An in-flight experimental investigation of helicopter main rotor/tail rotor interactions

by

Lieutenant Commander A D S Ellin Royal Navy
Defence Research Agency
and
University of Glasgow

Dissertation submitted to the University of Glasgow
for the degree of Doctor of Philosophy
April 1993

The research reported in this dissertation was funded by the UK MoD Strategic Research Programme (item AS011Q09)

ProQuest LLC.
789 East Eisenhower Parkway
P.O. Box 1346
Ann Arbor, MI 48106 – 1346

Preface

The work described in this dissertation was carried out by the author whilst a full-time student of the Department of Aerospace Engineering of the University of Glasgow during the period August 1990 to April 1993. The dissertation is original in content except where otherwise stated.

The author wishes to express his gratitude for the advice and encouragement given him by his supervisor, Professor R A McD Galbraith, during the course of this work. He would also like to thank Dr G D Padfield and the other members of the Helicopter Aeromechanics Section at DRA Bedford for their assistance.

Defence Research Agency, A D S Ellin

Bedford April 1993

Summary

Experience had shown that the fidelity of the yaw control characteristics of the computer simulation models used at DRA Bedford and elsewhere was not up to the standard required for ACT control law development. It was therefore decided that the DRA model, Helistab, should be improved in this respect and a research activity initiated. In the absence of suitable published information or detailed data on the performance of the tail rotor, two experimental flight test programmes were conducted, the first with a Puma, the second with a Lynx AH Mk5. This dissertation describes the planning and conduct of the second experiment and the analysis of the data collected in both.

Building on the DRA's considerable experience in main rotor research, the instrumented tail rotor blade for the Lynx was designed to make use of the Pressure Indicator Sensor technique which, provided that the local in-plane velocity is known, permits the local blade loading to be estimated from the pressures read at two points on the upper surface leading and trailing edges of the blade. The lack of this velocity information for the tail rotor presents problems, solutions to which are discussed.

With the aircraft experimental installation completed, it was flown for fifteen hours, during which time data on over 1200 flight conditions were collected from within the Lynx low speed flight envelope. New techniques had to be developed to allow efficient analysis of this large database so that the information contained therein could be extracted.

From the initial analysis of the data it was determined that the Lynx AH Mk5 low speed flight envelope can be sub-divided into six regions. In each of these regions, the mechanism of main rotor/tail rotor interaction is different. One or more flight conditions in each region were selected for in-depth analysis so that the detail of the mechanisms could be determined. Each interaction is covered in turn.

Once the predominant mechanisms of the main rotor/tail rotor interaction were isolated, their respective effects on the yaw performance of the helicopter could be assessed and a decision taken as to whether or not they should be included in the model. The dominant interaction, that taking place in quartering flight, should be included in all tail rotor models. This effect has been modelled and, when included in Helistab, the trim results obtained show a marked improvement over those previously available. The remaining interactions are not so significant and their inclusion would depend on the detail required in the model and the purpose for which it was intended.

The Lynx AH Mk5 experiment is seen as the first part of a comparative study: an additional trial with a Lynx AH Mk7, in which the tail rotor rotates in the opposite direction, is proposed as the second. The instrumented tail rotor blade designed for that aircraft includes an extra sensor that should enable the in-plane velocity to be determined.

In addition to the model improvements, this research has suggested the use of cyclic control of tail rotor pitch to improve tail rotor efficiency. The use of this control technique has the potential to expand the low speed flight envelope, though it could only be incorporated as part of a helicopter ACT system. It is recommended that tail rotor cyclic control, and some other aspects of tail rotor performance highlighted by this present research programme, be more fully investigated in the future.

Contents

Appendices.

Figures.

List of Figures.

4.3.1 Isometric presentation of frequency content.

4.3.2 Displaced presentation of frequency content.

4.3.3 Lynx AH Mk5 low speed flight envelope showing regions where different main rotor/tail rotor interactions were observed. Areas 3 & 4 have similar mechanisms.

4.4.1 Plot of variation in $-C_p$ for one revolution of the tail rotor in hover OGE. Aircraft AUM 4600kg.

4.4.2 Sequence of single revolution plots of Lynx AH Mk5 tail rotor -Cp data during 30kts forward flight OGE showing passage of main rotor blade trailing tip vortex interference effects. Aircraft AUM is 4700kg.

4.4.3 Plot of average $-C_p$ over 160 revolutions.

4.4.4 Standard deviation of -Cp over 160 revolutions.

4.4.5 Range of -Cp variation over 160 revolutions.

4.4.6 Standard plots of Compass heading, Pedal position, Yaw rate and 85% blade radius trailing edge pressure.

4.5.1 $-C_p$ data at 165° azimuth in the order as recorded.

4.5.2 Datum main rotor position for each tail rotor revolution.

4.5.3 Data in figure 4.5.1 reordered by nearest main rotor blade position.

4.5.4 Data in figure 4.5.1 reordered by red main rotor blade position.

4.5.5 Format used for original "cartoon" animation of Puma tail rotor pressure data.

5.2.1 Variation in bound circulation along a blade of an isolated rotor in the hover.

5.2.2 Position of tip vortices calculated for an isolated 4-bladed rotor in the hover. The marked change in direction of vortex movement after the first blade passage is indicated.

5.2.3 Comparison of Rankine & Scully vortex velocity distributions.

5.2.4 Velocity distribution at the blade of an isolated rotor in the hover.

5.2.5 Figure from Rossow(1977) showing 2 vortices of equal magnitude and sign rotating round each other.

5.2.6 Sketch showing how the wake behind a helicopter in forward flight resembles that of a fixed wing aircraft.

5.3.1 Variation of Puma main rotor leading edge $-C_p$ over one revolution in the hover.

5.3.2 Variation of Puma tail rotor leading edge $-C_p$ over one revolution in the hover.

5.3.3 Frequency content of puma tail rotor leading edge sensor signals in the hover.

5.3.4 Variation of Lynx AH Mk5 tail rotor leading edge $-C_p$ over one revolution in the hover. AUM=4610kg.

5.3.5 Frequency content of Lynx AH Mk5 tail rotor leading edge sensor signals in the hover.

5.3.6 Standard deviation of Lynx AH Mk5 tail rotor leading edge $-C_p$ over 160 revolutions in the hover.

5.3.7 Variation of Lynx AH Mk5 tail rotor leading edge $-C_p$ over one revolution in the hover. AUM=3945kg.

5.4.1 Lynx tail rotor - 30 kts forward flight OGE. Leading edge pressure sensor frequency content.

5.4.2 Sequence of plots of single revolutions of Puma tail rotor leading edge - C_p in 10 kts forward flight OGE showing passage of main rotor blade trailing tip vortex interference effects.

5.4.3 Variation in $-C_p$ at the 98% blade radius leading edge sensor for one revolution of the tail rotor. The localised reduction in $-C_p$ indicated by the vertical line is caused by the interaction of a main rotor blade trailing tip vortex and the preceding tail rotor blade.

5.4.4 Variation in $-C_p$ at the 75% blade radius leading edge sensor for one revolution of the tail rotor. A main rotor vortex is approaching the

sensor and the localised increase in $-C_p$ indicated by the vertical line is due to the velocity induced by that vortex opposing blade rotation.

5.4.5 Variation in $-C_p$ at the 75% blade radius leading edge sensor for one revolution of the tail rotor. A main rotor vortex has just passed the sensor and the localised reduction in $-C_p$ indicated by the vertical line is due to the velocity induced by that vortex being with blade rotation.

5.4.6 Plot showing the position of the datum main rotor blade as the main rotor blade trailing tip vortex interference effect is detected at each tail rotor blade leading edge sensor.

5.4.1.1 Sketch of main rotor blade trailing tip vortex/tail rotor blade trailing tip vortex interaction showing three phases of interaction.

5.4.1.2 Vortex interaction model starting positions.

5.4.1.3 Plots showing calculated changes in the tail rotor blade trailing tip vortex produced by the model over the first 10 milliseconds. The main rotor vortex only showed a slight bulge in the same timescale.

5.4.2.1 Theoretical variation in V^2 with blade radius for a tail rotor rotating top blade forward. The effect of a main rotor blade trailing tip vortex is shown for three vortex locations (25, 50 & 75% rotor radius).

5.4.2.2 Theoretical variation in V^2 with blade radius for a tail rotor rotating top blade aft. The effect of a main rotor blade trailing tip vortex is shown for three vortex locations (25, 50 & 75% rotor radius).

5.5.1 Definition of quartering flight.

5.5.2 Direction of rotation of both "wing tip" vortices is bottom-away from aircraft centreline.

5.5.3 "Wing tip" vortex coincident with tail rotor.

5.5.4 "Wing tip" vortex forward of tail rotor.

5.5.5 Percentage change in overall tail rotor dynamic head as a representative "wing tip" vortex tracks diametrically across the disc. Tail rotor radius is 1.1m.

5.5.6 Signal frequency content in quartering flight.

5.5.7 Variation in minimum separation distance between individual blade trailing tip vortices within the "wing tip" vortices with aircraft speed as calculated for a Lynx AH Mk5.

5.5.8 Standard deviation of Lynx AH Mk5 tail rotor leading edge $-C_p$ over 160 revolutions in flight 20 kts/60° OGE.

5.5.9 Variation in trailing edge C_p at 85% blade radius with tail rotor blade azimuth over 160 revolutions in flight 20kts/060° OGE.

5.5.10 Variation in total tail rotor dynamic head as calculated using Helistab in conjunction with the Beddoes wake model.

5.5.11 Variation in tail rotor blade root pitch angle as calculated using Helistab in conjunction with the Beddoes main rotor wake model.

5.5.12 Frequency content of the 84% tail rotor radius leading edge sensor on the Puma during tail rotor buzz.

5.6.1 Puma tail rotor blade leading edge sensor frequency content in flight 20kts/180° OGE.

5.6.2 Lynx tail rotor blade leading edge sensor frequency content in flight 30kts/150° OGE.

5.6.3 Lynx AH Mk5 tail rotor leading edge $-C_p$ averaged over 160 revolutions in flight 30kts/150° OGE.

5.6.4 Standard deviation of Lynx AH Mk5 tail rotor leading edge $-C_p$ over 160 revolutions in flight 30kts/150° OGE.

5.6.5 Variation of $-C_p$ with tail rotor azimuth and main rotor azimuth during flight at 30kts/210° OGE. Interpretation of plot is fully explained in text.

5.6.6 Lynx leading edge pressure sensor frequency content during flight at 30kts/300° OGE.

6.2.1 Figure showing Bo105 yaw rate response to a pedal input and Helistab model response to the same input.

6.3.1 Beddoes main rotor wake model configured as a Lynx at 30 kts.

Chapter 1.

Introductory

1.1 Introduction

The yaw control device of a helicopter has three primary functions. These are:

i. To provide a moment to counteract the main rotor torque reaction on the fuselage.

ii. To enable the pilot to select a desired heading whilst in the hover or a desired sideslip angle in translational flight.

iii. To enable the pilot to apply yawing moments in manoeuvre to effect coordinated and uncoordinated turns.

With the possible exception of it's use in certain 'aerobatic' manoeuvres, main rotor torque induced yawing motion of the fuselage is an unwanted effect. It would be beneficial if the yaw control device fitted to the helicopter could automatically provide the requisite moment to counter any such motion without conscious effort from the pilot.

It would also be desirable if heading or sideslip angle control could be achieved smoothly, linearly and progressively. Yaw control in a helicopter is the one 'attitude' control that is the most 'mission oriented', especially in the hover, and is often used in the performance of some pointing task such as fixed weapon firing. It should therefore be instinctive and unobtrusive so that the pilot attention is not unnecessarily distracted from his mission.

Unfortunately yaw control implementation in current generation helicopters requires considerable effort from the pilot and, in many cases, falls far short of providing the quality of control described above. There are several reasons for this; those affecting the conventional open tail rotor are as follows:

The tail rotor is not the only part of the helicopter that can provide a moment to counter the main rotor torque reaction. When the aircraft is flying with a relative wind from any direction other than straight ahead or backwards, the wind acting on the fuselage will try to turn the fuselage so that it is pointing nose to wind. The moment produced by this weathercocking effect will act either with or against the main rotor torque reaction depending on the relative wind direction. The main rotor downwash over the rear fuselage can also produce a yawing moment that changes with speed and direction of travel. In addition, the main rotor torque reaction will vary with the aircraft's all up mass. It can therefore be seen that, when all these factors are taken into account, the thrust required from the tail rotor to counter whatever yawing moment exists will vary quite considerably with flight condition.

Once the thrust required from the tail rotor is known the air mass flow rate required to produce it can be calculated if required and, under uniform flow conditions, the tail rotor blade pitch angle required to achieve this set. However, the operating regime of the tail rotor is seldom uniform. The flow field round the tail rotor is affected by the main rotor downwash, the influence of the rear fuselage and fin and, under certain flight conditions, the proximity of the ground. The relative proportions of these effects will vary significantly with flight condition and, to some extent, on the tail rotor thrust itself. The tail rotor blade pitch angle required to produce a given thrust will therefore change markedly with flight condition.

The end result of this changing thrust requirement and tail rotor operating environment is a yaw control that is anything but smooth, linear or progressive. An illustration of these non-linearities is given at figure 1.1.1. This portrays the variation in

yaw control-margin with relative wind speed and direction for the Westland Lynx AH Mk5 aircraft. The centre point on the plot indicates a still-air-hover with radial distance out from the centre, the relative wind speed. Zero degree sideslip indicates a relative wind from ahead with 90° sideslip, a wind on the starboard (right) beam. It highlights the major reduction in pedal margin when the relative wind is approximately 50 degrees right of the nose at 15 - 25 knots. These circumstances can potentially limit the achievable yaw acceleration, and hence flight in situations where heading accuracy can be vital. This has implications in nap-of-earth and deck operations for example where any restrictions in the out-of-wind capabilities of the aircraft can seriously affect its operational effectiveness. The tail rotor is not unique in possessing these characteristics. The other less conventional methods of yaw control each suffer from their own idiosyncrasies giving rise to comparable non-linearities in control.

As helicopters become more and more complex it is incumbent on designers to minimise pure piloting effort within the accepted technologies. Currently, Active Control Technology (ACT) is considered one of the most effective ways of achieving this end whilst maintaining or improving vehicle performance. When applied to the yaw axis, ACT should be capable of controlling tail rotor thrust automatically, thus reducing that part of the pilot's workload.

Experience with the implementation of ACT systems on fixed wing aircraft has highlighted the requirement for a high level understanding of the factors governing control of the vehicle. It would be difficult to develop the necessary control laws without an accurate model of the aircraft response. Contemporary yaw control models have major shortcomings and this provided the impetus for the present work. The deficiencies in our understanding are illustrated in figure 1.1.2. This shows how the DRA helicopter simulation model, Helistab (Padfield (1981)), predicts the Lynx AH Mk5 yaw control-margin plot and the disparities between this and figure 1.1.1 are evident. These discrepancies are largely due to the absence of any main rotor or fuselage flowfield effects in the tail rotor model.

The preliminary objective was to check whether or not the then available data were sufficient to improve the Padfield model. As shall be discussed in section 1.2 no suitable data could be found and so the present investigation was initiated. Tail rotor blade surface pressures were recorded in flight using specially instrumented blades on both Puma and, more extensively, Lynx AH Mk5 helicopters. Analysis routines were developed to permit the large quantities of data to be studied as efficiently as possible. Initial observation of the data revealed strong similarities between the features noted on the two aircraft types. The presence of six different variations of main rotor/tail rotor interaction were detected within the Lynx AH Mk5 low speed flight envelope and, from a more rigourous analysis of some of the data, detailed mechanisms determined for the three most significant. From the understanding of tail rotor operation gained a more accurate model of yaw control performance has been formulated. This now has the potential to be included in either Helistab or the next generation simulation model, thus achieving the aims of the programme.

This introductory chapter will continue with a review of the existing work carried out in this field. Section 1.3 will discuss the initial stages of the RAE/DRA tail rotor research programme before the scope of the present study is described in section 1.4. Finally the nomenclature and display conventions used throughout this report will be laid out in section 1.5.

1.2 Review of existing work.

Despite its extensive use in helicopter designs, the aerodynamics of the tail rotor has been minimally researched when compared to its companion main rotor. As an increase in main rotor efficiency has a greater effect on the overall vehicle performance than a comparative tail rotor improvement, resources expended on the main rotor has always been easier to justify.

Early tail rotor design work normally made use of main rotor or propeller theory though some theoretical work was carried out by Amer & Gessow (1954) which considered the tail rotor effect on directional stability. Tail rotor design has tended to be of an iterative nature with each manufacturer broadly sticking with a basic tried and tested design as the start point for a new aircraft and making subsequent small variations as required. In many cases, it was only when the yaw handling of a new helicopter was unsatisfactory that research was carried out. Although understanding of the tail rotor has improved over the years, new tail rotor designs are regularly proving to be deficient necessitating re-working either before or after the aircraft enters service.

One well documented case is that of the YAH-64 Apache Helicopter (Prouty & Amer 1982) This aircraft was fitted with 5 different designs of horizontal stabiliser and 2 different designs of tail rotor before handling was considered satisfactory. Changes to the UH-1 series of aircraft were described by Lynn,Robinson,Batra & Duhon (1969). The UH-1 tail rotor was altered from a tractor to a pusher configuration. The original five bladed, symmetrical section tail rotor fitted to the Westland Sea King was replaced when the thrust developed became insufficient for the weight growth of the aircraft. A new six bladed rotor was fitted in conjunction with a tail boom strake which sufficiently off-loaded the tail rotor in right sideways flight (Brocklehurst (1985)). Following the development of a cambered tail rotor blade section (Wilby (1976)) and subsequent trials on a Sea King (Hansford (1976) & Cook (1976)) which indicated an increased tail rotor thrust, new versions of the aircraft reverted to a five bladed rotor. The Westland Lynx is also on it's second tail rotor design. The original rotor rotated top blade forwards and had blades of RAE 9615 section. This has been replaced by a rotor rotating top blade aft with blades of RAE 9670 section. This greatly improved the aircraft's handling, especially in quartering flight (Phipps (1985) & Phipps (1987)). A reduction in the aeroacoustic signature of the aircraft was also apparent (Leverton, Pollard & Wills (1975) & Leverton (1981)). Changes in tail rotor design of the Westland/Agusta EH101 have yet to be fully documented.

Some tail rotor research has been undertaken by operators rather than manufacturers of aircraft. The Royal Australian Airforce had perceived a problem with the yaw handling of their Bell 206B-1 helicopters and their investigation, although it was not particularly conclusive, was reported by Ward (1981) and included an interesting discussion on tail rotor vortex ring states. Several studies simply gave a "state of the art" report on tail rotors and their inherent problems, eg.Cook (1978). The initial report of this current investigation (Smith(1987)) was produced to bring the RAE to an equivalent level of understanding.

The reports discussed above concentrated on the manifestations of the problems and their solutions. Very little mention was made of the mechanisms associated with and hence possible causality of the problems. A similar statement could easily be made for the majority of the non-aircraft-type-specific reports that considered tail rotors. With the exception of some full scale tests conducted on an isolated Lynx AH Mk5 tail rotor on an outdoor whirl stand (Signor, Yamauchi, Smith & Hagen (1989)), the remainder of the reports studied documented work carried out using models in wind tunnels.

Most of these wind tunnel experiments concentrated on the overall effects of the tail rotor interactions on the aircraft rather than the interactions themselves. Huston & Morris (1971) considered the ground vortex effect in low speed flight. This work, in conjunction with the later study by Yeager, Young & Mantay (1974), using the same experimental set-up, highlighted the manner in which the aircraft fin force varied with relative wind speed and angle, with tail rotor/fin separation, with tail rotor thrust and, more surprisingly, with tail rotor direction of rotation. These findings were corroborated by Weisner & Kohler (1973 & 1974) and Sheridan, Hanker & Blake (1984), who demonstrated the effect of change in height above the ground. Although each of these reports illucidate different aspects of the various tail rotor interactions, it was considered that the interaction mechanisms had to be determined prior to satisfactory modelling.

In 1985 Alan Brocklehurst of Westland Helicopters Limited conducted a series of wind tunnel experiments which specifically considered main rotor/tail rotor/fin interactions. His work on fin blockage effects (Brocklehurst (1985/3) & (1985/4)) did not fully support the findings of Yeager, Young & Mantay (1974) since he found that the fin force was independent of tail rotor thrust, provided that blade stall had not occurred. Equations, derived from his observations, were given to allow fin blockage effects to be taken into account. Brocklehurst (1985/1) considered the effect of the tail rotor wake on the main rotor and observed distortions to the tail rotor wake. These distortions caused the wake to wrap around the edge of the main rotor disc in flight conditions approaching the hover. This mechanism was then invoked to explain the azimuthal variations observed in main rotor pressure distributions on the RAE Puma (Tarttelin (1989)). An aspect of the interaction that was not considered was the similar effect on the tail rotor pressure distribution in the hover; this will be discussed in chapter 5. Brocklehurst (1985/1) also discusses the effect of changing the position of a trailing blade tip vortex in relation to the following blade and how that affects the loading distribution on that following blade. This was helpful during the development of the proposed mechanism associated with main rotor blade trailing tip vortex effects on the outer portion of a tail rotor blade in low speed forward flight; discussed in section 5.4.1.

Of this series of Westland reports, Brocklehurst(1985/2) provides the most comprehensive coverage of the predominant interaction affecting tail rotor performance. It discusses how, in quartering flight, the tail rotor can be immersed in the rolled up tip vortices trailed from the edge of the main rotor disc. The resultant flow field changes the dynamic head at the tail rotor blade giving the quoted 20% difference in the tail rotor thrust/pitch gradient between rotors rotating top-blade-forward and top-blade-aft. Brocklehurst concludes by stating that an accurate main rotor wake geometry model is required to reproduce the effect. Such a model will be described in chapter 6 with it's use noted in section 5.4.

Not all reports on tail rotor performance have been written from an aerodynamic standpoint. With the increasing requirement for military helicopters to avoid detection and for civil helicopters to be more "environmentally friendly", aeroacoustics has become a major field of study. As the acoustic signature is produced by the aerodynamic effects at the blades, valuable information on the performance might come from study of acoustic data. In addition to the two reports on Lynx aeroacoustics mentioned above, other reports on the topic include Pegg & Shidler (1978), Schreier (1982) and Fitzgerald & Kohlhepp (1988). The latter two of these reports discuss the effect of variations in tail rotor thrust on the noise generated. Tadghighi & Cheeseman (1983), although specifically referring to tail rotors in the title, considered the noise generated from an isolated rotor in smooth air conditions and cannot be said to relate to the noise emanating from a tail rotor in flight. Of more interest , however, was the work of Schinker & Amiet (1983)who considered the interaction of the tail rotor with a main rotor trailing tip vortex in low speed forward flight. Although the interference between the main rotor blade trailing tip vortex and it's tail rotor counterpart was not mentioned, it's effect, when interfering with the blade itself, is given significant coverage.

At an early stage, it became apparent that a good knowledge of the features of the main rotor wake would be required. There are several hundred reports pertaining to main rotor wakes, not all of which are directly relevant to the current work. Immediately following the Second World War, the RAE started investigating main rotor wake distributions. Brotherhood (1947) and (1952) showed detail of the flow in hover and vertical descent. Elsewhere,Heyson & Katzoff (1957) described experimentally and theoretically derived data for the induced velocity distribution of a lifting rotor disc and so formed a foundation for much of the work that followed. Simons, Pacifico & Jones (1967) gave information on blade trailing tip vortices and discusses the time taken these to roll up (up to 60 degrees of blade rotation). Experimental studies of the main rotor wake in the hover, leading to prescribed wake formulations for that flight

condition, were described by both Landgrebe (1971) and Kocurek, Berkowitz & Harris (1980). For forward flight, however, the prescribed wake model from Beddoes (1985) has been found to give good correlation with flight data and will be further discussed in Chapter 6. Few people have considered the main rotor wake with the intention of improving tail rotor performance prediction. Fortunately Quackenbush, Bliss & Mahajan (1989) and other reports by the same author(s) who did consider the interactions of interest, presented useful information for the present study. Recently, Gray (1991) reviewed the USA effort producing a good introduction to this area of interest. The work carried out by Messrs. Young and Markiewicz at RAE (now DRA) Farnborough also deserves mention even though their main rotor loading prediction methods can not be directly applied to the tail rotor.

There have been many reports on blade/vortex interaction, for example Horner, Saliveros &Galbraith (1991/1) and (1991/2) but almost all are concerned with main rotor interactions of the parallel configuration. Although this may cover some of the tail rotor interactions, the interactions between main rotor vortices and the tail rotor are not catered for.

The conventional tail rotor is but one of a variety of yaw control methods investigated. For example Mouille (1970) and (1979), Vuillet & Morelli (1986) and Vuillet (1989) are a few of the papers representing Aerospatiale experience with the Fenestron, the latter offering a comparison between the Fenestron and an equivalent tail rotor. Lemont (1982) considered the ringfin augmentation technique. McDonnell Douglas have persevered with their NOTAR to effect as discussed by Van Horn (1982) and Bregger & Dawson(1992) amongst others. The Fantail fitted to the Commanche has also been considered (Clemmons(1992)).

The reports mentioned above constitute a representative sample of the wide and comprehensive coverage given to many aspects of rotor aerodynamic research. The desire for an improved understanding of main rotor tail rotor interactions was a

reoccurring theme, though little action has hitherto been taken to address it. Although pertinent, the reports were not found to contain the detailed information on tail rotor operation and performance required to fulfil the needs of this programme.

1.3 Initial phases of the RAE/DRA tail rotor research programme.

The RAE tail rotor research programme was instigated in 1985 with the first phase undertaken by Lieutenant Commander A C Smith Royal Navy. As reported in Smith (1987), he conducted a limited literature search to acquire an appreciation of yaw related phenomena within the low speed flight envelope. These he identified as being:

1. Operation of the tail rotor in vortex ring in left sideways flight.

2. Main rotor torque variation in sideways flight inside ground effect (IGE).

3. Increased tail rotor inflow in right sideways flight.

4. Main rotor wake/tail rotor interaction; especially in quartering flight.

5. The effects of the fuselage shape on yaw stability. This includes weathercocking and the effects of tail boom strakes.

The following should be added to the list for it to detail all the most significant factors affecting yaw control:

6. The effect of the main rotor ground vortex in rearward flight IGE.

7. The interference between the main rotor wake and the tail fin.

In addition to the above, Smith also considered the effects of tail rotor configuration and the alternative Fenestron form of yaw control.

As Smith's work progressed it was decided that an instrumented tail rotor trial should be conducted using the RAE Flight Research Puma helicopter (figure 1.3.1). Design of the instrumented tail rotor assembly was commenced and, by the time that Lt Cdr Smith RN was relieved at Bedford by Lieutenant S F Baldwin Royal Navy in 1987, the blades and hub were being manufactured. Whilst these were under construction, it had been decided that a short flight trial would take place with a standard, non-instrumented tail rotor fitted to the Puma. The intention was to identify those regions of the low speed flight envelope that warranted in-depth investigation with the instrumented rotor. With this complete and the instrumented tail rotor fitted, the aircraft was taken to IAF Villafranca in the Po Valley of Northern Italy in April 1988 to conduct the trial with The instrumented rotor. Villafranca was selected as the trial location for the reasons given in section 3.2. All the intended flight conditions were flown and the aircraft returned for Bedford.

Unfortunately, no provision had been made for data quality checks at Villafranca. It was not until the data tapes were inspected at Bedford that the tail rotor sliprings failure part-way through the flight programme was discovered. The consequence of this was that, although aircraft rates, accelerations and control inputs had been recorded, no tail rotor pressure data had been collected after the fourth of eighteen flights. This notwithstanding, the collected data were of good quality and subsequently produced much useful information.

The design and manufacture of the Puma's instrumented tail rotor , the results obtained with the standard tail rotor and the conduct of, and some sample pressure plots from, the instrumented blade trial were recorded in Baldwin & Handley (1988). Lt Baldwin RN left Bedford In 1988 and was replaced by the author before any detailed analysis of the data collected could take place . It is appreciated that the achievements of the present work built on that of Lt Cdr Smith RN and Lt Baldwin RN together with the efforts of the Helicopter Aeromechanics Section of the DRA Flight Systems Division.

1.4 Scope of the present study.

Shortly after the instrumented tail rotor trial discussed in the previous section, the Puma was replaced by a Westland Lynx AH Mk5 (figure 1.4.1). As the Mk5 Lynx was only bought in small numbers by the MOD it had been decided that they should all be converted to Lynx AH Mk7 standard by the end of 1991. One of the most significant changes to the aircraft included in the modification programme was that the tail rotor was changed from the original, which rotated top-blade-forward, to one with a different blade section that rotated top-blade-aft. As the direction of rotation of the tail rotor had been identified as one of the most significant configuration changes affecting it's performance (Smith (1987), Lynn, Robinson,Batra &Duhon (1969)), it was recognised that the RAE had an excellent, and probably unique, opportunity to look in depth at the effects of tail rotor rotational direction with the two different tail rotors mounted on the same aircraft. It was therefore decided to pressure instrument a tail rotor blade on the Lynx AH Mk5 and conduct flight trials, before repeating the exercise with the Lynx AH Mk7.

An instrumented tail rotor was designed and manufactured to make use of the Pressure Indicator Sensor Technique of blade pressure measurement and load estimation (Brotherhood & Riley (1990)). Due to the restricted timescale imposed by the date of the Mk7 conversion, the instrumentation followed closely that used on the Puma. Even though the local blade in-plane velocity, an important part of the Pressure Indicator Sensor Technique, could not be established, it was decided that this instrumentation layout would lead to significant advances in the understanding of tail rotor aerodynamic phenomena. Details of the system are given in Chapter 2.

Following a thorough testing of the aircraft instrumentation system, the flight trials were conducted at IAF Villafranca in April 1991 and utilised the experience gained from the earlier work with the Puma. A portable data replay system had been acquired

and was used to inspect each data tape soon after recording. This was particularly important for it was clear that this was to be the last trial of an instrumented tail rotor on a Lynx AH Mk5 (Bedford's was the last remaining Lynx of this Mark). To make maximum use of the opportunity, more test points were flown than were strictly required for the present investigation. For example, in addition to the steady flight conditions within the low speed flight envelope, data were also collected in high speed and manoeuvring flight. The conduct of the experiment will be presented in Chapter 3.

Whilst the Lynx Ah Mk5 instrumented tail rotor was being built, the pressure data collected on the Puma was investigated. Due to the rate at which tail rotor pressure data varies in comparison with equivalent main rotor data, the analysis routines developed at RAE for the main rotor research were not directly applicable. A suite of analysis programs were therefore developed and applied to the Puma data in such a way that they could be adapted for use on the Lynx data. During this process, the speed of the data analysis was greatly improved by increased automation and an appreciation gained of the interactional phenomena observed. Both frequency and time domain analysis techniques were used and a method evolved for re-ordering the data so that animation techniques could be employed to highlight the finer features not apparent on a steady image; these routines will be discussed in Chapter 4.

On completion of the flight trial, the Lynx data were inspected and found to be of a contemporary high quality. A significant quantity of the data from the 1270 test points flown were processed using the developed analysis routines. After cursory inspection it was reassuring to observe that the features noted and identified in the Puma data were also evident for the Lynx. A consideration of the frequency content of the Lynx data, from steady sideslips, revealed different characteristics in different regions of the envelope. This indicated that different main rotor/tail rotor interactions were taking place dependant on flight condition. From each of the six regions identified a few test points were selected for further analysis.

In forward flight two different interactional mechanisms were determined; one between the main rotor blade trailing tip vortex and the tail rotor blade trailing tip vortex and the other between the main rotor blade trailing tip vortex and the inboard region of the tail rotor blade. The effect on the performance of these interactions was found to be quite small. This was not the case with the interaction between the main rotor wake and the tail rotor in quartering flight, where the tail rotor blade dynamic head could be reduced by as much as 35% for a tail rotor rotating top-blade forward. A detailed description of these interactions, and to a lesser extent those occurring in rearward flight is given in Chapter 5.

The limitations of current tail rotor computer models have already been mentioned in section 1.1. In order to test the hypotheses for the main rotor/tail rotor interactions discussed above it has been necessary to develop suitable models. For the forward flight case it was necessary for the model to consider the individual blade vortex interaction in detail whilst that for the quartering flight case could employ a more "broad-brush" treatment. It was found that by taking a prescribed main rotor wake model already developed for the calculation of main rotor blade loadings (Beddoes (1985)) it was possible to generate an appropriate flow in the region of the tail rotor. The incorporation of this model in the Helistab program resulted in a marked improvement in the prediction of yaw control margins (figure 1.4.2). A discussion of the different facets of tail rotor modeling will be given in Chapter 6.

In addition to detailing the conclusions drawn from this research programme, Chapter 7 will give recommendations for additional work to be carried out in this field including a comparable flight trial programme with a pressure instrumented tail rotor blade fitted to a Lynx AH Mk7.The standard tail rotor on the Lynx AH Mk7 is made predominantly of composite material rather than metal as used on the Mk5. This will enable a better instrumented tail rotor to be constructed for the second part of the comparative trial that should allow the in-plane velocities to be determined. From the

deduced blade loading data it should be possible to assess how evenly the tail rotor is loaded around it's azimuth for the different phases of flight.

Although the primary aim of the research programme has been the improvement of yaw control modelling for conventional and ACT control law development, there has also been the potential for improvements in tail rotor design, leading to increased efficiency. An example of this may be the use of cyclic control of tail rotor pitch enabling the redistribution of tail rotor lift in flight conditions where a large disparity in blade loading around the disc is currently experienced. The future flight experiment with the Lynx AH Mk7 and the possible advantages of tail rotor cyclic control will be discussed, together with the conclusions from the present investigation, in Chapter 7.

1.5 Nomenclature, abbreviations and display conventions.

a	Lift curve slope
A&AEE	Aircraft & Armament Experimental Establishment
AH	Army Helicopter
ASE	Auto Stabilisation Equipment
b	Number of blades
C_p	Coefficient of pressure
C_N	Normal force coefficient
c	Blade chord
DRA	Defence Research Agency
FCF	Flight Clearance Form
FTI	Flight Trials Instruction
IAF	Italian Air Force
IGE	Inside Ground Effect
L	Lift
MODAS	MOdular Data Acquisition System

N_r	Main rotor rotational speed expressed as a percentage of 318.21 rpm.
OGE	Outside Ground Effect
P	Raw recorded pressure
P_0	Static pressure
PCB	Printed Circuit Board
PRIU	Processor Recorder Interface Unit
R	Main rotor fundamental frequency
R_t	Tail rotor blade radius. (1.105m for Lynx AH Mk5)
r_t	Radial position along tail rotor blade
RAE	Royal Aerospace Establishment
RAF	Royal Air Force
REME	Royal Electrical & Mechanical Engineers
T	Tail rotor fundamental frequency
U	Local inflow velocity
V	Local blade velocity
V_a	Aircraft's translational velocity
V_r	In-plane velocity induced by blade motion
V_v	In-plane velocity induced by main rotor vortex
z	Vertical distance above main rotor disc
α	Blade incidence angle
μ	Main rotor advance ratio
ρ	Air density
θ	Blade root pitch angle (No twist on blade)
Ψ_m	Main rotor blade azimuth
Ψ_t	Tail rotor blade azimuth
Ω_m	Main rotor angular velocity
Ω_t	Tail rotor angular velocity

The following display conventions are used throughout the report:

i. Zero degrees azimuth for both main and tail rotors is with the datum or instrumented blade pointing aft. Azimuth angles are given in degrees and increase in the direction of blade rotation.

ii. The tail rotor is viewed from the port (left) side of the aircraft. If the fin were shown, it would be behind the tail rotor on the Lynx but in front of it on the Puma.

iii. The rotor C_p data variations are shown by means of coloured contour lines connecting points of similar value. The solid line in each colour represents the lowest value of that colour in the key table. $-C_p$ is displayed for reasons given in the text.

iv. Relative winds may be quoted in the form "30kts/064°". This represents a wind speed of 30 knots coming from a direction 64 degrees to the right of the aircraft's nose. Note that, depending on aircraft type, the direction of increasing relative wind angle may be different from that of increasing main rotor azimuth angle.

Chapter 2.

Experimental set up and measurement techniques.

2.1 Introduction

The aim of the programme has been stated in section 1.1 as being to improve the fidelity of existing computer models of helicopter yaw handling and performance through improved understanding of the aerodynamic interaction mechanisms. In section 1.2 a search of the available literature established that there were insufficient data already existing to achieve this goal. It was therefore decided to conduct an experiment during which suitable flight test data would be collected. The subsequent analysis of that data would then provide the information required to enable the model to be improved. Although the data analysis was the most significant part of the experiment, the correct data had to be recorded in a suitable manner so that the analysis could yield the desired results. This chapter discusses the design of the data collection phase of the experiment.

With all the factors that can affect the tail rotor thrust, it was not considered sufficient to measure the total thrust provided by the tail rotor but rather to arrive at this figure by integrating up the blade loads produced over the tail rotor disc. Indeed, at this stage in the programme, a sensor had yet to be designed that would give a single output of tail rotor thrust. The various methods of instrumenting rotors shall be discussed in section 2.2, with the Pressure Indicator Sensor Technique actually employed described in section 2.3. Originally developed for main rotor research, the technique relies on a knowledge of the local in-plane velocity at the blade which, as detailed in section 2.3, cannot be directly inferred for the tail rotor. The different techniques that can overcome this problem, some of which can be applied retrospectively to existing data, are covered in section 2.4.

The design and manufacture of an instrumented tail rotor for the Lynx AH Mk5 is covered in section 2.5. Once the pressures were detected at the blade sensors, the electrical signals they produced, suitably amplified, filtered and digitised, were recorded on the aircraft tape recorder. Subsequently, the data, suitably calibrated, were transcribed onto a different medium on a ground replay unit for long term storage and analysis. The aircraft instrumentation system and ground replay facilities are discussed in section 2.6 with system calibration and testing described in section 2.7.

2.2 Methods of rotor blade instrumentation

As discussed in the previous section, the tail rotor had to be instrumented to allow the variations in blade loading over the disc to be estimated. From this a value for total tail rotor thrust could then be derived. Theoretically it should be possible to derive the thrust directly from the blade coning angle, a technique used with some success on the main rotor. The variation in tail rotor blade coning angle is found to be very small in practice, partly because of the effect of the $\Delta 3$ hinge in reducing blade flap. Derivation of thrust from this angle is therefore subject to significant measurement errors. A sensor to measure tail rotor thrust directly from the tail rotor gearbox is currently under development and will be discussed in Chapter 7.

The blade loading could be derived from the local axial flow velocity changes induced by the tail rotor. This would necessitate the measurement of the velocity both upstream and downstream of the rotor to account for variations in the flow caused by agencies other than the tail rotor itself. It would also be necessary to record at discrete points over the whole disc. A rake of pitot tubes would be cumbersome and adversely affect the flow characteristics. Laser velocimetry techniques could be used. This method, although widely used in the controlled environment of the wind-tunnel and for the measurement of gust turbulence at a single point relative to a wing, is not one that lends itself readily to the recording of a rapidly changing field over a large area. In

addition, the Helicopter Aeromechanics Section at Bedford had no previous experience in the use of lasers in flight investigations and insufficient time within the programme to explore this technology. The use of high speed cameras to record the motion of smoke or other particles was not considered compatible with the accuracy required although, qualitatively, it would have proved quite useful. Hot film sensors bonded to the blade surface could show the location of the stagnation point at the blade leading edge and the transition point but previous experience within the Section had not shown their use to be particularly rewarding.

Any variation in loading will cause a rotor blade to deform. The strains induced in the blade could be recorded with a suitable array of strain gauges from which the deformation could subsequently be reconstituted. A method of strain pattern analysis (SPA) is currently under development for use on the main rotor of the DRA Flight Research Lynx AH MK7 helicopter. The analysis is complex and relies on a comprehensive calibration of the blade displacement / induced strain relationship. The tail rotor blade on a Lynx AH Mk5 is quite rigid and the deformations induced by the loading variation small. It is highly unlikely that any such method would be able to show the effects of a main rotor blade trailing tip vortex passing over the tail rotor disc.

The derivation of blade loading from surface mounted pressure sensors had previously been used with effect and was the method selected. A full description of the technique employed is given in the next section.

2.3 The Pressure Indicator Sensor technique.

The Helicopter Aeromechanics section at DRA Bedford has, over many years, developed expertise in performing in-flight rotor blade pressure measurement. Early research aimed at investigating the attributes of different aerofoil sections used an array of approximately twenty pressure sensors placed about the main rotor blade test section at one radial station. The recorded pressures could then be integrated to derive the blade

loading. This technique gave accurate results but required the use of a large number of individual sensors to measure the total loading. More recent research has been aimed at improving understanding of the loading variations over the whole rotor disc in flight. To use twenty sensors at each of up to twenty radial stations on a main rotor blade would necessitate the use of a recording system more capable than that currently available. The number of sensors required at each radial station had to be significantly reduced to make the research viable.

During the course of the work with the full chordwise sensor arrays just described, it had been noted that there was, under most conditions, a good general correlation between the variation in the local blade loading and the change in C_p measured at 2% chord on the upper surface of the blade (figure 2.3.1). Further research showed that wind tunnel data could be used to produce unique relationships over a range of Mach numbers between the C_p at this point on the blade chord and the local C_N and α (figures 2.3.2 & 2.3.3). These relationships have been expressed in tabular form for ease of use in analysis routines. The 2% chord position is in the vicinity of the aerofoil's suction peak and so has optimum sensitivity to loading variation. Unfortunately the relationships break down when the aerofoil stalls. A second sensor must therefore be fitted close to the blade trailing edge to detect flow separation in that region. When stall has occurred the value of C_N must be calculated in a different way; in the current analysis routines the C_N is held at it's immediately pre-stall value whilst the flow remains separated. The use of one leading edge and one trailing edge pressure sensor to derive local blade incidence and loading has become a standard method at DRA Bedford known as the Pressure Indicator Sensor Technique (Brotherhood & Riley(1990)). Brotherhood & Riley(1990) also discuss the effects of compressibility and phase lead of C_N to C_p on the results obtained.

The presence of different lines for each Mach number in figures 2.3.2 & 2.3.3 illustrates the techniques susceptibility to errors caused by inaccuracy in the value of local Mach number used. For main rotor work, this does not normally present a

problem since the local in-plane velocity can be obtained from a knowledge of the blades rotational velocity, the sensor radial location, the blade azimuth angle and the aircraft's translational velocity,ie:

$$V=\Omega_m r + V_a \sin \Psi_m \qquad \text{Eqn 2.1}$$

Although in-plane velocities induced by the main rotor's own tip vortices are ignored, this gives a close approximation for the majority of cases.

Unfortunately this is not the case for the tail rotor as the in-plane velocity is unknown and can be significantly affected by the main rotor wake and the influences of the fuselage, fin and ground in varying combinations. A representative value for tail rotor blade tip speed could be approximately 700 ft/sec and the corresponding main rotor downwash velocity, 60 ft/sec. If the tail rotor was fully immersed in the main rotor wake, it's blades would experience a variation of in-plane velocity of ±9% at the tip and ±20% at the root. If the tail rotor were only partially immersed in the main rotor wake the velocity changes experienced by its blades would be different. In this situation, the main rotor blade trailing tip vortices would also cause localised variations as they crossed the tail rotor disc, especially as the velocities they induced would be strongest in the plane of the tail rotor.

The use of tail rotor C_p calculated using a similar equation to Eqn 2.1 would generally result in a very poor approximation to C_N and α, although under certain flight conditions such as hover and low speed rearwards flight OGE, the effect of the main rotor wake would be small and this approach might be acceptable. For the rest of the flight envelope, however, an alternative method must be used to calculate the in-plane velocity. Some candidate techniques will be discussed in the next section.

Use of the Pressure Indicator Sensor Technique will not give as accurate a value for local blade loading as the use of a chordwise array of twenty sensors. There is a research programme at DRA Bedford to further investigate the source of the errors and

thus improve the analysis routines (Brotherhood (1992)). The pressure instrumented main rotor blade manufactured for the DRA Flight Research Lynx AH Mk7 helicopter has two chordwise arrays fitted in addition to the arrays of leading edge and trailing edge sensors so permitting continuation of this research(Tarttelin(1990)). The principle source of error when using the technique to study the tail rotor is in the estimation of the in-plane velocity. Once this error is reduced to an acceptable level, the detailed improvements currently being embodied in the main rotor analysis routines will be incorporated in their tail rotor counterparts. Experience gained during analysis of the tail rotor data so far undertaken has allowed these velocity-induced errors to be taken into account during the interpretation of the data; the techniques used and the information gleaned will be detailed in the chapters that follow.

2.4 Derivation of chordwise velocity.

It has already been established that a knowledge of the local chordwise velocity is required before the Pressure Indicator Sensor technique can be used to derive values for C_N and α. Where this velocity can be closely approximated by Eqn 2.1 for the main rotor, the same can not be said for the tail rotor. Three different methods of producing this velocity data have been established which are as follows:

i. By calculation using main rotor wake models.

ii. Using twin leading edge sensors.

iii. Tip pitot.

Of these three techniques, all but the first require extra sensors to be fitted to the instrumented blade which must therefore be embodied in the design stage. For a blade fitted with just the standard single leading edge and trailing edge sensors, the velocity can only be estimated by calculation. As, however, it is intended that a second experiment be carried out with a more comprehensively instrumented tail rotor blade

fitted to ZD559 after conversion to Mk7 standard, it should be possible to take data on the flow field affecting the tail rotor from that experiment and apply it retrospectively to test points flown at the same flight conditions as a Mk5. As the only design change that could affect the aircraft aerodynamics has been in the tail rotor itself, the effect on that rotor's flow field of the main rotor wake, the fuselage, fin and ground should be substantially the same.

The 3 methods are discussed in more detail below.

2.4.1 Derivation of velocity field by computation.

As stated in section 2.3, the local in-plane velocity at the leading edge sensors on main rotor blades has been determined by calculation using equation 2.1. This simple calculation yields a reasonably accurate velocity over the majority of the main rotor disc with the exception of those areas where a close blade/vortex interaction occurs. It should be possible to calculate the positions where such interactions occur and produce more accurate velocity values for those locations. Over the past 20 years much effort has been applied to the problem of predicting the wake beneath a rotor in hovering and translational flight, Landgrebe (1971) and Kocurek, Berkowitz & Harris (1980) being two of the many reports covering the hover and Beddoes (1985), forward flight. The research on which these reports are based has been aimed at improving main rotor loading predictions.

When considering tail rotor in-plane velocity distributions, the proportion of the disc affected by blade/main rotor wake interactions is significantly greater than on the main rotor discussed above. There is, however, no reason why the same philosophy cannot be adopted. If a main rotor wake model of sufficient accuracy could be formulated, the main rotor induced velocity distribution it produced for the tail rotor region could be applied to the tail rotor data. The most significant research into producing an accurate model of the main rotor flow field in the vicinity of the tail rotor

has been carried out by Continuum Dynamics Inc of New Jersey, USA; one of several reports on the work being Quackenbush, Bliss & Mahajan (1989). The main rotor flow field produced by their analysis predicts the passage of the main rotor blade trailing tip vortices with some accuracy but, at present does not consider the distortions to that flow field caused by the tail rotor.

When applying the in-plane velocities produced by such an analysis to the tail rotor pressure data the effects of this distortion could be taken into account. From an examination of the leading edge data in pressure coefficient form with the in-plane velocity derived from equation 2.1 it would be possible to plot the paths of the main rotor blade trailing tip vortices as they cut across the tail rotor disc and judge the age of that tip vortex in terms of main rotor azimuth angle. Using this information it should then be possible to adjust the position of the main rotor wake produced by the analysis to match that observed. The velocity field thus generated could then be applied to the pressure data and accurate loading calculations performed.

The technique just described would be expensive in terms of the computing time required as each tail rotor revolution would need to be matched to a flow field generated at the appropriate main rotor azimuth position. A result of reasonable accuracy could be achieved by a slightly different technique. Just as the velocities induced by direct blade/vortex interaction are ignored in DRA main rotor analysis as affecting a small area, the same could be done on the tail rotor. As above, the tail rotor pressure data could be examined to ascertain the path of the main rotor blade trailing tip vortices. A time averaged main rotor wake velocity distribution could then be positioned over the tail rotor using the tip vortex path as a locator and loading calculations subsequently performed. For a given flight condition it should therefore be sufficient to make one calculation of the main rotor wake distribution instead of one per tail rotor revolution. The loading distribution thus achieved would take into account the broader features of the main rotor flow without the complications of the smaller detail. Because of the

simplification it ought to be possible to use a less rigorous main rotor wake model than the Continuum Dynamics flow field discussed above.

There is no pretence that velocity distributions derived by computation would be as accurate as those directly measured at the blade. This technique does, however, provide a means of producing loading distributions of reasonable accuracy where the instrumentation required to measure the in-plane velocities was not available at the time of the experiment.

2.4.2 Twin leading edge sensor.

Without any velocity information, the single leading edge sensor of the standard Pressure Indicator Sensor technique can only provide a value for the local pressure. From wind tunnel data it is possible to construct a graph showing the relationship between the dynamic pressure measured and the local incidence and Mach number (figure 2.4.2.1). Without velocity information it is impossible to convert these $P-P_0$ values into incidence.

If the leading edge sensor were mounted at a different point along the chord line the slope of the lines of constant dynamic pressure would be different. By mounting a second sensor on the chordline it should be possible to chose a location such that the two lines of constant dynamic pressure from the two sensors intercept uniquely and thus define both the incidence and the Mach number (figure 2.4.2.2).

In choosing the location of the two sensors, the 2% chord position fulfils the criterion for one of them, namely high sensitivity to incidence. For the second sensor the sensitivity must be significantly less in order to provide a good intercept but not so low as to make the measurements overly susceptible to recording errors. The requirements for a good intercept and the reduction of compressibility effects dictate that the second sensor be placed further aft along the chord at approximately 40-50%

chord. A suitable fairing must be produced to cover both sensors without significantly altering the blade section. Although 50% chord can hardly be called the blade leading edge, the sensor at that location is referred to as a leading edge sensor to maintain the differentiation between the sensors used to derive C_N and α and the trailing edge sensor that must still be fitted to detect flow separation.

As with the single sensor technique, the accuracy of this method relies on the free-stream airflow along the chordline being uniform. Any velocity gradient in the flow affecting the blade will result in a change in the pressure profile round the aerofoil and thus change the value of velocity returned. The sensitivity of the technique to changing velocity must be determined. It is not expected that it will give accurate results during the passage of a main rotor vortex core.

2.4.3 Tip pitot

The use of a pitot tube mounted at the tip of a tail rotor blade, used in conjunction with the aircraft static system, probably represents the simplest method of measuring the broader features of the tail rotor flow regime. The tip pitot measures the dynamic pressure at the blade tip and once the contributions of rotor rotation and aircraft translation are removed will give the velocity at the blade tip due to the main rotor wake etc. It can therefore be used to measure the background features of the flow but will not give detail of the velocity variations induced by main rotor tip vortices as they pass over the tail rotor disc unless they happen to affect the pitot itself.

A tail rotor tip pitot for the Lynx AH Mk7 would have to be designed with care to keep it's weight to a minimum as the rivets fitted to retain the blade tip weight assembly are already highly loaded when the blade is rotating. As only the broader details of the flow would be measured there would be no additional advantage in fitting the pitot to the instrumented blade over fitting it to one of the others; indeed it would be

better to fit it to the opposite blade to assist in balancing the rotor system. The tip pitot fitted to the Lynx Main rotor is shown in figure 2.4.3.1.

2.5 Design and manufacture of the Lynx AH Mk5 instrumented blade and tail rotor assembly.

The design of the instrumented tail rotor blade for the Lynx AH Mk5 flight trial was similar to that used previously on the Puma which, in turn, had been based on the design of the main rotor instrumented blades. When the Lynx programme was initiated, timescales were such that the design of the blade had to be finalised at a very early stage and manufacture started. For this reason, even though the basic principles of the multiple leading edge sensor technique were evolved before instrumentation was complete, it was decided to stick with the original single leading edge plus trailing edge sensor layout. It was however decided that any instrumented tail rotor blade for the Lynx AH Mk7 would be fitted with multiple leading edge sensors.

The layout of the sensors on the blade was as shown at figure 2.5.1. Seven leading edge sensors were fitted at 2% chord with a concentration biased towards the tip; three with trailing edge sensors mounted directly behind them at 95% chord. This configuration was chosen to give a better coverage of the loading peak near the tip. This layout would give a more accurate estimate of blade thrust and improved understanding of the main rotor blade trailing tip vortex/tail rotor blade trailing tip vortex interaction at the expense of information on the interactions occurring inboard. Some strain gauges were fitted to monitor blade flap lag and torsion but the signals from all but three of these sensors were not recorded due to slip ring constraints. The wiring layout was designed to minimise connections and components on the blade surface with as many interconnections as possible, and all sensor temperature compensation resistors, at the blade root. The pressure sensor tag strips, strain gauges and wiring were bonded to the blade surface after paint removal as shown at figures 2.5.2 & 2.5.3; all work being

carried out in accordance with the relevant Westlands process sheet. The pressure sensors themselves were fitted after construction of the leading edge fairing. The pressure sensors used were Kulite pressure transducers type LQS-61-125-25SG, all of which had previously been used during main rotor investigations and then comprehensively tested prior to re-use

With metal main rotor blades built round an extruded alloy main spar there is generally sufficient metal at 2% chord to allow the sensor to be set down within the existing blade profile. With metal tail rotor blades that is not the case as a proportionally much greater part of the spar would have to be removed. The leading edge sensor must therefore be surface mounted and covered by a suitable fairing to restore the aerodynamic shape. The Lynx AH Mk5 tail rotor blade was of RAE 9615 section which, whilst based on the NACA 0012 section, had a drooped leading edge. Blade chord was 185mm. The external profile of the fairing was RAE 9615 for the first 15% of blade chord but with ordinates based on the 190mm chordlength that had been calculated to give sufficient depth of fairing to bury the sensor. The drooped leading edge of the blade provided extra clearance at the sensor location thus reducing the size of the fairing required. Aft of 15% chord the profile was faired back to that of the original blade by the point of it's maximum thickness ensuring that continuity of profile gradient was maintained. This fairing profile, shown in figure 2.5.4, was chosen as it was considered that a sensor mounted in it at 2% chord would respond to changes in velocity and incidence as if it were buried within a pure RAE 9615 section. In other words, the departures from RAE 9615 were small enough and sufficiently downstream of the sensor that their effect on the pressure recorded at the sensor could be neglected. The addition of the fairing shifted the quarter chord position of the aerofoil forward from that of the original blade but the structural implications of this and the additional weight of the instrumentation and fairing were not considered significant by Westlands. The fairing was made from balsa wood bonded to the outside of the blade anti-erosion shield and covered with a thin glass fibre scrim. The fact that the anti-

erosion shield was still in place, albeit no longer at the blade surface, meant that, although the fairing might be affected by impact damage, the structural integrity of the blade would not be affected. The balsa wood was fitted in three sections each covering approximately a third of the length of the working section of the blade to reduce the imbalance that would occur should part of the fairing become unbonded. All four blades were given identical fairings for ease of balancing and for uniformity of flow.

As the purpose of the trailing edge sensors is to detect flow separation at stall, minor discontinuities in the profile at this point could be tolerated. The trailing edge sensors were therefore bonded directly to the blade at 95% chord and surrounded with a small blister fairing.

When all 4 blades had been completed each of the non instrumented blades were statically balanced against the instrumented blade on a simple beam balance. Weight adjustments were achieved by judicious application of paint, care being taken to ensure that the edges were well feathered to reduce the likelihood of the paint layers separating in the airflow.

As originally schemed, it had been intended that the signals from the sensors would pass through a 44 way slip ring assembly prior to being amplified in the aircraft. It was however discovered that the 44 way slip ring, designed to fit on the tail rotor gearbox of a Lynx AH Mk7 was not compatible with that on the Mk5. The design of the installation was modified to make use of the 18 way slip ring assembly already fitted to the aircraft for the fatigue monitoring instrumentation. An amplifier unit was designed and manufactured to fit on the outside of the tail rotor pitch change beam (figure 2.5.5). The signals from the sensors were amplified to a level compatible with the 10 volt full scale deflection of the recording system and filtered at 600Hz; this frequency selected to give 7 samples per cycle at the 10th harmonic of the tail rotor fundamental frequency for good amplitude resolution. All tail rotor data was sampled at 4096Hz giving an azimuthal resolution of 2.7 degrees. By amplifying before the

sliprings the number of slipring channels required was virtually halved(1 wire per sensor plus a common 0 volts reference as opposed to 2 wires per sensor) and the potential impact of any noise generated by the slip rings reduced. The amplifier unit also included a power supply unit to convert the ±15 volts from the aircraft system to the ±5 volts required by the sensors. With this unit, the signals from the 10 pressure sensors, the 3 strain gauge bridges required for the fatigue monitoring package and the instrumented blade flap angle sensor could all be recorded. Tail rotor specific instrumentation fitted to the fuselage included a tail rotor azimuth sensor and tail rotor servo jack position indicator. By combining the output from the blade flap angle sensor with that from the servo jack position, the blade feather angle could be calculated. Although the aircraft had been fitted with a tail rotor torquemeter, this could not be made serviceable in time for the trial. The aircraft also had provision for recording the tail rotor near field noise with a microphone mounted on a tail boom access panel but again that was not fitted for this experiment. All the detailed design work required for this installation was carried out by the design staff of Aircraft Department, DRA Bedford. Blade instrumentation and manufacture of the tail rotor amplifier unit and all other items not commercially available were also done in house.

2.6 Aircraft instrumentation system and ground based replay facilities.

The instrumentation system fitted to the DRA flight research Lynx AH Mk5 helicopter at the time of the tail rotor investigation was based on the Plessey **Mo**dular **D**ata Acquisition System (MODAS) Mk1 PCM data recorder. The signals from the tail rotor sensors were passed into the fuselage via the slip ring assembly (figure 2.6.1) and thence down screened wire pairs down the length of the aircraft to the Signal Conditioning Unit on the instrumentation rack. This SCU was intended to house any additional signal conditioning cards that were required to bring the signals to the required standard. In the event no additional conditioning was required and the signals

passed unchanged through the SCU to the MODAS acquisition units. The heart of the MODAS was the Processor and Recorder Interface Unit (PRIU). This multiplexed the signals from acquisition units and fed the multiplexed data out to a 1" tape recorder. The total system sampling rate was 128k with each acquisition unit able to handle signals from 128 sensors. The rate at which each signal was sampled was controlled by a program within the PRIU, a different program being written for each experiment depending on the data required. When writing the program care was required in selecting the correct sampling rate as having too high a sampling rate can be as bad as having one too low. In addition, sensors in the same area, eg the tail rotor pressure sensors, must be sampled as close together as practicable to reduce the time skew in the data. As configured the system had two acquisition units; the MIPROC being the one handling all data from the main rotor slip rings with the other taking the data from the rest of the aircraft. A complete list of all sensors monitored during this investigation is given at Appendix 1. Each 1" flight tape could record up to 40 minutes of flight and was used only once to reduce data corruption. The data was recorded on the tape as counts, the range 0-4095 counts reflecting a 10 volt change in the amplified signal.

Two levels of ground replay were available. The first was a portable replay system which allowed selected signals from the flight tape to be inspected on hard copy as counts without any calibration. This unit was invaluable for monitoring recording system integrity. The second fixed base ground replay system was used to transfer calibrated data in edit sequences taken from the flight tape to 0.5" computer compatible tape whence the data could be de-multiplexed and analysed.

2.7 Instrumentation Calibration and test.

All the aircraft instrumentation was calibrated prior to the experiment. With the exception of the instrumentation fitted specifically for this experiment, all the other sensors had been calibrated in the past. A repeat calibration was carried out on these

sensors to ensure that they had not drifted and that, if the wiring had been disturbed, the sensor had been reconnected to the appropriate MODAS channel in the correct sense. As well as checking for operation over the sensor full range, the output signal was also inspected for noise and, where excessive noise was found, the source located and the problem dealt with. The sensors were all exercised in both directions to check for hysteresis. Calibrations were performed on the complete recording system, ie. with the sensor being fed by the aircraft power supply and recording the output on the aircraft MODAS equipment. Where a sensor had to be removed from the aircraft for calibration, eg rate gyro calibration on a rate table, it was connected to the aircraft system by a specially made wiring harness to ensure minimum disruption to the aircraft system.

As the tail rotor instrumentation was new for the experiment, additional work was required to ensure an adequate calibration. An estimate was made of the range of operation of the sensors in flight and the amplifier gains were set from the published sensor voltage output to give as large a MODAS count variation as possible. A quick calibration was then carried out to check the range and to allow adjustment of the amplifier offset. On completion of these adjustments a full calibration was then performed. If it became apparent during the test flying that the range or offset was incorrect an adjustment would be made and a further calibration performed. The blade pressure sensors were calibrated by removing the instrumented blade from the aircraft and placing it in a heavy gauge steel pressure vessel (figure 2.7.1) with electrical connection to the aircraft via a wiring harness. The air pressure in the vessel was then varied from 11 psi below atmospheric to 10 psi above in 1 psi steps and all 10 sensors calibrated together. Unlike that used for main rotor blade calibrations,the tail rotor blade pressure vessel was made air portable and taken to the trial location so that repeat calibrations could be performed as required. Following calibration of the blade flap angle sensor and yaw servo jack position indicator, these 2 parameters were varied together and the resultant blade feather angle recorded. All tail rotor calibrations were

carried out on site immediately before flying commenced and repeated again on completion.

Installation testing had two separate phases. It is a requirement that all changes to the aircraft that might affect it's control, performance or handling qualities be subjected to a rigourous flight test programme with it's own Flight Trial Instruction. As the tail rotor is a vital part of the helicopters control system in which any failure or restriction could have a potentially catastrophic result, this flight clearance flight programme was approached with some care. Without electrical power to the instrumentation itself, the rotor system was run at 100% N_r for 30 seconds before shutting down to inspect the tail rotor blade fairings and amplifier unit for security. This inspection was repeated after each element of a test schedule designed to gradually increase the tail rotor loading. This schedule, flown at a heavy all up mass, covered hover IGE and OGE, spot turns, low speed manoeuvres, high speed flight in and out of balance and culminating in an aerobatic sequence. Where a manoeuvre could be flown in 2 directions, eg spot turns to the left and the right, the first of the pair flown would be that which required the higher tail rotor loading to initiate and thus the lower thrust for recovery. As no security problems were found and the pilot reported no appreciable changes to handling or performance, the aircraft was cleared for flight throughout it's normal envelope with the instrumented tail rotor installed. When, during the experiment with the instrumented tail rotor fitted, the pilot experienced an airframe vibration that he had not previously noted, that same flight condition was repeated at the end of the experiment once the standard rotor had been refitted. As a very similar vibration was once more experienced, this ruled out the possibility that the vibration was due to the installation and gave extra confidence in the assumption that the instrumentation had not markedly affected the tail rotor's performance.

Once the physical safety of the installation had been assured, it could then be switched on in flight and it's operation assessed. This could be checked in 2 different ways. One single sensor of interest could be dialed up on the MODAS control panel

and the variation in the counts monitored on the digital display. With a rapidly changing signal the display turned into a blur but this at least gave confidence that the sensor was responding. For a more detailed check a test tape would be recorded in flight an the output inspected on the ground to ensure that it was sensible, that the amplifier gain and offset were appropriate and that signal quality was up to standard with the minimum of noise. A problem with the tail rotor instrumentation became immediately apparent when all the tail rotor sensors shut down as the rotor speed passed 95% N_r. This was eventually traced to some capacitors on the power supply board within the tail rotor amplifier unit that had been insufficiently secured to withstand the rotation and were breaking circuit. New fly-leads were soldered to the components which were then bonded to the circuit board with epoxy resin. Some of the wiring in the tail pylon was also replaced at this time as it was considered that faulty insulation was affecting the signals. No further problems of this nature were experienced.

Discovery of this problem reinforced the decision that a portable replay system was an essential part of the experimental equipment. Without it, this defect would have gone undetected and a lot of effort and considerable expense would have been wasted recording worthless data tapes. As it was, a check on the health of the recording system could be made at the end of each sortie to minimise data loss in the event of further failures.

2.8 Concluding remarks.

The aim of the experiment as reiterated in the Introduction to this chapter was to improve the fidelity of helicopter yaw control modelling; this chapter has described how the experiment was set up to record the data required to achieve that goal.

The tail rotor had to be instrumented so that changes in blade loading with both time and blade azimuth could be deduced. Of all the measurement techniques discussed in section 2.2, the use of pressure sensors acting as Pressure Indicator Sensors was

selected. Section 2.3 detailed the operation of the Pressure Indicator Sensor Technique and discussed the means by which the maximum amount of information on the loading distribution could be derived from the fewest possible sensors. The bounds of applicability of the technique were discussed, as was the problem of in-plane velocity measurement. Different methods of overcoming this problem were discussed in section 2.4, one of which, the use of computed flow fields, does not require any additional instrumentation on the blade. The remaining methods, which supply more accurate velocity information should be implemented on the instrumented tail rotor blade for the Lynx AH Mk7. As will be discussed in Chapter 4, the lack of any in-plane velocity information does not prevent significant advances being made on the understanding of main rotor/tail rotor interactions. The use of calculated velocity fields, application of which has yet to be fully investigated, is recommended for study at a later date.

A set of tail rotor blades were acquired for the Lynx AH Mk5 and instrumented as described in section 2.5 with the full aircraft installation discussed in section 2.6 and calibration in section 2.7. The instrumentation technique chosen was limited and, indeed, will not be used in the updated follow-on phase of the programme but, given the constraints of time and our initial understanding of the problem, it has permitted the recording of data that has fulfilled the requirements and allowed the aim of the programme to be achieved. The procedure followed to collect all the test points during the flight trial required will be covered in the next Chapter.

Chapter 3.

Experimental procedure.

3.1 Introduction

Any experimental flight research programme is an expensive and potentially dangerous undertaking. The utmost care must therefore be taken during the programme design phase to ensure that maximum value is obtained from each hour's flying and that test manoeuvres are carried out in accordance with carefully thought out and approved procedures.

Whilst the aircraft is engaged in an instrumented rotor trials programme, it is not available to earn revenue doing other work. Special weather conditions were required for this programme that are not regularly experienced at Bedford. The extra time spent waiting for these conditions would add to the length of the trial and overtime costs would be incurred. It therefore made good operational and fiscal sense to perform the trial away from base. The reasoning behind the choice of IAF Villafranca as the trial location is given in Section 3.2

The selection of test points and the manner in which they were to be flown were laid down in a Flight Trials Instruction. This FTI, which had to be fully authorised before any flying could commence, is included as Appendix 2. The reasoning behind the choice of test points is discussed in Section 3.3. During the course of the flight programme it was decided that time would be better spent if this initial selection were slightly amended. A summary of the test points actually collected is also given. Although great thought had been applied to the design of the instrumentation and the experimental programme, some unforseen problems did occur. These are described in Section 3.4.

3.2 Choice of Location.

Some care had to be taken in selecting a suitable location for the experiment. Meteorological conditions were the prime driver. As the helicopter yaw axis response is particularly sensitive to changes in relative wind speed and direction it had been decided to conduct the experiment in an area where very low ambient wind conditions could be expected on a daily basis. In addition, the susceptibility of the tail rotor blade leading edge fairings to impact damage ruled out operation from an unprepared site or flight in precipitation, dust or over cut grass. In addition to these requirements the conduct of the experiment would require undisturbed access to a long strip of runway/taxiway for the length of the flight, thus precluding operation from any busy airfield. Taking these constraints into consideration, DRA Bedford Airfield was ruled out due to excessive wind and a meteorological survey was carried out to determine which areas of the world would best fulfil the requirements. Two areas emerged as possibilities. The first was Colorado in the United States of America, a location favoured by A&AEE Boscombe Down. This was ruled out as the war in the Gulf was employing all available RAF Hercules aircraft and transporting the Lynx to America by sea would not fit the available time scale. The alternative was the Po Valley in Northern Italy which was within sensible Lynx flying distance and had been used previously during the earlier tail rotor investigation with the Puma (Baldwin & Handley, 1988).

A request was therefore sent to the authorities at IAF Villafranca, near Verona, through the British Embassy in Rome asking for permission to conduct the experiment at Villafranca and outline approval received. Details of our requirements were sent to the airfield and the finer points were all sorted out by the Project Officer and the Project Pilot during a 2 day visit to the airfield a month before the experiment was due to commence. Hangarage was arranged and permission received to operate along the main taxiway at Villafranca, a one mile stretch of concrete (figure 3.2.1), on the understanding that the movements of the indigenous Starfighters and AMXs took priority.

For the transit flight from Bedford to Villafranca, a standard tail rotor was fitted to the Lynx because of the limited life of the instrumented tail rotor blade set and the flight restrictions they imposed. The Lynx was flown to Italy over 3 days with night stops at Reims and Nice in France. The remainder of the experimental equipment and the REME maintenance team were flown to Villafranca in one of the DRA BAC 1-11s to arrive at the same time as the helicopter. The instrumented tail rotor was then fitted, calibrated and tested before the experimental data was collected.

It was found that the airfield lived up to expectation. By flying between 0530 and 0900 each day almost calm wind conditions could be expected and sufficient data points collected before the remainder of the airfield sprang to life. Provided that the Italian military movements were minimal, as at weekends, no problems were experienced with other conflicting traffic as is illustrated in figure 3.2.2.

3.3 Choice of test points

The test points flown during the flight programme were designed to exercise the tail rotor in a controlled manner to the limits of the aircraft low speed flight envelope. Complete descriptions of each manoeuvre including all safety precautions to be observed were laid out in the Flight Trials Instruction given at Appendix 2. The FTI formed the definitive document on which the conduct of the experimental flying was based and had to be authorised by the Commanding Officer of the DRA's Experimental Flying Wing prior to the trial.

Two factors were taken into consideration when choosing the flight conditions to be flown during the experiment. An initial selection was made knowing the depth and capabilities of the analysis to be undertaken in this phase of the research programme. Experience gained whilst working with the data collected on the Puma had shown that the analysis technique worked best on steady flight data. For this reason the majority of the programme consisted of pure hovers, straight and level flight with

relative winds of different speed and direction and constant yaw rate spot turns over a range of rotational velocities. Each test point was flown at 2 different all up weights, thus altering the tail rotor thrust requirement. They were also flown both inside and outside ground effect (IGE and OGE) to examine the effect of ground proximity.

An additional selection of test conditions was made on the basis that the experiment was unrepeatable. As ZD559 was programmed for conversion from a Lynx AH Mk5 to a Lynx AH Mk7 within weeks of completion of this experiment, it would not be possible to refit the instrumented tail rotor for an additional flight trials programme at a later date. It was therefore decided to fly some manoeuvres that were beyond the capabilities of the current analysis routines but that exercised the tail rotor more rigorously than was possible under steady conditions. These manoeuvres included sidesteps over a fixed distance and sidewards and rearwards accelerations. Some high speed flight cases were also flown, mainly to provide data for aeroacousticians.

Although the conduct of each test point was explicitly detailed in the FTI, some margin was allowed to permit extra events of the same type to be flown to further investigate regions of interest that became apparent during the course of the experiment. It had originally only been intended to perform sideslips to port in 30 degree steps. However, when these test points were flown, a higher than usual vibration was experienced. The interval was therefore changed to 10 degrees to more fully investigate the phenomenon. It was also discovered that there was little point in flying the hover turns as described in the FTI since they did not tax the aircraft's yaw performance any more than the spot turns already flown; they were therefore omitted. A full tabulation of the test points flown is given at Appendix 3.

3.4 Problems experienced and lessons learned.

The effort that had been put into making the FTI as comprehensive as possible paid dividends in Italy. Once the instrumentation was up and running, all the test points were flown well within the three weeks programmed, even allowing for days lost due to the passage of several unseasonal frontal systems. In the 15 hours of recorded flying, all the test cases were flown; in most instances more than once.

The only major problem experienced, other than that already covered in section 2.7, was impact damage to the balsa wood fairings on the tail rotor blades. No similar problem had been experienced on the Puma and the hardstanding and taxiways used were all in good condition and swept regularly. Even so, at the end of early flights at Villafranca, small stones up to the size of a large grain of rice were found embedded in the blade leading edge fairings. The one difference between the Lynx configuration and the Puma's that may have been a contributory factor was the Lynx's lower tail rotor ground clearance. The problem was overcome by covering the blade leading edges with a 4" wide strip of thin self-adhesive plastic film which, although it eventually started to come off after several hours flight, provided sufficient cushioning and protection to prevent recurrence of the damage.

At the end of the trial, all those involved at Villafranca discussed the flying programme and compiled a list of lessons learned and factors that would improve the Lynx Mk7 programme, if the flying were again carried out at Villafranca. The pertinent ones were as listed below:

1. Don't plan to arrive on a Friday - the Italians stop work at 1400. Wednesday would appear to be the best day to plan to arrive as that would enable the transit flight out to start on the Monday.

2. Plan to fly daily from 0600-0800. Once the AMXs and Starfighters start operating after 0800 the taxiway is in regular use preventing useful trials flying. For this reason, the weekend would be the most productive period.

3. Civil servants to wear greens and servicemen uniform on the airfield at all times. This should help to prevent identity problems with the local soldiers.

4. Arrange to receive daily phonecalls from base from the outset. It is difficult to phone home except from the Hotel.

5. Take the following stores:
   - Bladefold Kit
   - Tail rotor gust lock
   - NATO to LYNX Hydraulic adaptor
   - Jacking point adaptor
   - Lifting eye
   - Microfiche reader

6. Formally arrange all stores requirements in advance with DRA Aircraft Department.

7. Arrange procedures to obtain spares during the detachment. It may not be required but it's easier than having to arrange it by phone.

8. Check the pace car daily before and after use.

9. The replay system is essential. It is not possible to send tapes home to be checked.

10. Give the pilot a structured sortie. Have daily/weekly briefings and produce a sortie planning chart.

3.5 Study of data quality.

As previously mentioned a proportion of the data was examined at the end of each flight to ensure that the instrumentation system was still functioning correctly and that an unacceptable number of drop-outs had not been experienced. Once the instrumentation was up and running, to everyone's relief, no problems of this nature were encountered.

Once back at Bedford a more detailed inspection of the data took place. As a whole the data was found to be of a contemporary high quality. Very few drop-outs were found and few other anomalies discovered. Those that were found were due to low signal levels and thus lower signal to noise ratio.

Figure 3.5.1 shows a plot against time of the pressure coefficient calculated for the trailing edge pressure sensor at 85% rotor radius for one flight condition and shows a marked high frequency oscillation. Inspection of the frequency content of this signal (Figure 3.5.2) shows a degree of noise on the signal at frequencies between 550 and 650Hz. The cut-off frequency of the filter used on this channel was 600Hz and the noise is assumed to be an artifact of the filter. For comparison, the frequency content of one of the leading edge pressure sensors was also inspected (Figure 3.5.3) and, although that same noise is thought to be there, it is lost in the background frequencies of the measured signal. Indeed the high frequency variation in the signal is also present at the same amplitude but it is not so significant when compared with the rest of the data (Figure 3.5.4). During the analysis of the data, which shall be discussed in Chapter 4, no further filtration was made of the leading edge sensor as the high frequency noise was above the frequencies of interest and did not significantly affect the results. However, as the amplitude of the pressure variations at the blade trailing edge were much smaller and the shape of the signal important for detecting the bounds of flow separation, it was decided that that data should be filtered before subsequent analysis as

indicated on Figure 3.5.5. Having been filtered in this manner, the initial value of the time base of the data had to be carefully adjusted to ensure that skewing of the data did not occur.

The tail rotor blade flap angle sensor signal also contained this same high frequency noise and has been treated in the same manner as the trailing edge pressure data.

The sensors in the fuselage were not found to suffer from this problem; they had a different filter and a lower sampling rate. The care taken to screen all the signal leads, provide good quality earthing and isolate the signals from the 400Hz aircraft power supplies was rewarded by the acquisition of good quality data. With the exception of the tail rotor torquemeter which, as already reported, could not be made to function, all of the sensors have produced data which subsequently caused few problems in analysis and of which the trials team felt they could justifiably be proud.

3.6 Concluding remarks

This chapter set out to describe the experimental procedure and it's brevity is an illustration of the value of a comprehensive Flight Trials Instruction. Once the aircraft, trials personnel and support equipment arrived at the selected location and the instrumentation was assembled and checked, the programme ran as laid down in that document. As an end result, 15 hours experimental flying yielded 1277 test events of which all those so far inspected have provided data of a contemporary high quality. When the trials team returned home to Britain, they could do so in the knowledge that they had achieved what they had set out to do in a logical and professional manner.

Chapter 4.

Analysis techniques and data presentation.

4.1 Introduction

The fifteen hours of experimental flight data collected as described in the previous chapter represent a substantial data-base of Lynx AH Mk5 tail rotor blade leading and trailing edge pressure time histories. The aim of the research programme, however, was not just to collect this data-base but primarily to analyse enough of it that the mechanisms producing the variations observed could be explained. With such a large quantity of information it was important to establish an efficient analysis routine with which the data could be processed in a predominantly automatic fashion. The function of this routine was to highlight the significant features of the raw flight data so that the important phenomenological detail embedded in little pockets within it could be recovered. Once that detail was detected, it could then be more thoroughly investigated to determine the mechanisms causing the effects observed.

Just as with the main rotor, blade loading distribution on the tail rotor varies from flight condition to flight condition. The variations will stem from a changing tail rotor thrust requirement caused by changing main rotor torque and fuselage sideforce in addition to alterations in the effects of the fuselage, fin and ground on the flow through the tail rotor. As well as long term rotor trim changes there will be shorter term, revolution to revolution, variations in loading distribution brought about by the cyclical nature of the main rotor flow field. The analysis routine was designed to show the presence of both the long term and short term loading patterns in as efficient a manner as could be found within a reasonable timescale. The routine was built up from individual programs employing both frequency and time domain techniques. Inspection of the data in the frequency domain showed the natural frequencies of the agencies

causing the loading variations. It was also necessary to look at these variations in the time domain to see how the interaction effects changed across the tail rotor disc.

It has already been stated in section 2.3 that more complete local velocity information would be required before accurate loading and thrust calculations could be carried out for the majority of flight conditions. This chapter will commence with a discussion as to why that detail is not essential for the determination of the interaction mechanisms. The next two sections will discuss the frequency and time domain analyses with section 4.5 showing how the data can be manipulated to allow the time domain techniques to be extended by means of data animation.

The analysis routine has been developed for use on data collected whilst the helicopter was in a steady flight condition and is not readily transferable to that collected in manoeuvring flight. The reasons for this are discussed in section 4.6 and, although the analysis of manoeuvring flight is beyond the aims of this current phase of the tail rotor research, some pointers are given as to the perceived way forward with this aspect of the work.

4.2 The velocity problem.

Chapter 2 discussed the Pressure Indicator Sensor technique that the instrumentation on the Lynx AH Mk5 tail rotor blade was designed to employ. The problems associated with derivation of an accurate value of local chordwise velocity were also detailed. The conventional metal construction of the standard Lynx AH Mk5 tail rotor blade meant that the multiple leading edge sensor method for measuring the chordwise velocity (discussed in section 2.4.2) would have been very difficult to embody. This and the short time available before aircraft conversion to Mk7 standard resulted in the blade being manufactured with only the single leading edge and trailing edge sensor arrays.

Although there was no means of measuring the local chordwise velocity built into the Lynx AH Mk5 instrumented tail rotor blade, it was considered that the data collected with it would allow a considerable extension of the understanding of tail rotor operation gained using the data collected on the Puma (Baldwin & Handley (1988)). When working with the Puma data it had been found that the lack of this velocity information did not significantly hinder the advances made in improving our understanding of tail rotor interactions. If loading calculations were needed, a computed flow field could potentially be used to generate the velocities required. However, for flight conditions where the main rotor wake does not impinge on the tail rotor, such as in sideways and rearwards flight, estimates of tail rotor loading could be made without recourse to such a flow field.

With the advances in main rotor wake prediction already discussed in section 2.4.1, the more sophisticated models should produce velocity fields of reasonable accuracy. One area where these models can be inaccurate is in the placing of the main rotor vortices as they cross the tail rotor. By first examining the pressure data without the use of a calculated velocity field it is possible, especially in forward flight, to position the main rotor vortices quite precisely within the computed flow field and thus improve the accuracy of the pressure coefficients calculated.

So far, few calculations have been made with applied velocity fields for the present data. In the analysis programs the raw pressures have been non-dimensionalised with respect to the blade rotational and aircraft translational velocities:

$$C_p = \frac{P - P_0}{\frac{1}{2}\rho V^2} \qquad 4.1$$

where $$V = \Omega_t r_t + V_a \sin\Psi_t \qquad 4.2$$

The value of pressure coefficient thus created is somewhat artificial as the remaining velocity terms, some of which can be significant, are ignored. This non-

dimensionalisation step has been taken as it allows the pressure data recorded to be compared between flights in a form similar to that previously experienced during main rotor blade studies. If these C_p values were to be used to calculate C_N and α, unknown errors could be introduced. If, however, the analysis process is halted at the C_p stage, the effects of the errors could be more easily understood and accounted for. This would still allow the effects of the various main rotor/tail rotor interactions to be determined.

The blade local velocity can be split into three components; spanwise, normal to the chord and in the plane of the disc. Changes in the spanwise component will have little or no effect on the pressure distribution provided that conditions of supercritical or separated flow are not encountered. A change in the normal component will directly affect the local blade incidence (figure 4.2.1) and will therefore be detected by the sensor and displayed accordingly. Changes in the in-plane component, however, cannot be inferred from the sensor (figure 4.2.2). As this velocity component has been artificially constrained in the analysis as discussed above, a change of in-plane velocity would be incorrectly presented as a change in incidence, were this to be calculated. The effects of the errors introduced will be covered in more detail in chapter 5.

4.3 Frequency domain analysis.

Any helicopter has, almost by definition, a large number of rotating parts. All of the major rotating components rotate at speeds that are designed to be non-integer multiples of each other to reduce the risk of a vibration from one component exciting a harmonic of another. Just as the analysis of the frequency content of a vibration measured at a point within the airframe can be of assistance in the diagnosis of a fault on the helicopter, examination of the instrumented tail rotor blade pressure sensor signals in the frequency domain can give guidance as to which rotating parts of the aircraft are affecting the performance of the tail rotor.

The airflow through the tail rotor is never uniform, whatever the flight condition. It is rarely possible to select a point on the tail rotor blade where the flow conditions remain constant for a complete revolution. The frequency content of the signals recorded at the leading edge pressure sensors will therefore include the tail rotor fundamental frequency, 1T, and the tail rotor harmonics, 2T, 3T, 4T etc. A listing of the principle rotor frequencies for both the Puma and Lynx AH Mk5 is given in Appendix 5. The relative power of each frequency at any one sensor will vary with flight condition. It will also change with sensor radial location. Under most flight conditions within the low speed flight envelope the change in inflow induced by the fin will be the most significant source of once per revolution variation in the signals.

Unless the aircraft is perfectly trimmed the pilot will be making small corrections to maintain the required flight condition. The resultant changes in tail rotor pitch will be reflected in the frequency response as a low frequency peak. The size of that peak can be used as a guide to the amount of control activity required to maintain the flight condition.

Other than the tail rotor itself, the most significant rotating component influencing the signals from the pressure sensors will be the main rotor. This can affect the tail rotor airflow in a variety of ways and, although on occasion main rotor/tail rotor interactions will induce variations at the main rotor fundamental frequency, 1R, the most common forcing frequency will be the main rotor blade passing frequency which for the Puma and Lynx is 4R. In addition to the responses at 4R and it's harmonics, the interference between the main and tail rotors will induce beat frequencies at nT±4R. Again these will be present in varying proportions dependant on flight condition.

As part of the standard set of plots made from each event, two different plots of the sensor signal frequency content have been created as shown in figures 4.3.1 and 4.3.2. It has been found that by comparing these plots for sideslips at different relative wind speeds and directions it is possible to split the low speed envelope up into

regions where the frequency content contained similar features as shown in figure 4.3.3. The boundaries between the regions are not hard. The effects change gradually from one region to the next over a small area. The features in the frequency content observed in each region will be described in the appropriate section of Chapter 5.

4.4 Time domain analysis.

Once the data has been examined in the frequency domain and the presence of a main rotor/tail rotor interaction noted, it must then be studied in the time domain so that the interaction mechanism(s) can be determined.

Study of the varying pressure at an individual sensor in the time domain is not particularly enlightening. The simplest meaningful display format for the data is as polar contour plots of tail rotor blade leading edge $-C_p$ (figure 4.4.1). Negative C_p is conventionally plotted as a suction peak produces an area of increased blade loading. Some care must be exercised when studying these plots as, although they appear to represent the effect at the rotor at one instant in time, the data give a time history as the tail rotor blade sweeps from 0° to 360° azimuth. The interval of $1/\Omega_t$ must be taken into account, especially when observing effects at the rear of the disc where each revolution starts and finishes, or when following the passage of a main rotor tip vortex from one side of the tail rotor disc to the other. That break point was chosen as the majority of the interactional features of interest happen to the front of the disc. If the discontinuity does mar display of an effect, then the break point should be repositioned elsewhere.

Prior to producing any such polar plots some thought is required as to the purpose for which those plots is intended. When looking at plots of main rotor data recorded in steady flight, consecutive plots will not differ markedly from each other. It is therefore generally sufficient to study only one revolution in detail. With the tail rotor, however, the data can change from revolution to revolution due to the passage of the main rotor interactional effects. This changing pattern will repeat after an interval

dictated by the main rotor/tail rotor gearing ratio, so it may prove necessary to study up to 200 revolutions to observe a complete cycle. Plotting out this many revolutions is very time consuming but if full detail on the interaction is required there are few alternatives. Careful selection of a smaller number of revolutions may be sufficient to show the general trend of movement of an interaction as shown in figure 4.4.2. A detailed description of the interactional effects in this figure will be given in Section 5.4.

If, however, the data is being examined with a view to determining the tail rotor thrust for trim, it is worth considering that the aircraft's yaw rate response will not be high enough to react to the thrust changes from one revolution of the tail rotor to the next. A composite revolution could be constructed by taking the average of all data values for each sensor at each azimuthal position (figure 4.4.3) and using that, the long term tail rotor thrust value could be calculated. The revolution to revolution changes may be felt as a high frequency (probably 4R) vibration. Some idea as to the significance of the changes could be gained by studying the standard deviation or range of data values at each point (figures 4.4.4 &4.4.5). These last two plots will also help to highlight the areas of the disc where the stronger cyclical interactional effects exist. The variations exposed on these plots will be greater if the pilot has not maintained a steady flight condition through the event. To gauge the quality of the event, plots were taken from the raw data as shown in figure 4.4.6 showing the variation in compass heading, yaw rate and pedal position with time. The opportunity was also taken to include a plot of a sample of the signal from one of the trailing edge pressure sensors. This would give a visual indication as to whether the presence of trailing edge flow separation was likely in that event. Although analysis of the trailing edge data forms an integral part of the Pressure Indicator Sensor Technique it was not performed during the work carried out to date. It's true significance only comes into play when values of C_N and loading are calculated which are beyond the scope of the present study.

Derivation of a method for the analysis of the trailing edge pressure data will be required in the future and is briefly discussed in Chapter 7.

In order to reduce the plotting undertaken, only plots of data average, standard deviation and range have been made for each event inspected. Plots of individual revolutions have just been produced for those events selected for more complete analysis.

4.5 Data animation.

The production of a series of selected single revolution polar plots is a good simple method for permitting the study of the more obvious activity within the tail rotor disc. It is not, however, so good for spotting the more unexpected smaller effects or for observing phase shifts within the data. It has been found that the use of dynamic graphics can highlight these features as the movement makes them stand out. The animation can be produced by the rapid sequential display of a series of individual revolutions either on a computer terminal capable of performing this function or by the use of standard cartoon making techniques. As a suitable computer was not available at the start of the programme, animation was achieved by the very time consuming process of producing individual hard copies of each frame and then filming each one in sequence at the desired frame rate.As well as being a lengthy process, an additional drawback with this technique was that the format or view direction, once selected, could not be changed without repeating the process. The use of computer animation is therefore preferable and for that reason an Iris Indigo computer was acquired towards the end of the programme with a resultant improvement in flexibility and throughput..

Which ever method is employed, the correct frame order for the data must be found. An attempt to animate the data by showing the revolutions in the order in which they were recorded would show very little of the main rotor/tail rotor interaction. The relative gearing between the main and tail rotors on the Lynx (1:5.8) is such that a

trailing tip vortex from a main rotor blade would be detected only once or twice by the instrumented tail rotor blade as it crossed the tail rotor disc. The visible result of the non-integer nature of the gearing ratio is that a series of successive tail rotor revolutions would display a pseudo randomness in the main rotor induced activity which would not be at all conducive to smooth animation. This is demonstrated in figure 4.5.1 which shows, for the event illustrated in figure 4.4.2, the variation in negative C_p for each successive revolution as the instrumented tail rotor blade passes 165 degrees azimuth. For the eye to see steady motion with the data in this order, they would have to be smoothed to such an extent that the only movement visible would be that caused by the low frequency control inputs. A method of interpolation is required to increase the data rate.

In order that the aircraft would be flying in non turbulent air, the maximum wind speed permitted for the experiment was 3 knots. As a result, the wake from each main rotor blade could be assumed to be repeatable and that, as each main rotor blade passes through the same azimuthal position, the total main rotor wake would affect the tail rotor in a similar manner each time. The logical consequence of this would be that if the plots of tail rotor revolutions were re-ordered such that their datum main rotor blade positions were in ascending order, then the main rotor interference effect would advance accordingly. The datum main rotor blade position for a tail rotor revolution has been arbitrarily defined as the position of the main rotor when the instrumented tail rotor blade was at 180 degrees azimuth. If the radial distributions shown in figure 4.5.1 were re-ordered in this manner such that the position of the most rearward main rotor blade advances from 315 to 045 degrees (see figure 4.5.2), the resultant plot would be as shown in figure 4.5.3. This plot shows that the main rotor interference effects have been brought into some semblance of order by this transformation.

Unfortunately display of the revolutions in this order still failed to give a smooth image. Study of the inboard sensor data in figure 4.5.3 reveals an unacceptable spread in the passage of the interference effects. This variation is the product of the

incorrect assumption that all 4 main rotor blades produce the same wake. Even small changes in main rotor blade trim will produce variations in the wake pattern. Changing the assumption to read that each individual blade will produce the same wake each time it passes the same azimuth position once again re-orders the revolutions. With them now ordered such that the datum (red) main rotor blade position advances from 0 to 360 degrees (figure 4.5.4), animation is now possible and shows smooth progression of the interference effects. Even so, animation by this technique will only work for a steady flight condition. If it were attempted on a manoeuvre case the changes in tail rotor trim would, when the revolutions were re-ordered, make the animation too jumpy to be of any use.

The polar contour plot used for single hard copy display is not a suitable format for animation. The algorithms employed to position the contour lines must interpolate between the sensor positions and, where the distance between the sensors is large, small changes at the sensors can result in large variations in the positions of the contours. It is also possible for the interaction feature to fall between 2 sensors and not to significantly affect either of them. As the contour plot is continuous and does not show the sensor locations, the eye is deceived into thinking that it depicts the truth at all points. A better display format is one that only shows what is happening at the sensor locations. The format shown in figure 4.5.5 was that used with the original cartoon technique. Although the shape of the plot was hard to relate to the shape of the tail rotor disc, it was quick to produce and did show the interference effects. Several different display formats were used on the Indigo and no one of these was found to fulfil all requirements. The ease at which these formats could be interchanged and adjusted, however, made the need for one single format less pressing than it had been previously.

4.6 Analysis of manoeuvre.

Once an acceptable understanding of the operation of the tail rotor under steady conditions has been achieved, the next logical stage would be the analysis of the data recorded during manoeuvre. As discussed in the previous section, it would not be possible to reorder and animate the data in the same way to highlight the interactional effects and some other technique will be required. It is however expected that the interaction mechanisms determined for the differing steady flight conditions will apply as the aircraft manoeuvres through that flight condition. Though this has not been attempted to date, it should be possible to examine the data to see if that assumption holds and proceed accordingly .

4.7 Concluding remarks.

The work detailed in this chapter commenced with the requirement to take a large data-base of tail rotor pressure time histories and distil from it nuggets of information on the interactions affecting tail rotor blade loading distributions. The work was carried out under the assumption that the interaction mechanisms could be determined without a detailed knowledge of the blade local chordwise velocities and that most loading calculations performed would be to some extent erroneous.

An analysis routine was developed to reduce the data from each event down to three polar plots showing the long term variations in pressure coefficient and those areas of the disc most affected by the shorter term main rotor induced effects. An additional multi-graph plot designed to demonstrate the quality of the flying in the event and to indicate the possible presence of blade trailing edge flow separation has also been produced. The frequency content of the leading edge sensor pressure coefficients has been plotted in two different formats so that the relative proportions of the various forcing frequencies could be observed. From these plots it has been possible to divide

the Lynx AH Mk5 low speed flight envelope into six regions. Events within a region exhibited common features that were not found in most of the other five. It has also been possible to select a representative event from each region for further in-depth analysis. Each of these regions will be discussed in the next chapter.

An additional tool in the form of data animation has also been developed. Although it was not generally meaningful to attempt to animate the data in the order recorded, re-ordering in the manner described has allowed extra detail on the interactions to be observed that would otherwise have remained hidden.

Given time, a more effective suite of analysis programs could undoubtedly have been developed. However, that used has proved to be effective in allowing the information required to be extracted.

Chapter 5.

Features of tail rotor loading distributions.

5.1 Introduction

The preceding four chapters have discussed the background and aims of the current research programme, the aircraft installation, the conduct of the experiment and the analysis routine applied to each data event. Section 4.3 concluded by stating that, from the frequency domain analysis of each event, the low speed flight envelope of the Lynx AH Mk5 could be split up into 6 different regions (figure 4.3.3), each with it's own characteristics. This chapter will examine each of those areas in turn, discussing the features revealed by the analysis routine. Additionally, from the in-depth investigation of one or more event in each area, the interaction mechanisms explaining the phenomena observed will be described.

As the understanding of those mechanisms will depend on a good knowledge of the wake produced by a rotor, the chapter will commence with a brief description of the wake of an isolated rotor (ie one rotor, no fuselage, no ground) and the factors that affect it. Section 5.3 will cover the effects noted on the tail rotor in the hover and show the close similarities between the data for the Lynx AH Mk5 and that of the Puma, even though the tail rotors rotate in opposite directions. Section 5.4 will discuss the effects in low speed forward flight and show how the interaction mechanism changes depending on the position of the trailed main rotor blade tip vortex with relation to the tail rotor blade span. Section 5.5 will look at the most significant main rotor/tail rotor interaction which occurs in quartering flight (areas 3 & 4 on figure 4.3.3). Here the effects of variation in tail rotor blade dynamic head caused by the main rotor blade trailing tip vortices will be discussed. Deductions about the interactions taking place in sideways and rearwards flight will finally be presented in section 5.6.

The investigation has concentrated on the interactions between the tail rotor and the main rotor wake. The effect of the fin has not been studied in depth and will only be mentioned where it has significance in the effect of the main rotor.

5.2 The wake of an isolated rotor

Research into the geometry and characteristics of main rotor wakes has been taking place since the advent of the helicopter. Although much of this work has been carried out in the wind tunnel, a proportion has taken place in flight with sometimes quite rudimentary instrumentation. Early RAE reports on the subject (eg. Brotherhood (1947)&(1952)) describe the use of smoke either held by hand on a pole beneath a hovering rotor, mounted on the fuselage beneath the rotor in vertical flight or trailed behind another aircraft in forward flight. The use of smoke or other particulate display media is also much favoured in wind tunnel rotor experiments.

One of the more thorough reports on the geometry of the wake of a hovering rotor is Landgrebe (1971), others such as Kocurek, Berkowitz & Harris (1980) offering broadly similar results. In a pure steady hover the bound circulation on a rotor blade will vary with blade radius in the form shown in see figure 5.2.1. From zero at the blade root, it will rise to a maximum before dropping back to zero again. The position of maximum bound circulation will, for reasons described shortly, be just inboard of the blade tip. A sheet vortex will be shed behind the blade between the root and the point of maximum circulation with another of opposite sense between that point and the tip. These vortex sheets will tend to roll up at the root and the tip. The rate of roll up will be dependant on the rate of change of bound circulation with distance along that part of the blade from which that sheet vortex was shed. For the tip vortex, roll up will be complete within approximately 60 degrees of blade rotation (Simons, Pacifico & Jones (1967)), roll up at the root will be significantly slower (in excess of 3 or 4

revolutions). Although the rolled up vortex trailed from the root may have little effect on the blade bound circulation, that trailed from the tip will be quite significant.

As the wake contracts beneath the rotor, the rolled up tip vortex has been shown to move rapidly inwards towards the rotor axis until it passes close beneath the following rotor blade (figure 5.2.2). At this point it's rate of descent will increase and the relative rate of radial motion will be reduced. In practice, it has generally proved possible to track the first four or five blade trailing tip vortices beneath the rotor disc. After this point the path followed by individual vortices will vary because of interaction between the vortices and turbulence in the wake causing the structure of the wake to progressively break down. Before a shed vortex sheet rolls up it will descend beneath the blade at a faster rate than a corresponding rolled up trailing vortex at the same radial position(Landgrebe(1971)). Swirl velocities within the wake will be small, so the vortices can be considered to move almost vertically downwards.

The mechanism of tip vortex roll up has been examined in great detail (eg Saffman (1974)). Although not technically correct, the rolled up vortex can be considered to consist of an inviscid core with an associated velocity field. The core radius will be approximately 5% of the chord of the blade behind which that vortex is trailed (Simons, Pacifico & Jones (1967)). The strength of the velocity field will vary with distance from the vortex axis. The simplest model of the vortex is that given by Rankine (Milne-Thomson (1958)) though a more accurate representation is given by Scully (1975). A comparison between these two models is given at figure 5.2.3. Once formed the trailing tip vortices will maintain their form for a protracted period until they eventually breakdown and disperse (Saffman (1974). The structure of the vortex core is such that there will be some axial flow within the core moving towards the blade from which the vortex is trailed (Moore & Saffman (1973). the magnitude of this flow is small and, for the purposes of this study has been ignored.

As the rotor blade rotates it will pass over the trailing tip vortices and shed sheet vortices from preceding blades. As it does so it will be affected by the velocity fields associated with those vortices. The velocity field associated with a vortex sheet is not as significant as that from a rolled up trailing vortex and, as the vortex sheet is descending at approximately twice the speed of the trailing tip vortex, the velocities it induces at the blade will be relatively small. The trailing tip vorticies will have a major effect on the local velocity at the blade with the vortex trailed from the immediately preceding blade having the strongest effect of all. If the effect of all the shed and trailed vortices are summed, the axial velocity at the blade will be as shown in figure 5.2.4, thus explaining the location of the point of maximum blade circulation. As the tip vortex trailed behind the immediately preceding blade has such a significant effect on the bound circulation, any change in it's location relative to the blade being studied will have a major effect on that blade's loading distribution. A brief investigation of this effect was given in Brocklehurst (1985/1). The effect of the vortices on the overall disc loading distribution will be to form an axis-symmetric loading peak around the disc towards the blade tip.

Consider now the wake as the rotor moves off from the hover to level forward flight. The vortices will also no longer be of uniform strength but will vary with azimuth as the blade incidence changes with alterations in cyclic pitch and in-plane velocity. The relative rate of descent of the tip vortices will also change with those trailed from the rear of the disc moving down faster than those at the front. The vortices at the front of the disc can, under certain conditions, pass over, instead of under, the following blade. This variation will increase the effect on a blade of the tip vortex trailed from the immediately preceding blade at the front of the rotor disc with the opposite effect at the rear.

The helical form of the trailing tip vortices will skew as the rotor translates. Even at a very low advance ratio equating to 10-15 knots, the trailing tip vortices shed at the rear of the disc will no longer pass under the blade but, when viewed from

above, be left behind by the aircraft's motion. The effect of this on the rotor disc loading distribution will be to reduce the loading peak at the rear of the disc; the small inflow peak remaining being due to the blade dynamic head. Similarly, at the front of the disk, the trailing tip vortices will move backwards relative to the disc to leave a broader or double peak of smaller magnitude; the effect of the vortices moving inboard away from that of the dynamic head at the tip. As the advance ratio increases, so the position of the tip vortices will change in relation to the rotor disc with associated variations in loading distribution.

The effect of aircraft translation on the vortices trailed from the two edges of the disc (ie. approximately 90 and 270 degrees main rotor azimuth) will be to reduce the separation between vortices trailed from adjacent blades. It has already been stated that each tip vortex can be considered to have a solid inviscid core. Each vortex core will therefore be affected by the velocity field associated with each other vortex and, where sufficient curvature of that vortex's axis exists, by the velocity field of other parts of the same vortex. Two vortices of similar sign and strength (like two trailing tip vortices from adjacent blades for example) will each affect the other such that they are caused to rotate about each other whilst maintaining constant separation (figure 5.2.5 from Rossow(1977)). This effect need not be constrained to only 2 vortices, any number can join in with their relative rates of rotation being dependant on their strengths and separation. The individual blade tip vortices will therefore roll round each other and form a pair of large "wingtip" vortices somewhat akin to those trailed behind the wingtips of a fixed wing aircraft (figure 5.2.6). These "wingtip" vortices will descend at a comparatively slow rate dependant on their strength and separation.

From the preceding paragraphs it can be appreciated that, in forward flight, the blade trailing tip vortices descend at different rates depending on the position of the blade as they were formed; the effect of this variation is well covered by a notable report by Heyson & Katzoff (1957). For accuracy these effects must be included in any prescribed rotor wake model. This is done in the model described in Beddoes (1985)

which, although it does not fully represent the formation of the "wingtip" vortices, has proved quite accurate and most useful. This model and its uses for tail rotor studies will be covered in Chapter 6.

This brief discussion of rotor wake geometry has only considered steady non-manoeuvring flight OGE but should give sufficient background to render the remainder of this chapter more meaningful.

5.3 The hover

From the previous section it would be expected that rotor disc loading in the hover would be axis-symmetric with a marked loading peak just inboard from the blade tip. The Helicopter Aeromechanics Section at Bedford had, in the past, conducted an investigation of main rotor loading distributions in the hover with it's flight research Puma helicopter. A plot showing one revolutions worth of data from that programme is given in figure 5.3.1. This plot of variation in negative C_p displays such a loading peak and is virtually axis-symmetric with the exception of the region between 300 and 360 degrees rotor azimuth where the loading peak is absent. When initially observed this feature was thought to be caused by the aircraft drifting slightly in the 150 degree azimuth direction. Because the flights were conducted at altitude with minimal natural visual cues, positioning was achieved by formating on a brown smoke puff fired from a Very pistol to check for vertical movement. Fore & aft and lateral motion was countered by the pilot reacting to an observer in the cabin describing the motion of a tell-tale string attached to a ball suspended beneath the aircraft. Even with these aids it took precise flying to achieve good hover accuracy; even 10 knots of translational velocity would be enough to produce a similar effect to the one shown. It was not until the data from the instrumented tail rotor programme on the Puma was inspected that it was realised that the presence of a similar feature on the tail rotor indicated that the gap in the loading peak on the main rotor was caused by the tail rotor and vice verca.

A plot showing the Puma tail rotor in a hover OGE is given at figure 5.3.2. Again the almost axis-symmetric loading peak is present, indicated by the ring of high negative C_p values. As just mentioned, there is a gap in the loading peak, this time between approximately 165 and 240 degrees blade azimuth. The other main feature of note is the region of increased negative C_p at approximately 120 degrees blade azimuth. This is the result of the rotor inflow being locally reduced by the fin which is positioned just upstream of the tail rotor at this point. The reduced inflow velocity results in an increase in blade incidence thus giving rise to increased loading and the rise in negative C_p shown.

Examination of the pressure signals' frequency content in a similar manner to that described for the Lynx in section 4.3 showed little evidence of main rotor frequencies and mainly featured the tail rotor harmonics and evidence of control activity (figure 5.3.3 and Appendix 5). This indicated that, although the tail rotor loading distribution was being affected by the main rotor wake as discussed in the previous paragraph, it was not wholly or partially immersed in it. This fact was reinforced by the invariance in the tail rotor data from revolution to revolution. Brocklehurst (1986/1) shows photographs taken in a wind tunnel of a representative main rotor/tail rotor system in a hover and illustrates the tail rotor wake wrapping round the outside of the main rotor disc in this condition. A mechanism offering an explanation of the effect is also given. This phenomenon indicates that neither of the two rotors need to be immersed in the wake of the other for there to be a resultant change to their loading distributions.

The first Lynx AH Mk5 data to be examined was that recorded in a heavy (4610kg) hover OGE. A principal reason for selecting this case was comparison of the collected data with the corresponding Puma hover data just described. Figure 5.3.4 shows the variation in negative C_p for one revolution of the Lynx tail rotor for this flight condition. The strong similarities between this plot and its Puma equivalent shown previously in figure 5.3.2 are readily apparent; the loading peak with it's

missing segment and the effect of the fin interference are both present. Study of the frequency content of the data in this event (figure 5.3.5) again reveals the absence of any main rotor frequencies. Figure 5.3.6 shows the standard deviation of the C_p data as described in section 4.4 and, because of the small values, illustrates the steady nature of the data with little variation from revolution to revolution.

The location of the gap in the loading peak is not always the same. Figure 5.3.7 shows the variation in negative C_p for one revolution of the Lynx AH Mk5 tail rotor in a hover OGE but in this case at the much lighter weight of 3945kg. The missing segment is lower down on the tail rotor disc than before indicating a slightly different main rotor wake geometry.

The indicative features in the data discussed above are not only found in an absolute hover but also exist in a limited region about the hover as depicted in area 1 on figure 4.3.3. With a forward speed above 5 knots the main rotor wake starts to cross the tail rotor disc rather than passing in front of it. Similarly, as translational velocities build up in other directions the relative positioning of the main rotor wake and the tail rotor/tail rotor wake is altered and different effects are observed.

5.4 Forward flight.

As discussed in section 5.3, the front of the tail rotor disc will start to be immersed in the rearward part of the main rotor wake as the aircraft forward speed increases above 5 knots (Region 2 on figure 4.3.3). This can be identified from the frequency content of the tail rotor leading edge C_p data as frequencies attributable to the main rotor are observed (figure 5.4.1). The fundamental main rotor frequency is that of the blade passing frequency, 4R, rather than the main rotor rotational frequency. The beat frequencies caused by the interaction between the two rotor systems, ie nT±4R, are commonly more significant than the 4R frequency itself. Comparing the frequency content of the signals from the different sensors, that of the fourth (85%) sensor is

often the strongest. The reason for this will be made apparent shortly. As expected, at speeds where the main rotor wake just clips the front of the tail rotor disc, main rotor frequency content towards the root of the tail rotor blade is reduced.

In forward flight, the Puma data and the Lynx data again show strong similarities although the change in direction of tail rotor rotation creates some differences in the effect of the interaction of the main rotor blade trailing tip vortices and the inner part of the tail rotor blade. A sequence of plots showing the passage of a main rotor blade trailing tip vortex across the Lynx tail rotor in 30 knots forward flight OGE has already been given in figure 4.4.2. A similar sequence for the Puma at 10 knots forward flight OGE is shown at figure 5.4.2. The path of the interaction for the two aircraft at the same flight speed will not be the same as the aircraft attitude and the positioning of the tail rotor with respect to the main rotor will be different. Ignoring the main rotor interference, the fin interference effect will be observed as in the hover, though slightly further aft. The blade tip loading peak is only present at the front of the disk as the tail rotor blade trailing tip vorticies that produce it have been left behind, as described in section 5.2.

In both figure 4.4.2 and figure 5.4.2 the individual plots have been ordered to show the effect of the main rotor blade trailing tip vortex advancing across the tail rotor disc. The interaction has two different effects. Outboard, within the tip loading peak region, the main rotor vortices cause a local reduction in negative C_p. Figure 5.4.3 is a plot of the negative C_p calculated for the 98% blade radius leading edge sensor on the Lynx for one revolution of the tail rotor blade at 25 knots forward flight OGE and illustrates this effect. Inboard, on the Lynx AH Mk5, the main rotor vortices cause a local peak followed by a trough in the negative C_p values. These are illustrated in figures 5.4.4 & 5.4.5 which show the variation in negative C_p over two different revolutions of the tail rotor as calculated for the 75% rotor radius sensor at the same 25 knot flight condition. The peak shown in figure 5.4.4 is stronger than the trough in figure 5.4.5; quite commonly the trough does not stand out at all. On the Puma, with

it's opposite direction of tail rotor rotation, the trough should come before the peak though it is seldom observed.

The position of the interactional features are not always as easily identifiable as in the two cases illustrated here. The plot of the standard deviation of the C_p values (figure 4.4.4) can help to ease this problem. A comparison between this figure and figure 4.4.2 showed how the standard deviation plot identified the location of the interaction with the Lynx. It was thought that the plot of the range of the data (figure 4.4.5) might yield some additional information but that has not proved to be the case.

Close examination of these interactional effects, especially with the data animated as described in section 4.5, revealed a discontinuity between the timings of the passage of the effect outboard to that on the inner part of the tail rotor blade. Figure 5.4.6 shows the main rotor azimuth position at which the interactional effects were noted at the various sensor locations on the Lynx blade. If it is assumed that the main rotor vortex passes the inboard sensors midway between the peak and the trough (as shall be discussed in section 5.4.2), then this plot reveals a phase shift of approximately 15.5 degrees of main rotor rotation between the effects noted outboard and those inboard. 15.5 degrees of main rotor rotation equates to 90 degrees of tail rotor rotation on this aircraft. A similar phase shift was apparent on the Puma. The effect of this phase shift is to delay the appearance of the interactional feature at the tip until after it has appeared further inboard. This would suggest that two different interactional mechanisms are employed, one covering the interaction between a main rotor blade trailing tip vortex and it's tail rotor counterpart and the other between that main rotor vortex and the tail rotor blade itself. These two mechanisms will be discussed in more detail in the sections that follow. There would appear to be a region on the blade that is affected to some extent by both mechanisms; this in the vicinity of the 85% sensor, thus giving rise to the increased main rotor frequency content at that sensor.

Although the two interactions described have a noticeable effect on the tail rotor C_p distribution, their overall effect on the tail rotor thrust is small. It is considered that there would be little to be gained from any attempt to reduce their effect still further. The relative magnitude of the overall tail rotor loading variation should be considered when deciding whether to include the effects of these interactions in a computer model. On a simple model of tail rotor thrust they could perhaps be ignored.

5.4.1 The interaction between a main rotor blade trailing tip vortex and a tail rotor blade trailing tip vortex in forward flight.

The interactional mechanism described in this section takes place in flight conditions where the tip vortices trailed from the main rotor blades are cut by the tail rotor blades. For there to be an effect on the tail rotor loading distribution this intersection must take place when the tail rotor blade in question is at an azimuth angle where the loading peak is evident. This will limit the visible effect of this interaction to the front of the tail rotor disc.

Assuming that the wakes from the main rotor and the tail rotor were independent and that each had no effect upon the other, the blade trailing tip vortex systems from the two rotors could be drawn as skewed helices. To add complication, the shape of each element on the helices trailed from a rotor would be distorted by the wake contraction and the influence of all the other vortex elements in that rotor's wake. The relative geometry of the main rotor and tail rotor dictates that the helical wake systems from the two rotors will intermesh orthogonally. As the external influences on both wake systems are the same at any given point, the separation between a vortex trailed from a main rotor blade and one from a tail rotor blade will remain constant. The separation between a main rotor vortex element and a tail rotor vortex element will therefore be dependant on the location of that main rotor vortex element when the tail rotor vortex element was formed. As already described in section 5.2, a tail rotor blade

trailing tip vortex is formed by the rolling up of the vortex sheet shed from the blade outboard of the point of maximum circulation. This roll up process is complete by the time that the blade tip has travelled one rotor radius (ie 60 degrees of blade rotation) (Simons, Pacifico & Jones (1967)) and the main rotor blade trailing tip vortex will have been present at it's final location whilst this roll up was taking place. The separation distance between successive main rotor and tail rotor vortices will be different because of the non-integer gearing ratio between the two rotors.

Contrary to the assumption made at the beginning of the last paragraph, the two wake systems are not independent and each main rotor vortex element will induce motion in each tail rotor vortex element and vice versa. The velocities induced will depend on the strengths of the vortices and the distance between them. Figure 5.4.1.1 shows a sketch of the tip of a tail rotor blade with the trailing tip vortex rolling up behind it. The tail rotor blade is about to cut a main rotor blade trailing tip vortex. That main rotor vortex can induce large variations in the local chordwise velocity at the blade, possibly affecting the point of maximum circulation on the blade and thus subsequently the strength and location of the tip vortex. The vortex sheet shed by the blade may be distorted by the velocities induced by the main rotor vortex. This would affect the roll up process which would again change the properties of the tail rotor tip vortex. Once the roll up process has been completed the two vortices would continue to interact.

The overall mechanism of this interaction process is indeed complex. In an attempt to illucidate the interaction that would occur once the tail rotor blade trailing tip vortex was fully formed (and there is some doubt as to whether this would happen) a simple computer model was constructed. Two Scully vortices of approximately Lynx main and tail rotor vortex strengths were placed, one along the x-axis and the other parallel to the z-axis as shown in figure 5.4.1.2. The minimum separation distance between the centrelines of the two vortices was set as being the sum of the two vortex core diameters (10 cm). The vortices were initially divided up into 4mm long elements.

The Biot-Savart Law (Landgrebe (1971) Appendix 3) was then employed to calculate the velocities induced at the core of each vortex element node by the velocity field of each vortex element from both vortices. Neglecting any inertial effects, the displacement of each node was then calculated over a 1 millisecond timestep. This process was then repeated several times. The distortion induced in the tail rotor vortex after each time step is shown in figure 5.4.1.3. The interaction produced was very unstable with the vortex cores touching after only four iterations and the convoluted bundle of distorted vortices growing rapidly thereafter. It was observed that the vortex elements close to the interaction were very rapidly stretched. To reduce the errors introduced by using straight vortex elements in regions of high vortex curvature, each element was kept close to it's original length by cutting it in half whenever it stretched to twice it's original length. This model, though simple and restrictive, illustrates the stretching of the vortex elements close to the original point of minimum separation which is considered to be significant.

Theoretical research has been carried out on the effect of strain on a line vortex (Moore & Saffman (1970)). This suggested that a line vortex will "disintegrate" (their word) if the ratio of applied strain rate over vortex circulation strength exceeds a given value. Applying this principle to the interaction under consideration, each vortex element is subjected to a varying strain by the others. This may suggest that, when the main and tail rotor blade trailing tip vortices are close enough together, then at least the tail rotor vortex, and possibly the stronger main rotor vortex, would disintegrate and the local induced velocity field(s) fall to zero. This would have only a minimal effect on the blade trailing the vortex. However section 5.1 discussed how the strength of the loading peak near the tip of a blade is most significantly affected by the location of the tip vortex trailed from the preceding blade. If that tip vortex had a discontinuity produced by the interaction just described, then a reduction in the loading peak on the next blade would follow.

For such an effect to be recorded on the instrumented tail rotor blade, the main rotor blade trailing tip vortex would have had to interact with the tip vortex trailed from the preceding tail rotor blade. This will affect the timing of the interactional feature noted in the data, effectively delaying it by 90 degrees of tail rotor rotation. This agrees with the phase shift noted on figure 5.4.6.

The reduction in the loading peak will not be limited to the passage of one tail rotor blade. The reduction in the loading peak on one blade will reduce the strength of the tip vortex trailed behind that blade and thus affect the loading peak on the next, though to a lesser extent. Therefore, although the loading peak will be rapidly reduced by the interaction , it will return to it's original value at a slower rate.

5.4.2 The interaction between a main rotor blade trailing tip vortex and the inboard region of a tail rotor blade in forward flight.

For the interaction described in section 5.4.1 to take place a main rotor blade trailing tip vortex must be cut by that part of a tail rotor blade that is outboard of the point of maximum bound circulation. If the main rotor vortex is positioned such that it will lie inboard of that point then a different interaction will occur. With the main rotor vortex far enough inboard, its distance from the tail rotor trailing tip vortex should result in there being insufficient strain on that vortex for disintegration to occur.

In low speed flight, the dominant loading variations over the region of the tail rotor blade inboard of the loading peak is caused by the change in the local chordwise velocity. This is in contrast with the dominant variations outboard being caused by changes in the inflow velocity. The inboard vortex sheet shed from a tail rotor blade does not have a particularly strong effect on the following blades. Any disruption of this shed vorticity by a main rotor blade trailing tip vortex will therefore not significantly alter the blade loading.

The axis of tail rotor rotation lies parallel to the centrelines of the main rotor blade trailing tip vortices that pass across it. Although there is some axial flow within the main rotor vortex core, it will only affect a very small part of the tail rotor disc (the core diameter being approximately 4cm) and can thus be ignored. The effects of the changes in tail rotor blade chordwise velocity induced by the main rotor vortex will vary dependent on the tail rotor's direction of rotation. The vortex's velocity field will always rotate in a top-forward direction.

The lift produced by an element of the blade, dr, at radius r is given by:

$$L=\frac{1}{2}\rho V^2 drca\alpha \qquad \text{Eqn 5.1}$$

where:

$$\alpha=\theta-\tan^{-1}\frac{U}{V} \qquad \text{Eqn 5.2}$$

giving:

$$L=\frac{1}{2}\rho drcaV^2(\theta-\tan^{-1}\frac{U}{V}) \qquad \text{Eqn 5.3}$$

The effect of the main rotor blade trailing tip vortices on the in-plane velocity at the tail rotor blade is of a very transitory nature. For this reason, it has been assumed that the local inflow velocity, U, will not have time to change in response to the changing in-plane velocity and incidence.Therefore, when the local chordwise velocity increases not only does the V^2 term increase but the local incidence does as well. Concentrating on the V^2 term and expanding:

$$V = V_r + V_v \qquad \text{Eqn 5.4}$$

If the chordwise component of the vortex induced velocity V_v is against the direction of blade rotation, then:

$$V^2=V_r^2 + 2V_r|V_v| + |V_v|^2 \qquad \text{Eqn 5.5}$$

If , however, V_v is in the direction of blade rotation:

$$V^2=V_r^2 - 2V_r|V_v| + |V_v|^2 \qquad \text{Eqn 5.6}$$

Therefore, at a given point on the blade, the increase in blade loading that results from a vortex induced chordwise velocity opposing blade motion will be greater than that from the same velocity in the direction of blade travel.The major perturbation in blade loading will therefore be a sharp upwards peak to one side of the vortex core with a much smaller downwards one on the other. For a tail rotor with top-blade-aft rotation, such as that on the Puma of Lynx AH Mk7 the region of reduced V^2 will be on the side of the vortex centreline closer to the rotor axis. As the value of V_r is lower the further you are from the blade tip the region of reduced loading will be smaller and have less effect than would be the case with a tail rotor rotating top-blade-forward. Figures 5.4.2.1 and 5.4.2.2 show plots of V^2 against tail rotor blade radius for the 2 different blade rotations. Main rotor vortices are shown in three locations demonstrating that, for both directions of blade rotation, the effect of the vortex decreases as it moves towards the centre of the rotor. It should be remembered that the interaction described in section 5.4.1 will mask the effect described in this section from about 80% rotor radius outwards at the front of the tail rotor disc in forward flight.

The observed effect of this interaction will be altered to some extent by the display technique used. As previously stated, the tail rotor pressure data has been displayed as plots of pressure coefficients with the velocity term based on the blade's rotational and aircraft translational velocities alone as expressed in equation 2.1. The C_p value will not, therefore, take account of the chordwise velocity changes that produce this particular interaction. If they were to do so, only the effects of changing incidence would be seen and a major part of the effect of this interaction would be masked.

5.5 Interaction between the main rotor wake and the tail rotor in quartering flight.

Of all the main rotor/tail rotor interactions examined in this study, that occurring in quartering flight and described in this section has the most significant effect on tail rotor performance. In this context, "quartering flight" describes the flight condition when the sideslip angle is such that the tail rotor is affected by the wake from the edge of the main rotor disc as depicted in figure 5.5.1. In forward flight the tail rotor will be in the centre of the main rotor wake and, where they affect the tail rotor, will cut each main rotor blade trailing tip vortex in sequence as they are trailed from the rear of the disc. In quartering flight, ie with a sideslip angle of between 45 and 70 degrees depending on aircraft configuration, the main rotor wake effect on the tail rotor can be much more significant as the tail rotor may be immersed in one of the two 'wingtip' vortices described in section 5.2.

The wingtip vortex is formed from a number of main rotor blade trailing tip vortices rotating round each other. In forward flight the velocity field of each of these trailing vortices will also be rotating such that motion below the vortex centreline will be directed outwards, away from the aircraft centreline as shown in figure 5.5.2. The wingtip vortex will therefore constitute a significant velocity field, all rotating in this direction. Once the aircraft develops a sideslip angle the wingtip vortices maintain their position with respect to the aircraft's track which will no longer be aligned with the axis of the helicopter. As just mentioned above, with a sideslip angle of 45 to 70 degrees the helicopter's tail rotor may end up tracking along one of these vortices. If the tail rotor rotates top-blade-forward and the centre of the wingtip vortex passes through the centre of the tail rotor disc as in figure 5.5.3, then the tail rotor blades will be rotating within a mass of air that already has a component moving in the same direction. The flow velocity over the blades will therefore be reduced. The resultant reduction in dynamic

head means that an increased tail rotor blade pitch is required to produce the necessary thrust. This increased pitch requirement is reflected in the helicopter transmission and control system by a reduction in pedal margin. The situation is the same whether the tail rotor is affected by the wingtip vortex from either the advancing or the retreating side of the main rotor disc (areas 3 & 4 on figure 4.3.3). The only difference that exists between the two is that when the tail rotor is affected by the vortex from the retreating side of the main rotor, the tail rotor is off-loaded to some extent by the weathercocking action of the fuselage and the change in tail rotor inflow due to the sideways motion. The yaw control margin is therefore greater than with the same relative wind from the other side of the nose and its reduction proportionally smaller. When the centre of the tail rotor disc is displaced from the vortex centreline as depicted in figure 5.5.4, that part of the tail rotor disc between the vortex centreline and the axis of rotor rotation will experience an increase in dynamic head. As shown in figure 5.5.5 the effect of a vortex tracking diametrically across the tail rotor will be an initial rise in dynamic head followed by a much larger fall before a mirror image effect on the other side of the disc. The strength of the vortex used in this figure is not representative of that behind a Lynx main rotor but merely illustrative to show the effect.

With a tail rotor that rotates top-blade-aft the effect of the wingtip vortex on the yaw control margin is reversed.

From the point of view of the measurement technique employed, calculated values of leading edge pressure coefficient will not take account of changes of in-plane velocity as already described. The effect of vortex induced changes in dynamic head will therefore be accentuated towards the centre of the tail rotor. Were true C_p values to be calculated using the correct in-plane velocity at each point, only the effects of the changes in incidence just described would be seen on a C_p plot, though accurate loading calculations could then be made.

If the position of the tail rotor along the length of the wingtip vortex were to be considered then it could be expected that the tail rotor would be closer to the start than the end of the roll up process. The velocity fields of the individual main rotor blade trailing tip vortices would therefore appear at the leading edge pressure sensors as a marked cyclical variation at the blade passing frequency or some multiple of it. Even if the roll up was well established this frequency would still be evident provided that the rolled up vortices retained their identities. As the effect of the main rotor wake on the tail rotor is stronger in quartering flight than in forward flight, it would be reasonable to expect that the main rotor induced frequencies would also be more significant. This has not been found to be the case. Figure 5.5.6 shows the frequency content of the leading edge sensor signals recorded when flying OGE with a relative wind of 25 knots at 064 degrees. The traces show an almost total lack of any main rotor induced frequency content. This would suggest that the individual main rotor blade trailing tip vortices have lost their individual centres of circulation and merged into one larger vortex. Vortex merging of this nature has been noted during research into wake minimisation techniques for large transport aircraft (Rossow (1977)). One of the most significant criteria that determined whether or not two vortices merged was found to be the ratio between the distance between their centrelines and the core diameters. If merging of this nature has occurred in the wingtip vortices by the time that they influence the tail rotor, it would suggest that the roll up process was approaching completion. The strength of the flow field of such rolled up wingtip vortices requires further investigation as does the rate of vortex dispersion.

In order to demonstrate whether this vortex merging was indeed the cause of the noted reduction in main rotor frequencies in the data, the Lynx main rotor wake model described in section 6.3 was created. The model was run at different flight speeds and the separation between the vortices noted (figure 5.5.7). Calculation of the vortex separation ratio discussed in the previous paragraph indicated that such merging was

possible at the flight speeds that the Lynx suffered from yaw control margin restrictions.

The absence of main rotor frequencies in figure 5.5.6 is reflected in the low standard deviation in the C_p values over most of the tail rotor disc as shown in figure 5.5.8. The exception to this is in the region of the tail fin were some marked C_p variations are to be found. Although full analysis of the data from the trailing edge sensors has yet to be carried out, visual inspection of the trailing edge negative C_p values when plotted against tail rotor azimuth angle for all 160 revolutions in the event (figure 5.5.9) shows a distinct peak as the instrumented blade passes the position of the tail fin. From experience with similar main rotor data, as briefly discussed in Chapter 4, this peak can be stated as indicating the presence of blade stall. This stall requires further investigation but is currently thought to be caused by the turbulent nature of the flow round the fin in a flight condition where the fin, when considered as an aerofoil, is at a very high angle of attack.

As the changes in dynamic head induced by the main rotor wingtip vortices cannot be derived from the instrumentation fitted to the Lynx AH Mk5 instrumented tail rotor, it was decided to use the main rotor wake model described above to produce a calculated value as shall be described in section 6.3. Figure 5.5.10 shows the plot of percentage reduction in dynamic head thus produced for all conditions of relative wind speed and direction within the low speed flight envelope. These values were then used in conjunction with the values of tail rotor pitch angle calculated with Helistab to produce an amended pitch angle (figure 5.5.11) which was subsequently translated into yaw control margin to give the plot already presented in figure 1.4.2. The close agreement between this plot and the equivalent plot of yaw control margin as measured on the aircraft (figure 1.1.1) indicates that:

i. Variation in dynamic head is one of the most significant factors affecting tail rotor performance throughout the low speed flight envelope, and

ii. The wake model used is sufficiently accurate to be able to provide reasonable velocity values at the tail rotor for steady trimmed flight.

That the yaw control margin in quartering flight is still slightly over predicted indicates that the effect of the fin interference must also be taken into account to include the effects of blade stall in this region.

As previously stated, the tail rotor on the Puma rotates top-blade-aft and so does not suffer from yaw pedal margin deficiencies in the same way as the Lynx AH Mk5. However, one feature was recorded on the Puma tail rotor in quartering flight that has not been found on the Lynx. Figure 5.5.12 shows the frequency content of the data recorded on the Puma tail rotor whilst the aircraft was translating IGE with a relative wind of 15 knots from 300 degrees. It should be remembered that, as the main rotor on the Puma rotates in the opposite direction to that on the Lynx, right sideslip angles on the Lynx equate to left sideslip on the Puma when considering the effects of the main rotor wake on the tail rotor. By comparing Figure 5.5.12 with Figure 5.3.3, it can be seen that in addition to the tail rotor and control induced frequency content previously observed, another peak is to be found at a frequency equating to twice the main rotor blade passing rate. This frequency is almost isolated having very weak harmonics and not producing any beat frequencies with the tail rotor at all. Whilst this event was being recorded the pilot experienced 'tail rotor buzz', a high frequency vibration felt through the airframe and pedals. The mechanism of this particular interaction has not been determined and it deserves some additional research for completeness.

5.6 Main rotor effects observed on the tail rotor in sidewards and rearwards flight.

In sidewards and rearward flight the Lynx main rotor wake does not approach the tail rotor and it was expected that the distinct lack of main rotor induced frequencies observed in the Puma data in rearwards flight (Figure 5.6.1) would be repeated. This

however was not found to be the case. Figure 5.6.2 shows the frequency content of the Lynx data with the aircraft translating OGE with a relative wind of 30 knots from 149 degrees. Although the main rotor blade passing frequency is only just apparent on the outer 3 sensors, the frequencies equating to T±4R are evident at a uniform strength along the blade. The plot of the average C_p (figure 5.6.3) shows that the remaining segment of the loading peak is now at the rear of the disc as the aircraft translation is essentially backwards. The plot of standard deviation of C_p (figure 5.6.4) indicates that the loading peak is almost steady and that the maximum variation is in the fin interference effect region. When the data was animated, no clear cyclical patterns were observed; the C_p variation in the lee of the fin was found to be almost random. The most likely cause of this latter effect was thought to be flow breakdown round the fin although no concrete evidence of blade stall was to be found.

On closer inspection by a different means a very slight cyclical variation at the main rotor blade passing frequency was found. Figure 5.6.5 shows a carpet plot of the C_p derived from the sensor at 85% tail rotor radius. The horizontal axis represents the tail rotor azimuth changing from 0 to 360 degrees. Equally spaced up the plot are the C_p values from all 160 tail rotor revolutions. The revolutions have been so ordered that the main rotor azimuth position increments from 0 to 360 degrees going up the plot. The contours have then been drawn through lines of equal C_p. If the green lines representing a C_p value of 1.33 towards the left-hand and right-hand edges of the plot are followed up the page, a four cycle oscillation can be observed. Four cycles in 360 degrees of main rotor rotation equate to the main rotor blade passing frequency. If the whole of the plot is studied in a similar manner, this same variation can be observed, except at the tail rotor azimuth position where the fin interference effect occurs.

In this instance, therefore, although the main rotor wake is passing well clear of the tail rotor, a main rotor induced cyclical variation is to be found over most of the disc. It is considered that the variations observed are caused by the main rotor wake exciting the fuselage, causing the tail to shake laterally and thus imparting a flapping

motion to the tail rotor blades. This would affect the C_p values in a similar manner to that shown and affect the whole disc.

This effect was noted over the whole of the rear half of the flight envelope as indicated in figure 4.3.3 as region 6. A related but slightly different effect was noted in region 5 where, instead of the main rotor blade passing frequency being present, the main rotor fundamental frequency was observed (Figure 5.6.6). The mechanism in this region is thought to be similar to that outlined above but with the main rotor exciting a different mode in the fuselage.

Neither of the two interactions described in this section are considered significant. It is for that reason that no more effort was spent refining the detail of the interaction mechanisms. There is, at present, not thought to be much advantage to be gained by the inclusion of the effects of these interactions in a computer model.

5.7 Concluding remarks.

In Chapter 4, it was shown that study of the frequency content of the data recorded on the Lynx AH Mk5 tail rotor had different attributes depending on aircraft relative speed and direction. The low speed flight envelope of the aircraft was thus divided into six regions. In this chapter, the effects noted in each of the six regions were investigated in some depth and details on the interaction mechanisms taking place revealed. Some of the mechanisms are clearly aircraft configuration related but it is thought that others will be more universal in their application. Nearly all of the mechanisms postulated warrant additional research, most of which would be best carried out in a controlled wind tunnel environment.

Chapter 6.

Aspects of tail rotor and yaw control modelling.

6.1 Introduction

In Chapter 1 the problems experienced with the current generation of helicopter yaw control models were mentioned. A plot given at Figure 1.1.2 showed the inaccuracies in the representation of the Lynx AH Mk5 yaw control margin as produced by the DRA's current helicopter model, Helistab. Low fidelity yaw control modelling is not unique to the DRA but is almost universally found to be a problem area. In many instances the tail rotor representation in a simulation model is less accurate than it's main rotor counterpart as deficiencies in the main rotor model have a greater impact on the overall model performance. In addition, the information to produce a high quality tail rotor model has not been available. One of the prerequisites of a high fidelity tail rotor model is an accurate main rotor wake model that will reproduce the wake geometry whatever the flight condition. This main rotor wake model must be able to run in real time for piloted simulation work.

This chapter will start with an overview of the tail rotor model in Helistab (Padfield (1981)) and discuss some of it's shortcomings. Section 6.3 will then look at the two different types of main rotor wake model and cover, in some detail, the use of a wake model that has been found to give encouraging results when applied to the tail rotor problem. Finally section 6.4 will discuss, in outline terms, a method by which such a wake model could be coupled into a piloted simulation model in an attempt to overcome some of the shortcomings previously encountered.

6.2 Current tail rotor modelling in Helistab.

In Helistab, the tail rotor is represented by a disc model which was developed using the same basic assumptions as the main rotor. It has rigid blades which are hinged at the shaft. Blade flapping motion is included, albeit in a simplified form, but there is no lag. As the tail rotor rotational frequency is high, the time taken for the blades to respond in flap is correspondingly fast. For this reason the dynamics of the tail rotor blades are modelled in a quasi-steady manner such that a tail rotor collective input results in an instantaneous alteration in thrust and tail rotor coning. Cyclic variation in flap is neglected so the thrust produced by the tail rotor is always along the shaft axis which is assumed to be uncanted. The Blackhawk, for example, with it's canted tail rotor cannot therefore be accurately modelled at present though a minor modification would make this possible. The tail rotor inflow is of the Glauert trapezoidal type and will respond to changes in sideslip angle etc. Only the uniform component of the inflow is, however, included.The tail rotor blade drag is calculated for each point on the disc and then averaged over the disc so that the tail rotor torque can be estimated. No fuselage reaction to changes in tail rotor torque is included. A simple model of fin blockage can be incorporated if required but there is no means by which the effect of the main rotor wake on the tail rotor can be represented. A model of the weathercocking action of the fuselage is also used.

When it is configured to represent the Lynx AH Mk5, these factors combine to give the model a yaw performance which, although it may be adequate for manoeuvres at higher speeds as illustrated in Figure 6.2.1, is less representative of that found in the real aircraft within the low speed flight envelope as demonstrated by a comparison between Figures 1.1.1 and 1.1.2. It is considered that improvements could be made to this aspect of Helistab and these will be discussed later in this chapter.

6.3 Steady main rotor wake model.

To reiterate what was said in the introduction to this chapter, no representative tail rotor model can exist in isolation. Instead it must operate in conjunction with a main rotor wake model so that the effects of the relevant main rotor/tail rotor interactions can be included at the appropriate flight conditions. This section will look at the requirements for such a main rotor wake model, discuss one that has been used to effect within this programme and show some of the results obtained with it.

Rotor wake models fall into two generic categories: the free wake and the prescribed wake representations. In a free wake model the initial conditions of the wake are laid out and then, as the rotor revolves the wake is left to evolve under the influences of the various velocity fields that affect it until, at each time step, it reaches an quasi-equilibrial condition. A good free wake model should be capable of producing an accurate wake geometry under most conditions but has the following drawbacks:

i. For the wake to form accurately all influences on it's geometry must be represented. To calculate the effect of each vortex element on all the other elements can be computationally intensive, especially since, for each time step, the calculation of the induced velocities must be repeated until equilibrium is achieved. Generally, when an isolated main rotor model is considered, time steps equating to not less than one twentieth of a main rotor revolution are used; any shorter an interval and the number of calculations increases dramatically. If a blade element tail rotor model were to be run along side that main rotor model the time step would have to equate to that same proportion of a tail rotor revolution to give adequate resolution. This would reduce the time step by a factor of the main rotor/tail rotor gearing ratio giving rise to an unacceptable computing burden. One method that has been used with some success to reduce the effects of this problem has been to artificially increase the size of the main rotor blade trailing tip vortex cores, thus reducing the resolution required,

performing the wake calculations and then subsequently modifying the result with a 'fudge factor' to reduce the vortices and their effects to scale proportions (Quackenbush, Bliss & Mahajan (1989) and other reports by the same authors).

ii. If an attempt is made to calculate the wake geometry in a low speed/high thrust condition, it is unlikely that a free wake model will achieve the equilibrium state required and will probably diverge. As discussed in the preceding chapters, most of the significant main rotor/tail rotor interactions take place at low speed when the main rotor will be at high thrust.

It is the second of these two points rather than the first which would tend to make a free wake main rotor wake model unsuitable for tail rotor modelling applications. That is not to say, however, that it could not be used when a high degree of accuracy is required in a high speed flight condition.

A prescribed rotor wake model produces a representation of the wake geometry in a significantly less computationally intensive manner. The rotor wake is studied either in flight or in a wind-tunnel and it's geometry noted. A set of equations are then derived which account for the distortions in the wake observed. These equations must effectively arrive at the quasi-equilibrium state in one step that is achieved by iteration in the free wake model. Prescribed wake models are seldom as accurate as free wake models and will not portray the finer details. The wake from which the equations were initially derived will be of one particular rotor configuration and care must be taken to ensure that wakes produced for other aircraft are accurate and that the parameters that prescribe the shape of the wake do not require adjustment.

Notwithstanding the above, the use of a prescribed main rotor wake in tail rotor investigations does have certain advantages. As iteration is not required to reach wake equilibrium, the model can be used for the low speed/high thrust situation described earlier. A prescribed rotor wake model will require orders of magnitude less computing

time than it's free wake counterpart and is thus better suited to real time or near real time operation.

Whilst investigating the main rotor/tail rotor interaction occurring in quartering flight, as described in section 5.5, the requirement arose for a main rotor wake model to aid in the investigation of some of the effects noted. Advice was taken from Mr Todd R Quackenbush of Continuum Dynamics Inc. of Princeton, New Jersey, as to the best form of model to use and some of his comments have been summarised above. He suggested the use of a flat wake model as described in Curtis & Quackenbush (1989). Although such a model would have been wholly appropriate in higher speed forward flight (μ above 0.15), it was not thought that it would be sufficiently accurate to model the effects occurring at low speed and high sideslip angles. The model used had to reflect the distortions found at the edge of the main rotor disc as detailed by Heyson & Katzoff (1957).

The model eventually selected was the prescribed wake model developed at Westland Helicopters Ltd by Mr Tom Beddoes (Beddoes (1985)). Originally intended for use in main rotor loading distribution calculations, all the equations required to generate the wake geometry are given in the report. Figure 6.3.1 shows the wake geometry created using the model. The vortices trailed from blades at the rear of the disc initially descend at a slightly faster speed than those from the front whilst those from the edges of the disc hardly descend at all, simulating the position of the blade vortices within the rolled up wingtip vortices trailing from this position. The model is not totally representative in this area as the blade vortices do not roll round each other as described in section 5.1. This has not, however, been found to be a problem in the uses to which the model has been put. Using the equations given, the main rotor wake model was coded up to represent a Lynx AH Mk5 with the facility to place the tail rotor at the correct place within the wake for any combination of speed and sideslip angle.

As discussed in section 5.5, the model was then used to calculate the change in dynamic head at the tail rotor. The wake model was configured to give 10 revolutions of the main rotor wake and the velocity induced at each point on the tail rotor disc by all the vortex elements calculated using a Scully vortex representation. The length of the wake was selected as being sufficiently long to reduce error but not so long as to incur excessive computational penalties. Undoubtedly a more efficient method could have been used to find the vortex elements having the most significant effect on the tail rotor (somewhat akin to that given in Beddoes (1985) perhaps) but, as this particular calculation was only to be performed once, it was not deemed to be worth spending the time developing it. All the in-plane velocities induced at each point on the tail rotor disc were then summed and a value of the dynamic head calculated at each location. These values were subsequently expressed as the percentage change they made to the dynamic head at that point on an isolated rotor. Finally, these percentages were averaged to give one percentage change figure over the whole tail rotor disc for a given flight condition. A plot of the data thus generated for all relative wind speeds and directions within the Lynx AH Mk5 low speed flight envelope has already been given at Figure 5.5.11 and discussed in that section.

It is considered that this model, however accurate the results it gives when employed as above, cannot be used to generate anything more precise than a single figure for the percentage change in dynamic head for application to the whole tail rotor disc. If the prescribed wake model was believed to be totally accurate, it would theoretically be possible to calculate values of velocity and incidence for each point on the tail rotor and then use this information in a tail rotor blade element model. However, as the main rotor wake model does not reproduce the formation of the wingtip vortices or any vortex merging that might occur, the localised detail in the wake cannot be held to be accurate. This being said, the circulation content of the main rotor wake will be reasonably accurate and allow the more broad brush dynamic head calculations described above to be made.

The method used to calculate the induced velocity at each point on the tail rotor disc was computationally expensive and could not be made to run in anything approaching real time. An alternative route for arriving at this figure using the model has therefore been sought. During the initial stages of model development a plot was made showing the number of main rotor blade trailing tip vortices calculated to pass through the tail rotor for any given relative wind speed and direction (Figure 6.3.2). When compared with Figure 5.5.10 a close comparison was observed. When the number of vortices passing through the tail rotor were multiplied by a suitable factor (found by experiment to be approximately 2.6 for the Lynx), the plot given in Figure 6.3.3 was created. When yaw control margins are calculated using this data as described in section 5.5, the resultant plot (Figure 6.3.4) shows only slight departures from that created by the more intensive method (Figure 1.4.2) though with the use of significantly reduced computing time. Theoretically this simplified model should also take account of the vortices just outside the tail rotor which have the opposite effect to those passing through it as discussed in section 5.5. This requires investigation.

It is considered that this main rotor wake/tail rotor model, when used in the manner described in the preceding paragraph to calculate tail rotor dynamic head, is worthy of further research for use in real time simulation. This application of the model, or a derivative of it will be discussed in the next section.

6.4 Potential improvements in tail rotor modelling.

Given the current standard of tail rotor modelling outlined in section 6.2 and the increased fidelity of the yaw control margin achieved using the Beddoes main rotor wake model detailed in section 6.3, this section will discuss some modifications to the basic Helistab tail rotor model that could potentially improve it's tail rotor and yaw control performance.

In section 6.3 it was shown that, for a Lynx AH Mk5, the percentage change in dynamic head at the tail rotor could be calculated with reasonable accuracy using a prescribed main rotor wake model. The calculations performed have been for the helicopter in steady trimmed flight. The requirement for simulation modelling is to be able to predict the pedal margin for the tail rotor in manoeuvring flight and from this the excess tail rotor thrust available to produce acceleration in yaw. The model must be able to achieve this for all helicopters fitted with a conventional tail rotor.

Taking that last point first, when the main rotor wake model was used to calculate the percentage change in dynamic head for the Lynx Ah Mk5 by summation of the induced velocities at the tail rotor, the Lynx parameters used in the programme were not adjusted in an attempt to influence the accuracy of the result. This gives some confidence that use of the model in other aircraft configurations would yield similarly accurate results, though this will require verification. The multiplication factor used to produce the percentage change in dynamic head from the number of main rotor vortices passing through the tail rotor may change from aircraft type to aircraft type and would need to be checked by comparing the results from the two calculation methods discussed.

Assuming that this method were applicable to all appropriate helicopter types, it must be capable of covering manoeuvring as well as steady flight. In gentle manoeuvres, the main rotor wake experienced by the tail rotor at a given instant will not be significantly different from that in steady flight at the same flight condition. As the severity of the manoeuvre increased, so would the errors induced by use of this model. As no work has been done to look at the effect of the model in manoeuvring flight, these errors have yet to be quantified.

Since the initial report on this main rotor model was written(Beddoes (1985)) additional work on it has been performed under a joint programme by Westland Helicopters Limited and DRA Farnborough. Under this programme the wake model

has been modified to enable the loads on the main rotor in manoeuvring flight to be determined (Harrison (1991)). The changes to the model have yet to be examined in detail but, unless the code that produces the main rotor wake geometry for manoeuvring flight is significantly more complex than that for steady flight, it would appear that this manoeuvre model would offer the most accurate means of calculating the tail rotor dynamic head. It is envisaged that, at each time interval, the main rotor wake coordinates would be calculated and from this the number of vortices passing through the tail rotor determined. This would then be converted into the percentage change in dynamic head from which the pedal margin required to maintain the current yaw acceleration could be derived. The use of this method will require detailed investigation; some factors which will need to be considered are as follows:

i. How the multiplication factor required to obtain the percentage change in dynamic head from the number of main rotor vortices will vary with manoeuvre.

ii. The number of revolutions in the main rotor wake required before all main rotor vortices are out of the vicinity of the tail rotor. This number will vary with flight condition. Once a main rotor trailing tip vortex has penetrated the tail rotor, if it is going to do so at all, if it subsequently does not encounter the tail rotor for one complete revolution, then it is unlikely to do so again.

As discussed in section 6.3, the dynamic head calculations should only be made on the basis of one figure for the whole tail rotor disc. For this reason the disc representation of the tail rotor in Helistab should be retained and used to calculate blade motions. A blade element model could, however, be used to calculate blade loading distribution.

Other areas of the yaw performance implementation in Helistab could be improved with effect. These are as follows:

i. Cyclic flap motion and pitch control input. Although on a conventional tail rotor only collective control inputs can be applied to the tail rotor, tail rotor cyclic flapping can be significant, especially at high speed. Section 7.7 will discuss the potential advantages to be gained from the use of cyclic control of tail rotor pitch. In order to investigate this new departure in the use of the tail rotor it would be beneficial to have a computer model that could represent it. Any such model would need to have the capability for cyclic control inputs, tail rotor blade flapping, and tail rotor thrust along a line not coincident with the tail rotor drive shaft. Tail rotor lag motion would also be an advantage. If cyclic control inputs were being used it may be advantageous if the $\Delta 3$ blade flap/pitch coupling effect could be disabled.Even if the use of cyclic control inputs were not required for a given application, the remainder of this package would improve the results obtained.

ii. A more representative and validated model of fuselage weathercocking effects and fin blockage, including the influence of the main rotor downwash on the fuselage flowfield..

It is considered that the modifications suggested in this section would improve the yaw control representation with Helistab. The ability of the model to accept cyclic tail rotor pitch control inputs will also be a distinct advantage if research into that topic is continued.

6.5 Concluding remarks.

In the introductory paragraphs to chapter 1 it was stated that accurate computer models of an aircraft were required before the control laws required for an ACT system could be developed. This chapter has looked at the yaw control aspects of one such model. Although the model is reasonably accurate in some areas, it does have deficiencies in the low speed flight regime; one where yaw control is critical. A major

shortcoming of the model was identified as being the lack of any main rotor wake influence on the tail rotor. A main rotor wake model has been used as part of this research programme and has produced encouraging improvements in the modelling of the yaw control margin in trimmed steady flight within the low speed flight envelope. This was discussed, as was the use of a variation on this wake model designed for manoeuvring flight. Other detailed improvements to the yaw control model were also discussed, in particular the ability of the model to be able to introduce cyclic control of tail rotor pitch. The reason behind the desirability of this last feature will be made clear in the following and final chapter.

Chapter 7.

Conclusions and recommendations for further research.

7.1 Introduction.

The development of ACT control laws require accurate system models. This programme of research into helicopter tail rotor handling and performance was originally instigated with the aim of improving the understanding of the factors affecting the tail rotor to a point where their effects could be included in such a model. The programme commenced in 1985 with a review of the problem (Smith (1985)). This dissertation forms the final report from this phase of the DRA tail rotor research programme.

This dissertation has set out to document the selection of a data recording technique, the design and manufacture of an instrumented tail rotor for the DRA's flight research Lynx AH Mk5 helicopter to use that technique and then, using that rotor, the planning and conduct of the experimental flight trial to collect the data. The collection of that data was just a stepping stone, albeit an important one, on the route towards the final goal. Once the quality of the data had been confirmed, an analysis package had to be developed so that a significant quantity of the data collected could be inspected in a predominantly automated fashion. From the insights gained from this process, the low speed flight envelope of the Lynx AH Mk5 could be split up into six regions and the differing main rotor/tail rotor interactions occurring in each of those regions examined in detail. From the understanding thus gained of the tail rotor's operating regime, some modifications to Helistab, one of the DRA's helicopter computer models, could be investigated and proposed.

The previous paragraph galloped through the work of several years in just a few sentences but, in doing so, showed that the major aim of the programme, namely the improvements to the computer model, has been achieved. This final chapter of the

dissertation will go through each of the areas of the programme in turn, outline the conclusions made in each and then make some recommendations for additional work that could be carried out in the future.

At the start of the programme there was no intention to do anything but investigate the performance of the current generation tail rotor. However, certain aspects of the research undertaken have suggested a novel tail rotor control strategy that may be of benefit to the helicopters of the future. This, the use of cyclic control of tail rotor pitch, although outside the aims of this research programme, will be briefly discussed at the end of the chapter.

7.2 Experimental set up and measurement technique

Chapter 2 discussed the choice of measurement technique to be used. This choice was made on the basis that the mechanisms of the main rotor/tail rotor interactions to be determinable from the data collected. The technique selected was that of the Pressure Indicator Sensor. The following conclusions can be made about its suitability for use in tail rotor applications:

i. Use of the Pressure Indicator Sensor technique has allowed some of the mechanisms of main rotor/tail rotor interaction to be determined.

ii. Use of the technique has allowed this information to be obtained from a minimal quantity of sensors on the tail rotor blade.

iii. When used to its full potential, the technique permits the derivation of blade loading and incidence. However, for this to be possible an accurate estimate of the local in-plane velocity component is required at each blade station.

iv. Various methods have been proposed to enable an estimate of the in-plane velocity to be made. This velocity component could be derived from

computational main rotor wake models and then applied retrospectively to existing pressure data. The velocity at the blade tip could be measured by means of a tip pitot to give the background features of the flow but not the fine detail around points of vortex interaction. The preferred method would be one that allowed the velocity to be estimated from the analysis of data collected on the blade. One such method involves the use of an extra pressure sensor at 50% chord on the upper surface of the tail rotor blade at each station. This method requires verification; this will be possible with the main rotor chordwise array data to be recorded on the DRA Lynx AH Mk7.

v. When mounting pressure sensors on conventional metal-sparred tail rotor blades there is generally insufficient metal in the spar to allow the sensors to be mounted within the blade profile. They therefore must be surface mounted under a suitable fairing. Similar fairings must be applied to each blade in the tail rotor set adding to the cost of the trial unless a set of old blades can be acquired.

vi. All signals from the rotor should be amplified before being passed through the sliprings to reduce the signal to noise ratio. All signal wires should be adequately screened wherever possible. Extreme care must be taken when routing cables over hinges and other moving joints. Sampling rates should be chosen to give a minimum of seven samples per cycle at the tenth harmonic of the fundamental frequency of interest to give good amplitude resolution.

vii. A quick method of being able to replay each tape at the end of each flight is essential to reduce lost data due to malfunction and to maintain confidence in the instrumentation. All sensors should be calibrated before and after the trial, whenever they have been disturbed and whenever there is any doubt about the existing calibration.

The instrumentation system fitted to the Lynx AH Mk5 was not identical to that which would be employed if the experiment were to be repeated. The major change

would be the fitment of the extra sensor at 50% blade chord described above. The instrumentation schemed for the Lynx AH Mk7 composite tail rotor blade incorporates this sensor. The design of this blade is such that no leading edge fairing is required and thus only one or, at most two special blades are required. The cost and duration of any experimental flight programme with that aircraft would therefore be reduced. A description of the instrumentation for that blade is given at Appendix 4. It is recommended that, before that blade is built, the use of two sensors at 2% and 50% chord on the upper surface of the blade to derive in-plane velocity is investigated. This could be done using data from the full chordwise arrays fitted to the main rotor of Lynx ZD559. The principles of the velocity estimation technique could thus be fully established and the location of the 50% chord sensor confirmed.

7.3 Experimental procedure.

The experimental flight trial with the Lynx AH Mk5 had to be completed within a short timescale. The decision to go abroad to seek better weather conditions for the flight phase of the programme ensured that it was completed on schedule. The use of a military airfield that did not charge for its use or for facilities and the employment of a military maintenance team who did not charge overtime helped to keep the costs down.

The success of the flight trial was largely due to the planning that preceded it. The requirement to produce a detailed Flight Trials Instruction (Appendix 1) before any experimental flying could take place helped to ensure that all the relevant factors, particularly flight safety, had been considered. Inevitably some problems did occur but none of these proved insuperable. If a similar trial were to be repeated in the future it would be recommended that the lessons learned during this flight trial and given in section 3.4 were studied. As the instrumentation schemed for the Lynx AH Mk7 tail rotor should prove easier to assemble and disassemble, the requirement to conduct a trial with that aircraft at one go may not be as pressing. The advantages of being able to

analyse some of the data between flights and adjust the flight programme accordingly should not be ignored.

The experimental flying phase of this programme was a success. Over twelve hundred test points were flown covering all the flight conditions then deemed of interest. This was carried out in the desired meteorological conditions within the allotted time scale and the data recorded have proven to be of a contemporary high standard.

7.4 Analysis techniques and data presentation.

At the end of the experimental flight phase of this programme, a member of the Army team maintaining the aircraft calculated that, if the all data collected were to be analysed using the techniques available at the start of the study, that process would take approximately 652 man years to complete. That a significant proportion of the data has been analysed to a common basic level in less than two man years indicates that the analysis routines developed during the course of the programme have enhanced the DRA's ability to process this type of tail rotor flight test data. The analysis routines must be constantly appraised to determine whether further improvements are possible.

The following conclusions concerning the analysis of this form of data can be drawn:

i. As each six second event recorded contains some one hundred and sixty tail rotor revolutions, all of which may be different, some form of semi-automated process is required to indicate the information contained in each event with a handful of meaningful plots. The analysis package developed has met this requirement.

ii. Examination of the data in the frequency domain can reveal the presence of different main rotor/tail rotor interactions. Each interaction so far studied would appear to have its own signature. This was revealed by a comparison of the

relative powers in the main rotor induced frequencies in each leading edge pressure sensor signal.

iii. The detail of the interactional mechanisms cannot be determined in the frequency domain. The areas of the tail rotor disc affected by an interaction can be found through study of the data in the time domain. Plots showing the average and standard deviation of the data at each radial and azimuthal location were found to be most useful in this respect. Once an interaction has been detected within a region of the helicopter's low speed envelope, one event could be selected from that region for more in-depth analysis.

iv. This in-depth analysis was, in the majority of cases, greatly assisted by the use of dynamic graphics. This technique revealed detail in the timing of interactions that was not evident from the study of a sequence of individual revolutions. Smaller effects could also be emphasised by animation. Different formats were tried but no one was found to fulfil all requirements. The use of computer generated animation, as opposed to hard copy cartoon techniques, was found to be invaluable.

v. The analysis routines developed were designed for use on data collected in steady flight and would not all be suitable for tail rotor investigations in manoeuvring flight. Some ideas on a possible way forward in the analysis of manoeuvring flight were given in section 4.6. The technique does, however, require to be substantiated.

7.5 Features of tail rotor loading distributions.

From the frequency domain analysis of the Lynx AH Mk5 data carried out as described in Chapter 4 it is evident that the tail rotor experiences different interactions depending on flight condition. It has been possible to divide the low speed flight

envelope of the aircraft into six regions (figure 4.3.3), each with its own variety of main rotor/tail rotor interaction. The following conclusions have been drawn about the interaction mechanisms in each region:

Region 1. Near hover.

i. The main rotor wake does not cut across the tail rotor and main rotor induced frequencies in the tail rotor data are negligible. The tail rotor loading distribution does not vary significantly from revolution to revolution.

ii. The tail rotor wake is distorted by the main rotor wake and can be induced to curve round the outside of the main rotor disc as described by Brocklehurst (1986/1).

iii. Although for most modelling purposes the effect on the tail rotor is small, this interaction can have a more significant effect on the main rotor loading. It is therefore recommended for further study to improve main rotor hover loading prediction.

Region 2. Forward flight.

i. In low speed forward flight, two different interactional mechanisms are active; one between the main rotor blade trailing tip vortices and the tail rotor blade trailing tip vortices, the other between the main rotor blade trailing tip vortices and the tail rotor blade itself.

ii. The separation between the individual blade tip vortex elements trailed from the two rotors is dependant on the position of the main rotor vortex when the tail rotor vortex was formed. The strength of the interaction depends on this distance.

iii. Where the separation is small enough the main rotor blade trailing tip vortex may interfere with the formation of the vortex trailed from the tail rotor blade.

Assuming that tail rotor vortex roll-up does occur, that vortex will be subjected to a localised strain by the main rotor blade trailing tip vortex. This, if sufficiently strong, will cause the tail rotor blade trailing tip vortex to disintegrate, leaving a small gap in the vortex core.

iv. This gap will have a minimal effect on the blade from which the vortex was trailed but will produce a localised reduction in the tip loading peak on the following blade(s). The interference effect is therefore detected 90° later than expected (for a four bladed tail rotor).

v. The effect noted on the inboard section of the tail rotor blade will be that of the main rotor blade trailing tip vortex on the local in-plane velocity at the blade. Depending on the direction of tail rotor rotation, it will produce a suction peak followed by a smaller trough (top-blade-forward) or a small trough followed by a larger peak (top-blade-aft). The trough will not always be present.

vi. Both of the above mechanisms will be experienced at the inboard edge of the tail rotor blade loading peak.

vii. Although the strength of the tail rotor blade tip loading peak can be significantly reduced by the main rotor interaction effect, it occurs over such small azimuth that the effect on the total blade thrust is small (less than 5%). It is not therefore considered worthwhile to attempt to minimise the interaction. If, however, a detailed blade element model of the tail rotor is required, more information on the detail of the interaction between the two trailing tip vortices would be required, particularly on the effect of the main rotor blade trailing tip vortex on the tail rotor tip vortex roll-up process. This would be best carried out in a wind tunnel.

Region 3. Quartering flight - advancing blade side.

i. Some or all of the tail rotor disc is immersed in the "wing-tip" vortex formed by the interaction of the blade tip vortices trailed from the edge of the main rotor disc.

ii. For a tail rotor rotating top-blade-forward, the "wing-tip" vortex flowfield will be rotating in the same direction as the tail rotor blade and, when that vortex is approximately centred on the tail rotor, the blade dynamic head will be significantly reduced. This will lead to an increased tail rotor blade root pitch angle for the same thrust.

iii. The reduction in the main rotor induced frequencies in the tail rotor pressure data would suggest that vortex merging has occurred and that the main rotor blade trailing tip vorticies have lost their individual identities by the time they reach the tail rotor.

iv. There is evidence that the tail rotor blade stalls as it passes the fin. This requires further investigation.

v. This is the most influential main rotor/tail rotor interaction; the only one that can significantly affect the handling and control of the aircraft. As such, its effects should be included in any model of helicopter low speed handling.

vi. The ill effects of the interaction are largely countered by fitment of a tail rotor rotating top blade aft. If this is done, the main adverse effects remaining are those of the flow round the fin.

Region 4. Quartering flight - retreating blade side.

i. The interaction mechanism is the same as that described for region 3 above. The magnitude of the blade root pitch angle change required will, however, be

reduced as the tail rotor is partially off-loaded by the weathercocking action of the fuselage.

ii. The comments for modeling the effect given for region 3 also apply.

Region 6. Sidewards and rearwards flight.

i. The tail rotor disc is not immersed in the main rotor wake. Main rotor induced frequencies are,however, still present in the tail rotor blade pressure data.

ii. This is thought to be caused by the main rotor wake acting on the fuselage and causing it to vibrate at the main rotor blade passing frequency. This motion is translated into a flapping motion at the tail rotor blade root giving rise to the variations observed.

iii. The magnitude of the interaction is dependent on aircraft configuration.

iv. The loading variation thus produced is of such small magnitude that it is not considered worthy of further attention or inclusion in all but the most detailed model.

Region 5. Left sidewards flight at approximately 30 knots.

i. The interaction observed is similar to that found in region 5 with the exception that the fundamental frequency is that of main rotor rotation as opposed to main rotor blade passing.

ii. Again, the effects of the interaction are configuration dependent and so small as not to warrant further investigation or inclusion in all but the most detailed model.

It has been encouraging that most of the significant interaction effects studied were to be found on both the Puma and the Lynx AH Mk5. As the two aircraft are so

different, this gives confidence that the mechanisms described would be found affecting the tail rotor on most conventional helicopter types.

7.6 Aspects of tail rotor and yaw control modelling.

As the fidelity of helicopter simulation models has improved, one aspect that has not received sufficient attention has been that of yaw response and control. This has largely been due to the lack of detailed understanding of the factors affecting yawing motion. It is believed that this programme, from its in-depth investigation of main rotor/tail rotor interactions, should help to restore the balance even though the effects of the fuselage and fin were not covered.

From the modelling work carried out within the programme, the following conclusions have been made:

i. Helistab, although reasonably accurate at higher speed, does not reflect the trim states found on the Lynx AH Mk5. The most important reason for this is the lack of any main rotor wake effects in the tail rotor model.It is believed that an acceptable method of including these effects has been found.

ii. When modelling the tail rotor in the low speed flight envelope, the high thrust/low speed conditions found preclude the use of a free wake model for either the main rotor or tail rotor wake. Instead a prescribed wake model must be used. One such model that has been found suitable for the main rotor wake is that described by Beddoes (1985).

iii. The change in dynamic head induced by the main rotor wake at the tail rotor blade has been found to have a significant effect on the yaw pedal margin. Although this can be rigourously calculated, an acceptably similar result can be obtained by counting the number of main rotor blade tip vortices passing through the tail rotor disc at any one time and multiplying this by the necessary

factor. This has only been tested for the Lynx AH Mk5 and must be repeated for other aircraft types.

iv. Although the method just outlined works for steady flight, it has yet to be extended to cater for manoeuvring flight. A suitable system has been outlined but requires additional research to develop its implementation.

v. Even though the effect of the main rotor wake on the tail rotor is the predominant effect, those of the fuselage side force and fin interference should not be ignored and should both be studied in more depth for inclusion in the models.

It is believed that, if the above effects are included in Helistab, that the yaw fidelity will be greatly enhanced, especially in steady state and manoeuvring flight within the low speed flight envelope.

7.7 Cyclic control of tail rotor pitch.

Although it was not stated as one of the original aims of this research programme, the study of the tail rotor data has suggested a novel form of tail rotor control; that of cyclic control of tail rotor pitch. The implications of the addition of tail rotor cyclic control have been discussed with Dr G D Padfield and Mr A McCallum in the Helicopter Aeromechanics Section and the ideas in this section contain their input as well as the author's. There are four perceived advantages of tail rotor cyclic control, each of which will now be discussed.

Study of the polar plots of tail rotor negative pressure coefficient has shown that the loading of the tail rotor disc is seldom uniform with part of the disc working harder than the rest. The variations in loading over the disc vary with flight condition. As no loading calculations have been carried out from the data collected for the reasons outlined in chapter 2, a full investigation of the loading variations has yet to be

undertaken. The most accurate results would be obtained from a trial with the Lynx AH Mk7 blade described in Appendix 4, though it is expected that reasonable results could be obtained using the existing data with a calculated in-plane velocity as discussed in section 2.4.1. It is thought that the loading could be more uniformly distributed over the tail rotor disc if the blade pitch could be controlled cyclicly as well as collectively. This should in turn reduce the tail rotor power consumption and thus improve the tail rotor efficiency.

One of the factors that limits helicopter manoeuvrability is the lag stresses induced in the tail rotor blades during rapid yawing motion. It is considered that cyclic control of tail rotor pitch could be used to limit the magnitude of the blade flapping motion that gives rise to the lag stress. If this were to be the case, the manoeuvre envelope of the aircraft would be enlarged, possibly to the extent of permitting snap turn manoeuvres in forward flight. During a snap turn, the aircraft head is yawed up to 90 degrees from track at speed to acquire and engage a target before yawing back to forward flight. Such a manoeuvre is currently only possible with a ducted fan tail rotor such as the Fenestron or Fantail where these lag stresses do not arise.

The flight safety implications of tail rotor drive failure are well documented. If the tail rotor disc could be canted backwards when such a failure occurred, it is possible that the tail rotor could be made to autorotate whilst still delivering a useful amount of thrust.

Horton(1988) discusses the advantages of being able to command fore and aft acceleration without changing aircraft pitch attitude as being improved pilot field of view and better fixed weapon targeting. It is thought that, by using vertical tail rotor cyclic control to counter fuselage pitching moments, aircraft pitch attitude could be controlled over a range of ± 10 degrees without excessive tail rotor thrust requirements, thus permitting acceleration up to 3.5 knots per second without change in pitch attitude. The main limiting factor would be the degree of main rotor blade flapping permitted.

It would be unrealistic to expect a pilot to exercise cyclic control over the tail rotor. An Active Control Technology system would therefore be a prerequisite before any of these effects could be tried in flight. It is recommended that the advantages of tail rotor cyclic control be investigated, possibly using inverse simulation techniques, and that, if it is subsequently considered that the advantages outweigh the penalties of increased tail rotor complexity, an ACT tail rotor demonstrator programme be instigated.

7.8 Concluding remarks.

The original aim of this programme was to make a significant contribution to the improved understanding of the operating environment and performance of the tail rotor so that it could be adequately modelled for ACT control law development. It is believed that, through the design and conduct of a suitable experiment and the subsequent analysis of the data collected, this aim has been achieved. The principle conclusions drawn from the programme outlined in this chapter should lead to measurable improvements in model fidelity, as should the recommendations given for future research in the field.

References.

Amer KB, Gessow A — 1954 — 'Charts for estimating tail-rotor contribution to helicopter directional stability and control in low-speed flight.' NACA Technical Note 3156.

Balch DT — 1983 — 'Experimental study of main rotor/tail rotor/airframe interaction in hover.' 39th American Helicopter Society Forum.

Baldwin SF, Handley CS — 1988 — 'Flight tests to explore tail rotor limitations in the low speed envelope.' 14th European Rotorcraft Forum, paper 111.

Balke RW, Bennett RL, Gaffey TM, Lynn RR — 1969 — 'Tail rotor design Part 2: Structural dynamics.' 25th American Helicopter Society Forum.

Beddoes TS — 1985 — 'A wake model for high resolution airloads.' Us Army/AHS conference on rotorcraft basic research (North Carolina)

Blachere G, D'Ambra F — 1981 — 'Tail rotor studies for satisfactory performance strength and dynamic behaviour.' 7th European Rotorcraft Forum, paper 74.

Bregger RE Dawson S 1992 'Sde-by-side hover performance comparison of MDHC 500 NOTAR and tail rotor anti-torque systems,' 48th American Helicopter Society Forum, pp689-697.

Brocklehurst A 1975 'An interim report on an investigation into the effects of design parameters on tail rotor performance.' Westlands Research Memorandum 319.

Brocklehurst A 1985 'A significant improvement to the low speed yaw control of the Sea King using a tail boom strake.' 11th European Rotorcraft Forum, paper 32.

Brocklehurst A 1986/1 'Main rotor/tail rotor interactions near hover.' Westlands Research Memorandum 535.

Brocklehurst A 1986/2 'An experimental study on the effect of the main rotor's wake on tail rotor performance in quartering flight.' Westlands Research Memorandum 536.

Brocklehurst A 1986/3 'Interactions between the tail rotor and fin in hover.' Westlands Research Memorandum 537.

Brocklehurst A 1986/4 'Experimental determination of tail rotor fin blockage in hover and right sideways flight.' Westlands Research Memorandum 538.

Brotherhood P 1947 'An investigation in flight of the induced velocity distribution under a helicopter rotor when hovering.' Minisrtry of Supply report Aero 2212

Brotherhood P 1952 'Flow through a helicopter rotor in vertical descent.' ARC Technical Report R&M 2735.

Brotherhood P 1978 'Flight experiments on aerodynamic features affecting
Riley MJ helicopter blade design.' Vertica vol2 pp27-42.

Brotherhood P 1990 'Experimental techniques in helicopter aerodynamics flight
Riley MJ research.' AGARD 1989-1990 Lecture Series No 5 Aerodynamics of Rotorcraft.

Brotherhood P 1992 'The determination of helicopter blade local normal force coefficient, incidence and stall boundaries from flight measurements of leading and trailing edge pressures,' DRA Technical Memorandum in preparation.

Clemmons MG 1992 'Antitorque safety and the RAH-66 Fantail,' 48th American Helicopter Society Forum, pp 169-177

Cook CV 1976 'Flight evaluation of a highly cambered tail rotor.' 2nd European Rotorcraft Forum, paper 24.

Cook CV 1978 'A review of tail rotor design and performance.' Vertica vol 2 pp 163-181.

Curtis HC Quackenbush TR	1989	'The influence of the rotor wake on rotorcraft stability and control.' 15th European Rotorcraft Forum, paper 70.
Ellis W Diamond J Fay CB	1976	'Design, development, and testing of the Boeing Vertol/Army YUH-61A.
Fitzgerald J Kohlhepp F	1988	'Research investigation of helicopter main rotor/tail rotor interaction noise.' NASA Contractor Report 4143.
Gray RB	1991	'Vortex Modeling for rotor aerodynamics - the 1991 Alexander A Nikolsky Lecture.' 47th American Helicopter Society Forum.
Hansford RE	1976	'Flight test results and performance assessment of a cambered section tail rotor.' Westlands Research Memorandum 400.
Harrison RJ	1991	'A manoeuvre wake model for the coupled rotor fuselage model (phase 2).' Westlands Research Paper RP 775.
Harvey KW Hughes CW	1979	'Design, analysis, and testing of a new generation tail rotor.' 35th American Helicopter Society Forum, paper 79-57.
Heyson HH Katzoff S	1957	'Induced velocities near a lifting rotor with nonuniform disk loading.' NACA report 1319.

Horner MB 1991/1 'An experimental investigation of the oblique blade-vortex
Saliveros E interaction.' 17th European Rotorcraft Forum, paper 91-62.
Galbraith RAMcD

Horner MB 1991/2 'An examination of vortex convection effects during blade-
Saliveros E vortex interaction.' AHS/RAES international technical
Galbraith RAMcD specialists meeting on rotorcraft acoustics and rotor fluid
dynamics, Philadelphia, USA.

Huber H 1982 'Studies on blade-to-blade and rotor-fuselage-tail
Polz G interferences.' AGARD fluid dynamics panel specialists'
meeting on prediction of aerodynamic loads on rotorcraft.

Huston RJ 1971 'A wind-tunnel investigation of helicopter directional control
Morris EK in rearward flight in ground effect.' NASA Technical Note
D-6118.

Kocurek JD 1980 'Hover performance methodology at Bell Helicopter.' 36th
Berkowitz LF American Helicopter Society Forum.
Harris FD

Kolwey HG 1991 'Analysis tools derived from investigating aerodynamic loss
of tail rotor effectiveness (LTE).' Proceedings of 22nd
annual symposium of the Society of Flight Test Engineers.

Landgrebe AJ 1971 'An analytical and experimental investigation of helicopter rotor hover performance and wake geometry characteristics.' USAAMRDL Technical Report 71-24.

Lemont HE 1982 'Ringfin augmentation effects.' 38th American Helicopter Society Forum.

Leverton JW 1975 'Main rotor wake/tail rotor interaction.' 1st European Pollard JS Rotorcraft Forum.
Wills CR

Leverton JW 1981 'Reduction of helicopter noise by use of a quiet tail rotor.' 6th European Rotorcraft Forum.

Lynn RR 1969 'Tail rotor design Part 1:Aerodynamics.' 25th American Robinson FD Helicopter Society Forum.
Batra NN
Duhon JM

Milne-Thomson LM 1958 'Theoretical Aerodynamics.' MacMillan.

Moore DW 1970 'Structure of a line vortex in an imposed strain.' Proceedings Saffman PG of symposium on Aircraft wake turbulence and it's detection, pp 339-354.

Moore DW 1973 'Axial flow in laminar trailing vortices.' Proc.R.Soc.Lond.
Saffman PG A333, pp491-508.

Mouille R 1970 'The "Fenestron" shrouded tail rotor of the SA.341 Gazelle.' Journal of the American Helicopter Society, Oct 1970 pp 31-37.

Mouille R 1979 'Ten years of Aerospatiale experience with the Fenestron and conventional tail rotor.' 35th American Helicopter Society Forum, paper 79-58.

Niebanck C 1978 'Sikorsky S-76 analysis, design, and development for
Girvan W successful dynamic Characteristics.' 34th American Helicopter Society Forum, paper 78-23.

Pegg RJ 1978 'Exploratory wind-tunnel investigation of the effect of main
Shidler PA rotor wake on the tail rotor.' NASA Conference Publication 2052 Part 1 pp205-220.

Padfield GD 1981 'A theoretical model of helicopter flight mechanics for application to piloted simulation.' RAE Technical Report 81048.

Phipps PD 1985 'Lynx low speed handling Characteristics with and without tailcone strake fitted.' Westlands W.E.R.141-06-00796.

Phipps PD 1987 'Lynx Mk 7 Tail Rotor Low Speed Performance.' Westlands Aerodynamics Technical Note Lynx/168.

Prouty RW 1982 'The YAH-64 empannage and tail rotor - a technical history.'
Amer KB 38th American Helicopter Society Forum.

Quackenbush TR 1989 'High resolution flowfield prediction for tail rotor
Bliss DB aeroacoustics.' 45th American Helicopter Society Forum.
Mahajan A

Robinson F 1970 'Increasing tail rotor thrust and comments on other yaw control devices.' Journal of the American Helicopter Society, Oct 1970, pp 46-52.

Rossow VJ 1977 'Convective merging of vortex cores in lift generated wakes.' Journal of Aircraft, Vol 14, No 3, pp283-290.

Saffman PG 1974 'The structure and decay of trailing vortices.' Archives of Mechanics, Vol 26 No 3 pp 423-439.

Schlinker RH 1983 'Tail rotor blade-vortex interaction noise.' USA AIAA-83-
Amiet RK 0720.

Schreier J 1982 'Fluctuating forces and rotor noise due to main rotor-tail rotor interaction.' 8th European Rotorcraft Forum, paper 9.2.

Scully MP 1975 'Computation of helicopter rotor wake geometry and its influence on rotor harmonic airloads.' ASRL TR 178-1.

Shenoy RK 1989 'Aeroacoustic flowfield and acoustics of a model helicopter tail rotor at high advance ratio.' 45th American Helicopter Society Forum.

Sheridan PF 1979 'Interactional aerodynamics - a new challenge to helicopter
Smith RP technology.' 35th American Helicopter Society Forum, paper 79-59.

Sheridan PF 1984 'Investigation of operational and design factors resulting
Hanker EJ from main rotor and tail rotor interactions.'
Blake BB USAAVRADCOM TR-82-D-40.

Signor DB 1989 'Performance and loads data from an outdoor hover test of a
Yamauchi GK Lynx Tail rotor.' NASA Technical Memorandum 101057.
Smith CA
Hagen MJ

Simons IA 1967 'The movement, structure and breakdown of trailing vortices
Pacifico RE from a rotor blade.' A.R.C. 28 993.
Jones JP

Smith AC 1987 'Review of helicopter low speed handling problems associated with the tail rotor.' RAE Technical Memorandum FS(B) 683.

Tadghighi H Cheeseman IC	1983	'A study of helicopter rotor noise, with special reference to tail rotors, using an acoustic wind tunnel.' Vertica Vol 7 No 1 pp9-32.
Tarttelin PC	1989	'Rotor loadings in hover - correlation of theory and experiment.' 15th European Rotorcraft Forum, Paper 19.
Tarttelin PC	1990	'Rotor aeromechanics research with the RAE Research Lynx - the experimental facility and test programme.' 16th European Rotorcraft Forum, paper II.7.4.
Van Horn JR	1986	'NOTAR (No Tail Rotor) hover testing using a scale model in water.' 42nd American Helicopter Society Forum.
Vuillet A Morelli F	1986	'New aerodynamic design of the fenestron for improved performance.' 12th European Rotorcraft Forum, paper 8.
Vuillet A	1989	'Operational advantages and power efficiency of the fenestron as compared to a conventional tail rotor.' Vertiflite, Jul/Aug 1989, pp24-29.
Ward LR	1981	'Bell 206B-1 directional control in low airspeed flight.' RAAF ARDU-T1-721.
Weisner W Kohler G	1973	'Tail rotor performance in presence of main rotor, ground and winds.' 29th American Helicopter Society Forum.

Weisner W 1974 'Tail rotor design guide.' USAAMRDL Technical Report
Kohler G 73-99.

Wilby PG 1976 'The aerodynamic Characteristics of a new helicopter tail rotor blade section.' RAE Technical Report 75142.

Yeager WT 1974 'A wind-tunnel investigation of parameters affecting
Young WH helicopter directional control at low speeds in ground effect.'
Mantay WR NASA Technical Note D-7694

Appendix 1.

Lynx AH Mk5 instrumentation.

Sensors were fitted to Lynx AH Mk5 ZD559 for the instrumented tail rotor investigation to monitor the following parameters:

Accelerations: normal, lateral & longitudinal

Airspeed

Altitude

ASE inputs in collective, pitch, roll & yaw

Attitudes: pitch & roll

Compass heading

Control positions: collective, longitudinal & lateral cyclic & pedals

Engine RPMs & Torques

Low air speed sensor data

Main rotor azimuth

Radar altitude

Rates: pitch, roll & yaw

Servo jack positions: collective, longitudinal & lateral cyclic & pedals

Tail rotor: Azimuth

Flap angle

Leading edge pressures at 55, 65, 75, 85, 91, 95 & 98% radii

Trailing edge pressures at 65, 85 & 95% radii

Appendix 2.

Lynx AH Mk5 Flight Trials Instruction.

Flight Systems (Bedford) Department

Building 109

4 March 1991

LYNX INSTRUMENTED TAIL ROTOR BLADE FLIGHT TRIALS

1. GENERAL INFORMATION AND PURPOSE OF TRIAL

1.1 Location. The trial will take place at IAF VILLAFRANCA or other suitable military/MOD airfield.

1.2 Authority for Trial. Helicopter Aeromechanics Section, Flight Systems 1 (Bedford) Dept are the sponsoring authority.

1.3 Cost Code. FS1H 5A2F051

1.4 Sponsor. Lt A D S ELLIN Royal Navy (ext 5367)

1.5 Sponsor's Trial Reference:

1.6 Personnel:

Project Officer Lt A D S ELLIN RN (ext 5367)

Project Pilot Lt Cdr C BROWN RN (ext 5784)

Trials Observers Mr I MANSFELD (ext 5549)

Mr SA PIGHILLS (ext 5204)

In the event of the project officer being unavailable, Mr I MANSFELD (ext 5549)will act on his behalf.

1.7 Purpose of Trial. A standard LYNX Tail Rotor Blade has been modified at RAE Bedford, to incorporate instrumentation, in order to carry out flight trials to investigate the yaw control of the LYNX helicopter throughout the low speed and high speed flight envelopes. The aim is to carry out detailed research on the aerodynamic conditions which exist at the tail rotor in the hover, and during low speed manoeuvres. Tests will be conducted in and out of ground effect, and at various AUWs. Some aerodynamic and aeroacoustic measurements will also be made during steady high speed flight.

1.8 Background. In 1988 a similar trial was flown with the RAE PUMA XW241. It is intended to repeat the trial with the LYNX both before and after Mk7 conversion to study the effects of tail rotor rotational direction and to improve the data base of tail rotor information. Much of the preliminary work carried out with the PUMA still applies.

2. SPECIAL AIRCRAFT OR STORES FIT

A standard LYNX tail rotor blade has been modified to incorporate instrumentation in the form of pressure sensors and strain gauges. Two sets of pressure sensors are fitted - one set along the leading edge at the 2% chord position, sunk into a balsa wood and glasscloth fairing which has been constructed around the leading edge of the blade, and extends along its length, and the second set along the trailing edge, at the 95% chord position, mounted in individual fairings. Both sets are positioned on the upper surface of the blade. A strain gauge array is mounted along the blade.

The balsa fairing extends the blade chord by 5.0mm, but by careful shaping of the fairing, the original RAE 9615 aerodynamic section has been maintained in the nose region. The other three blades, which make up the set, each have similar balsa

fairings constructed along their leading edges, though they have no instrumentation fitted. As all four blades have substantially the same aerodynamic shape as before, there should be no noticeable difference in flying qualities between them and other standard blades.

The signals from the sensors are amplified before being fed through sliprings into the aircraft recording system. A special amplifier can is fitted to the tail rotor pitch change beam for this purpose. A tail rotor torquemeter and external microphone are also fitted to the aircraft.

2.1 Flight Limitations. Normal Flight Limitations apply to flight with the Instrumented Tail Rotor Blade Set, as they should behave exactly as an ordinary blade set. (However, to avoid blocking the sensors, care must be taken when low flying, with regards potential recirculation problems of cut grass, FOD, etc.)

2.2 Weather Limitations. The Instrumented Tail Rotor Blade Set does not have anti-erosion protection strips along the leading edges, and therefore cannot be flown in any form of precipitation. (This includes flight in weather conditions where icing may occur). Liaison with the Meteorological Department for sortie timing and planning will be required.

2.4 Documentation. The following documentation refers to the Instrumented Tail Rotor Blade Set:

RAE Installation Instructions can be found in the following AS1's: No.s - 46,47,56,71,73,79,85,86,87,90,91,104,115,116,117,118,120,124,128

Flight Clearance Form No.559/104 gives all relevant flight clearance information including clearance of the blade set and amplifier can by WHL.

2.5 Other. Where maximum All Up Weight (AUW) is required, ballast is used to reach the required weight condition. This consists of ballast weights fitted at standard attachment points outside the airframe.

3. EXTERNAL REQUIREMENTS

The following facilities are required:

Instrumentation: + A/C MODAS recording system

Other: * Local ATC

* Pace Vehicle with: Wind Vane/Anemometer and indicator

Rope Marker

UHF/VHF Comms

* Marker Boards

* - Not required for every test

+ - Essential for every test

4. OPERATIONAL DETAILS

4.1 Desciption. These trials involve operating the Lynx, fitted with the Instrumented Tail Rotor Blade, in various flight conditions to investigate the aerodynamic environment at the tail rotor during low speed yaw control manoeuvres. These tests, which include both steady trim conditions and translational responses, include: Sideslip Tests, Acceleration Tests, Spot Turns and Agility Tests (specifically Lateral Sidesteps and Hover Turns). High speed flight at varying sideslip angles within the flight envelope will also be flown.

4.2 Trial Conditions. The tests will be made at two weights within the normal range of AUW, both IGE and OGE and with the lateral CG in the mid range. The crew will consist of a minimum of one pilot and one observer. General instructions and details of the test conditions are given at Annex A.

4.2.1 Aircraft Type. Lynx Mk5 ZD559

4.2.2 Aircraft Base. IAF VILLAFRANCA

4.2.3 Height

4.2.4 Speed See Table 1 for a tabulated set of test conditions.

4.2.5 Track

4.2.6 Method of Control. All manoeuvres where aircraft limitations may beapproached eg spot turns and sidesteps, are to be flown incrementally and checked by means of on line kine data (if available), stop watch etc.

4.2.7 Flight Limitations. All tests are to be flown with ASE disengaged, (although some check points with autostabs engaged may be requested), within the normal flight envelope, as defined by LYNX AH Mk1 Aircrew Manual

AP101C-1301-15 and CA(PE) LYNX5/ZD285/A/2 dated 23 May 1986.Where the lack of pitch autostabilisation causes a limitation in the low speed envelope the ASE pitch channel is to be engaged to allow operation in this area. The lateral C of G of the aircraft is to be kept in the mid-range for these trials. The longitudinal C of G is to remain approximately constant for each weight condition throughout the trial. All low flying will take place within the airfield boundary.

4.2.8 Weather Limitations. All tests are to be flown in day, VMC conditions. A max wind speed of 3 kts is required, except where stated otherwise. Due to the

Instrumented Blade set not having leading edge anti-erosion strips, flight is not permitted in precipitation conditions.

4.3 Trial Area. All tests will be flown at IAF VILLAFRANCA, within the airfield boundary or at another specified military/MOD airfield.

4.4 Trial Sequence. The majority of tests involve only the aircraft and aircrew, but where additional support is required (ie pace vehicle etc) the project officer will co-ordinate their actions.

4.5 Communication. In tests using a pace vehicle, the aircraft will maintain radio communication with the vehicle. Frequencies and callsigns will be determined and agreed at the flight briefing.

4.6 Safety Procedures. The helicopter is to be operated using standard safety procedures. Minimum height during test runs is to be 10 feet AGL. Tests which involve flying up to flight envelope boundaries will be incremental in nature, to ensure no limits are exceeded.

4.7 Emergency Procedures. Standard emergency procedures are to be used.

5. RECORDS AND RESULTS

The MODAS flight data recording system will be used for each sortie. In various cases, Kines and/or Telemetry records will also be used. Additionally, the project pilot will be required to submit a written debrief of the sortie content, with pilot handling qualities ratings for several of the tasks. All data analysis will be performed by the project officer.

Annex A

to FTI Number

Lynx 0014

LYNX INSTRUMENTED TAIL ROTOR BLADE FLIGHT TRIALS - TEST CONDITIONS

1. SIDESLIP TEST - AIRCRAFT TRANSLATING

1.1 Description. The aircraft is flown at various sideslip angles around the azimuth, while translating at fixed speeds. The speeds flown cover the range10-30 Kts, in 5 Kt increments, whilst remaining within the low speed flight envelope at all times. Tests are flown both IGE and OGE, at standard and maximum AUW. From this test, aircraft control margins can be determined, and areas of poor, or restricted performance, identified.

1.2 Weather Conditions. Wind speed for this test must be less than 4 Kts .

1.3 Method. As the aircraft ASI is inaccurate at very low speeds and large sideslip angles, a pace vehicle, fitted with an anemometer, is used to set the aircraft velocity. The vehicle will be driven along the runway, trailing a rope marker, remaining clear of the aircraft downwash, while the aircraft keeps station on the marker. The aircraft will fly at 30 degree sideslip angle increments around the azimuth, sideslip angle being maintained using compass headings. Each steady condition, once reached, is held for 10-15 seconds, to enable data to be recorded.

2. ACCELERATION TEST

2.1 Description. The aircraft accelerates laterally, from the hover, at various steady rates of acceleration. The aircraft continues to translate until the limiting flight envelope speed is reached, when the aircraft flies out into a normal

forward flight condition. The pilot must maintain heading, height and attitude during the course of the manoeuvre. The test is repeated for the aircraft accelerating to Port and Starboard, and Aft. All tests are flown both IGE and OGE and at two AUWs. This test is designed to evaluate the ability of the aircraft to maintain heading whilst translating, and to highlight control cross-couplings during the manoeuvre.

2.2 Weather Conditions. Wind speed for this test must be less than 4 Kts .

2.3 Method. The rates of acceleration are set using aircraft attitudes - roll angles when accelerating to Port and Starboard, and pitch angles when accelerating Aft. The aircraft initially hovers, nose into wind, and an input is applied to initiate translation in the desired direction. The required attitude is held until the limiting flight envelope speed is reached in that direction, when the aircraft recovers to the hover. Markers, placed at set distances apart, are used to set the start and end points for each run, to ensure flight envelope limits are not exceeded.

3. SPOT TURNS

3.1 Description. This test consists of several parts: yaw pedal step input responses are examined; steady yaw rates are established for recording trim conditions; and dynamic inputs are applied to the aircraft once steady yaw rate conditions have been achieved. Together, these tests are designed to evaluate the effectiveness of the tail rotor during zero velocity yawing manoeuvres, and to highlight control responses with varying yaw rates. The tests will be flown at maximum AUW, both IGE and OGE, to Port and Starboard.The aircraft is to be flown up to a safe limit of yaw rate, determined by the pilot. Tests will be flown in an incremental manner, the yaw rate being determined by timing complete revolutions with a stop watch.

3.2 Weather Conditions. Wind speed for these tests must be calm, previous trials having shown that results achieved are severely affected by wind.

3.3 Method.

3.3.1 Step Inputs. The aircraft is hovered and a yaw pedal step input, of known magnitude is applied (and held). The aircraft response is recorded until the aircraft reaches either: steady conditions, or a yaw rate which is determined to be a safe limit by the pilot. The test is repeated for various size step inputs both to Port and Starboard.

3.3.2 Steady Yaw Rates. The aircraft is hovered, and the pilot applies the necessary pedal inputs to establish, and maintain, a steady yaw rate. This test is carried out for various steady yaw rates both to Starboard and Port.

4. AGILITY TESTS

With the Instrumented Tail Rotor Blade fitted to the LYNX, it is a good opportunity to fly some well tried Agility Tests previously flown, to examine the aerodynamics of the Tail Rotor during these manoeuvres. Within the low speed flight envelope, the tests which have the greatest yaw channel input are Lateral Sidesteps and Hover Turns, both being similar to tests already being flown (namely Acceleration Tests and Spot Turns). Therefore, it is intended to include tests of these two techniques in this series of flight trials. Quick stops will also be flown.

4.1 LATERAL SIDESTEPS

4.1.1 Description. The aircraft must translate laterally between two markers, a set distance apart, in the shortest time possible. The aircraft begins in the hover at the first marker, accelerates laterally using a set angle of bank, recovering to the hover as the second marker is reached. Different angles of bank are used to set the 'task agression', and the pilot must remainwithin the task constraints while manoeuvring. The test is repeated for different length sidesteps (100 and 200 feet), both to Port and Starboard, IGE and OGE and at two AUWs.

4.1.2 Weather Conditions. Wind for this test must be 10 Kts (mean) or less.

4.2 HOVER TURNS

4.2.1 Description. The aircraft hovers over a fixed point, and changes heading a set amount, by applying a yaw pedal input, recovering to a stable hover on the new heading on completion. The pilot attempts to complete the manoeuvre in the minimum possible time for each condition. The heading change is set by markers and the test repeated for different sized heading changes and different sized yaw pedal inputs. The test is flown to Port and Starboard, and repeated both IGE and OGE, and at two AUWs.

4.2.2 Weather Conditions. This test will be repeated for two wind conditions: 0-3 Kts (max), and 10 Kts (mean) to assess the different handling qualities under the two conditions.

5. HIGH SPEED FLIGHT

High speed flight tests will be flown to look at tail rotor airflow and acoustic signature. The aircraft will be flown in straight and level flight at 100ft along the duty runway at three speeds and 2 different AUWs. For each condition 3 passes will be made in the same direction:

1st pass: Balanced flight

2nd pass: Flight with 30kt left sideslip component.

3rd pass: Flight with 30kt right sideslip component.

The sideslip angle required for these conditions will be calculated before flight and this angle added to or subtracted from the aircraft compass heading whilst maintaining track along the runway.

TABLE 1. Tail rotor investigation - test points to be flown.

Time	Weight	Height	Wind	
1.00	Std	A/R	10	Shake down flying - See FTI lynx 426
0.30	Std	A/R	10	Practice sideslips
1.00	Std	OGE	3	(Sideslips with sideslip angles varying
1.00	Std	IGE	3	(from 0 to 360 degrees in 30 degree steps
1.00	Max	OGE	3	(at speeds of 10,15,20,25 & 30 Knots.
1.00	Max	IGE	3	(
0.45	Std	OGE	3	((Sideslips with sideslip angles varying
0.45	Std	IGE	3	((between 030 & 100 degrees in 10 degree
0.45	Max	OGE	3	((steps at speeds of 10,15,20,25 & 30
0.45	Max	IGE	3	((Knots.
1.00	A/R	A/R	3	Repeat points as required
0.30	Std	A/R	10	Practice sidestep accels
1.00	Std	OGE	3	(Sidestep accels flown to port,starboard
1.00	Std	IGE	3	(& backwards, accelerating to 30 knots
1.00	Max	OGE	3	(with bank angles of 10,20,30 & 40 degrees.
1,00	Max	IGE	3	(

0.30 Std A/R 5 Practice hover turns & spot turns

1.00 Std OGE Calm (In each condition, carry out: Pure Hover,

1.00 Std IGE Calm (Pedal step inputs port/stbd with W,X,Y,Z%

1.00 Max OGE Calm (pedal, Steady turn rates port & starboard

1.00 Max IGE Calm (with turn rates of 20,30,40,50&60 Deg/sec.

1.00 Std OGE 10 (High speed flight with full left & right

1.00 Max OGE 10 (& no sideslip flown at 100,120 & 140 Knots.

0.30 Std A/R 10 Practice sidesteps

1.00 Std OGE/IGE 10 (Sidesteps over 100 & 200 ft with bank

1.00 Max OGE/IGE 10 (angles of 10,20,30 & 40 degrees.

0.30 Std OGE/IGE Calm (Hover turns through 45,90 & 180 degrees

0.30 Max OGE/IGE Calm (

Notes:

1 The flights may take place in any order with the low wind speed conditions taking precedence. Steady nil wind hover OGE takes precedence over all.

2 If the wind conditions change during a flight, alter points flown accordingly.

3 Flights requiring acoustic recording may need to be blocked together.

Appendix 3. Summary of data collected.

Tables 1 - 11 of this appendix list the flight conditions for which data was collected during the experiment. For each condition where data was recorded the flight number and event within that flight are given as (flight number/event number). Some flight conditions were recorded more than once.

It is worth noting that, if a flight condition appears to be missing from a sequence in the tables, it may not have been possible to hold that condition to allow a steady trimmed flight recording to be made. This is especially true in the region of reduced pedal margin during flight with starboard quartering winds. It is, however, likely that the attempts made to establish that condition were recorded and could be extracted from the flight tape if required.

Appendix 3 Table 1 Sideslips OGE Light.

	5 kts	10 kts	15 kts	20 kts	25 kts	30 kts
000	241/101 242/1	231/46 241/89	231/34 241/76	225/17 227/26 231/23 241/3 242/13 241/65	227/14 231/12 241/14 242/25 241/54	225/13 227/2 231/1 241/25 242/37 241/36
010				231/24 241/4	231/13 241/15	231/2 241/26
020				231/25 241/5	231/14 241/16	231/3 241/27
030	242/2 241/102	231/47 241/90	231/35 241/77	227/27 231/26 241/6 242/14	227/15 231/15 241/17 242/26	227/3 231/4 241/28 242/38
040				231/27 241/7	231/16 241/18	231/5 241/29
050				231/28 241/8	231/17 241/19	231/6 241/30
060	242/3 241/103	231/48 241/91	231/36 241/78	227/29 231/29 241/9 242/15	227/16 241/20 231/18 242/27	227/4 241/31 231/7 242/39
070				231/30 241/13	231/19 241/21	231/8 241/32
080				231/31 241/12	231/20 241/22	231/9 241/33
090	242/4 241/104	231/49 241/92	231/37 241/79	225/19 231/32 241/10 227/30 242/16	227/17 241/23 231/21 242/28	225/15 231/10 242/40 227/5 241/34
100				231/33 241/11	231/22 241/24	231/11
120	242/5	231/50 241/93	231/38 241/80	227/31 242/17	227/18 242/29	227/6 242/41
150	242/6	231/51 241/94	231/39 241/81	227/32 242/18	227/19 242/30	227/7 242/42
180	242/7	231/52 241/95	231/40 241/82	225/20 242/19 227/33	227/20 242/31	225/16 242/43 227/8
210	242/8	231/53 241/96	231/41 241/83	227/34 242/20	227/21 242/32	227/9 242/44
240	242/9	231/54 241/97	231/42 241/84	227/35 242/21	227/22 242/33	227/10 242/45
260				241/75	241/64	
270	242/10	231/55 241/98	231/43 241/85	225/18 242/22 227/36 421/74	227/23 242/34 241/63	225/14 242/46 227/11..241/45
280				241/73	241/62	241/44
290				241/72	241/61	241/43
300	242/11	231/56 241/99	231/44 241/87	227/37 242/23 241/71	227/24 242/35 241/60	227/12 242/47 241/42
310				241/70	241/59	241/41
320				241/69	241/58	241/40
330	242/12	231/57 241/100	231/45 241/88	227/38 242/24 241/68	227/25 242/36 241/57	227/13 242/48 241/39
340				241/67	241/56	241/38
350				241/66	241/55	241/37

Appendix 3 Table 2 Sideslips OGE Heavy

	5 kts	10 kts	15 kts	20 kts	25 kts	25 kts
000	239/1	230/46 239/13	230/34 239/26	226/28 239/38 230/24 240/1 243/1	226/16 239/51 230/14 240/10 243/12	226/4 239/63 230/3 240/21 243/23
010				230/25 240/2	230/15 240/11	230/4 240/22
020				230/26 240/3	230/16 240/12	230/5 240/23
030	239/2	230/47 239/14	230/35 239/27	226/29 239/39 230/27 240/4	226/17 239/52 230/17 240/13	226/5 239/64 230/6 240/24
040				230/28 240/9	230/18 240/14	230/7 240/31
050				230/29	230/19 240/15	230/8 240/30
060	239/3	230/48 239/15	230/36 239/28	226/30 239/41	226/18 239/54	226/6 239/65 230/9 240/29
070				230/33 240/8	230/23 240/20	230/13 240/28
080				230/32 240/7	230/22 240/19	230/12 240/27
090	239/4	230/49 239/16	230/37 239/29	226/31 239/40 230/30 240/5	226/19 239/53 230/20 240/16 240/17	226/7 239/66 230/10 240/25
100				230/31 240/6	230/21 240/18	230/11 240/26
120	239/5	230/50 239/17	230/38 239/30	226/32 239/42	226/20 239/55	226/8 239/67
150	239/6	230/51 239/18	230/39 239/31	226/33 239/43	226/21 239/56	226/9 239/68
180	239/7	230/52 239/19	230/40 239/32	226/34 239/44	226/22 239/57	226/10 239/69
210	239/8	230/53 239/20	230/41 239/33	226/35 239/45	226/23 239/58	226/15 239/70
240	239/9	230/54 239/21 239/22	230/42 239/34	226/36 239/47	226/24 239/59	226/14 239/71
260				243/11	243/22	243/33
270	239/10	230/55 230/56 239/23	230/43 239/35	226/37 239/48 243/10	226/25 239/60 243/21	226/13 239/72 243/32
280				243/9	243/20	243/31
290				243/8	243/19	243/30
300	239/11	230/57 239/24	230/44 239/36	226/38 239/49 243/7	226/40 239/61 243/18	226/12 239/73 243/29
310				243/6	243/17	243/28
320				243/5	243/16	243/27
330	239/12	230/58 239/25	230/45 239/37	226/39 239/50 243/4	226/41 239/62 243/15	226/11 239/74 243/26
340				243/3	243/14	243/25
350				243/2	243/13	243/24

Appendix 3 Table 3 Sideslips IGE Light

	5 kts	10 kts	15 kts	20 kts	25 kts	30 kts
000	246/3	233/37 246/15	233/49 247/27	233/25 233/61 246/39 246/94 247/3	233/14 233/73 246/50 246/83 247/16	233/3 233/85 246/61 246/72 247/28
010				233/26 246/95	233/15 246/84	233/4 246/73
020				233/27 246/96	233/16 246/85	233/5 246/74
030	246/4	233/38 246/16	233/50 246/28	233/28 233/62 246/97 247/4	233/17 233/74 246/86 247/17	233/6 233/86 246/75 247/29
040				233/29 246/98	233/18 246/87	233/7 246/76
050				233/30 246/99	233/19 246/88	233/8 246/77
060	246/5	233/39 246/17	233/51 246/29	233/31 233/63 246/100 247/5	233/20 233/75 246/89 247/18	233/9 233/87 246/78 247/31
070				233/32 246/101	233/21 246/90	233/10 246/79
080				233/33 246/102	233/22 246/91	233/11 246/80
090	246/6	233/40 246/18	233/52 246/30	233/34 233/35 233/64 246/103 247/6	233/23 233/76 246/92 247/19	233/12 233/88 246/81 247/30
100				233/36 246/104	233/24 246/93	233/13 246/82
120	246/7	233/41 246/19	233/53 246/31	233/65 247/8	233/77 247/20	233/89 247/32
150	246/8	233/42 246/20	233/54 246/32	233/66 247/9	233/78 247/21	234/1 247/33
180	246/9	233/43 246/21	233/55 246/33	233/67 247/10	233/79 247/22	234/2 237/34
210	246/10	233/44 246/22	233/56 246/34	233/68 247/11	233/80 247/23	234/3 234/4 247/35
240	246/11	233/45 246/23	233/57 246/35	233/69 247/12	233/81 247/24	234/5 247/36
260				246/49	246/60	246/71
270	246/12	233/46 246/24	233/58 246/36	233/70 246/48 247/13	233/82 246/59 247/25	234/6 246/70 247/37
280				246/47	246/58	246/69
290				246/46	246/57	246/68
300	246/13	233/47 246/25	233/59 246/37	233/71 246/45 247/14	233/83 246/56 247/26	234/7 246/67 247/38
310				246/44	246/55	246/66
320				246/43	246/54	246/65
330	246/14	233/48 246/26	233/60 246/38	233/72 246/42 247/15	233/84 246/53 247/27	234/8 246/64 247/39
340				246/41	246/52	246/63
350				246/40	246/51	246/62

Appendix 3 Table 4 Sideslips IGE Heavy

	5 kts	10 kts	15 kts	20 kts	25 kts	30 kts
000	245/2	232/2 245/14	232/14 245/26	232/26 243/58 236/2 243/71 244/37	232/38 243/46 236/11 243/80 244/23	232/49 243/34 236/19 244/1 243/90 244/12
010				236/3 243/72	236/12 243/81	236/20 244/2 243/91
020				236/4 243/73	236/13 243/82	236/21 244/3 243/92
030	245/3	232/3 245/15	232/15 245/27	232/27 243/59 236/5 243/74	232/39 243/47 236/14 243/83	232/50 244/4 243/35 236/22 243/94
040				236/6 243/75	236/15 243/84	236/23 244/5 243/94
050				236/7	243/85	236/24 244/6 243/95
060	245/4	232/4 245/16	232/16 245/28	232/28 243/62 243/79	243/49	232/51 244/11 236/25 243/96
070					243/89	236/26 244/10
080				236/9 243/78	236/17 243/88	236/27 244/9
090	245/5	232/5 245/17	232/17 245/29	232/29 243/61 236/8 243/76	232/40 243/48 236/16 243/86	232/52 244/7 243/36 243/97 236/28
100				236/10 243/77	236/18 243/87	236/29 244/8 243/98
120	245/6	232/6 245/18	232/18 245/30	232/30 243/63	232/41 243/50	232/53 243/37
150	245/7	232/7 245/19	232/19 245/31	232/31 243/64	232/42 243/51	232/54 243/39
180	245/8	232/8 245/20	232/20 245/32	232/32 243/65	232/43 243/52	232/55 243/40
210	245/9	232/9 245/21	232/21 245/33	232/33 243/66	232/44 243/53	232/56 243/41
240	245/10	232/10 245/22	232/22 245/34	232/34 243/67	232/45 243/54	232/57 243/42
260				244/47	244/33	244/22
270	245/11	232/11 245/23	232/23 245/35	232/35 243/68 244/46	232/46 243/55 244/32	232/58 243/43 244/21
280				244/45	244/31	244/20
290				244/44	244/30	244/19
300	245/12	232/12 245/24	232/24 245/36	232/36 243/69 244/43	232/47 243/56 244/29	232/59 243/44 244/18
310				244/42	244/28	244/17
320				244/41	244/27	244/16
330	245/13	232/13 245/25	232/25 245/37	232/37 243/70 244/40	232/48 243/57 244/26	232/60 232/45 244/15
340				244/39	244/25	244/14
350				244/38	244/24	244/13

Appendix 3 Table 5 Hovers

OGE LIGHT	OGE HEAVY	IGE LIGHT	IGE HEAVY
225/3	224/5	233/2	236/1
227/1	226/3	238/1	245/1
229/2	226/42	246/2	
241/2	228/2	247/2	
242/61	230/2		
	240/43		

Appendix 3 Table 6 Spot-turns

		10°/SEC	20°/SEC	30°/SEC	40°/SEC	50°/SEC	60°/SEC
OGE LIGHT	LEFT	231/58 242/49	231/59 242/50	231/60 242/51	231/61 242/52	231/62 242/53	231/63 242/54
	RIGHT	231/64 242/55	231/65 242/56	231/66 242/57	231/67 242/58	231/68 242/59	231/69 242/60
OGE HEAVY	LEFT	240/37	230/60 240/38	230/61 240/39	230/62 240/40	230/63 240/41	230/64 240/42
	RIGHT	230/67 240/32	230/68 240/33	230/69 240/34	230/70 240/35	230/71 240/36	230/72 240/36
IGE LIGHT	LEFT	238/2 247/40	238/3 247/41	238/4 247/42	238/5 247/43	238/6 247/44	238/7 247/45
	RIGHT	238/8 247/46	238/9 247/47	238/10 247/48	238/11 247/49	238/12 247/50	238/13 247/51
IGE HEAVY	LEFT	236/30 245/38	236/31 245/39	236/32 245/40	236/33 245/41	236/34 245/42	236/35 245/43
	RIGHT	236/36 245/44	236/37 245/45	236/38 245/46	236/39 245/47	236/40 245/48	236/41 245/50

Appendix 3 Table 7 200ft Side-steps

		10°AOB	20°AOB	30°AOB	40°AOB
OGE LIGHT	LEFT	238/23	238/25	238/27	238/29
	RIGHT	238/22	238/24	238/26	238/28
OGE HEAVY	LEFT	237/10	237/12	237/14	237/16
	RIGHT	237/9	237/11	237/13	237/15
IGE LIGHT	LEFT	234/10	234/12	234/14	234/16
	RIGHT	234/9	234/11	234/13	234/15
IGE HEAVY	LEFT	237/2	237/4	237/6	237/8
	RIGHT	237/1	237/3	237/5	237/7

Appendix 3 Table 8 Side-step Accelerations

		10¤AOB	20¤AOB	30¤AOB	40¤AOB
OGE LIGHT	LEFT	229/4 229/12	229/6 229/14	229/8 229/16	229/10 229/18
	RIGHT	229/3 229/11	229/5 229/13	229/7 229/15	229/9 229/17
OGE HEAVY	LEFT	228/4 237/48 228/12	228/6 228/14 27/50	228/8 228/16 237/52	228/10 228/18 237/53
	RIGHT	228/3 228/11 228/13 237/47	228/5 228/15 237/49	228/7 237/51	228/9 228/17
IGE LIGHT	LEFT	238/15	238/17	238/19	238/21
	RIGHT	238/14	238/16	238/18	238/20
IGE HEAVY	LEFT	236/43 237/55	236/45 237/57	236/47 237/59	236/49 237/60
	RIGHT	236/42 237/54	236/44 237/56	236/46 237/58	236/48

Appendix 3 Table 9 200ft Back-hops

	5¤ Nose up	10¤ Nose up	15¤ Nose up	20¤ Nose up	25¤ Nose up
OGE LIGHT	238/30	238/31	238/32	238/33	238/34
OGE HEAVY	237/17	237/18	237/19	237/20	237/21
IGE LIGHT	234/17	234/18	234/19	234/20	234/21
IGE HEAVY	236/50	236/51	236/52	236/53	236/54

Appendix 3 Table 10 Rearward Accelerations

	5¤ Nose up	10¤ Nose up	15¤ Nose up	20¤ Nose up	25¤ Nose up
OGE LIGHT	238/35	238/36	238/37	238/38	238/39
OGE HEAVY	237/22	237/23	237/24	237/25	237/26
IGE LIGHT	247/52	247/53	247/54	247/55	247/56
IGE HEAVY	236/55	236/56	236/57	236/58	236/59

Appendix 3 Table 11 High Speed Flight

	Sideslip	80 kts	100 kts	120 kts	140 kts
OGE LIGHT	NIL	234/24 234/28 234/26	234/29 234/33 234/31	234/34 234/36 234/38	234/39 234/41 234/43
	LEFT	225/6 234/25	225/7 234/30	225/9 234/35	225/11 234/40
	RIGHT	225/5 234/27	225/8 234/32	225/10 234/37	225/12 234/42
OGE HEAVY	NIL	237/27 237/29 237/31	237/32 237/34 237/36	237/37 237/39 237/41	237/42 237/44 237/46
	LEFT	224/6 237/28	224/8 237/33	224/10 237/38	224/12 237/43
	RIGHT	224/7 237/30	224/9 237/35	224/11 237/40	224/13 237/45

Appendix 4.

The design of the Lynx AH Mk7 instrumented tail rotor blade and thrust sensor.

The blade.

The pressure instrumented tail rotor blade for the Lynx AH Mk7 has been designed in the light of the experienced gained in the manufacture and operation of the instrumented blade used in the trial with the Lynx AH Mk5. The Mk5 blade had various shortcomings; these were as follows:

1. There was no method of directly deducing the local chordwise velocity from the blade instrumentation. Due to time constraints, the design of the instrumentation was based on that used on the Puma which had been a direct copy of that used on the main rotor. It was not until the blade was being instrumented that the problems of velocity measurement were examined and solutions developed.

2. Owing to the conventional metal construction of the blade, the pressure sensors had to be mounted on the blade surface with the leading edge shape restored by means of a balsa wood fairing. All four blades had to be fitted with similar fairings which increased the effort required to prepare the tail rotor for the trial considerably. Had four old blades not been available, the trial cost would also have been significantly increased. As well as slightly modifying the blade aerofoil section, the fairings proved to be highly susceptible to damage from small stones blown up from the hardstanding.

3. Problems were experienced in the operation of the blade in that the loom connecting the instrumented tail rotor blade to the amplifier assembly on the pitch change beam was inadequately secured. The PRC covering the loom was continually in need replacement with consequent three day delays whilst the PRC cured. This problem was exacerbated by the fact that the PRC was disturbed whenever the blade attachment bolts were removed.

As currently schemed, the design of the instrumentation for the Mk7 blade should partially or totally overcome these problems.

The problem of direct measurement of local chordwise velocity over the length of the instrumented blade was initially considered during the investigation of the data collected on the Puma. Since that time a technique for recording that velocity has been developed (see section 2.4.2) and it is considered that this should be incorporated on the Mk7 blade. This technique required an additional sensor to be placed on the top surface of the blade at 50% chord. There are sufficient amplifier channels to permit thirty pressure sensors to be fitted to the blade. This will enable nine sensors to be fitted to the blade top surface at 2% chord, nine to be fitted to the top surface at 50% chord and nine more to the top surface at close to the trailing edge.It is considered that the remaining three sensors should be fitted on the lower surface at 50% chord. The working section of the Mk7 blade only covers the outer half of the blade radius. Nine equally spaced stations within this length will result in a distance between sensors of approximately 65mm. It is considered that there is more to be gained from the sensors being equally spaced, allowing the various interactions to be better investigated, than in concentrating the sensors towards the tip to provide more detail of the tip loading peak; this should be adequately covered with the 65mm sensor separation proposed. The 3 lower surface sensors should be evenly spaced along the blade at the same radial

stations as the 2nd, 5th and 8th upper surface sensors. The proposed sensor layout is shown at figure A4.1

The basic tail rotor blade on the Lynx AH Mk7 is of composite construction. Once it has been laid up on an inflatable bag mandrel, the blade core is given its final shape by being baked in an autoclave in an accurately machined female aluminium mold. Consultation with the Composite Manufacturing Facility at Westland Helicopters Limited has shown that it is, in principle, possible to introduce minor deviations from this shape by temporarily securing metal strips to the inside of the mold. The depressions thus induced in the shape of the core should permit all the pressure sensors save those at the trailing edge to be mounted within the profile of the original blade surface. This will therefore do away with the requirement for the balsa wood fairing, thus greatly reducing the work required to prepare for the trial. It may still prove necessary to modify two blades as the weight increase on the instrumented blade may be beyond the scope of the adjustment permitted on the tip weights.

Details of the four depressions required are shown in Figure A4.2 and are as follows:

A. Back to a line normal to the top surface at 2% chord on full section. 1.5 mm maximum depth.

B. Same thickness as leading edge stainless steel strip back to 34mm behind leading edge of blade core and thence back to original surface via 5mm minimum radii.

C. Full depth 1.5mm from 75mm to 90mm behind leading edge of blade core. Either side faired back to original surface via 5mm minimum radii.

D. Full depth 1.5mm from 70mm to 105mm behind leading edge of blade core. Either side faired back to original surface via 5mm minimum radii.

The sensors at the 2% chord position should be cylindrical rather than flat and mounted in holes drilled right through the blade; the hole centreline being normal to the blade surface at the top surface. So that the wires can be buried within the profile, the stainless steel anti-erosion shield should be cut from the lower surface hole back to its rear edge. Westlands advise that this will not affect the lag stiffness of the blade.

The wires to the trailing edge sensors should run aft along the lower surface of the blade and round the trailing edge and given the minimum thickness of protective fairing.

It should be possible to mount all the temperature compensating resistors and all joints within the wiring on two printed circuit boards mounted on the top and bottom of the blade at the root end. If a multi-layered PCB is used, one layer would be for the signal tracks, one for the positive supply and the third, the negative supply. By cutting holes in the PCB, it should be possible to substantially bury the resistors in the thickness of the board. The PCBs will have to be bonded to the blade surface as no reduction of the blade thickness can be tolerated at the root. This should not affect the aerodynamic properties of the blade as it has a bluff leading edge at this point.

Although the aerodynamic shape of the blade has not been affect, its weight and balance has. Advice should be taken from Westlands as to the rectification required. It may be deemed necessary to balance all the blades to a heavier datum.

The thrust sensor.

When conducting main rotor research, it is possible to compare the integrated main rotor loading with the aircraft weight and load factor to determine the accuracy of the loading calculations. As the tail rotor does not provide all the moment required to balance the main rotor torque, this same procedure cannot be followed. An alternative method of deriving tail rotor thrust must therefore be schemed.

From study of the drawings of the Lynx AH Mk7 tail rotor hub and gearbox, it is apparent that the tail rotor thrust is transmitted from the hub to a lip on the gearbox output drive shaft via a seal ring (figure A4.3). If this ring were to be extended outboard and the hub reduced accordingly, it should be possible to mount strain gauges on the exposed portion of the ring and thus measure the compression forces it experiences. As a small proportion of the thrust is transmitted via to the hub nut to the end of the output drive shaft, it is thought that the tail rotor thrust should be measurable within 5% by this arrangement. This should then permit the accuracy of the thrust calculated from the pressure sensors to be assessed.

Appendix 5.

Principle Puma & Lynx AH Mk 5 frequencies.

The principle frequencies of interest for the Puma and Lynx AH Mk5 are tabulated below. The frequencies given may differ slightly from those seen in the figures if the main rotor speed was not precisely set at the value laid down in the aircrew manual. The ratio between the various frequencies and the main rotor speed, 1R, should, however, be as given below:

	Puma		Lynx Mk5	
	Hz	x 1R	Hz	x 1R
1R	4.42	1.0	5.3	1.0
4R	17.7	4.0	21.2	4.0
1T	21.3	4.83	30.7	5.8
8R	35.3	8.0	42.4	8.0
2T	42.6	9.66	61.3	11.6
12R	53.0	12.0	63.6	12.0
3T	63.9	14.49	92.0	17.3
4T	85.2	19.32	122.6	23.1

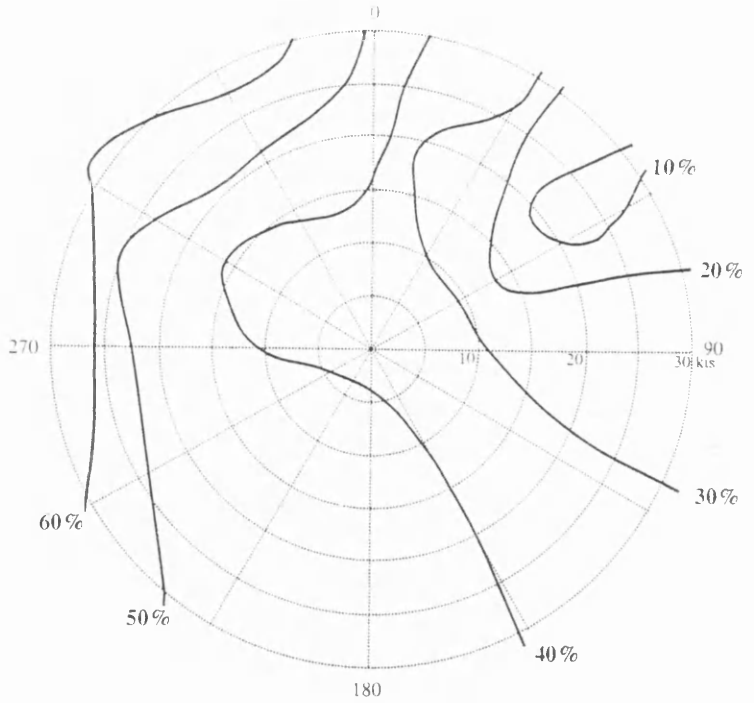

Figure1.1.1 Plot showing the variation in yaw control margin for changes in relative wind speed and direction for the Lynx AH Mk5 recorded during the flight trial. Aircraft all up mass is 4700kg.

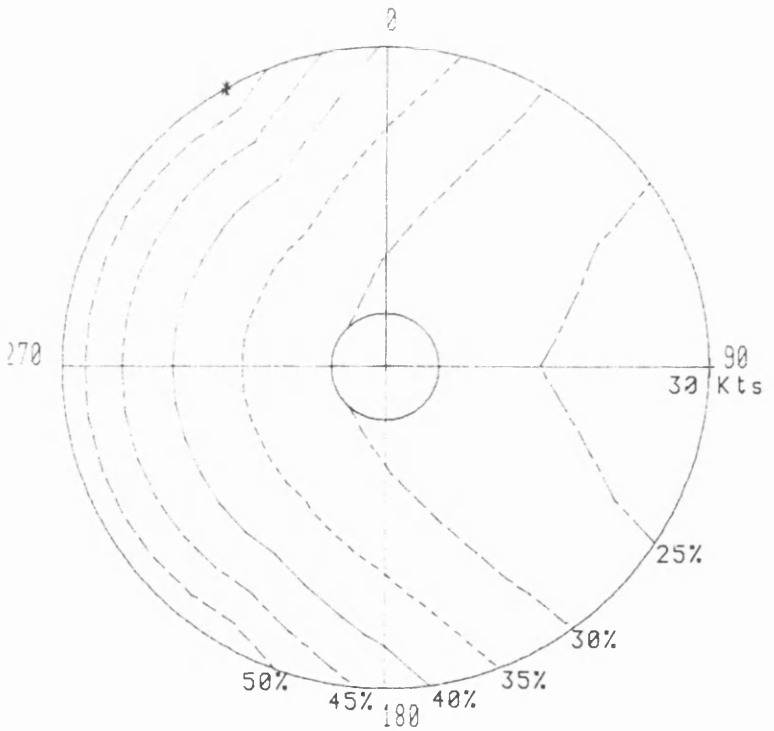

Figure1.1.2 Plot showing the variation in yaw control margin for changes in relative wind speed and direction as calculated by Helistab when configured as a Lynx AH Mk5.

Figure 1.3.1 RAE Bedford Flight Research Puma

Figure 1.4.1 RAE Bedford Flight Research Lynx AH Mk5

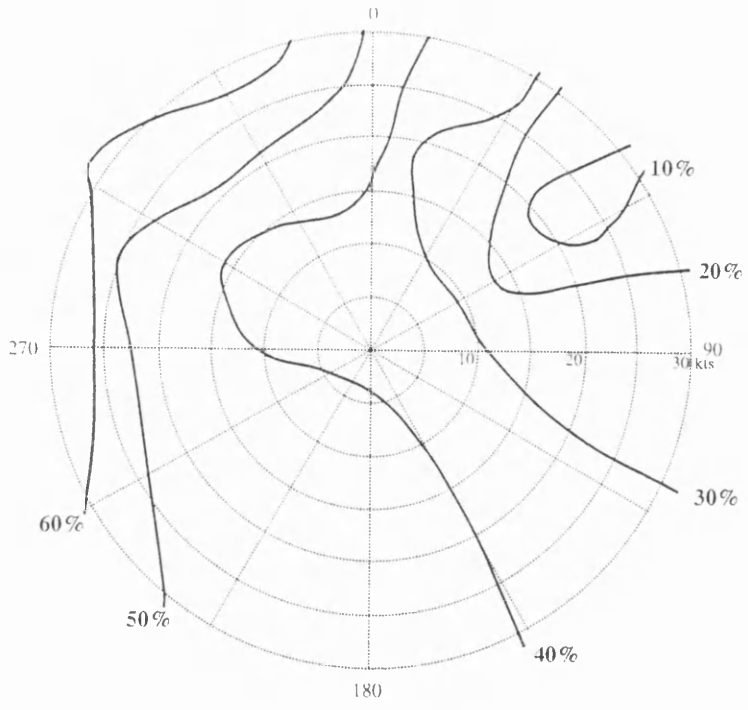

Figure 1.1.1 Repeated for ease of comparison.

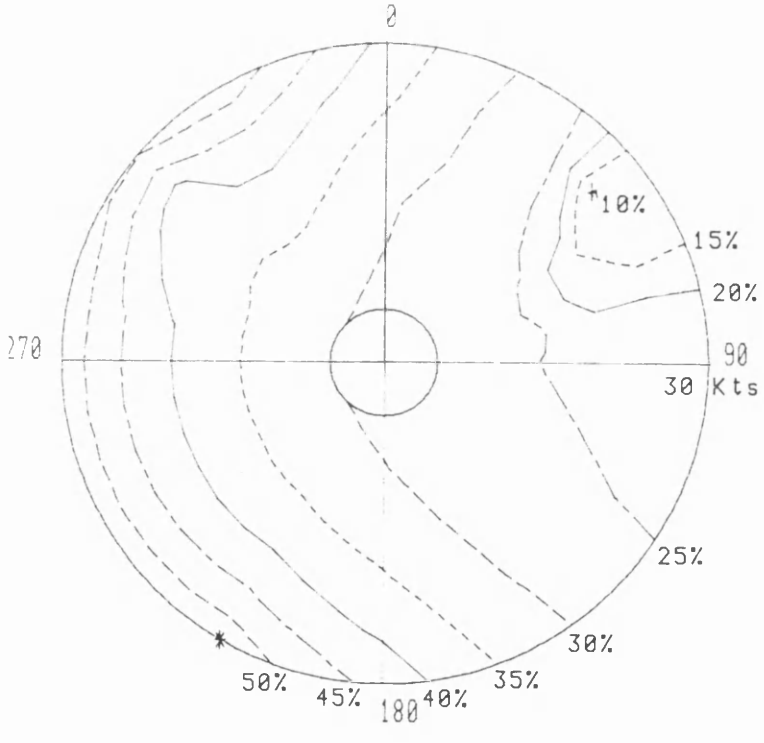

Figure 1.4.2 Plot showing the variation in yaw control margin for changes in relative wind speed and direction as calculated by Helistab when modified with the Beddoes main rotor wake model.

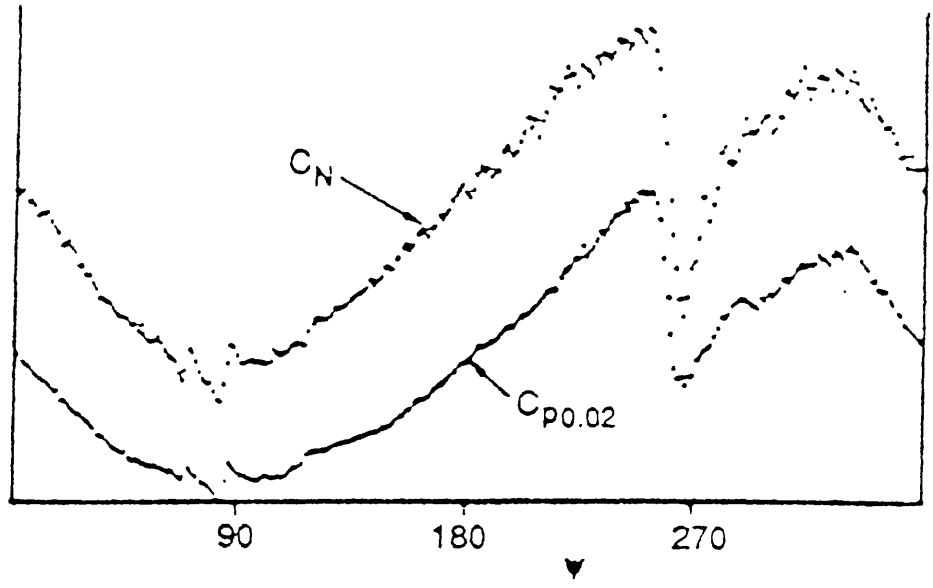

Figure2.3.1 **Comparison between normal force coefficient and leading edge pressure coefficient.**

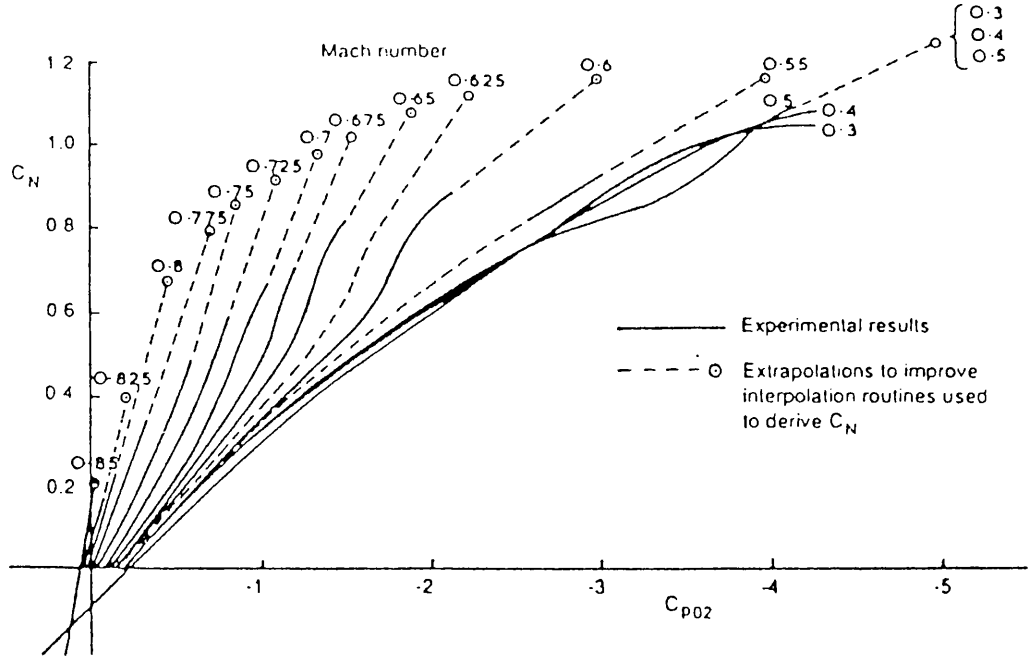

Figure2.3.2 **Correlation between lift and upper surface pressure coefficient at 2% chord derived from steady wind tunnel tests of NACA 0012 profile.**

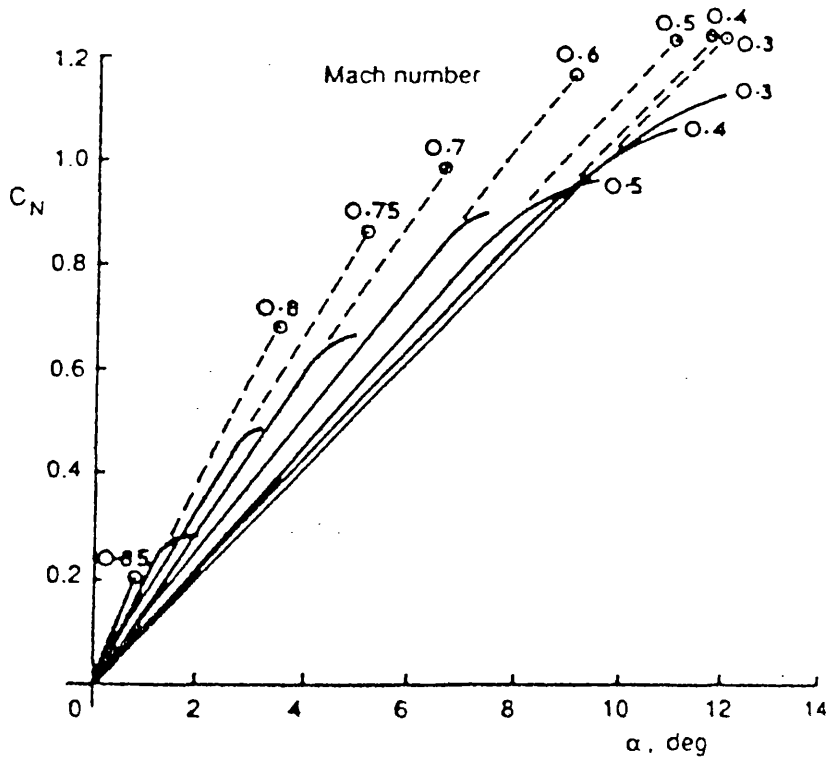

Figure2.3.3 **Correlation between lift and incidence derived from steady wind tunnel tests of NACA 0012 profile.**

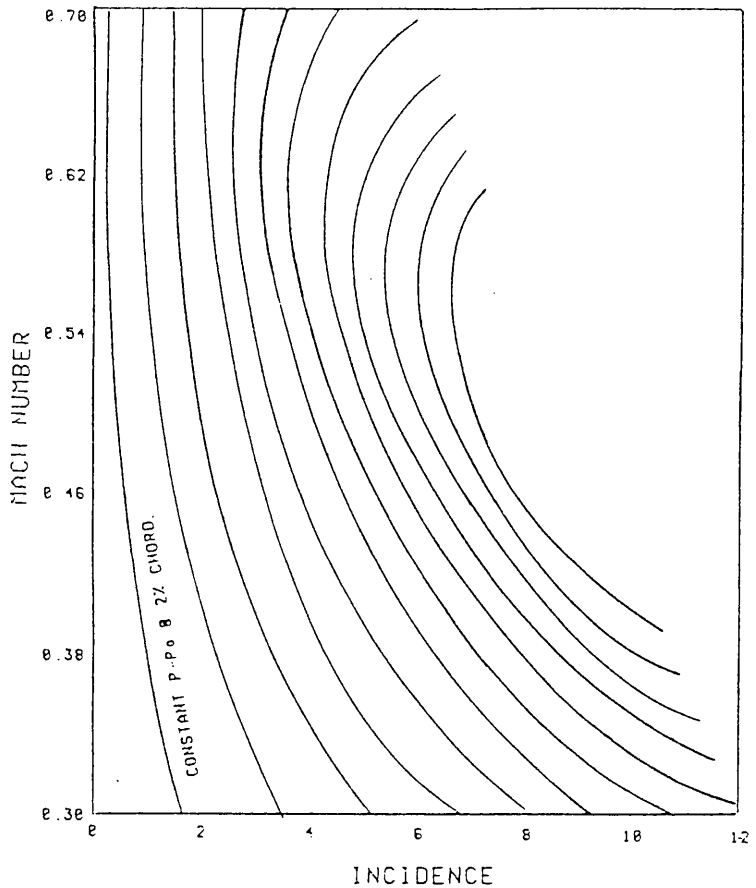

Figure2.4.2.1 Lines of constant dynamic head for sensor at 2% chord on the upper surface of NACA 0012 section.

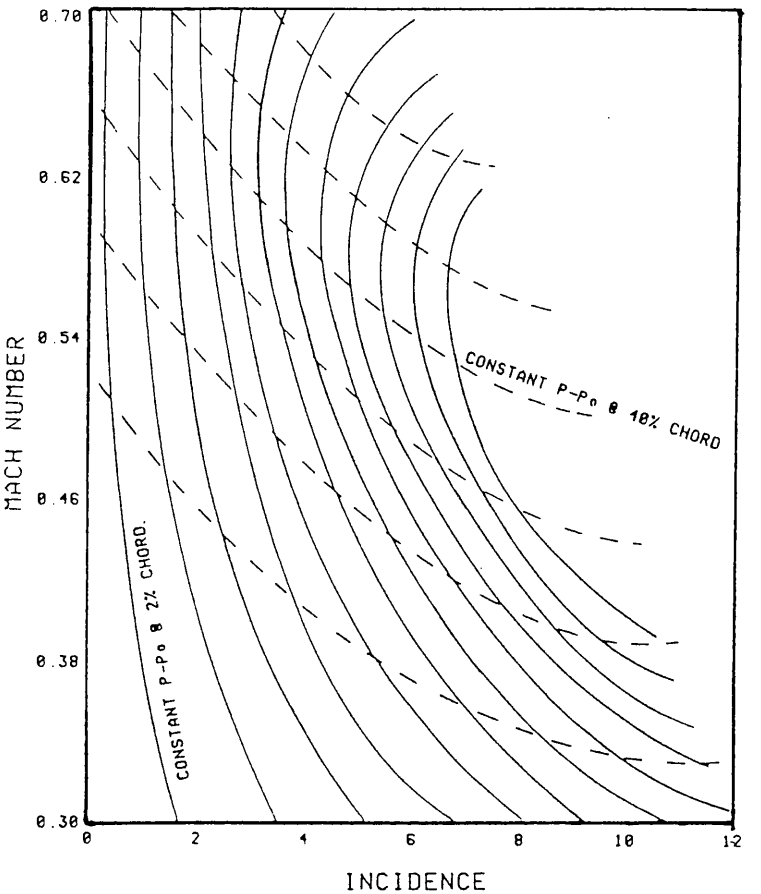

Figure2.4.2.2 Lines of constant dynamic head for sensors at 2% & 50% chord on the upper surface of NACA 0012 section showing unique nature of intercepts.

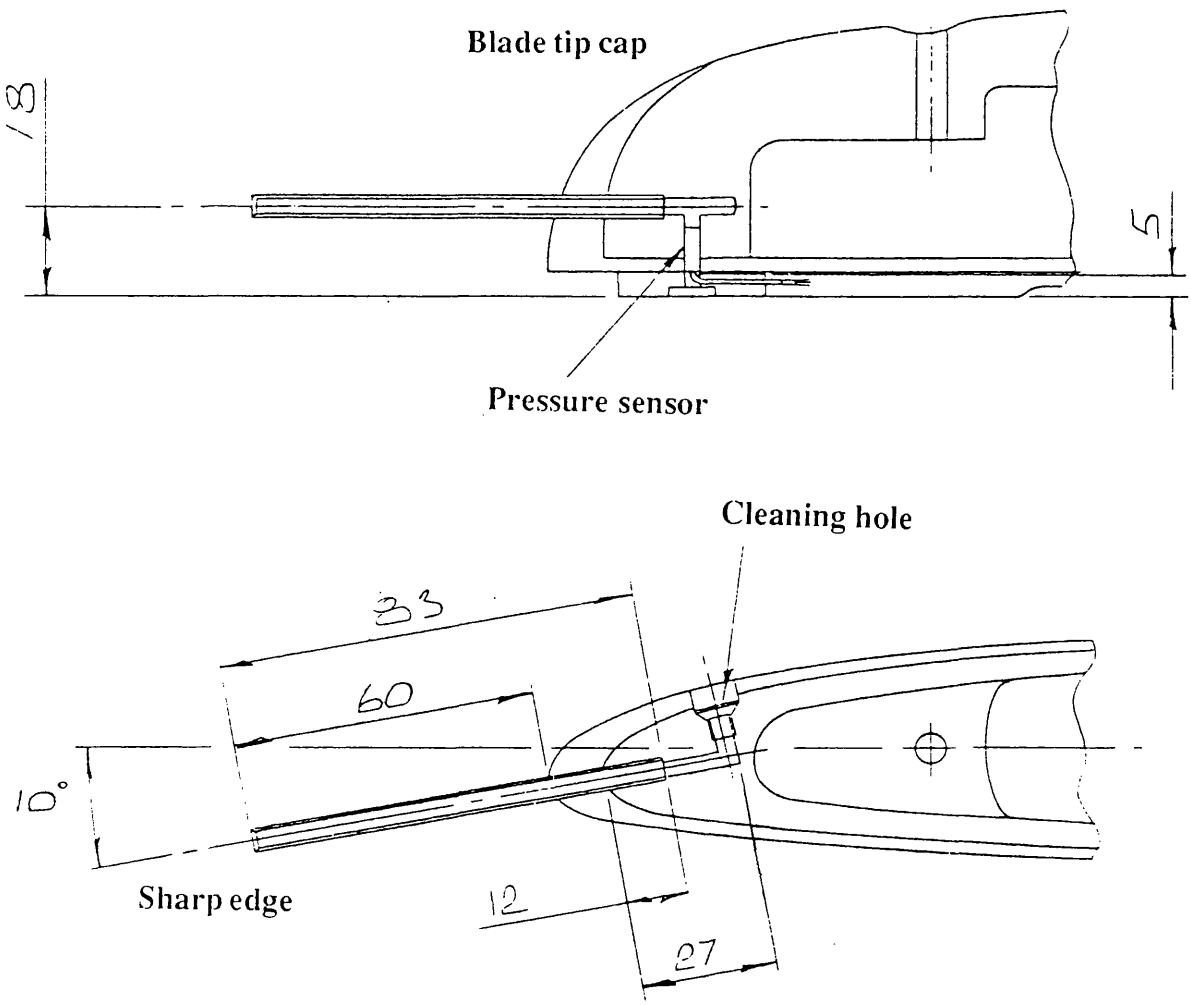

Figure2.4.3.1 Drawing of main rotor blade tip pitot fitted to Lynx AH Mk5 ZD559.

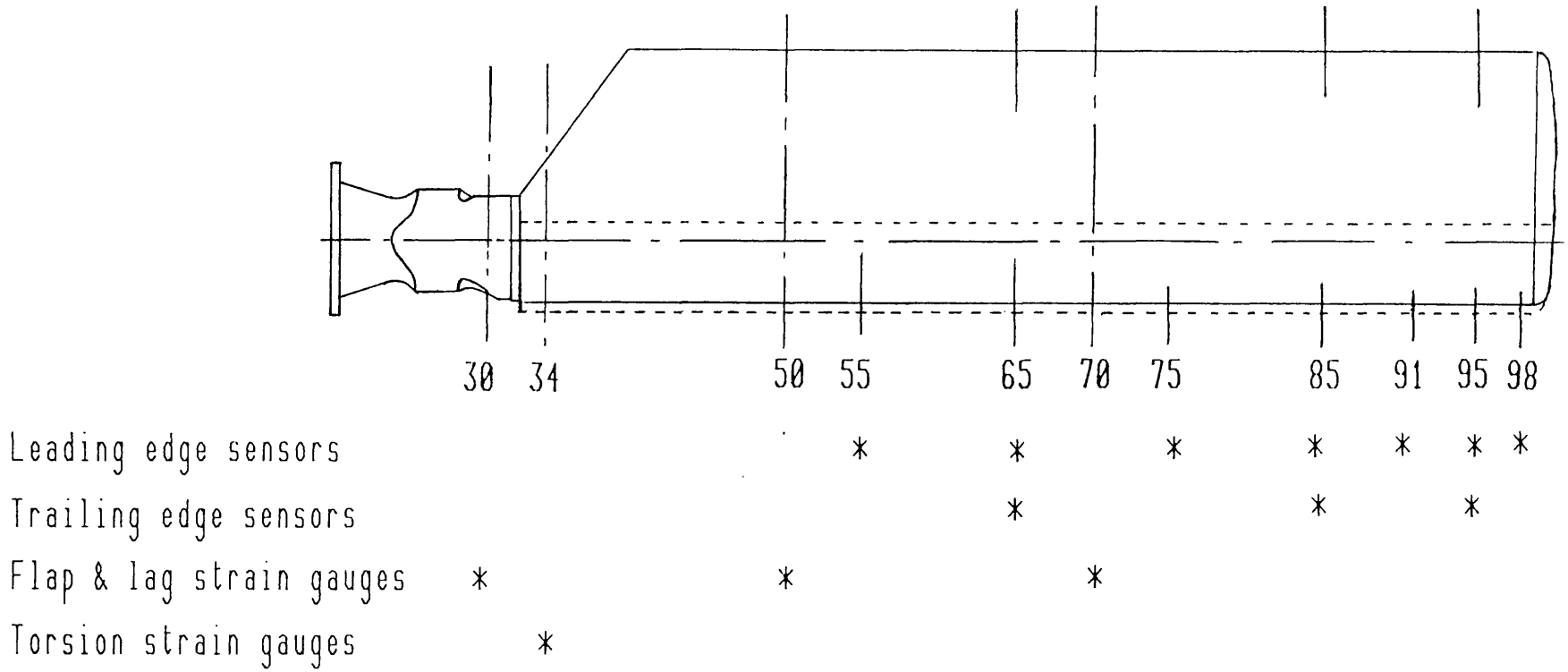

Figure2.5.1 Lynx AH Mk5 instrumented tail rotor blade schematic sensor layout.

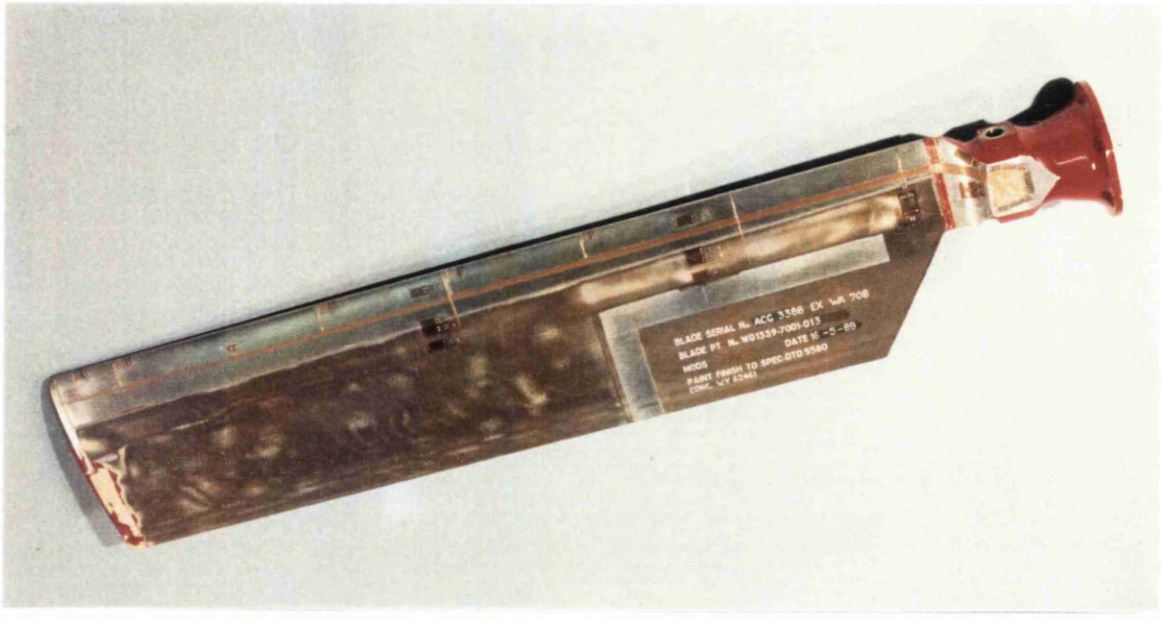

Figure2.5.2 Photograph of Lynx AH Mk5 instrumented tail rotor blade during construction showing one wiring loom, strain gauges and pressure sensor tag strips.

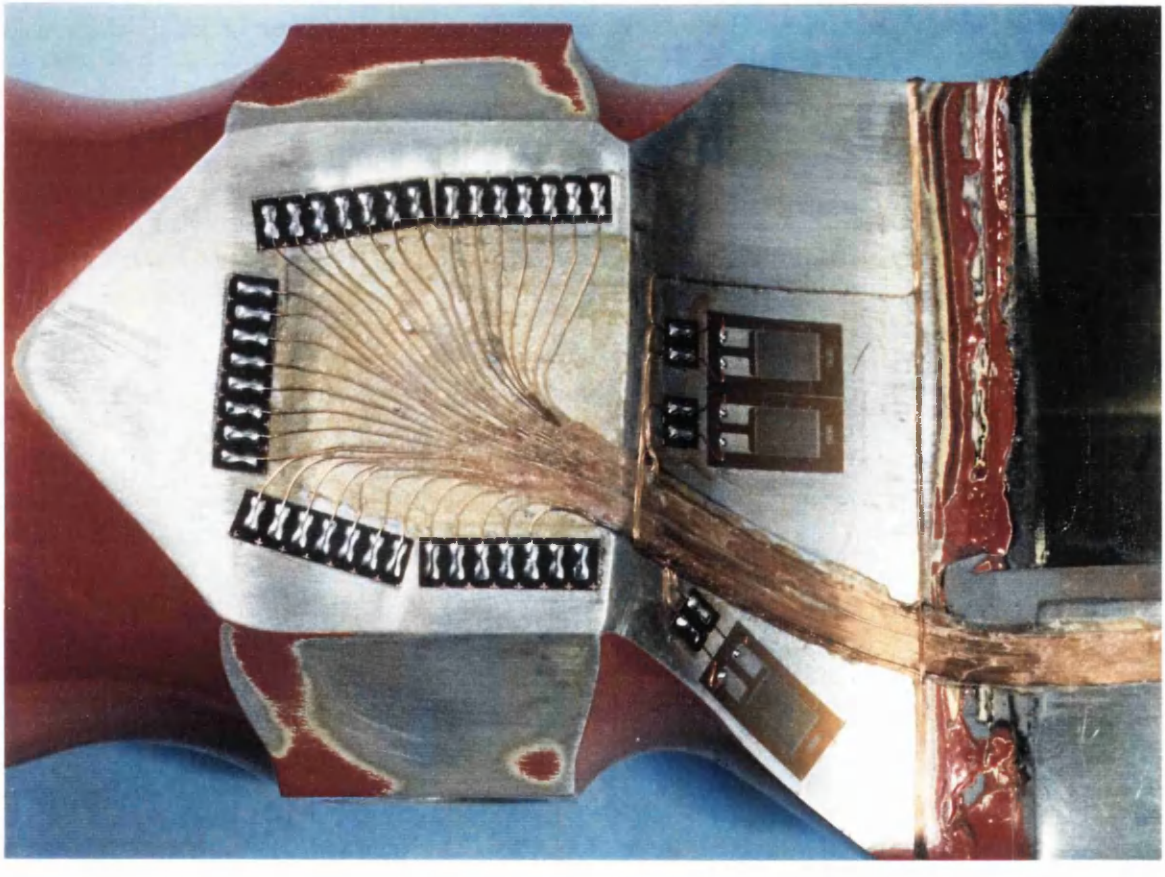

Figure2.5.3 Photograph of Lynx AH Mk5 instrumented tail rotor blade during construction showing blade root tag strip.

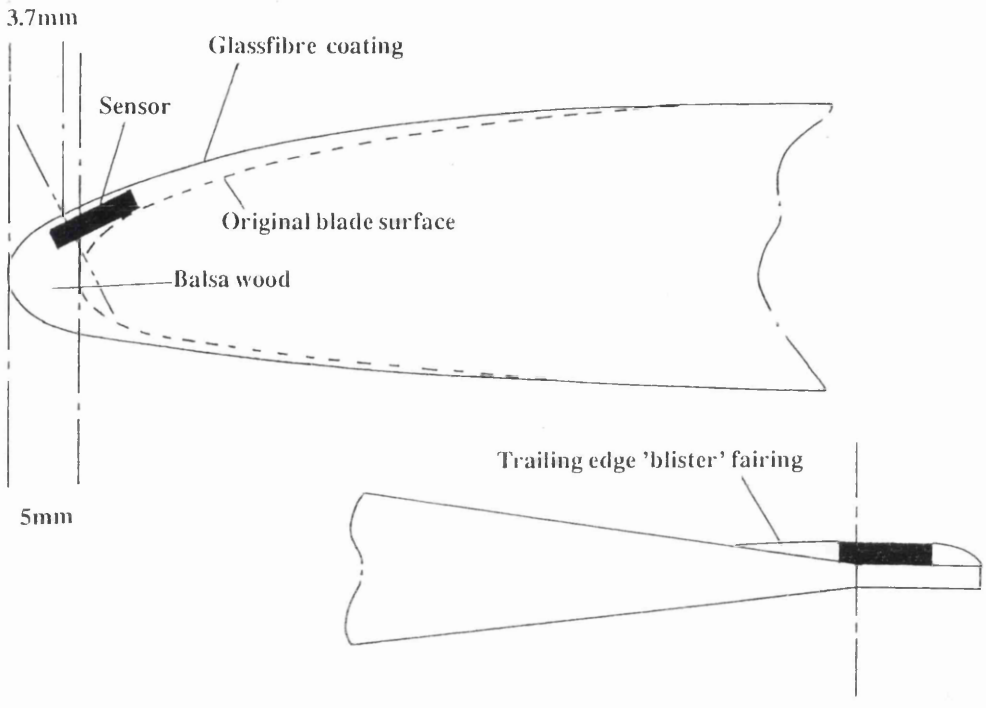

Figure2.5.4 Part cross–section of Lynx AH Mk5 instrumented tail rotor blade showing fairing profiles.

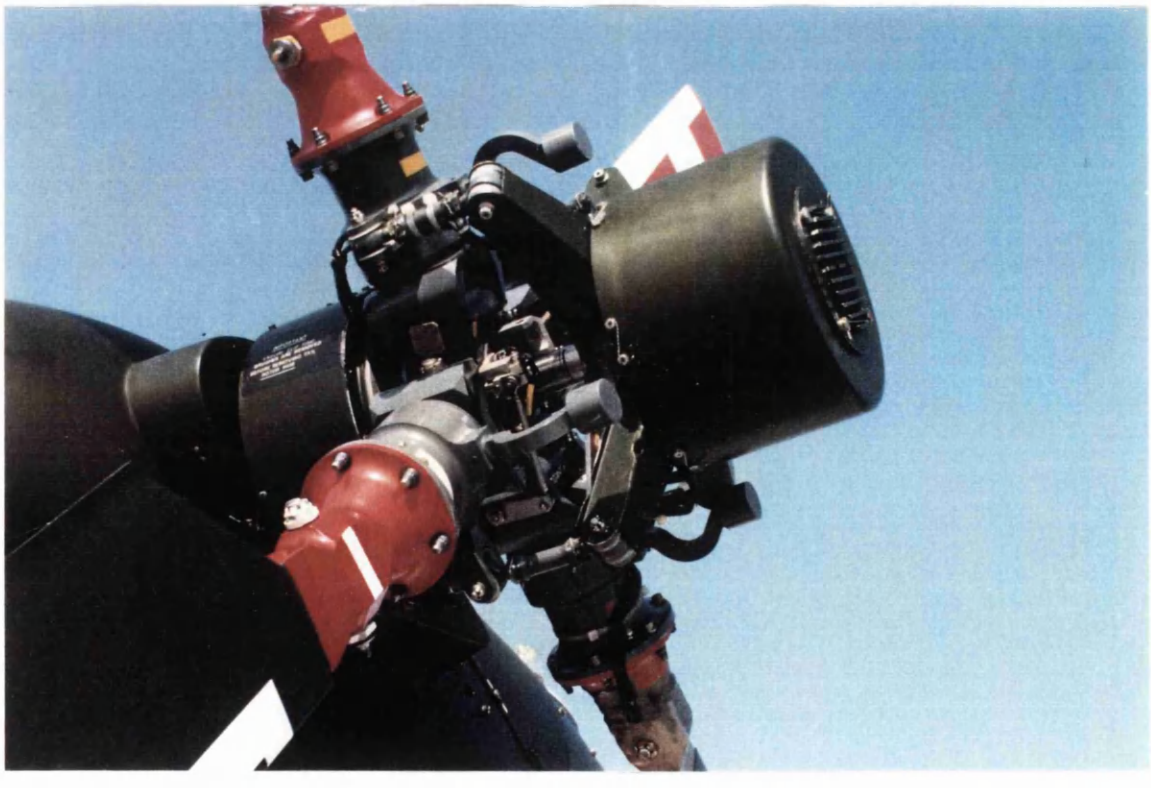

Figure2.5.5 Photograph of Lynx AH Mk5 tail rotor amplifier unit and 18–way slipring assembly.

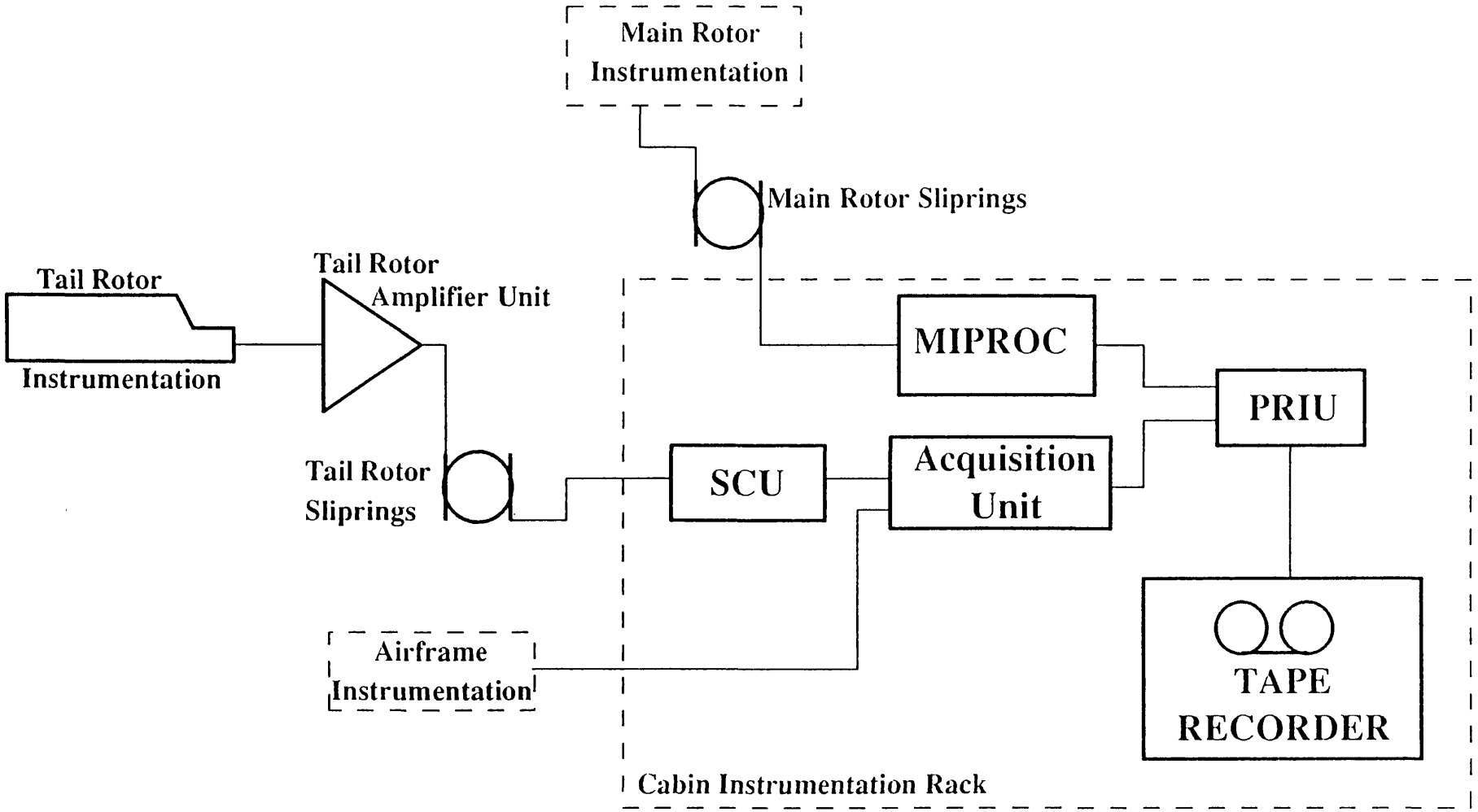

Figure2.6.1 Schematic Lynx AH Mk5 instrumentation diagram.

Figure2.7.1 Photograph of the pressure sensor calibration vessel.

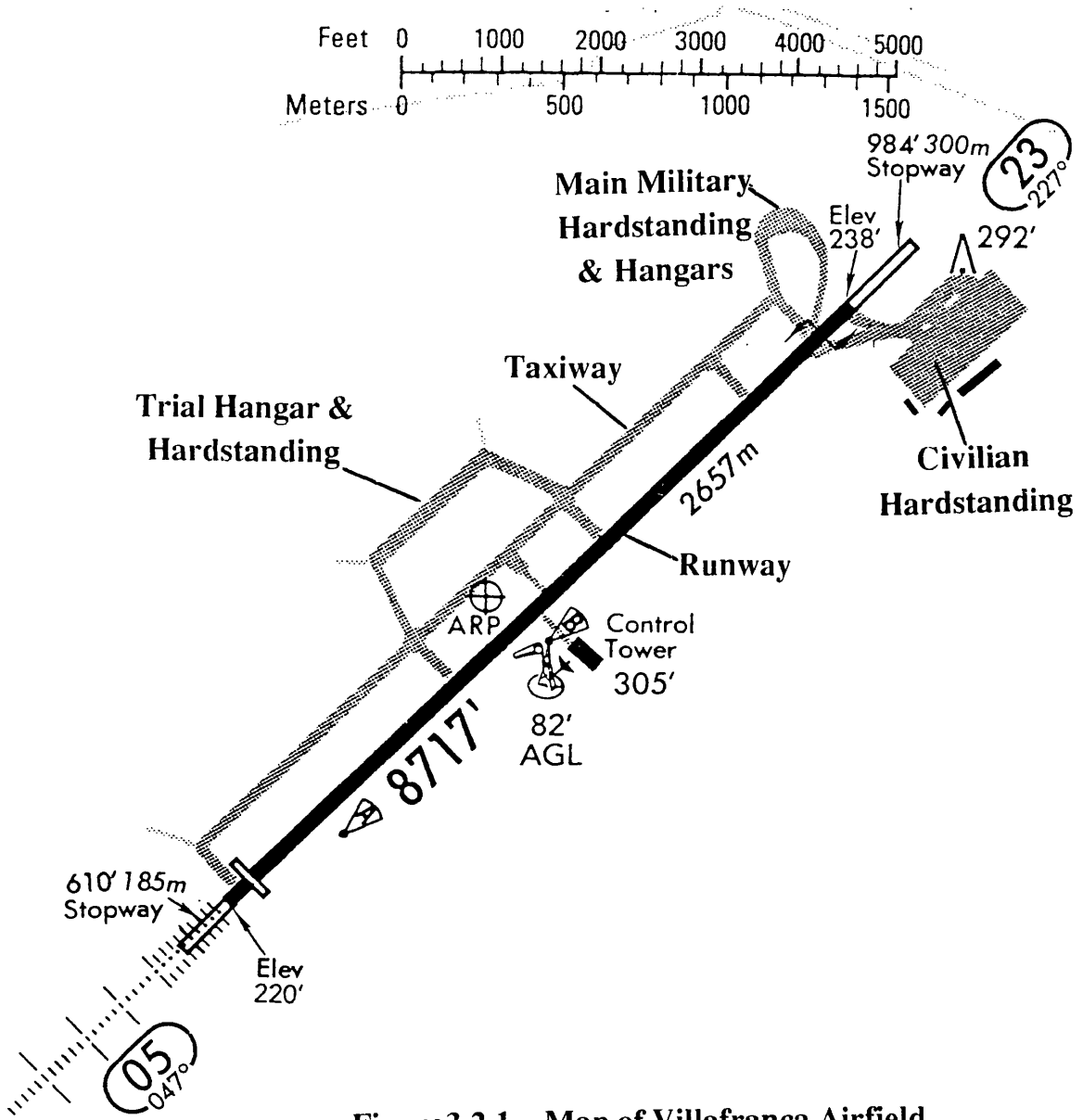

Figure3.2.1 Map of Villafranca Airfield

Figure3.2.2 The flight trial did not disrupt the routine operation of the airfield.

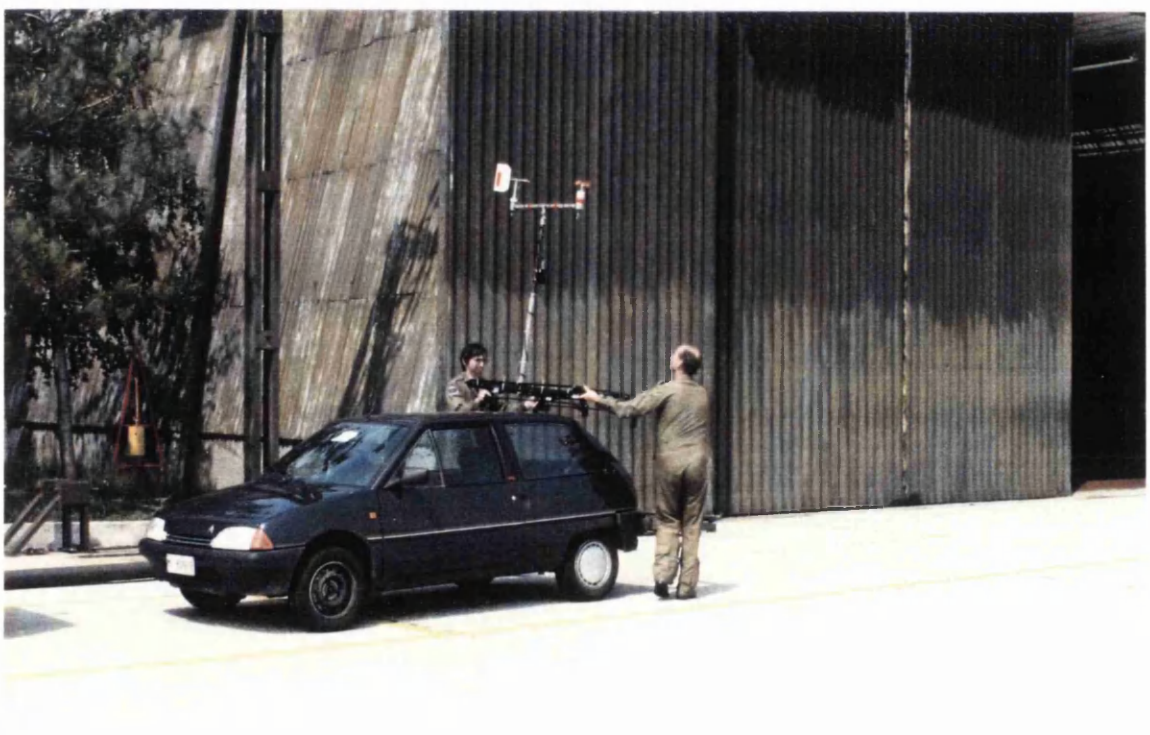

Figure3.2.3 Photograph of the car and anemometer.
This figure is not referenced in the text.

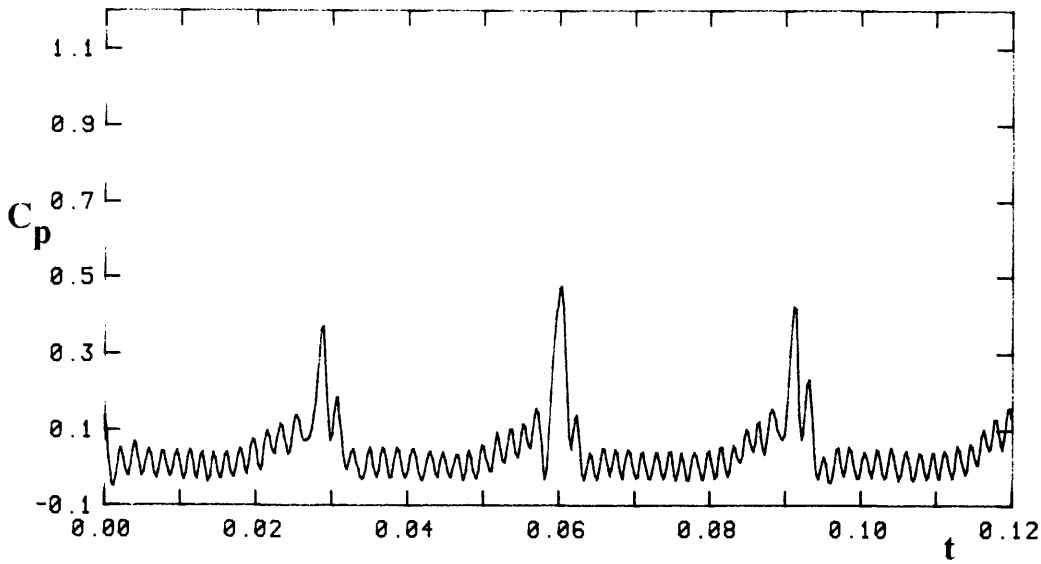

Figure3.5.1 **Pressure coefficient recorded at the 85% rotor radius trailing edge sensor showing high frequency oscillation. Relative wind is 20 kts at 064degrees.**

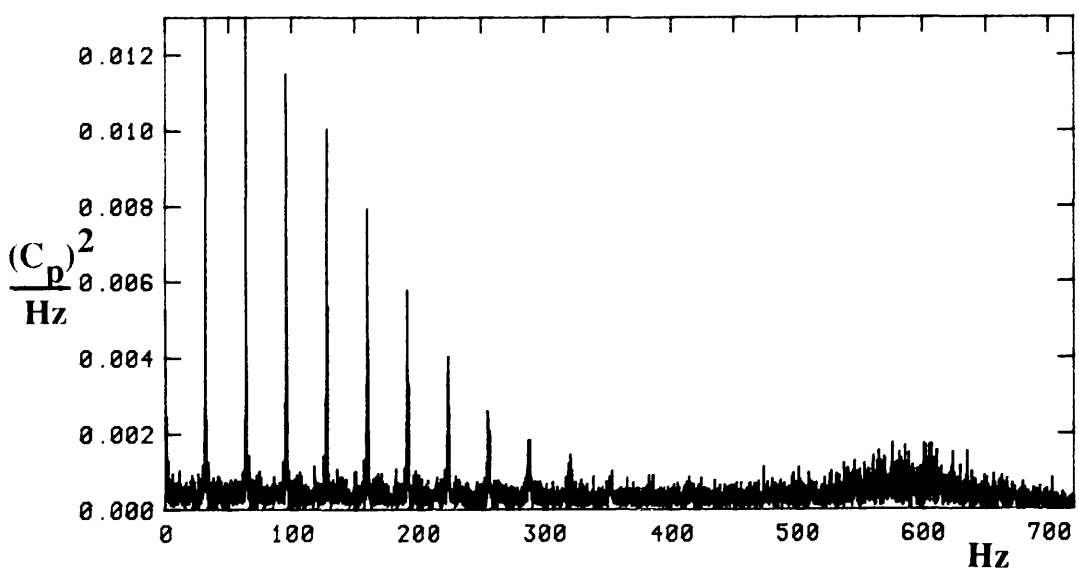

Figure3.5.2 **Power Spectral Density of the signal in Figure 3.5.1 showing increased noise round the filter cut-offfrequency, 600Hz..**

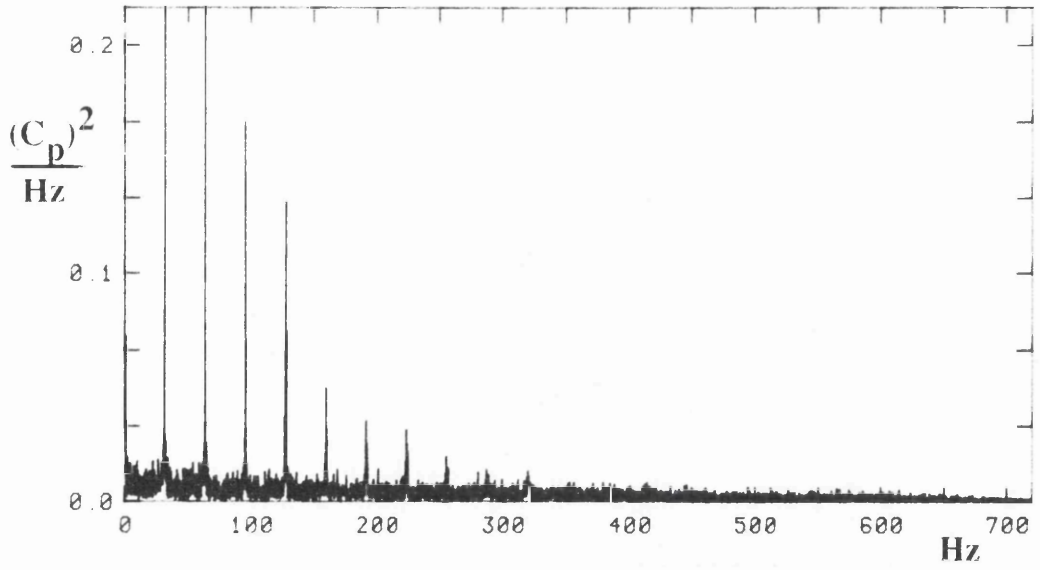

Figure3.5.3a Power Spectral Density of the signal recorded during the same event but on the 55% rotor radius leading edge sensor showing low level of noise compared with the tail rotor harmonics.

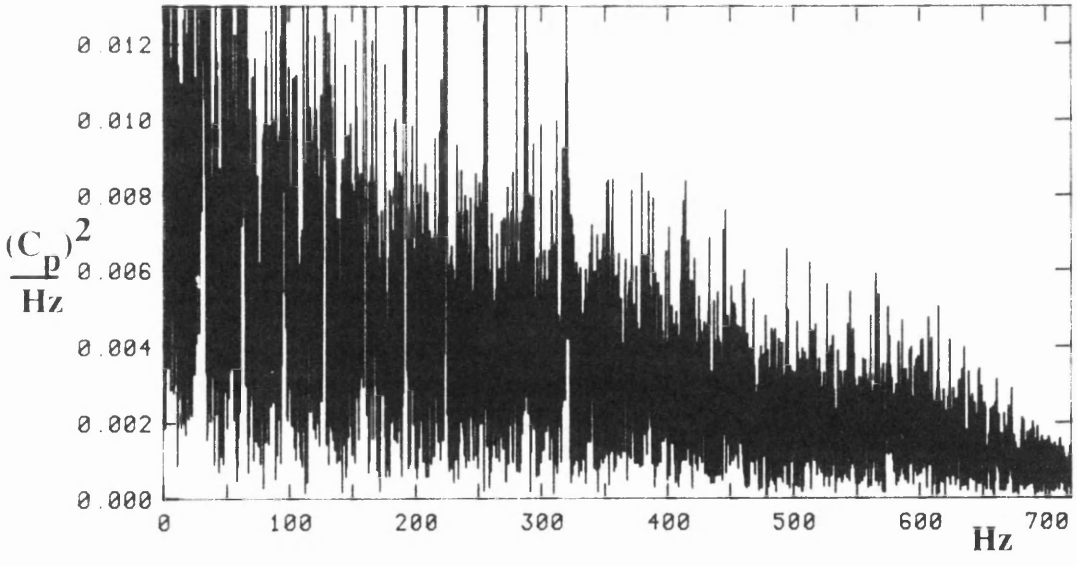

Figure3.5.3b Same data as above but to the same scale as Figure3.5.2.

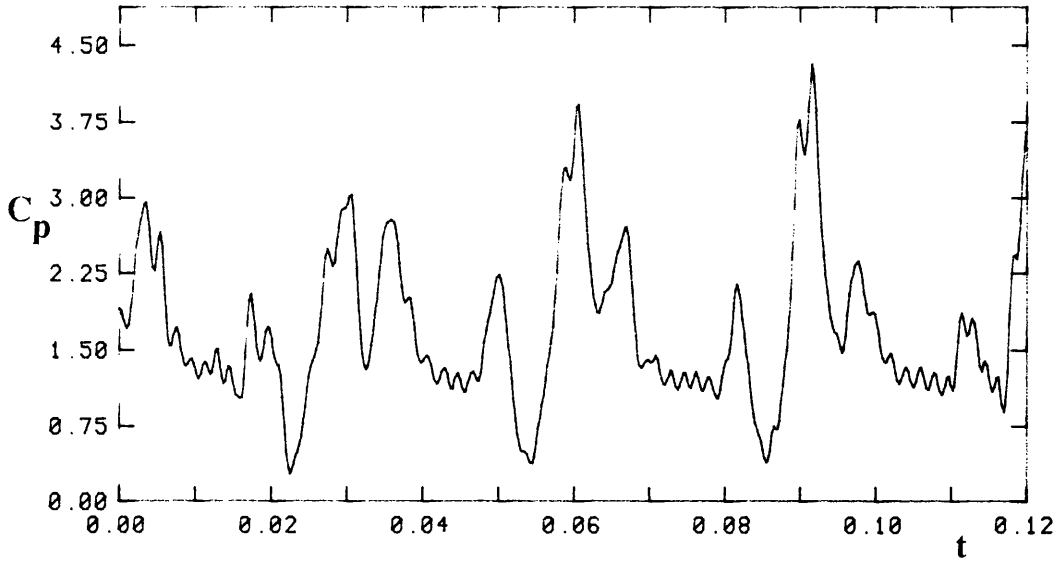

Figure3.5.4 Pressure coefficient time history for the data in Figure 3.5.3.

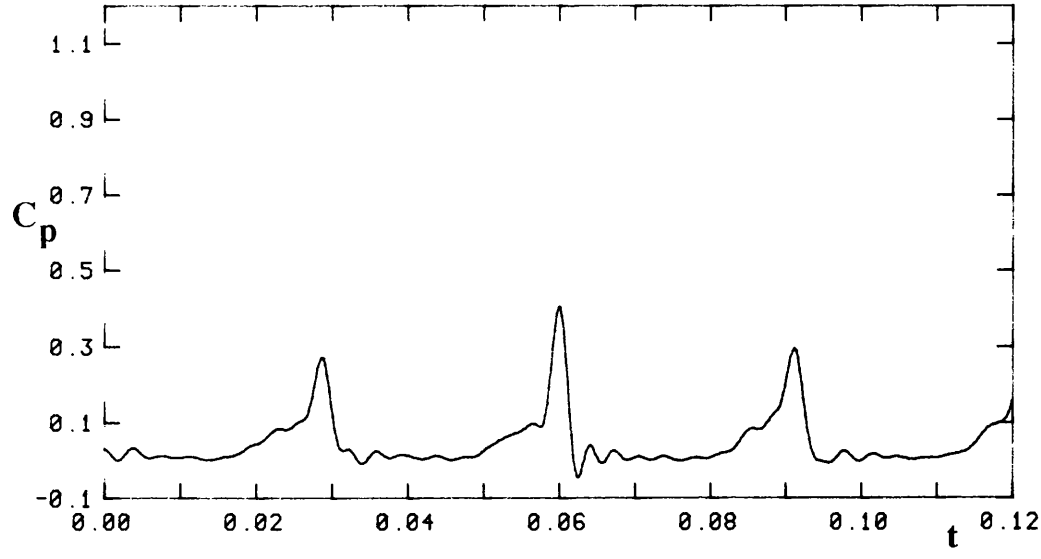

Figure3.5.5 Data in Figure 3.5.1 after being passed 5 times through a 300Hz Low pass Butterworth filter with the time base readjusted.

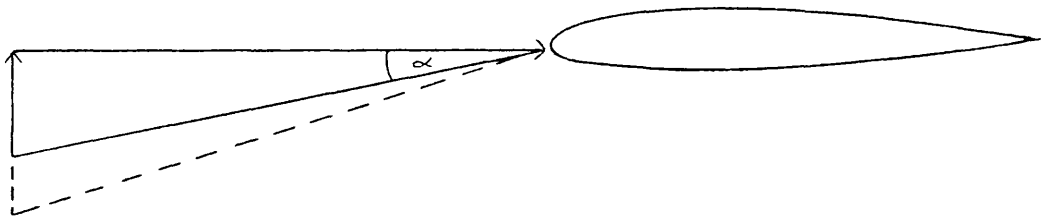

Increase in normal component = increase in incidence
slight increase in velocity

Figure 4.2.1 Effect of change in normal velocity component.

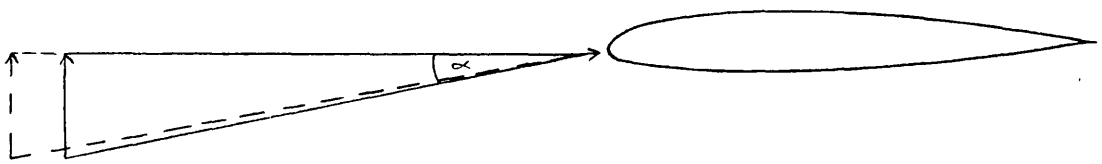

Increase in in–plane component = slight reduction in incidence
major increase in velocity

Figure4.2.2 Effect of change in in–plane velocity component.

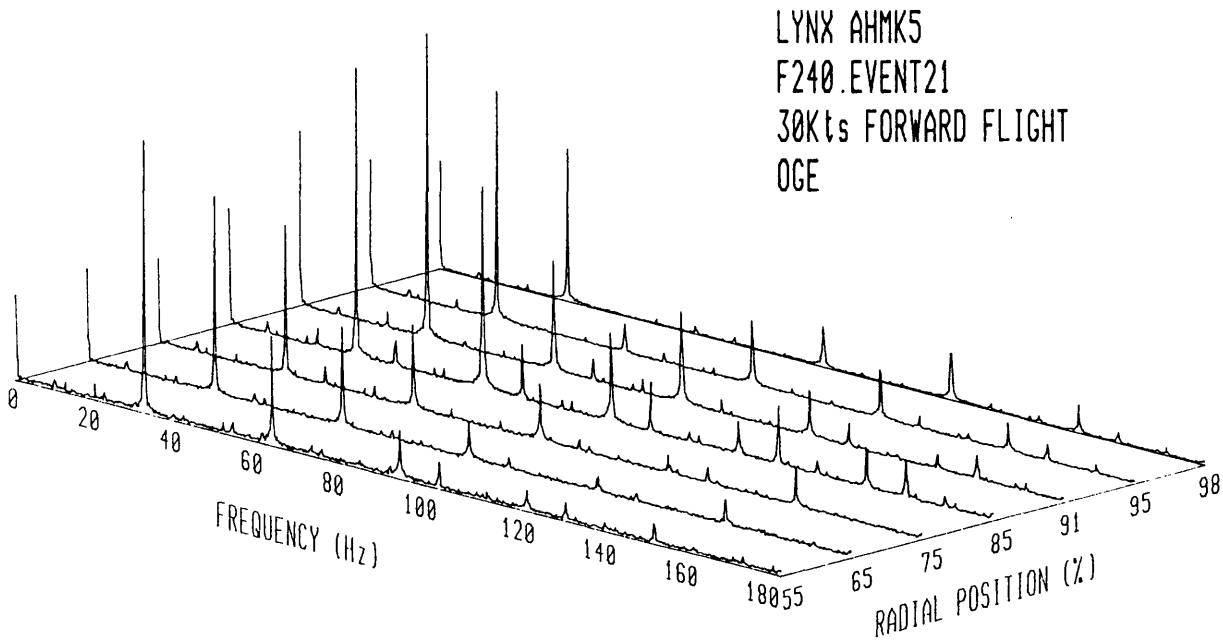

Figure4.3.1 Isometric presentation of frequency content.

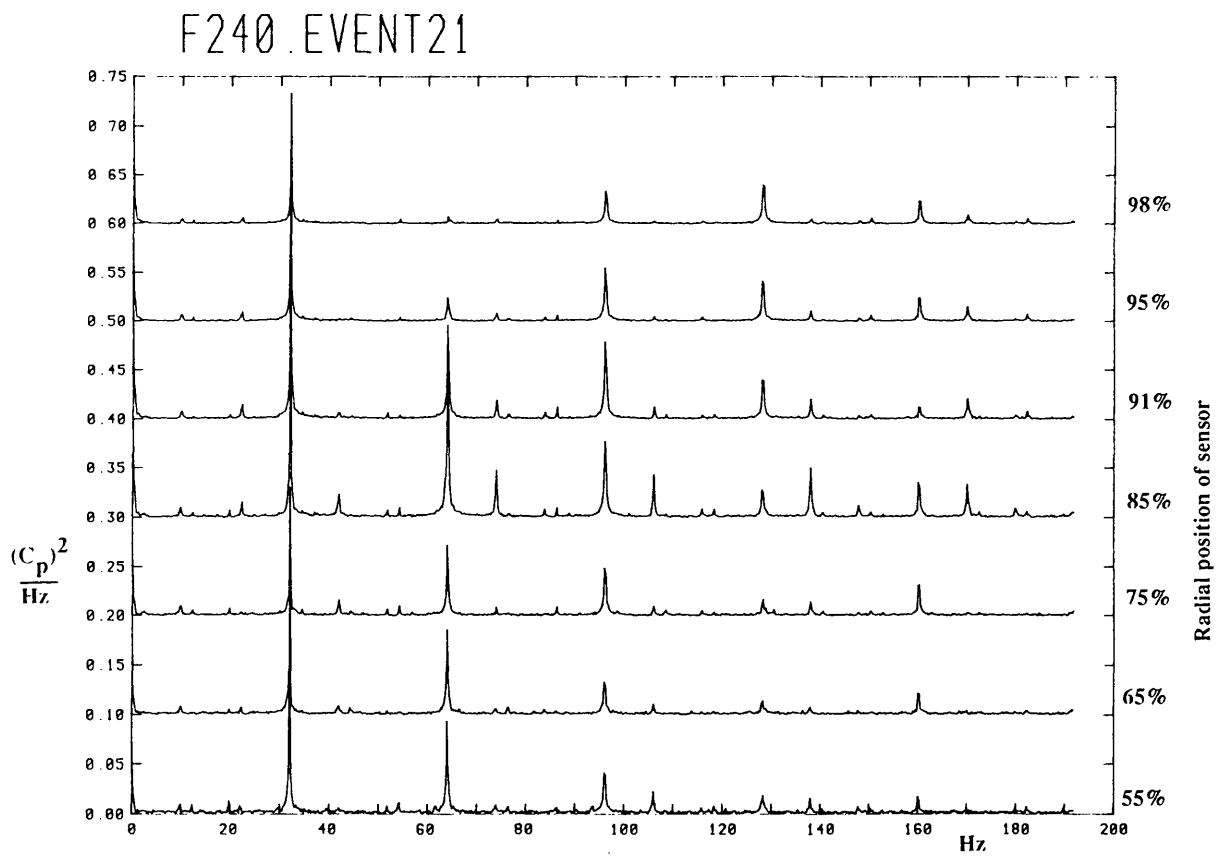

Figure4.3.2 Displaced presentation of frequency content.

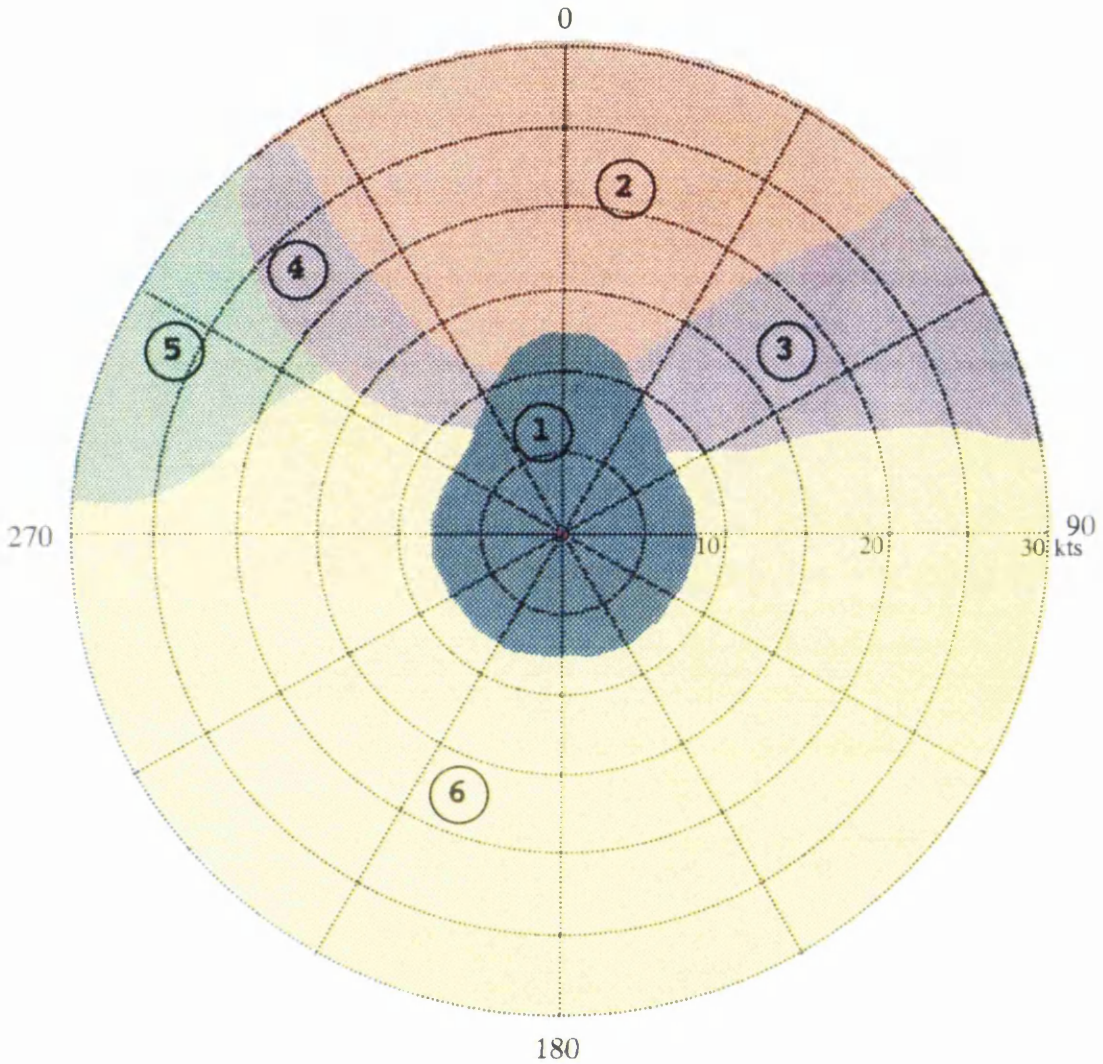

Figure 4.3.3 Lynx AH Mk5 low speed flight envelope showing regions where different main rotor/tail roto interactions were observed. Areas 3 & 4 have similar mechanisms.

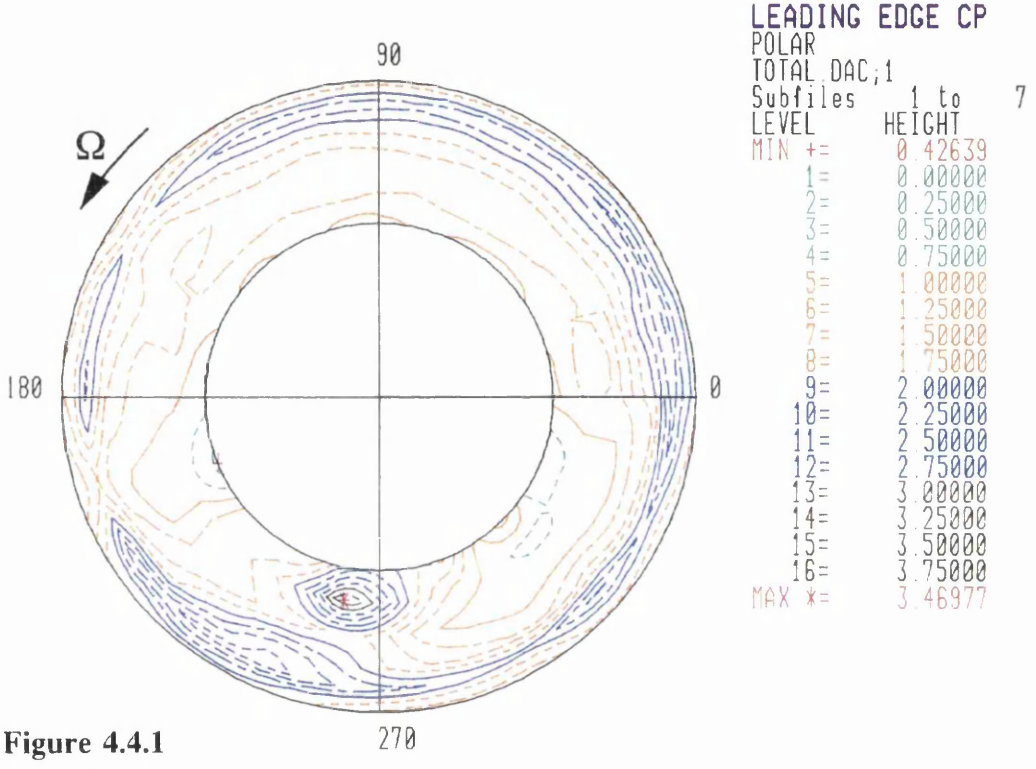

Figure 4.4.1

Plot of variation in $-C_p$ for one revolution of the tail rotor in Hover OGE. Aircraft AUM 4600kg.

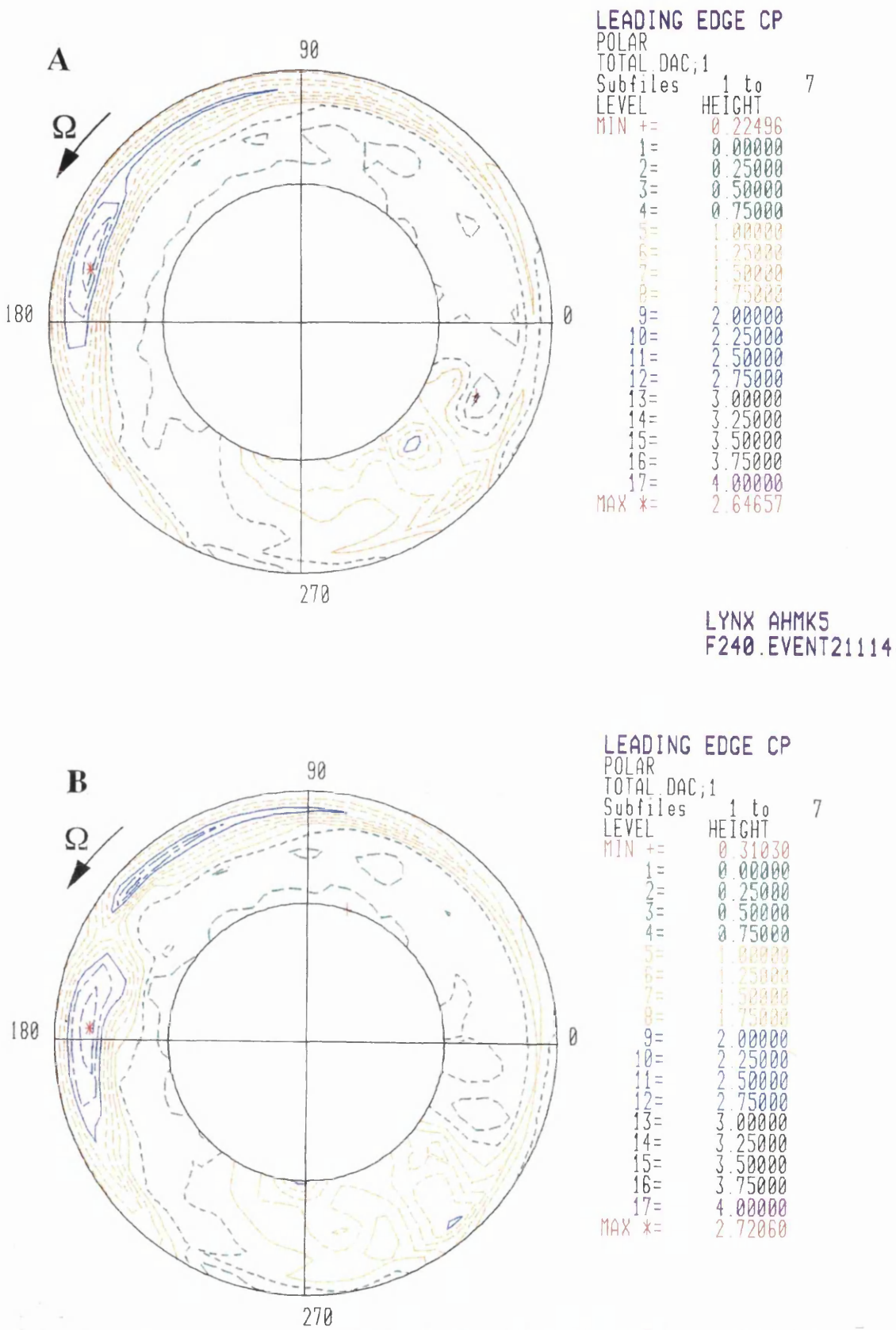

Figure 4.4.2 **Sequence of single revolution plots of Lynx AH Mk5 tail rotor $-C_p$ data during 30 kts forward flight OGE showing passage of main rotor blade trailing tip vortex interference effects. Aircraft AUM is 4700kg.**

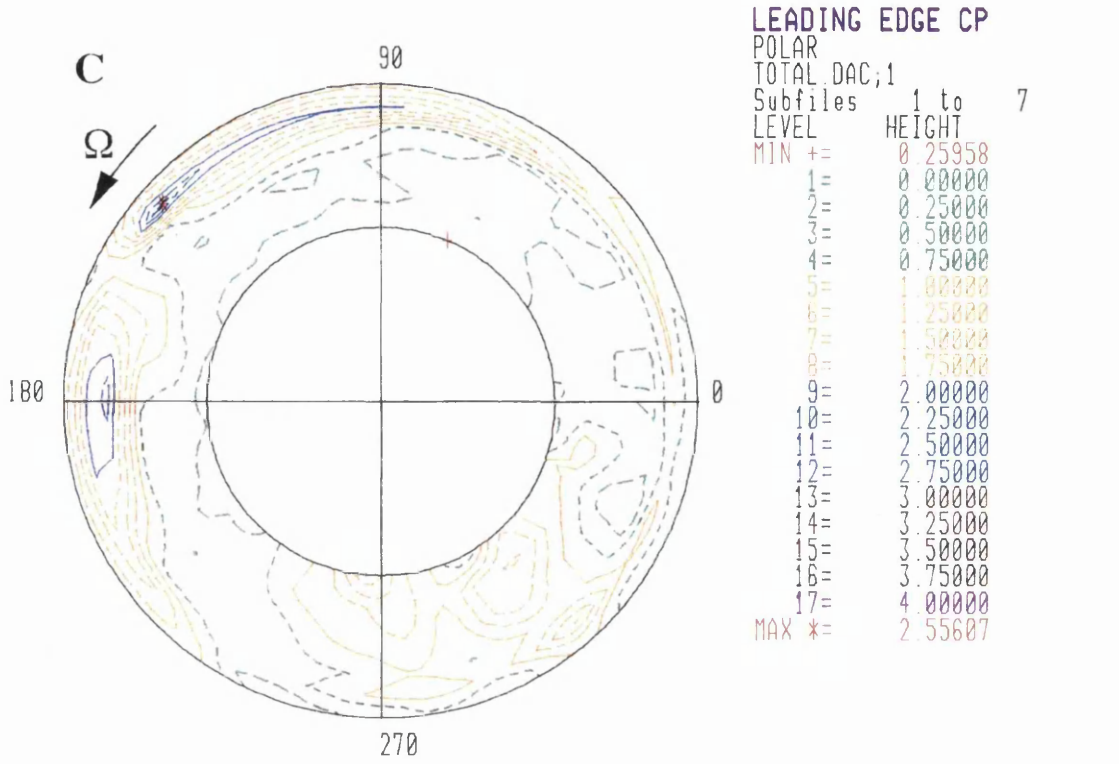

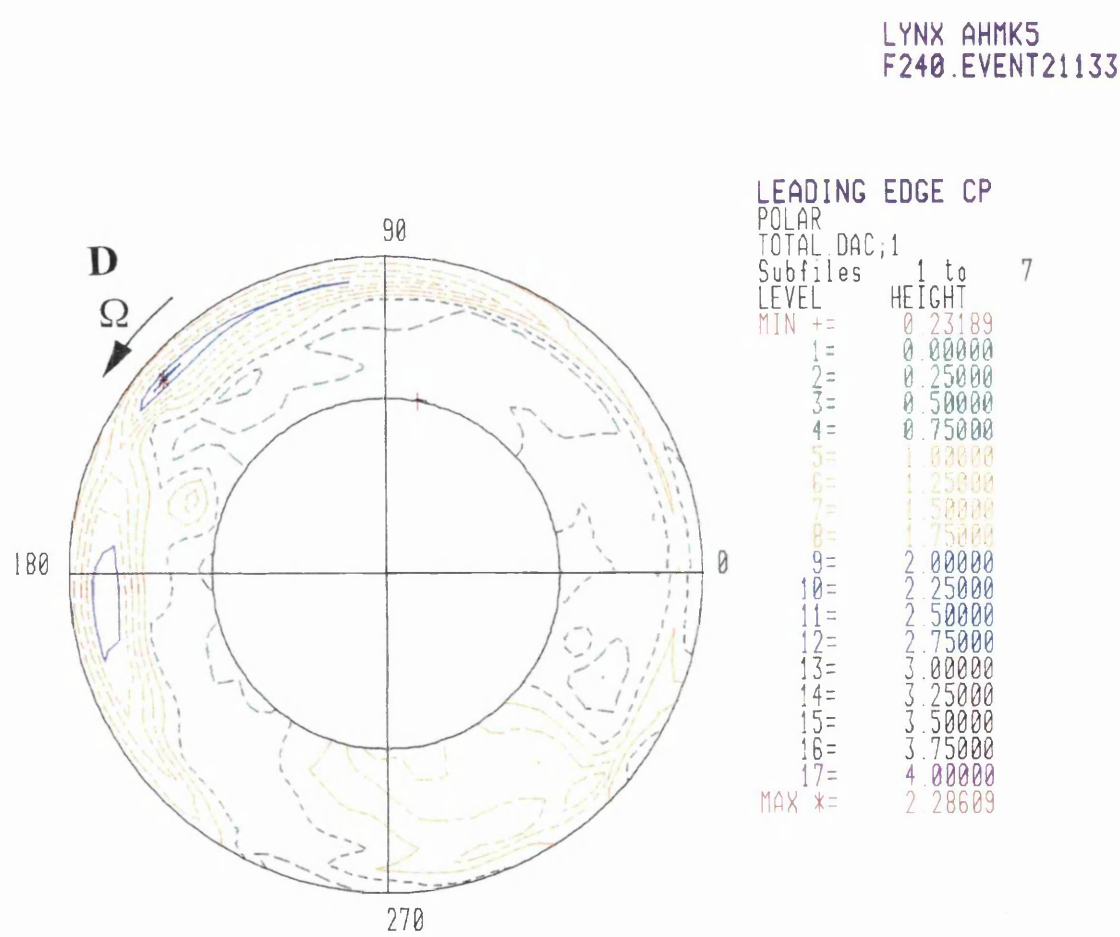

Figure 4.4.2 continued.

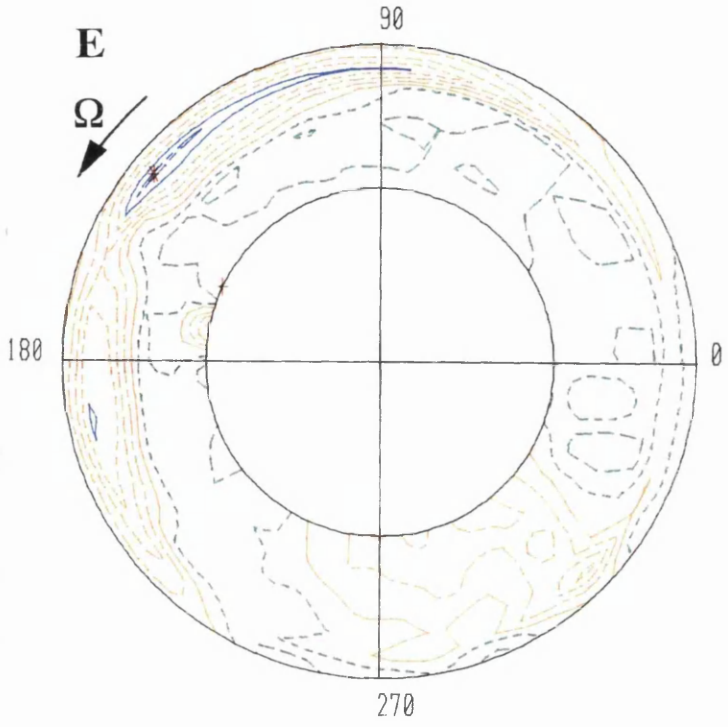

LYNX AHMK5
F240.EVENT21084

LEADING EDGE CP
POLAR
TOTAL DAC;1
Subfiles 1 to 7

LEVEL	HEIGHT
MIN +=	0.22699
1=	0.00000
2=	0.25000
3=	0.50000
4=	0.75000
5=	1.00000
6=	1.25000
7=	1.50000
8=	1.75000
9=	2.00000
10=	2.25000
11=	2.50000
12=	2.75000
13=	3.00000
14=	3.25000
15=	3.50000
16=	3.75000
17=	4.00000
MAX *=	2.31518

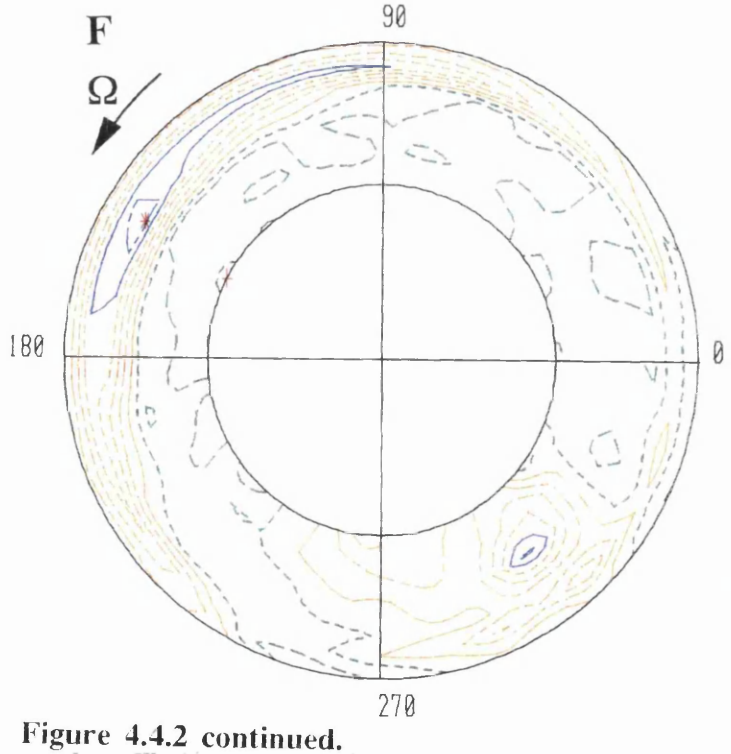

LYNX AHMK5
F240.EVENT21067

LEADING EDGE CP
POLAR
TOTAL DAC;1
Subfiles 1 to 7

LEVEL	HEIGHT
MIN +=	0.17906
1=	0.00000
2=	0.25000
3=	0.50000
4=	0.75000
5=	1.00000
6=	1.25000
7=	1.50000
8=	1.75000
9=	2.00000
10=	2.25000
11=	2.50000
12=	2.75000
13=	3.00000
14=	3.25000
15=	3.50000
16=	3.75000
17=	4.00000
MAX *=	2.36178

Figure 4.4.2 continued.

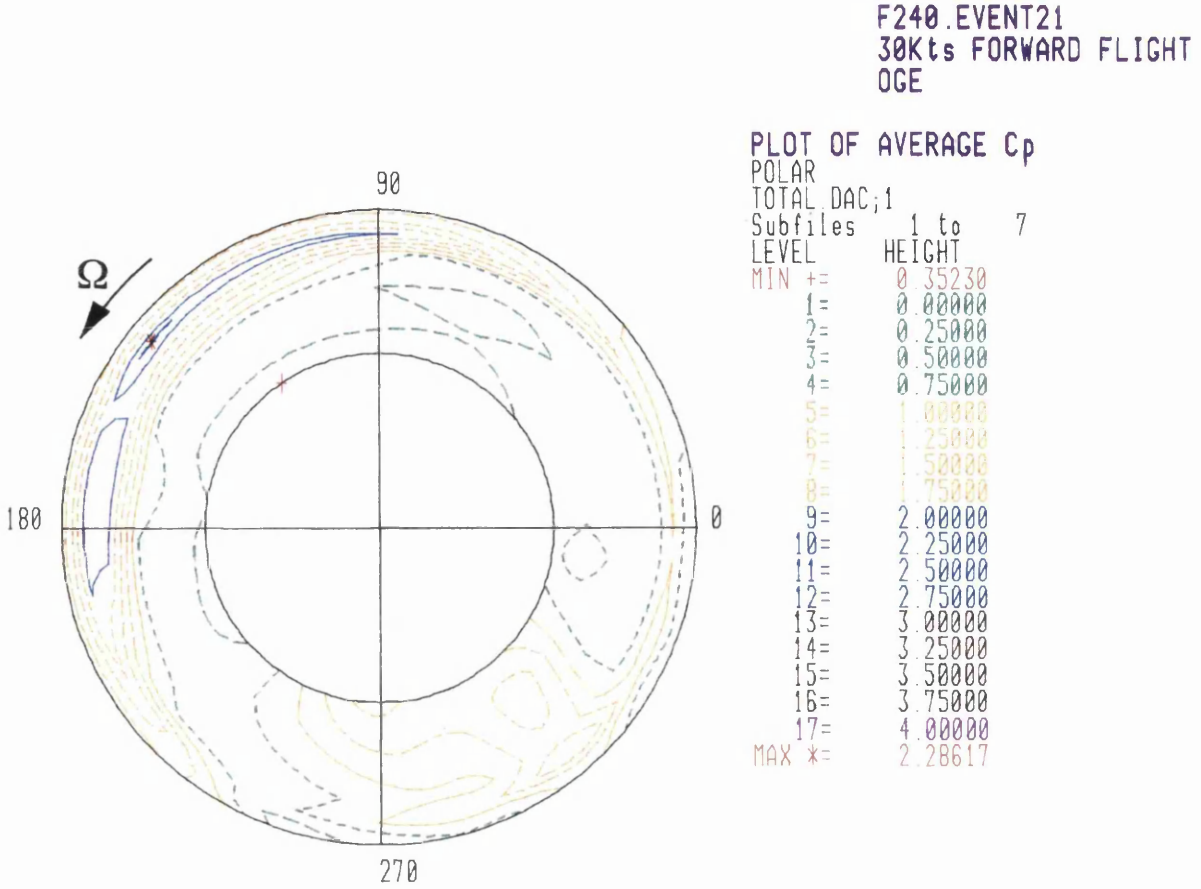

Figure 4.4.3 **Plot of average C_p over 160 revolutions.**

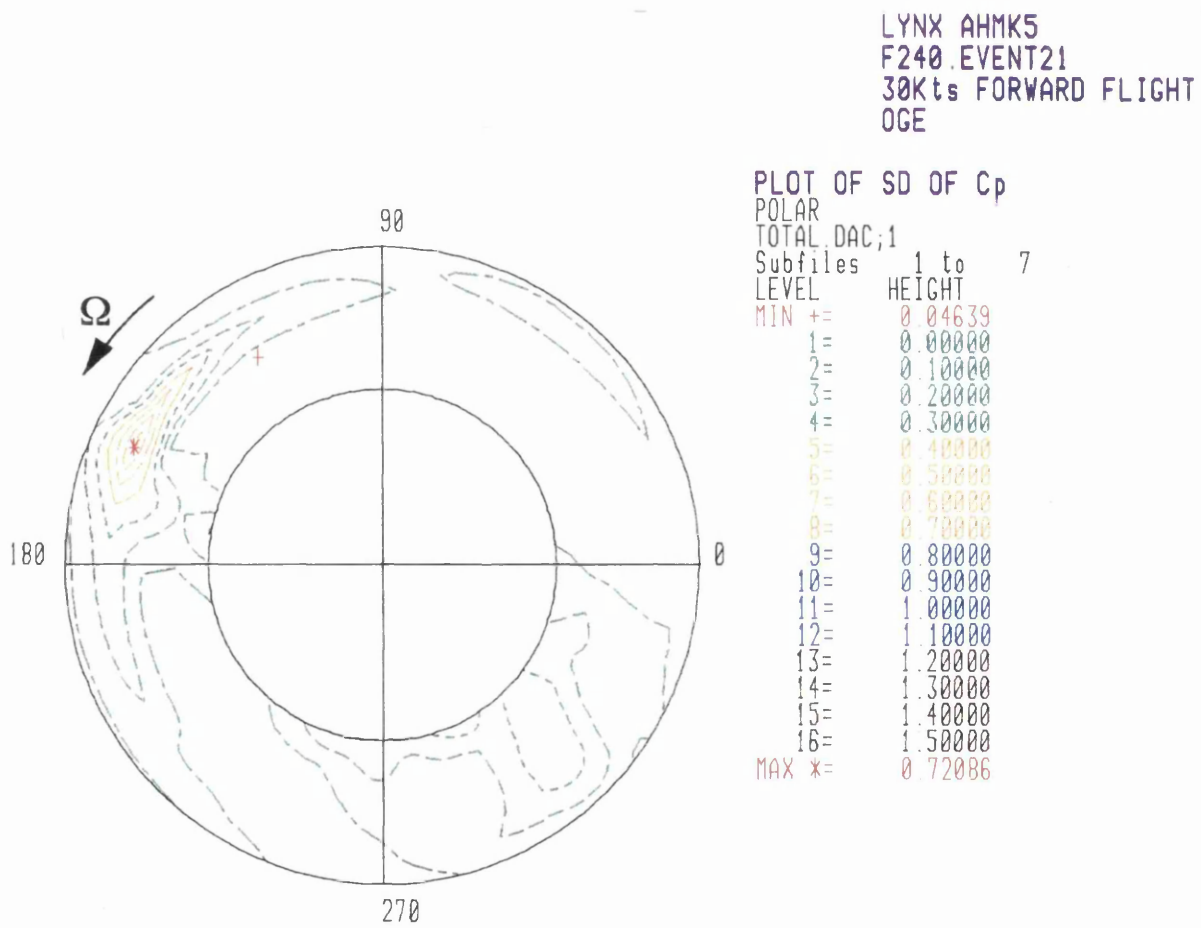

Figure 4.4.4 **Plot of standard deviation of C_p over 160 revolutions.**

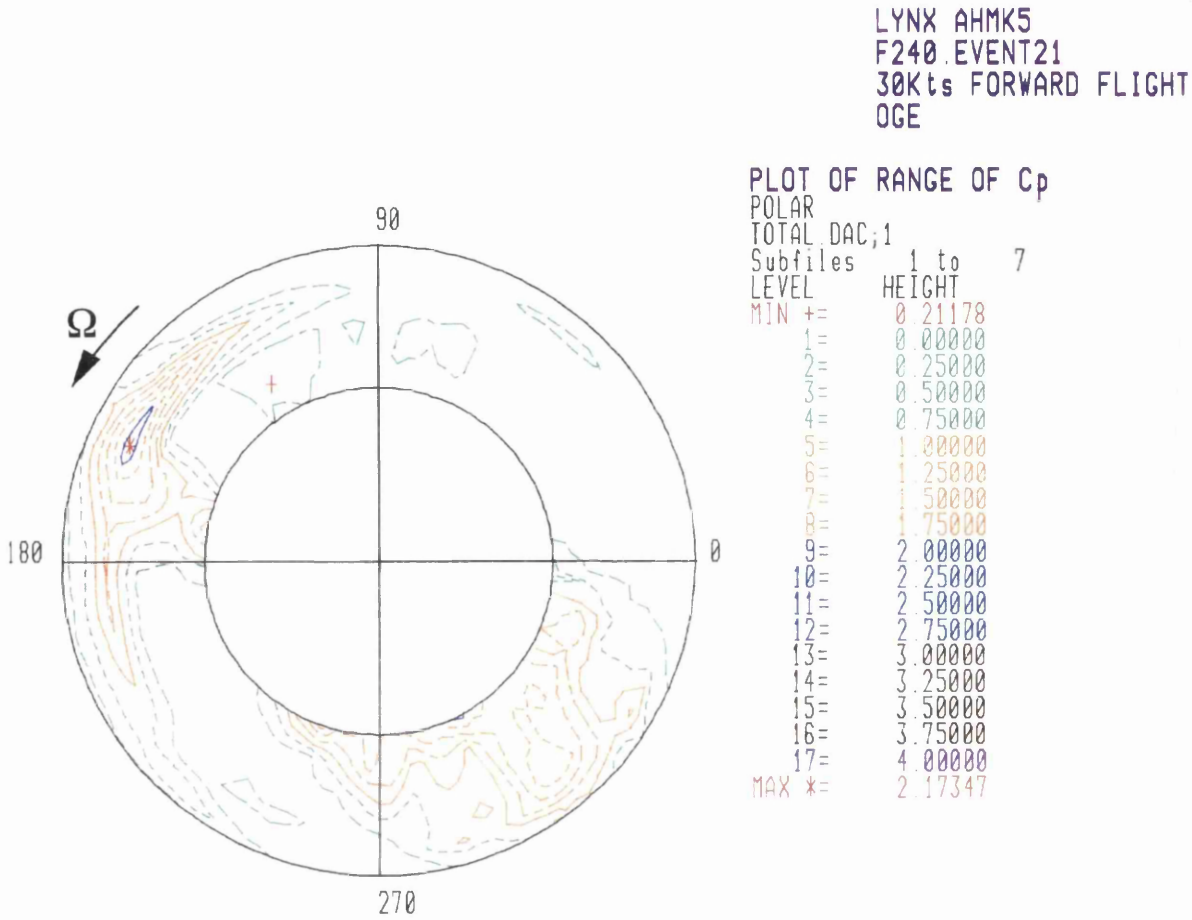

Figure 4.4.5 **Plot of range of C_p variation over 160 revolutions.**

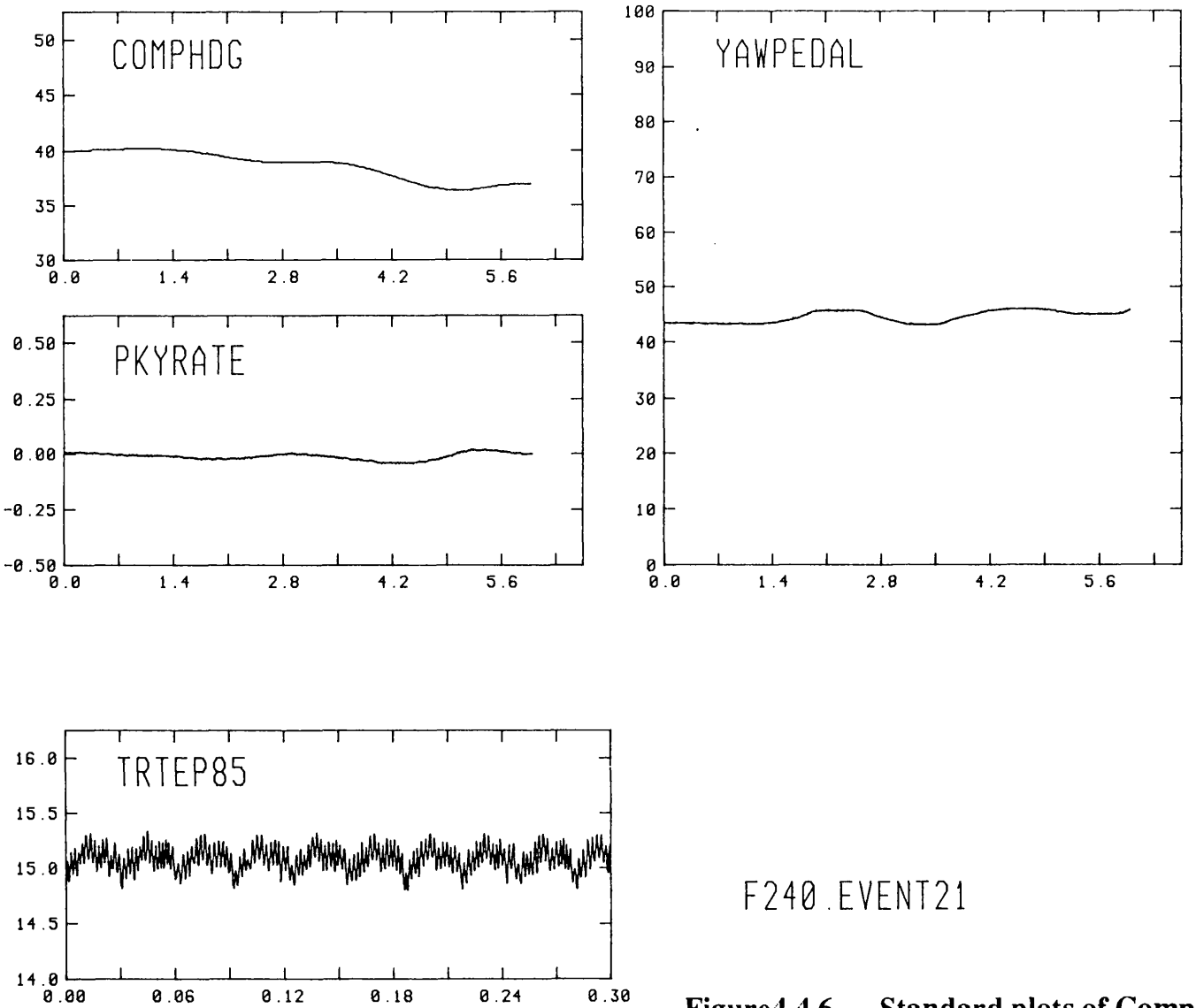

Figure4.4.6 Standard plots of Compass heading, Pedal position, Yaw rate and 85% blade radius trailing edge pressure.

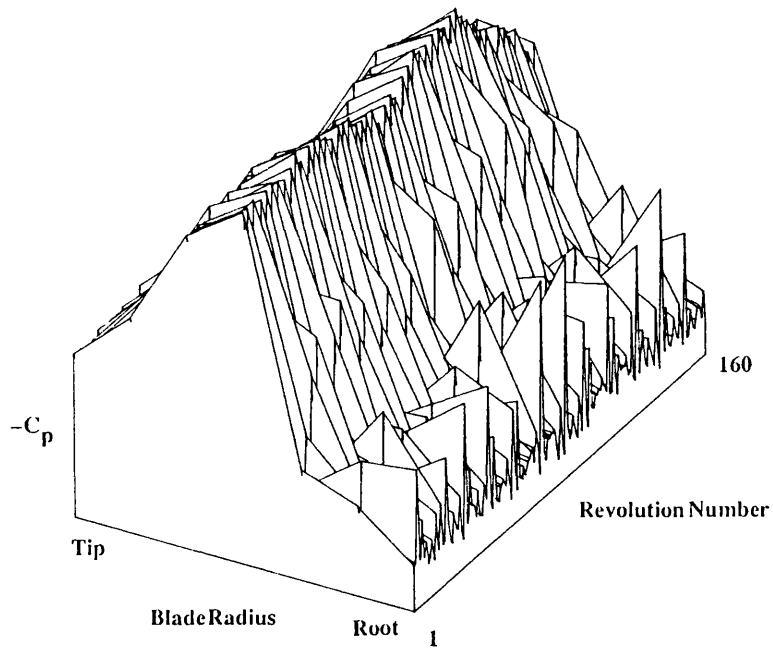

Figure 4.5.1 C_p data at 165° azimuth in the order as recorded.

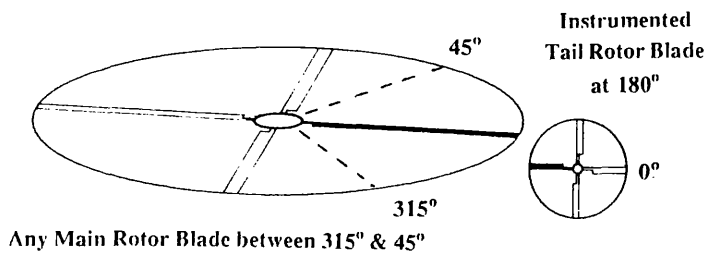

Figure 4.5.2 Datum main rotor position for each tail rotor revolution.

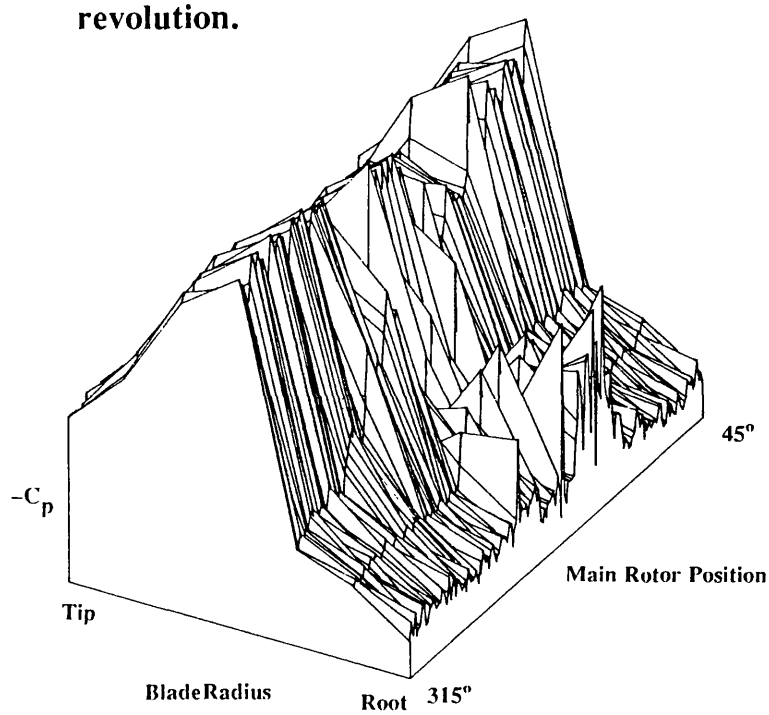

Figure 4.5.3 Data in Fig 4.5.1 reordered by nearest main rotor blade position.

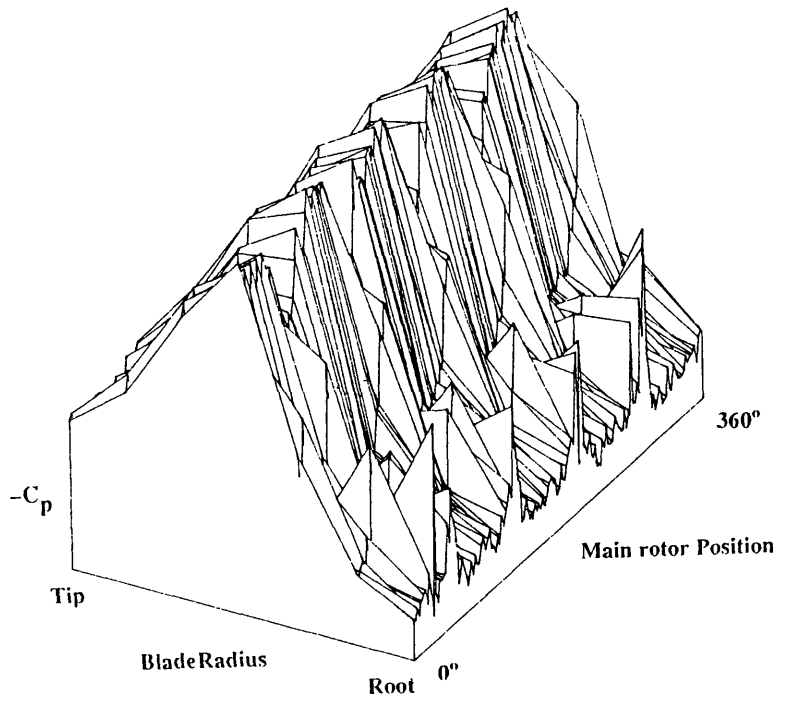

Figure 4.5.4 Data in Fig 4.5.1 reordered by red main rotor blade position.

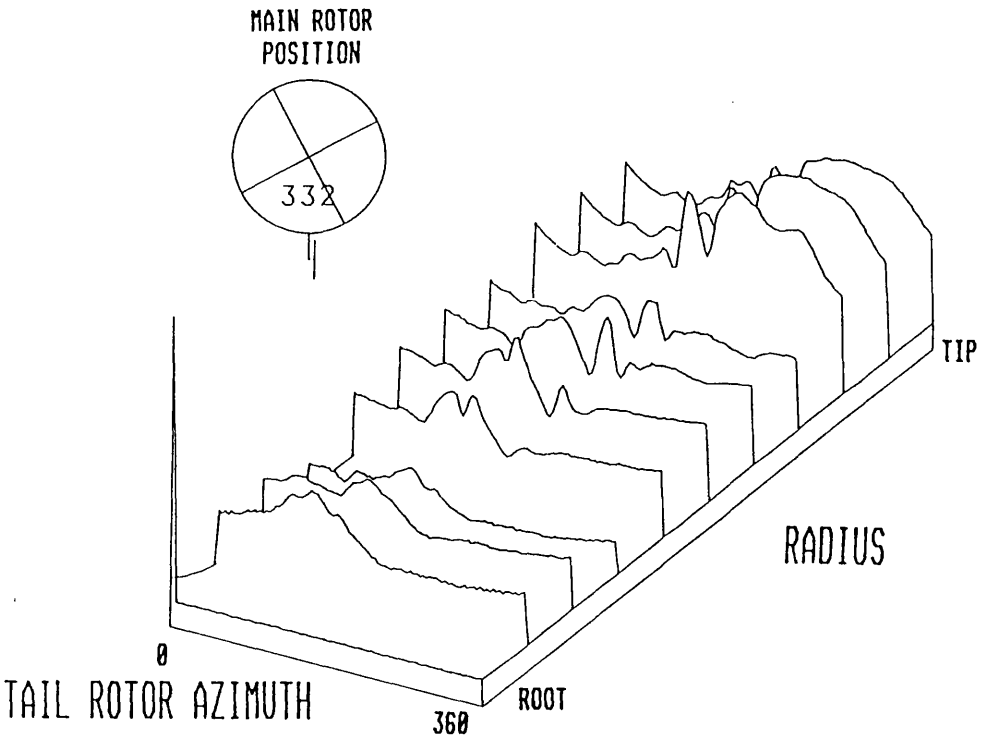

Figure 4.5.5 Format used for original "cartoon" animation of Puma tail rotor pressure data.

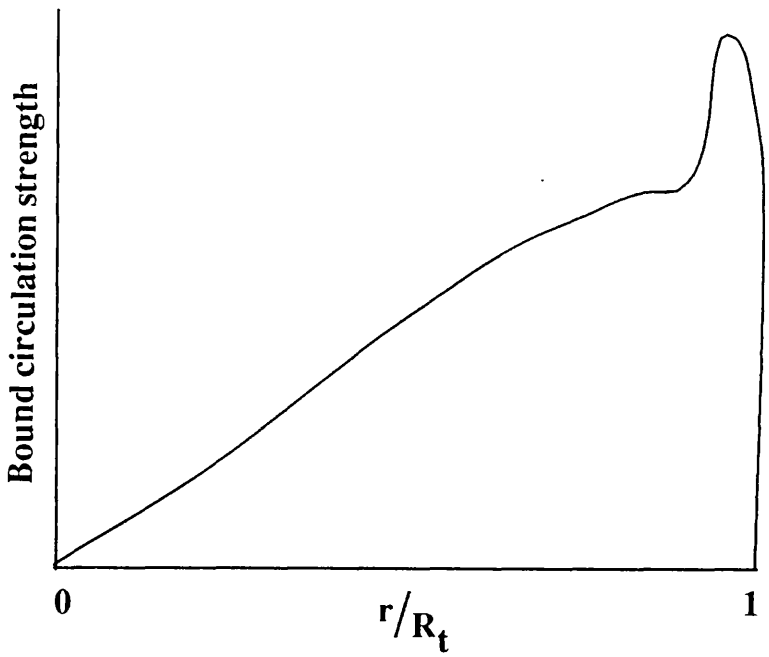

Figure5.2.1 Variation in bound circulation along a blade of an isolated rotor in the hover.

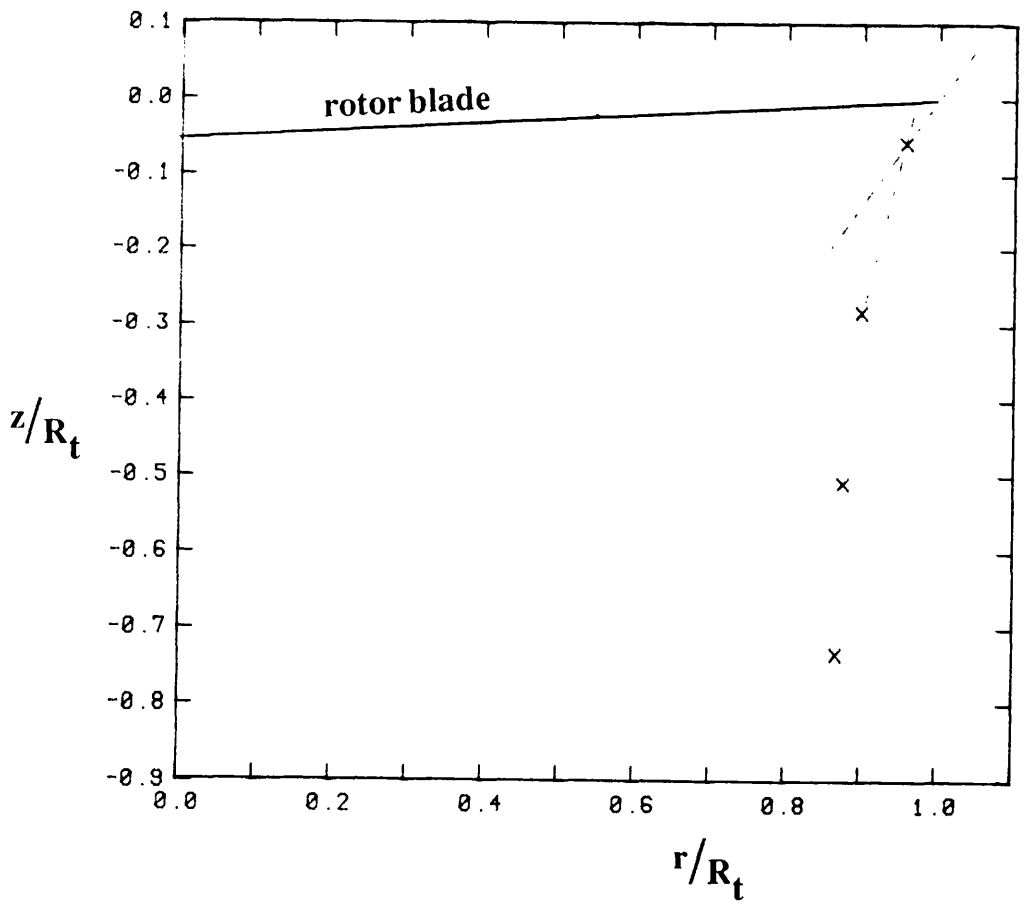

Figure5.2.2 Position of the tip vortices calculated for an isolated 4–bladed rotor in the hover. The marked change in direction of vortex movement after the first blade passage is indicated.

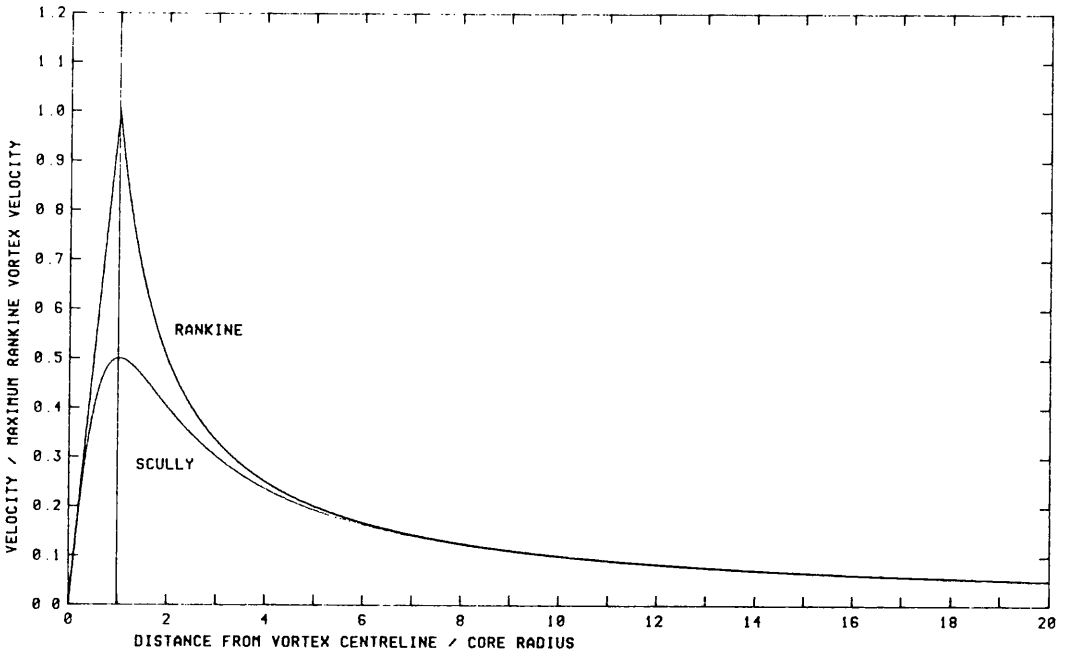

Figure5.2.3 Comparison between Rankine & Scully vortex velocity distributions.

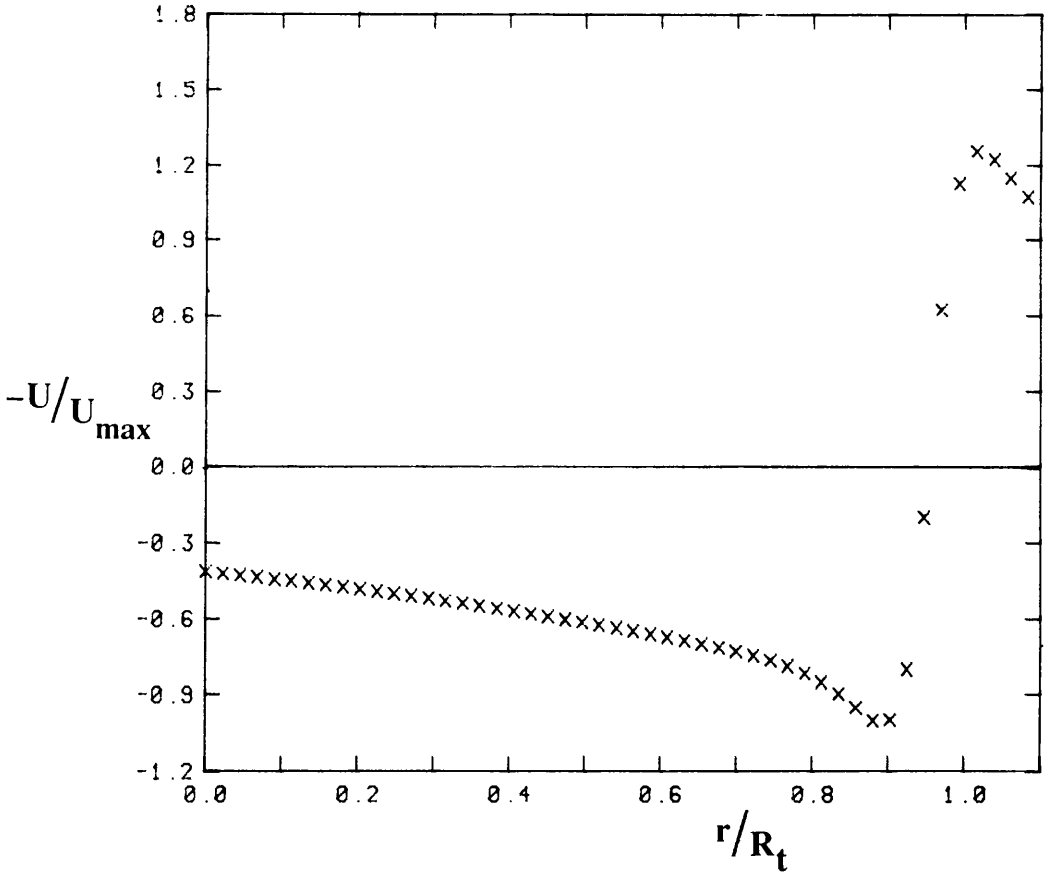

Figure5.2.4 Velocity distribution at the blade of an isolated rotor in the hover.

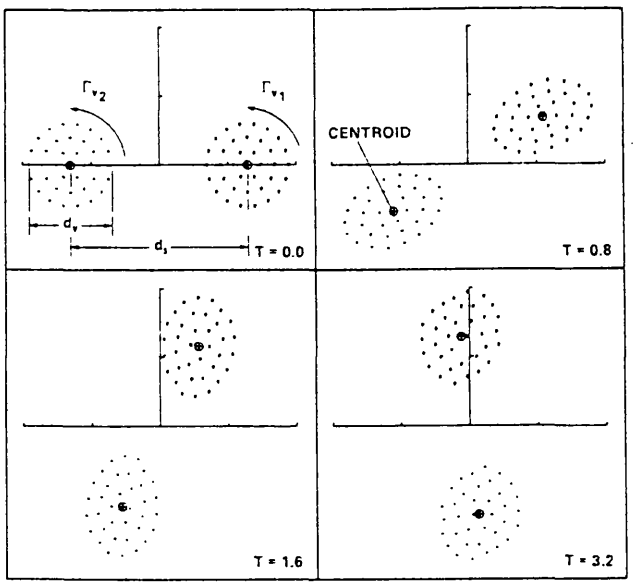

Figure5.2.5 **Figure from Rossow (1977) showing 2 vortices of equal magnitude and sign rotating round each other.**

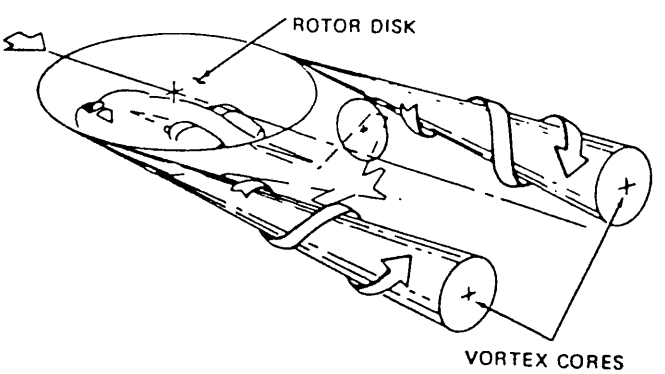

Figure5.2.6 **Sketch showing how the wake behind a helicopter in forward flight resembles that of a fixed wing aircraft.**

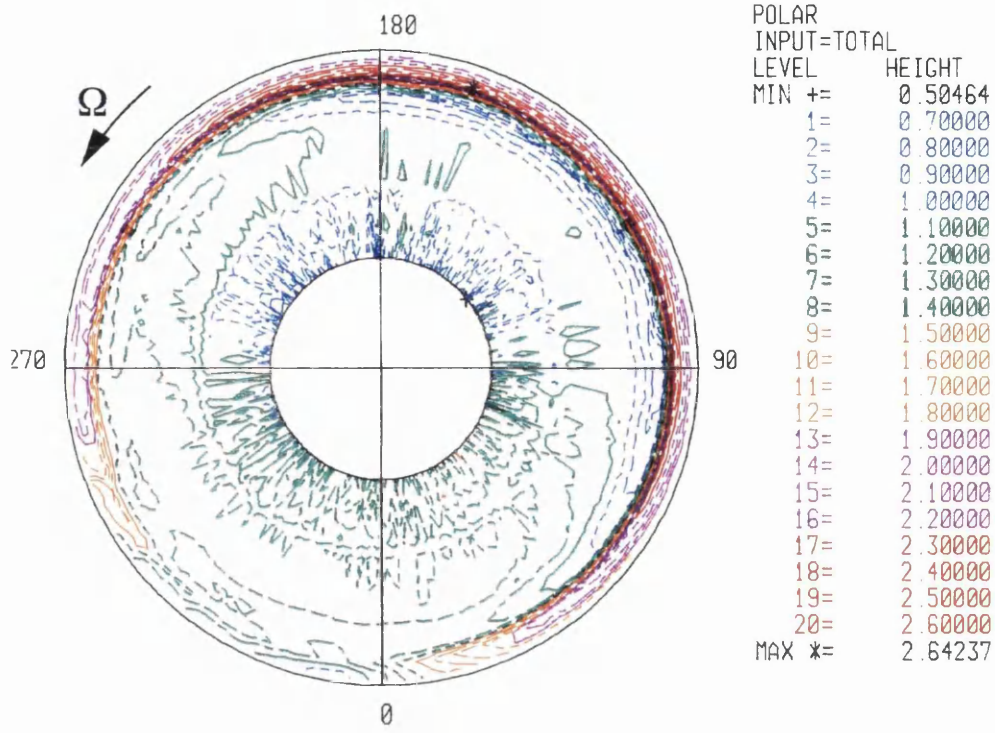

Figure 5.3.1 **Variation of Puma main rotor leading edge $-C_p$ over one revolution in the hover.**

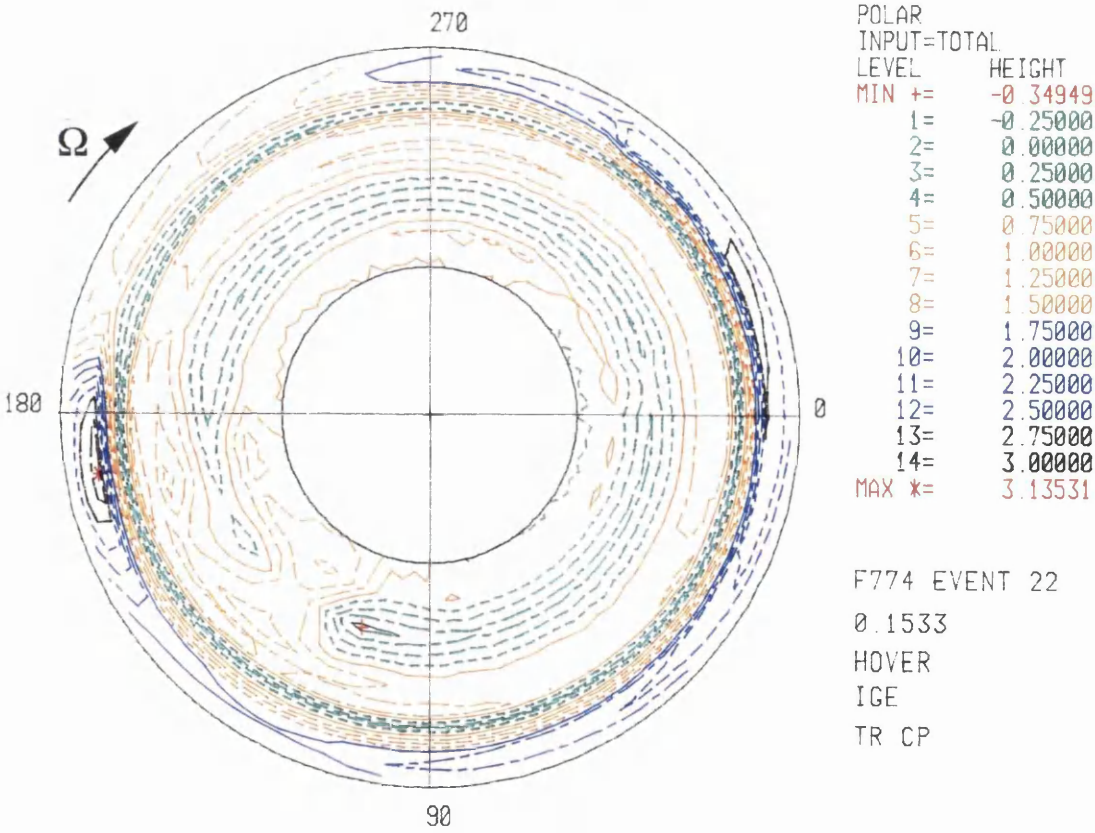

Figure 5.3.2 **Variation of Puma tail rotor leading edge $-C_p$ over one revolution in the hover.**

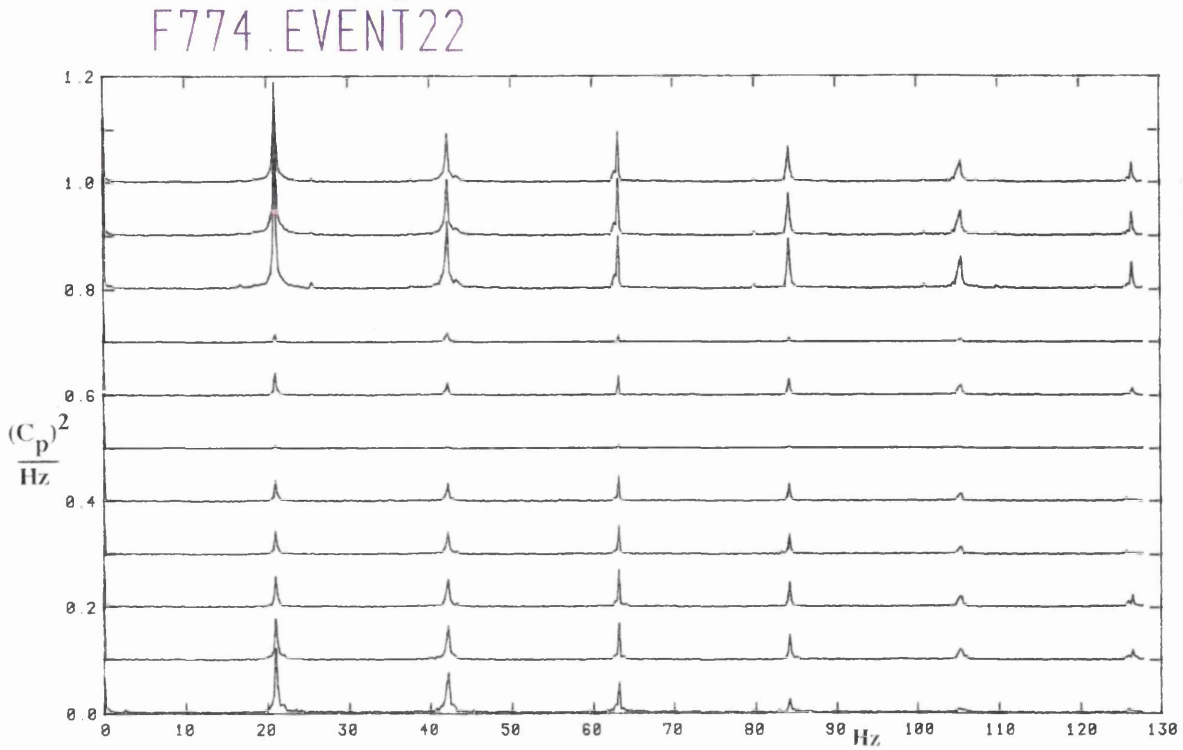

Figure 5.3.3 **Frequency content of Puma tail rotor leading edge sensor signals in the hover.**

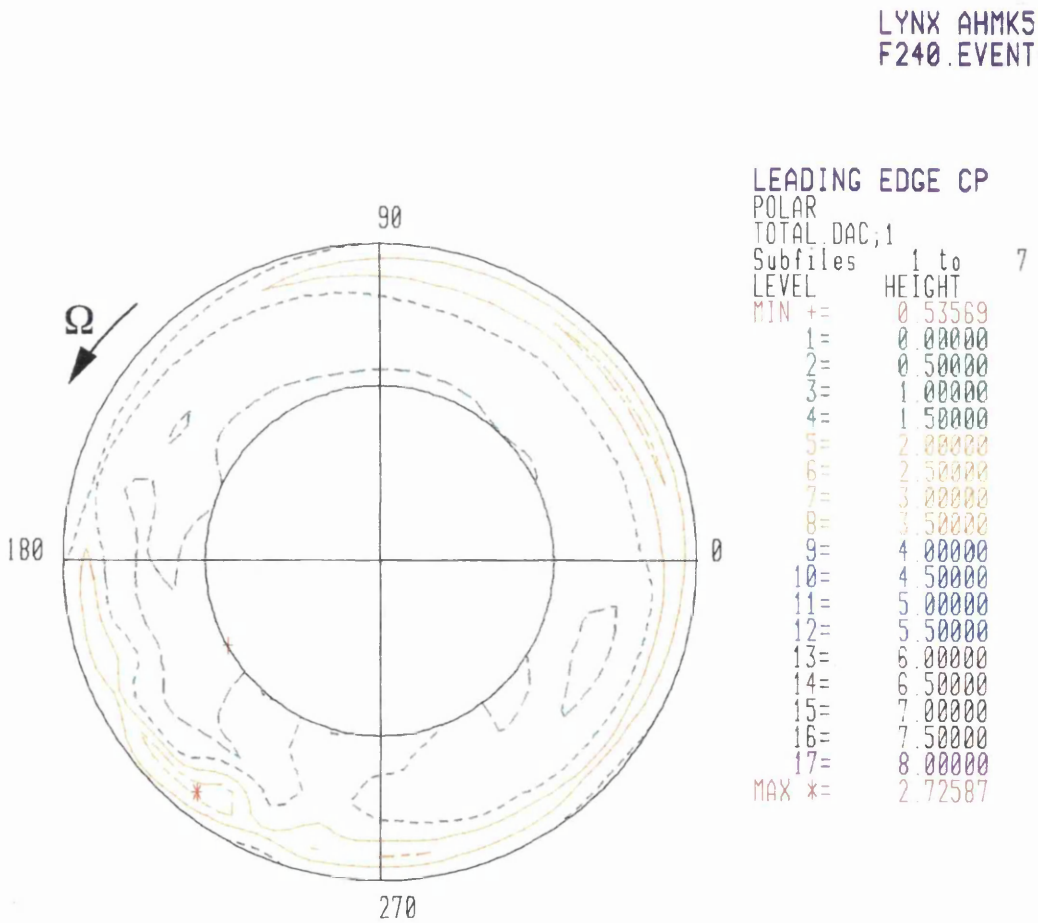

Figure 5.3.4 **Variation of Lynx AH Mk5 tail rotor leading edge $-C_p$ over one revolution in the hover. AUM = 4610kg**

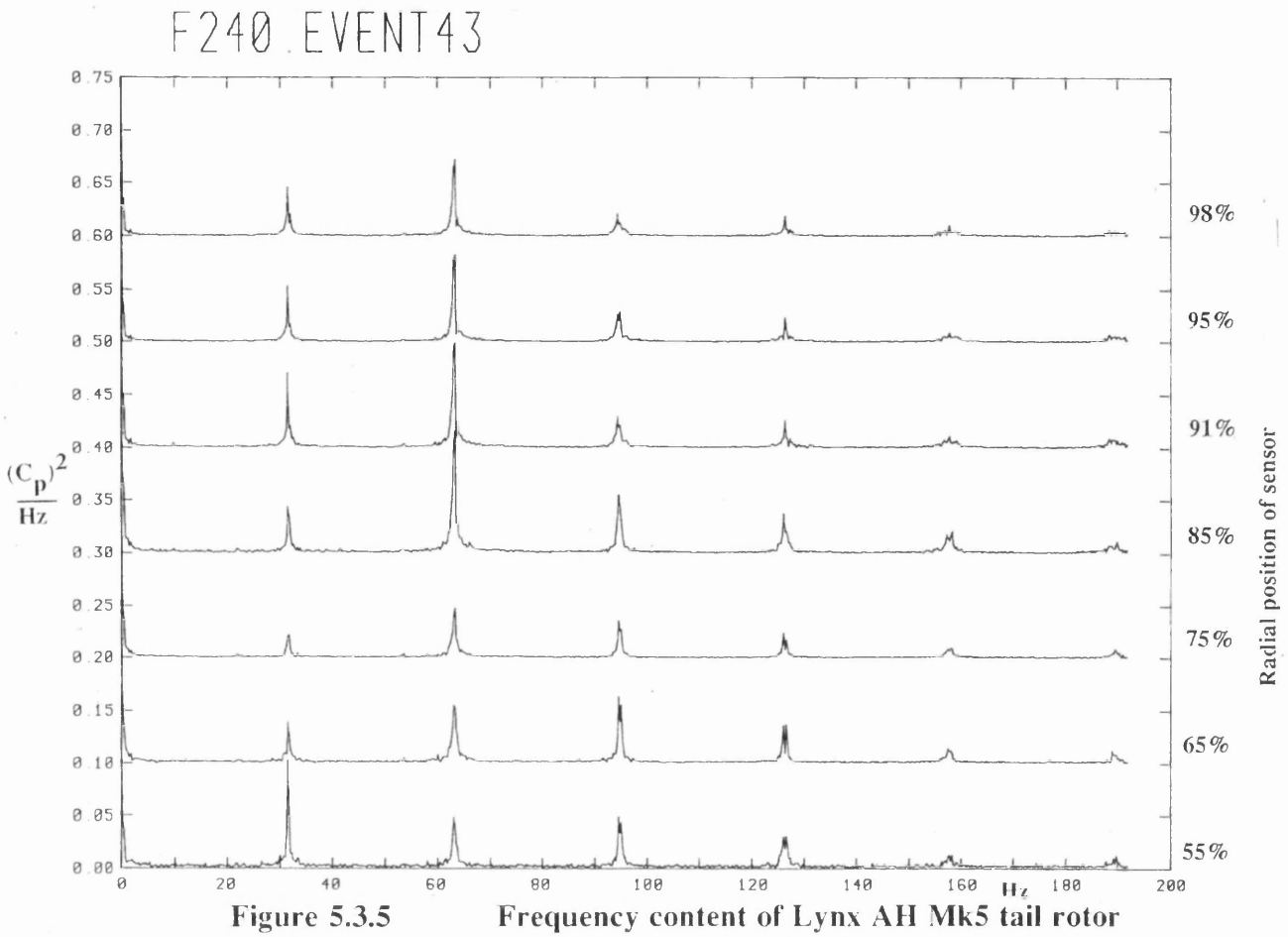

Figure 5.3.5 Frequency content of Lynx AH Mk5 tail rotor leading edge sensor signals in the hover.

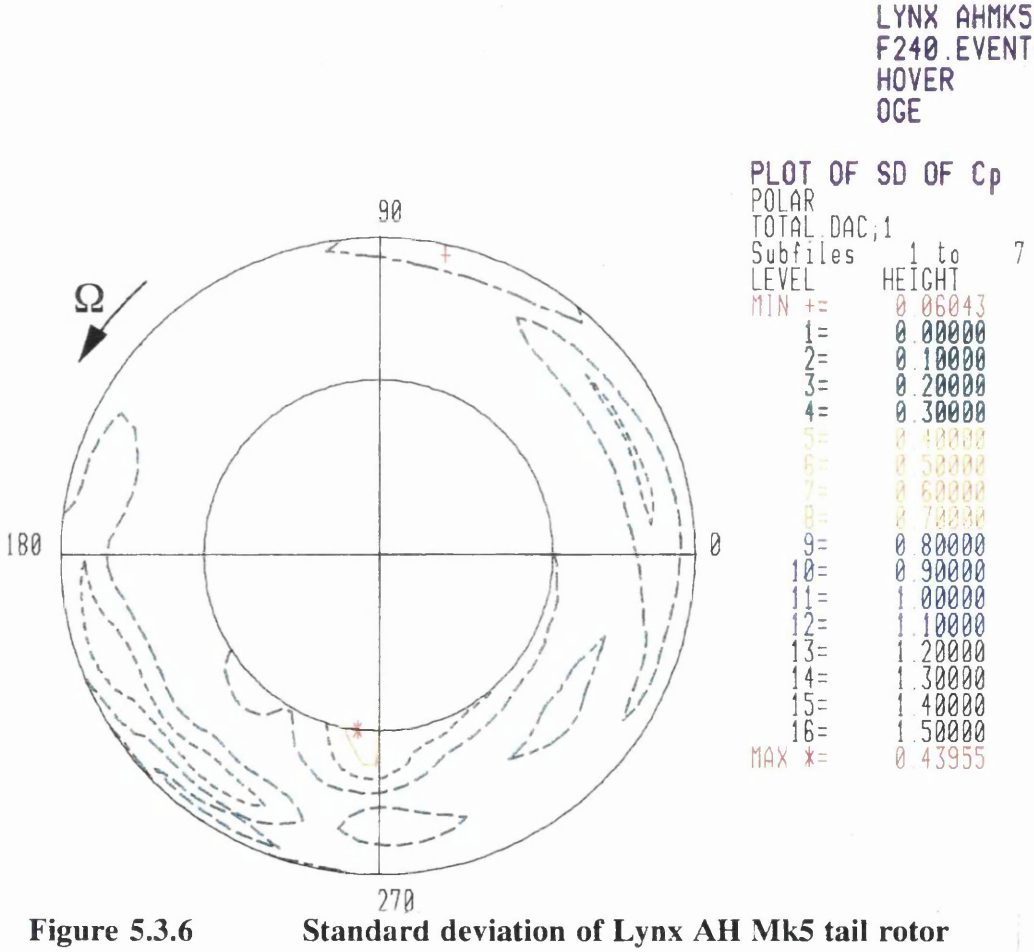

Figure 5.3.6 Standard deviation of Lynx AH Mk5 tail rotor leading edge $-C_p$ over 160 revolutions in the hover.

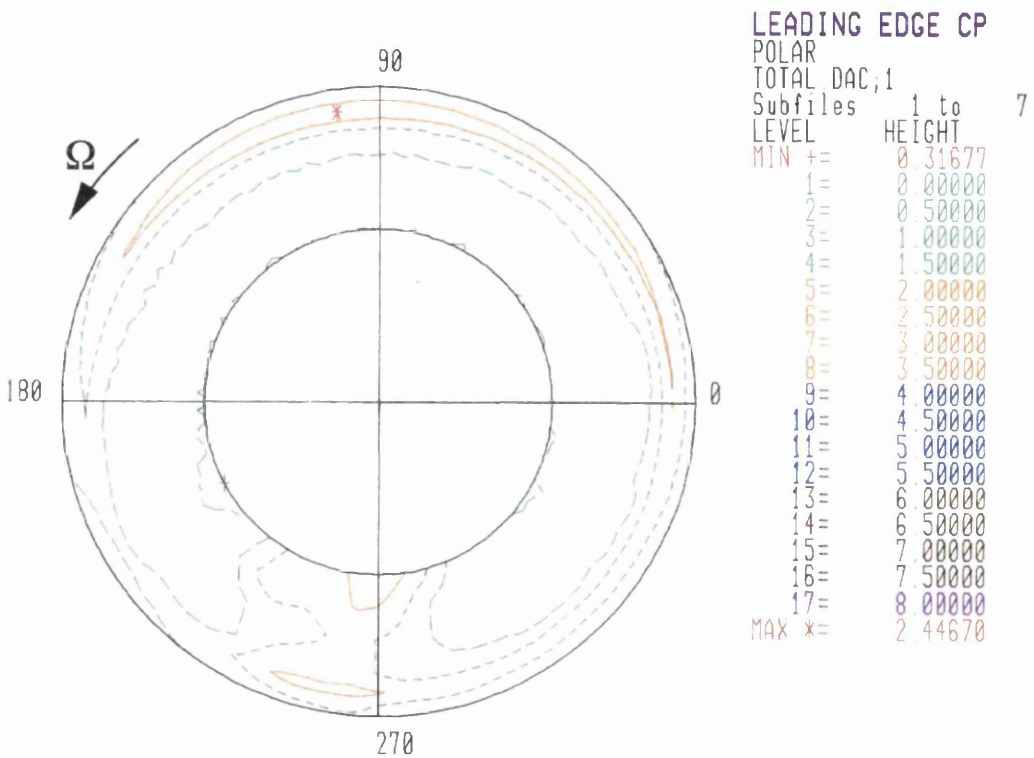

Figure 5.3.7 **Variation of Lynx AH Mk5 tail rotor leading edge $-C_p$ over one revolution in the hover. AUM = 3945kg**

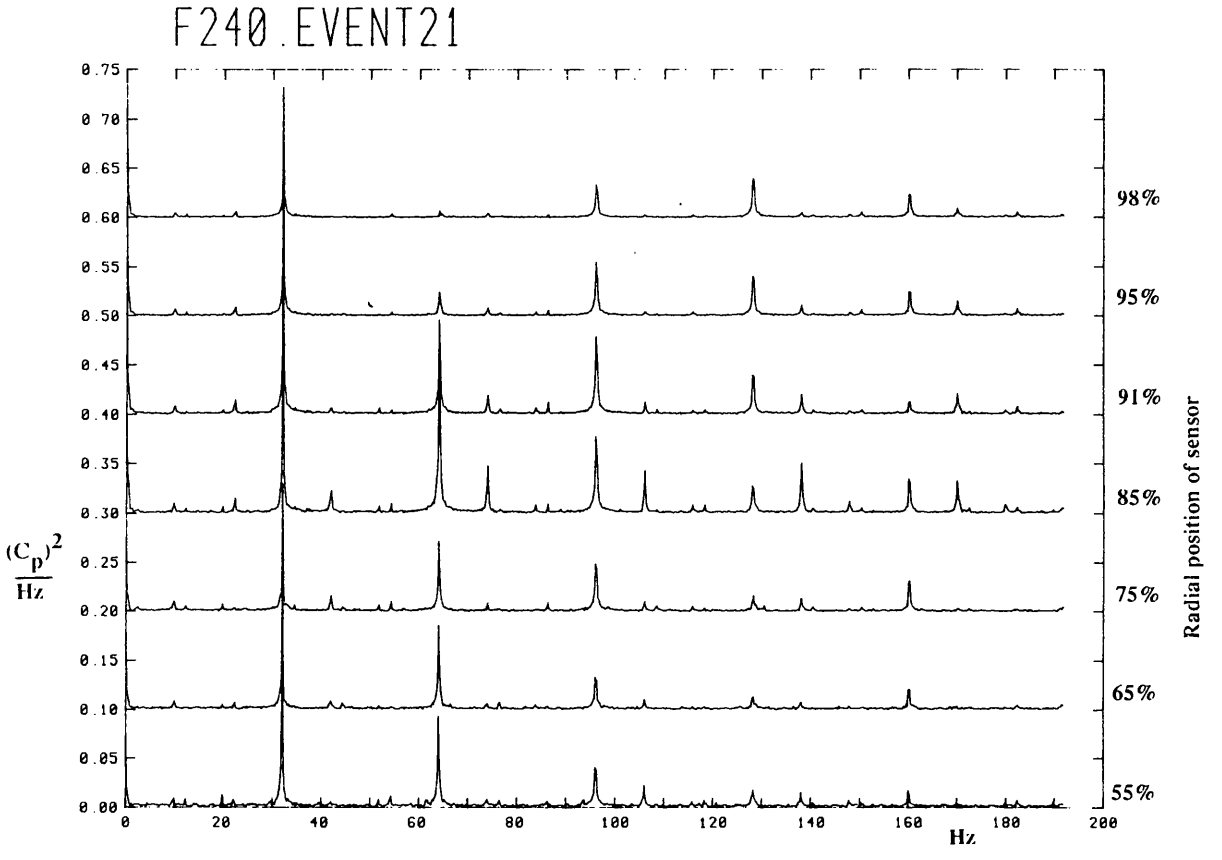

Figure5.4.1 Lynx tail rotor – 30 kts forward flight OGE Leading edge pressure sensor frequency content.

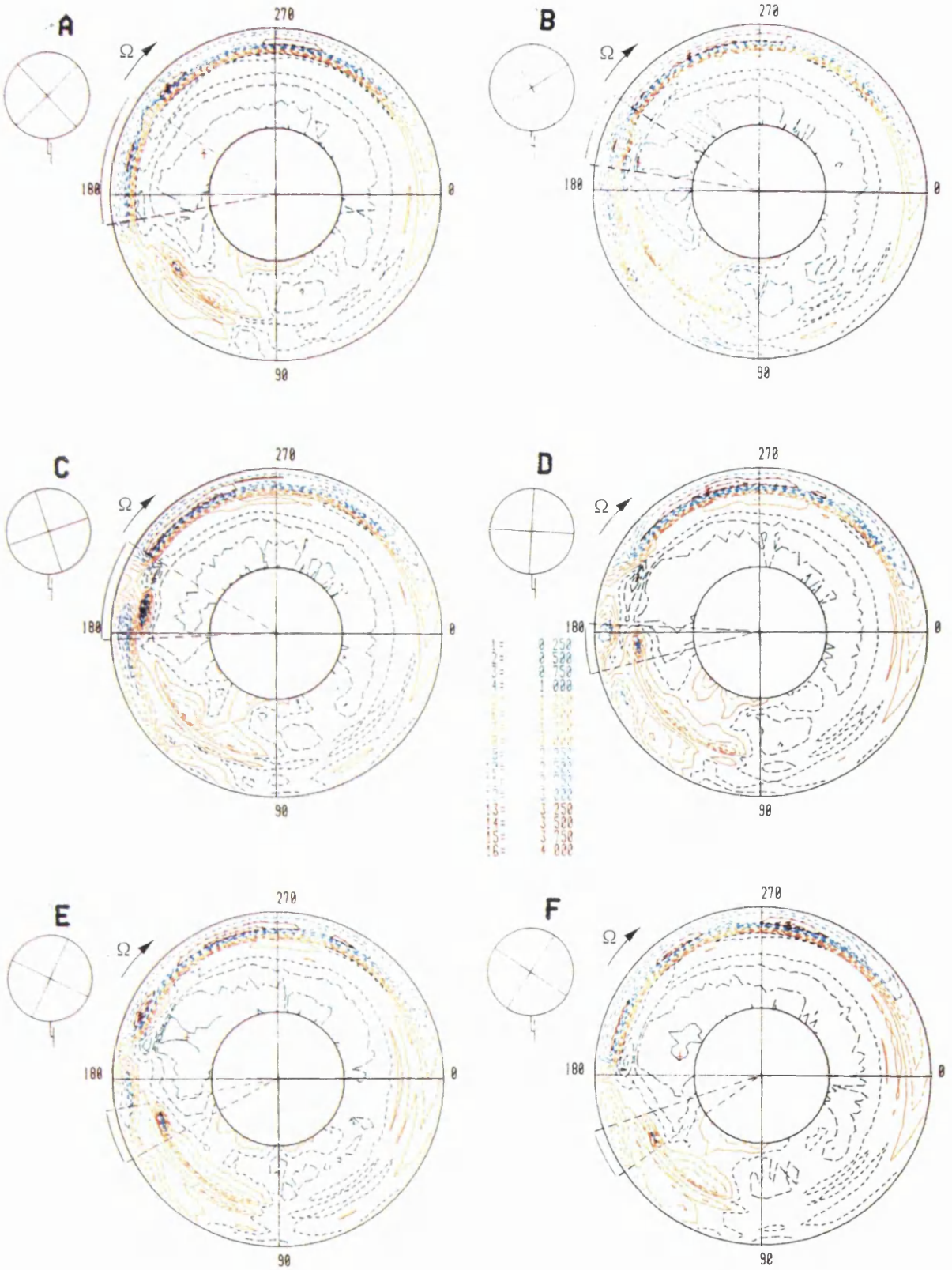

Figure5.4.2 Polar plots of Puma tail rotor $-C_p$ in 10 kts forward flight OGE

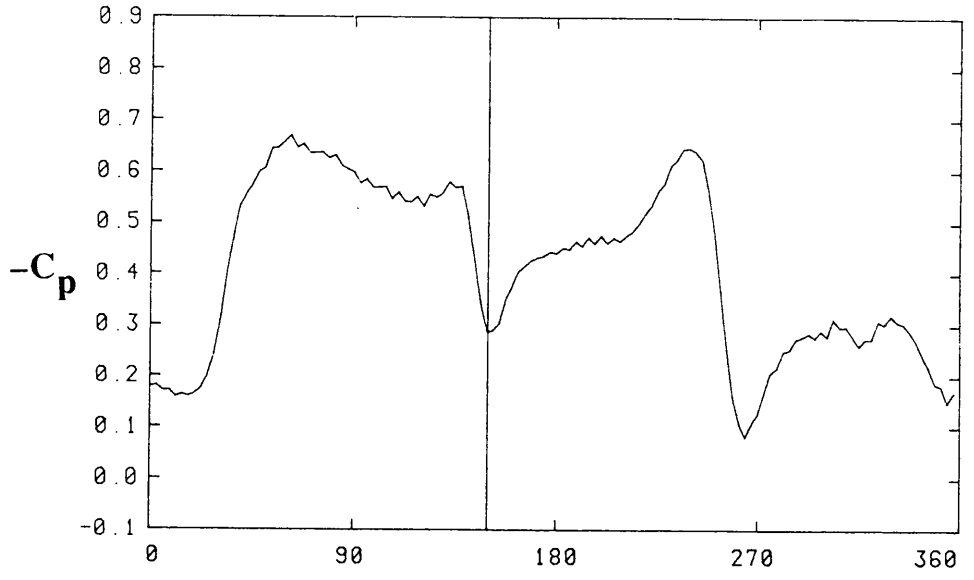

Figure5.4.3 **Variation in $-C_p$ at the 98% blade radius leading edge sensor for one revolution of the tail rotor.**
The localised reduction in $-C_p$ indicated by the vertical line is caused by the interaction of a main rotor blade trailing tip vortex and the preceding tail rotor blade.

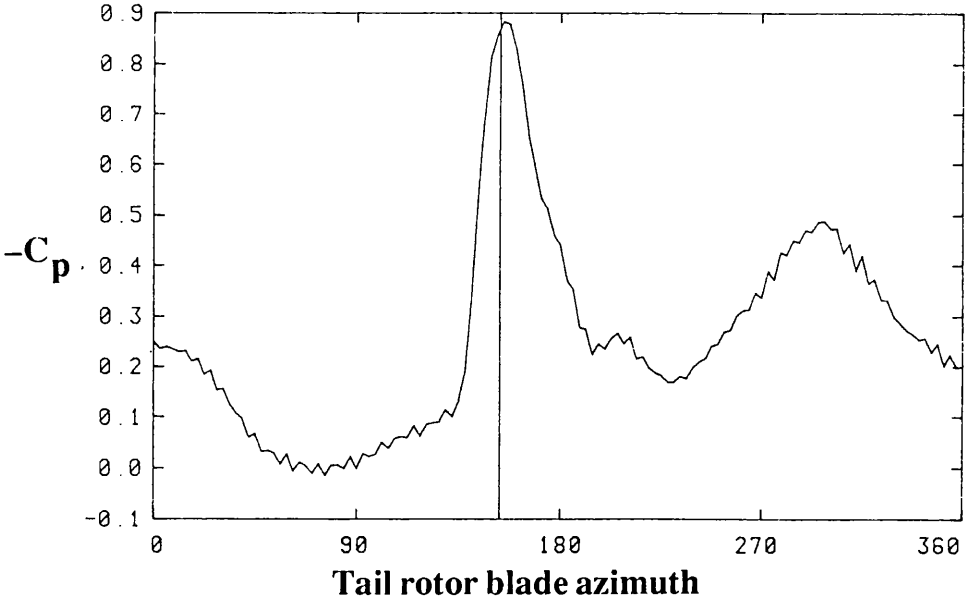

Figure5.4.4 **Variation in $-C_p$ at the 75% blade radius leading edge sensor for one revolution of the tail rotor.**
A main rotor vortex is approaching the sensor and the localised increase in $-C_p$ indicated by the vertical line is due to the velocity induced by that vortex opposing blade rotation.

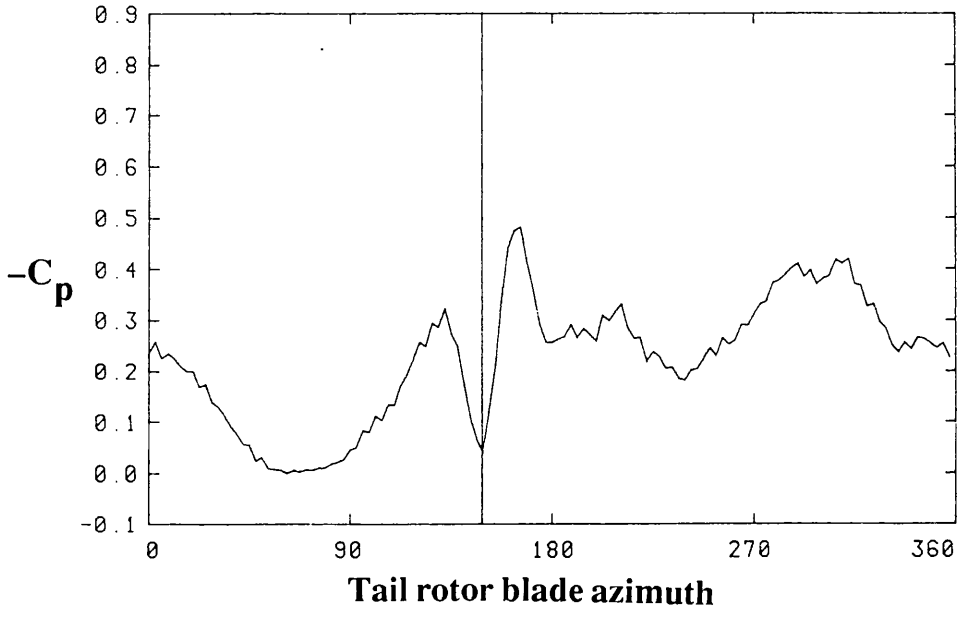

Figure5.4.5 Variation in $-C_p$ at the 75% blade radius leading edge sensor for one revolution of the tail rotor.
A main rotor vortex has just passed the sensor and the localised reduction in $-C_p$ indicated by the vertical line is due to the velocity induced by that vortex being with blade rotation.

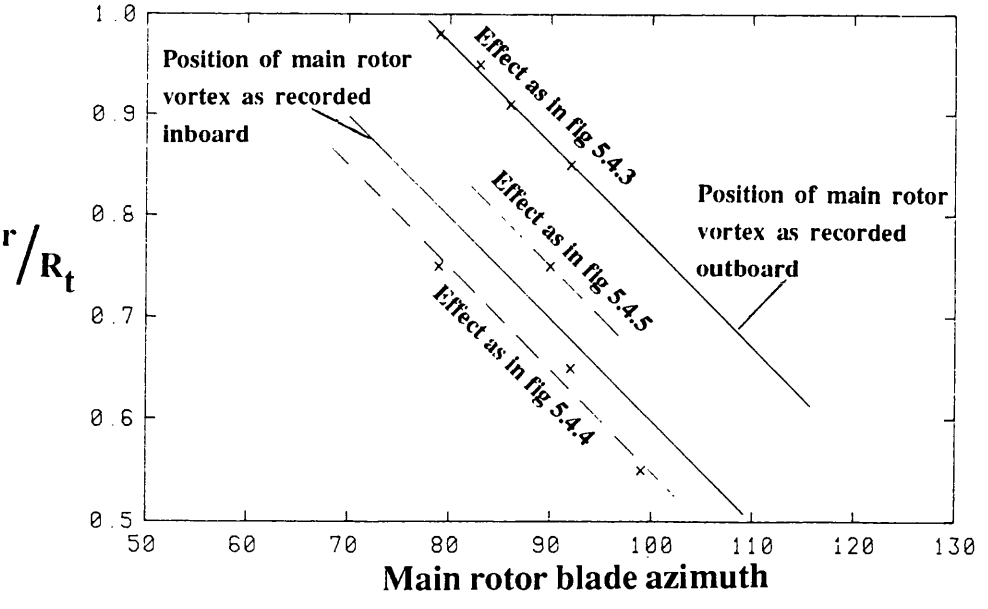

Figure5.4.6 Plot showing the position of the datum main rotor blade as the main rotor blade trailing tip vortex interference effect is detected at each tail rotor blade leading edge sensor.

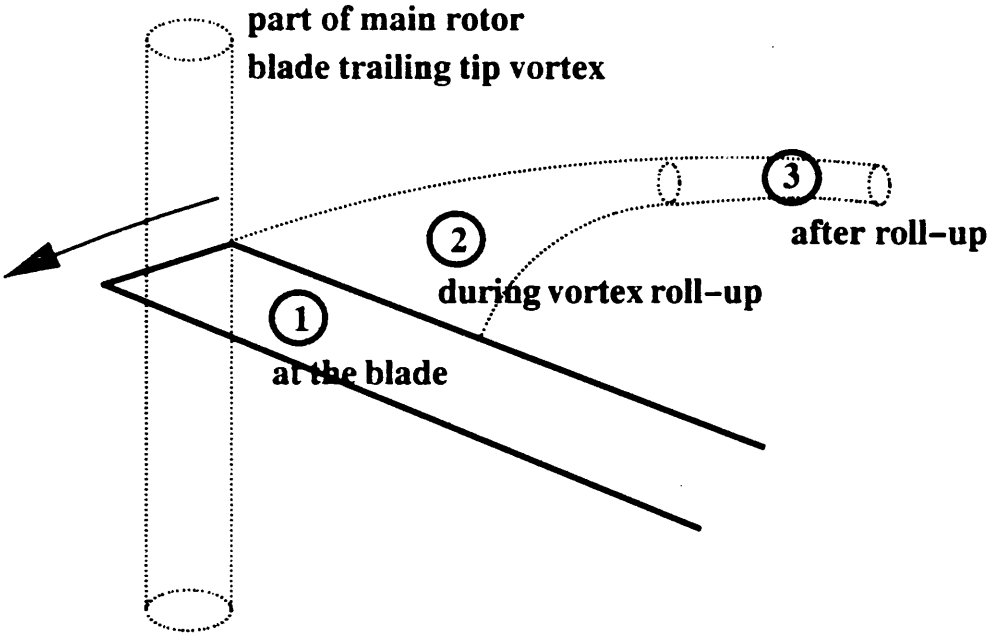

Figure 5.4.1.1 Sketch of main rotor blade trailing tip vortex/ tail rotor blade trailing tip vortex interaction showing three phases of interaction.

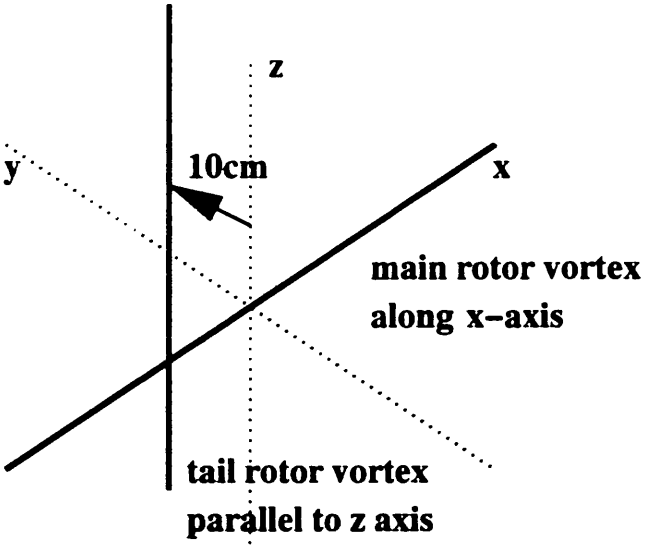

Figure 5.4.1.2 Vortex interaction model starting positions.

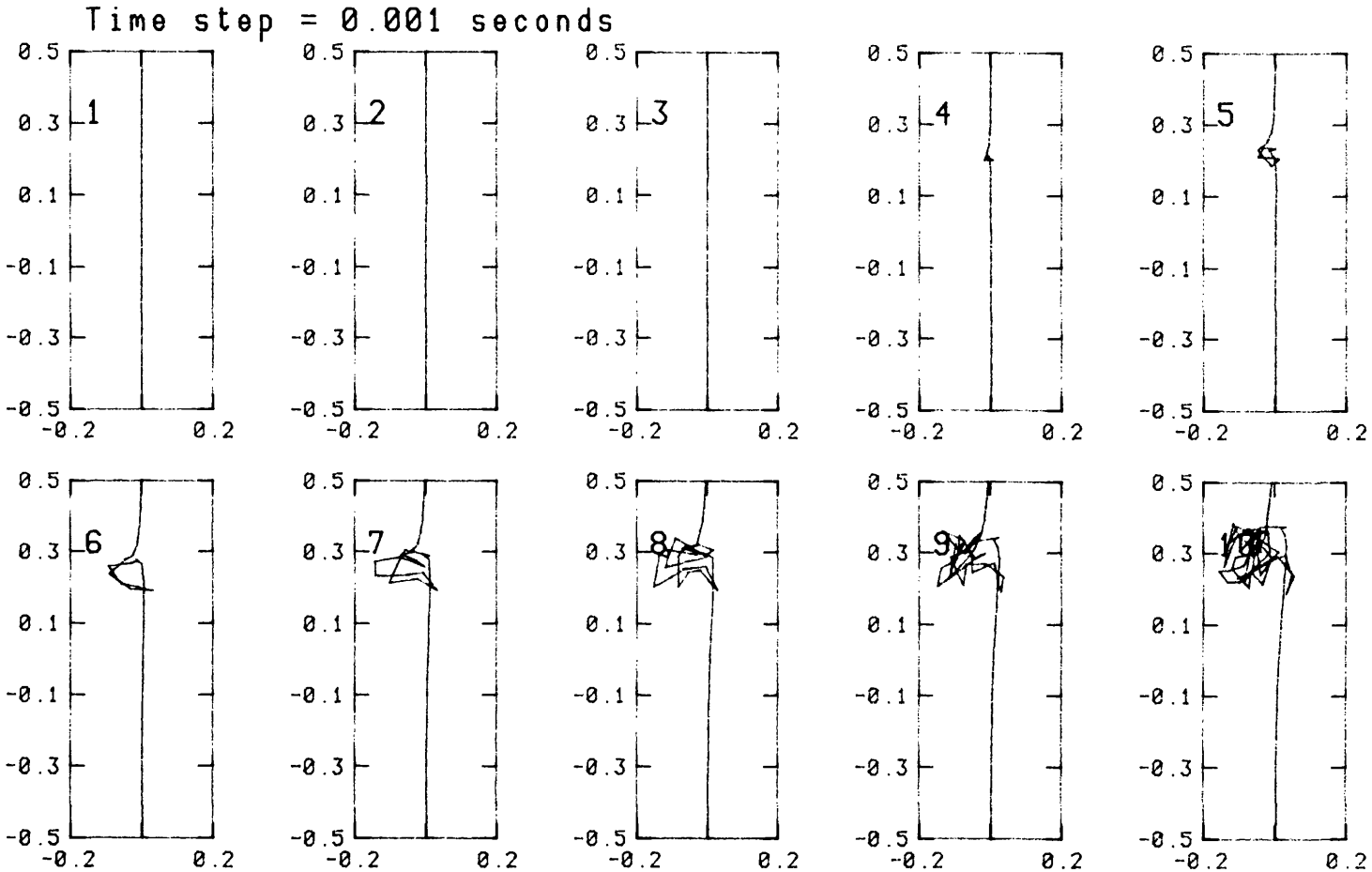

Figure5.4.1.3 Plots showing calculated changes in the tail rotor blade trailing tip vortex produced by the model over the first 10 milleseconds. The main rotor vortex only showed a slight bulge in the same timescale.

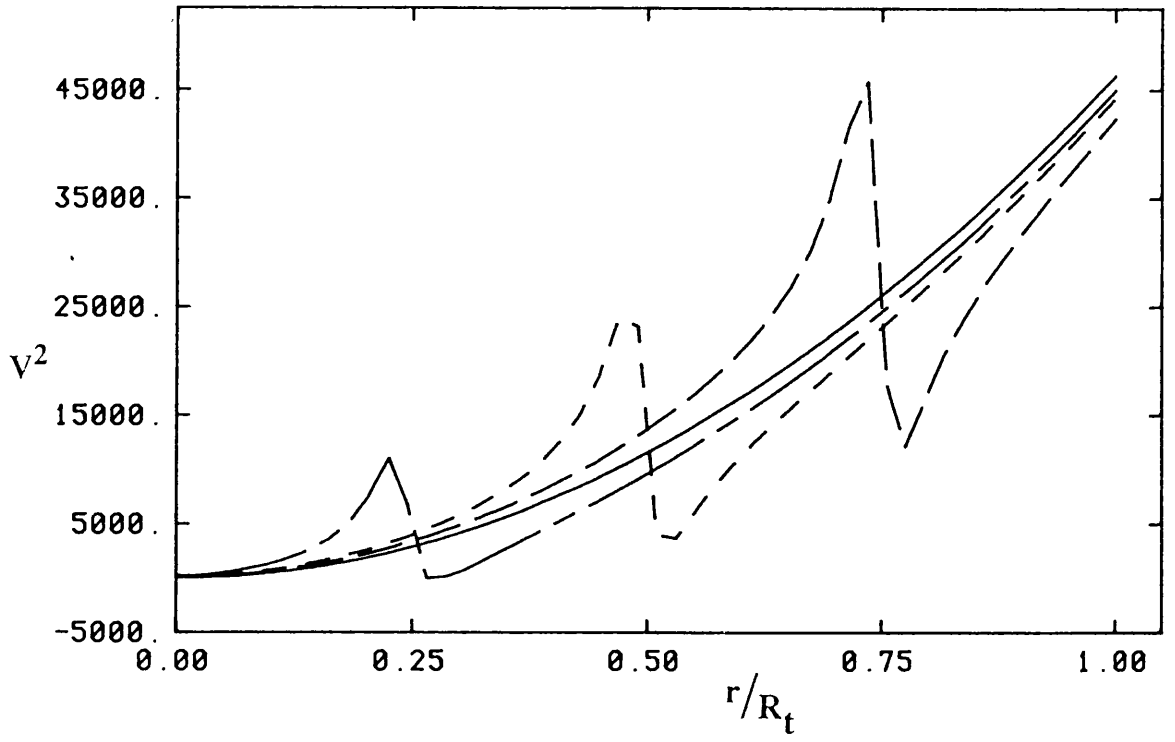

Figure5.4.2.1 Theoretical variation in V^2 with blade radius for a tail rotor rotating top blade forward. The effect of a main rotor blade trailing tip vortex is shown for three vortex locations (25, 50 & 75% rotor radius).

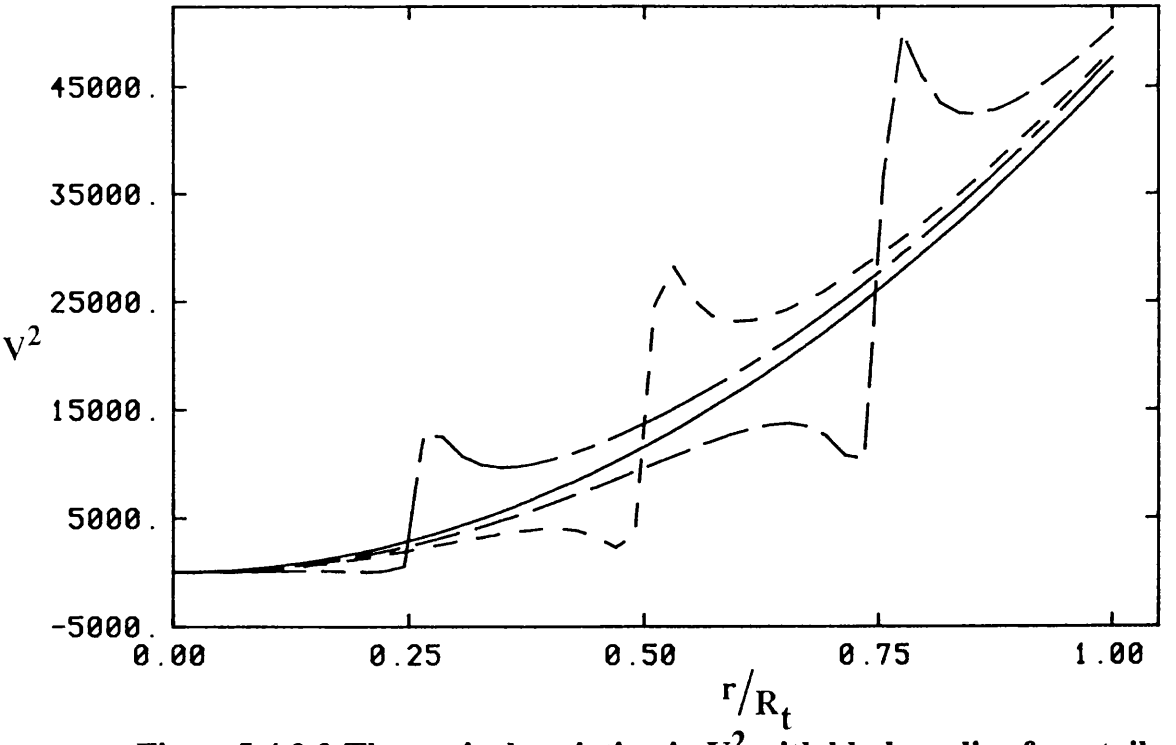

Figure5.4.2.2 Theoretical variation in V^2 with blade radius for a tail rotor rotating top blade aft. The effect of a main rotor blade trailing tip vortex is shown for three vortex locations (25, 50 & 75% rotor radius).

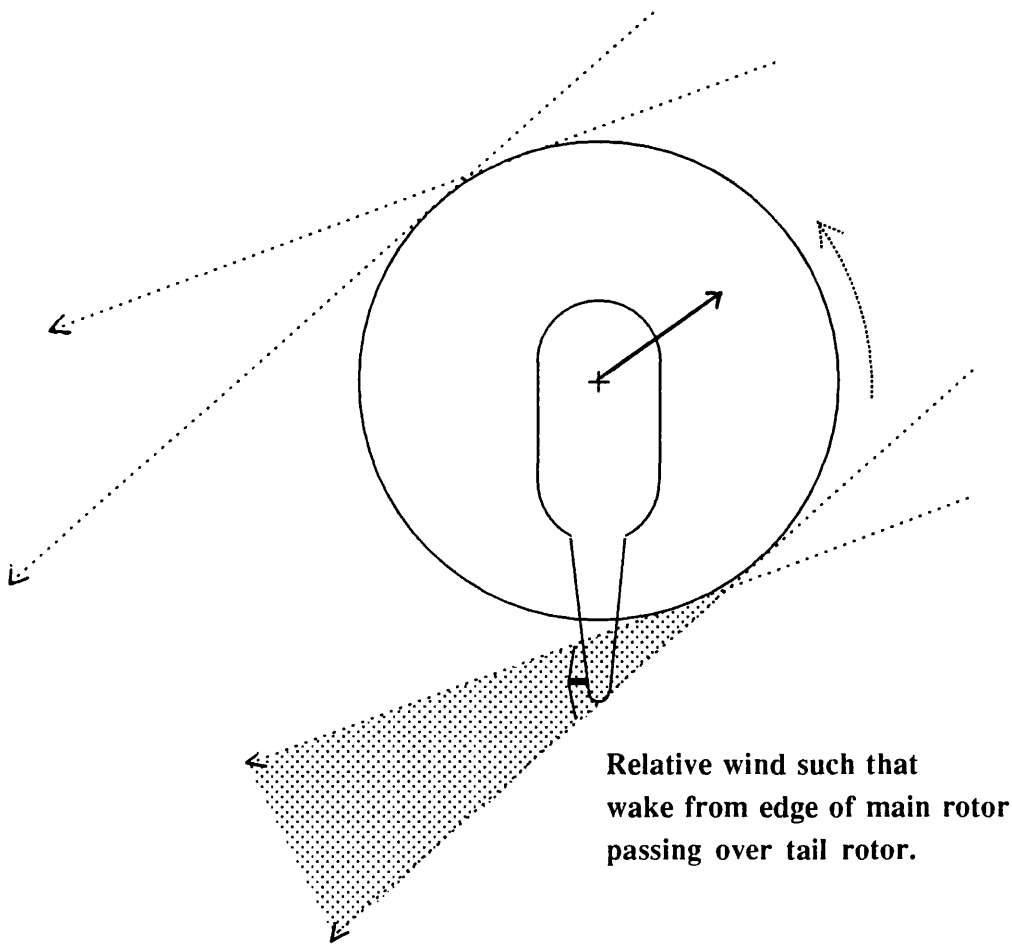

Figure5.5.1 Definition of quartering flight.

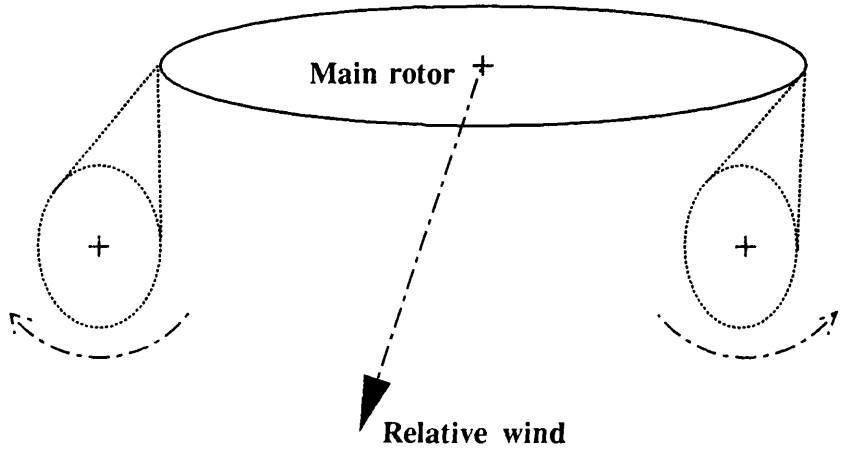

Figure5.5.2 Direction of rotation of both "wing tip" vortices is bottom–away from aircraft centreline.

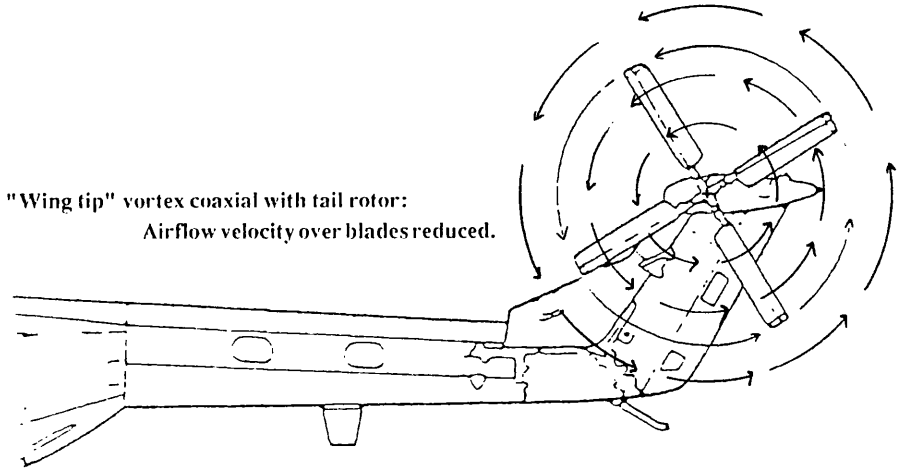

Figure5.5.3 "Wing tip" vortex coincident with tail rotor.

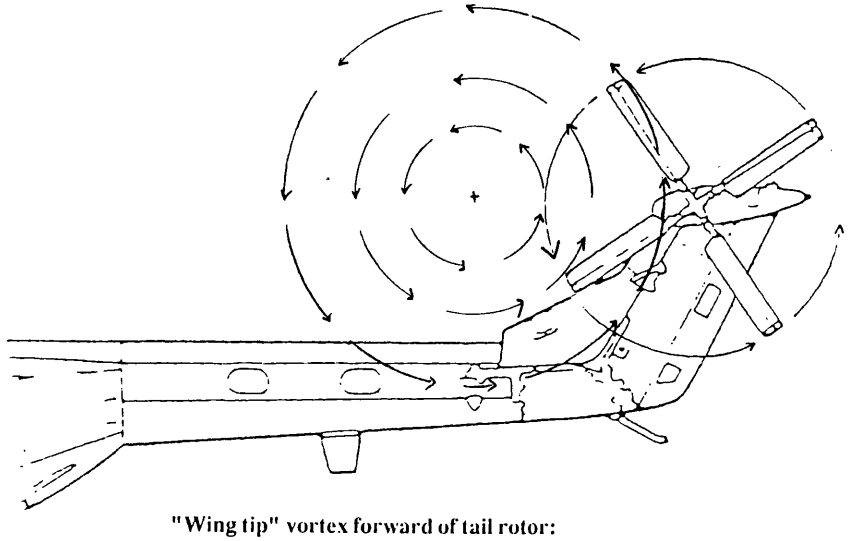

Figure5.5.4 "Wing tip" vortex forward of tail rotor.

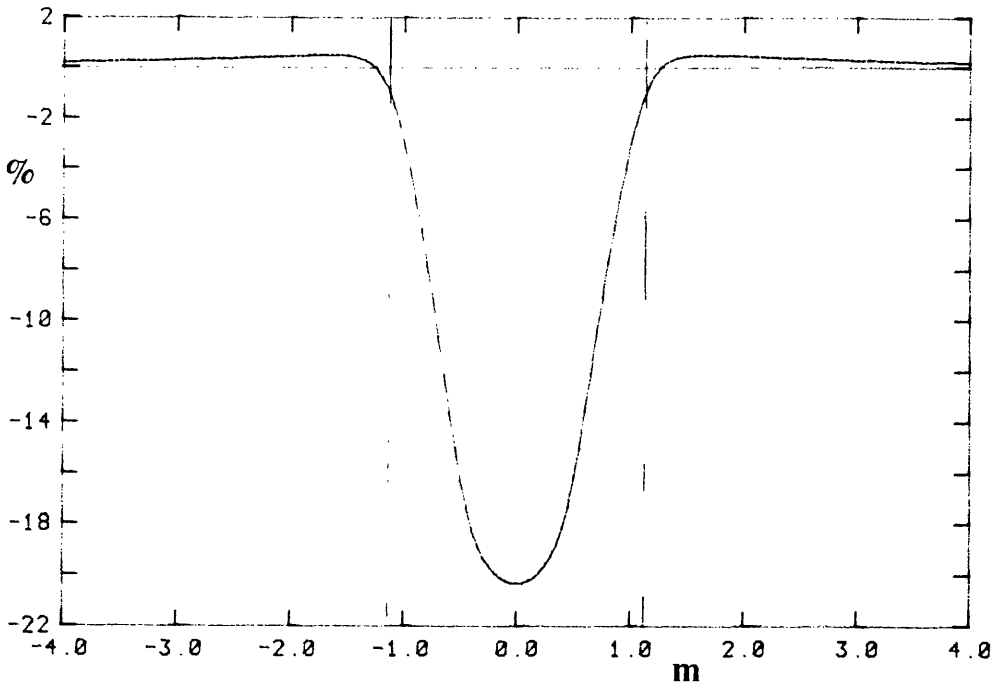

Figure5.5.5 Percentage change in overall tail rotor dynamic head as a representative "wing tip" vortex tracks diametrically across the disc. Tail rotor radius is 1.1m.

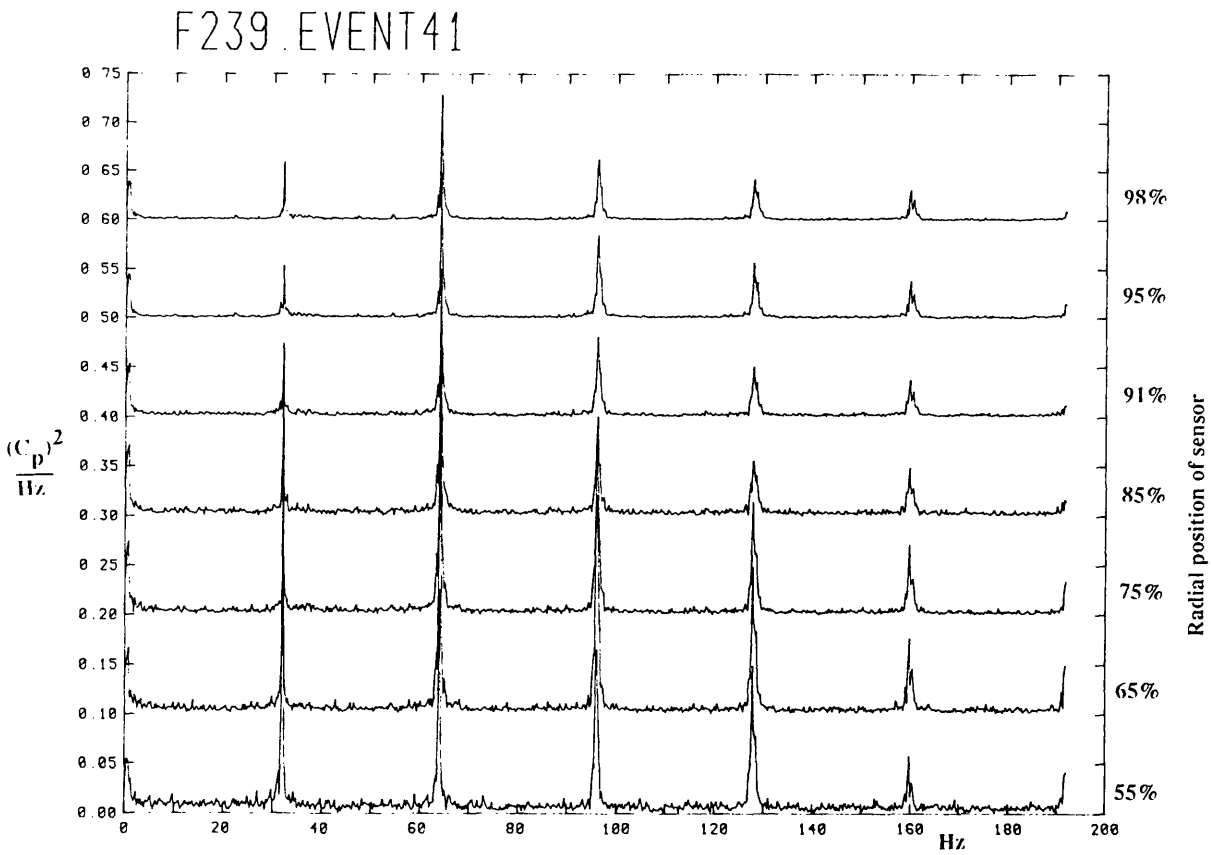

Figure 5.5.6 Signal frequency content in quartering flight.

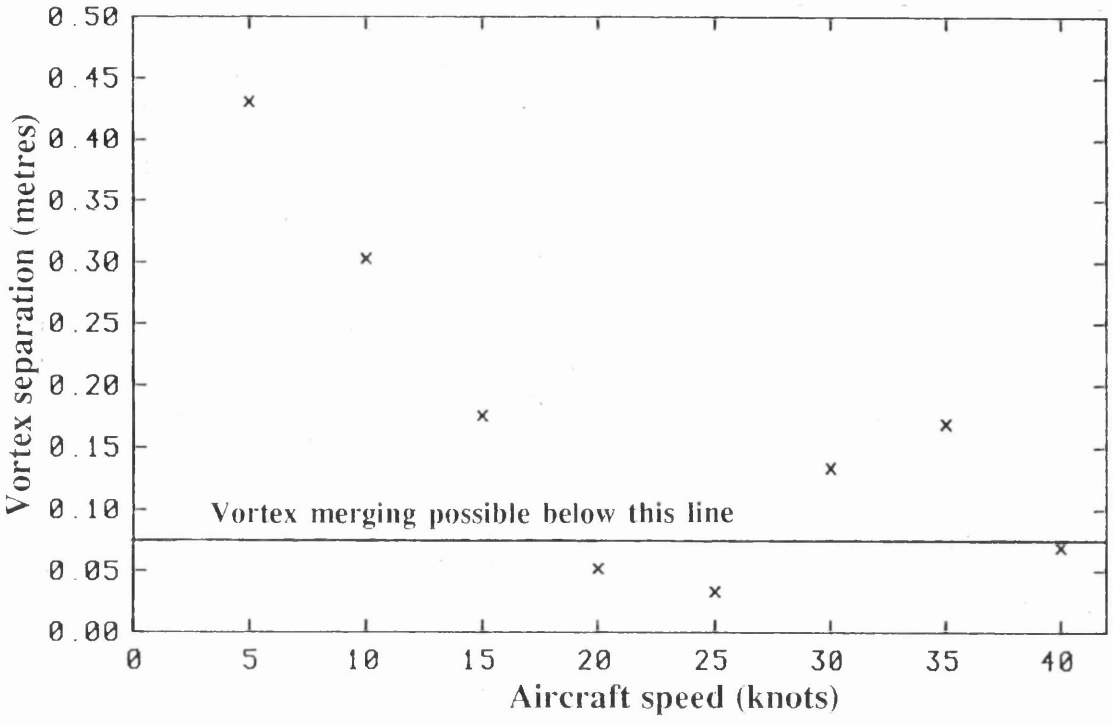

Figure 5.5.7 **Variation in minimum separation distance between individual blade trailing tip vortices within the "wingtip" vortices with aircraft speed as calculated for a Lynx AH Mk5.**

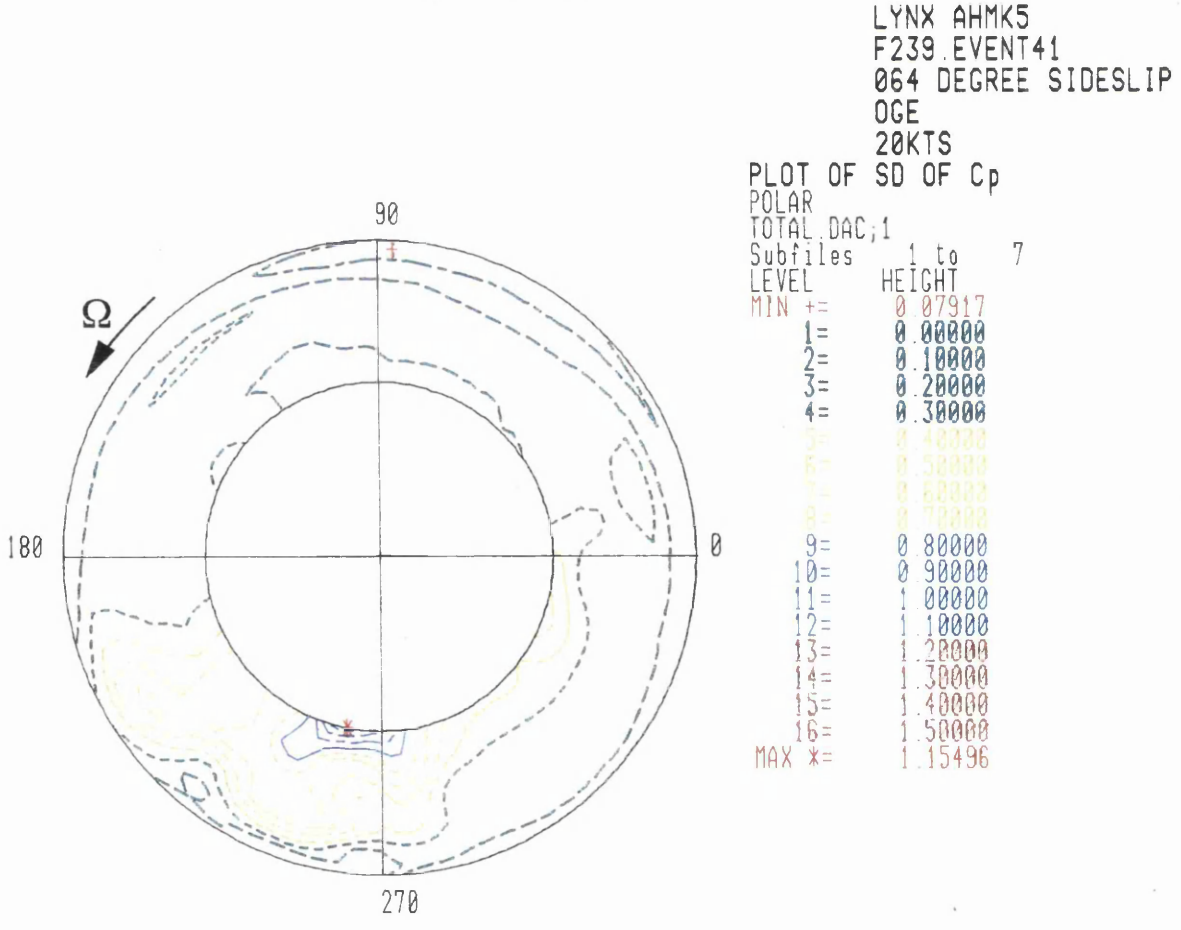

Figure 5.5.8 **Standard deviation of Lynx AH Mk5 tail rotor leading edge $-C_p$ over 160 revolutions in flight 20kts/60° OGE.**

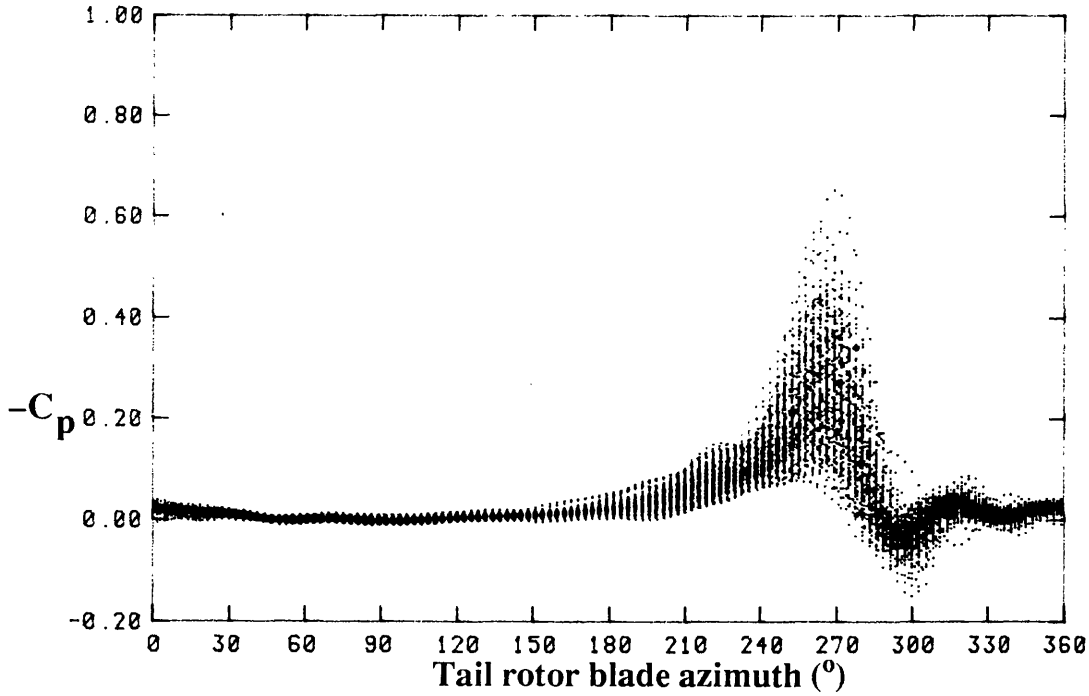

Figure 5.5.9 Variation of trailing edge C_p at 85 % blade radius with tail rotor blade azimuth over 160 revolutions on Lynx AH Mk5 during flight 20 kts/060° OGE

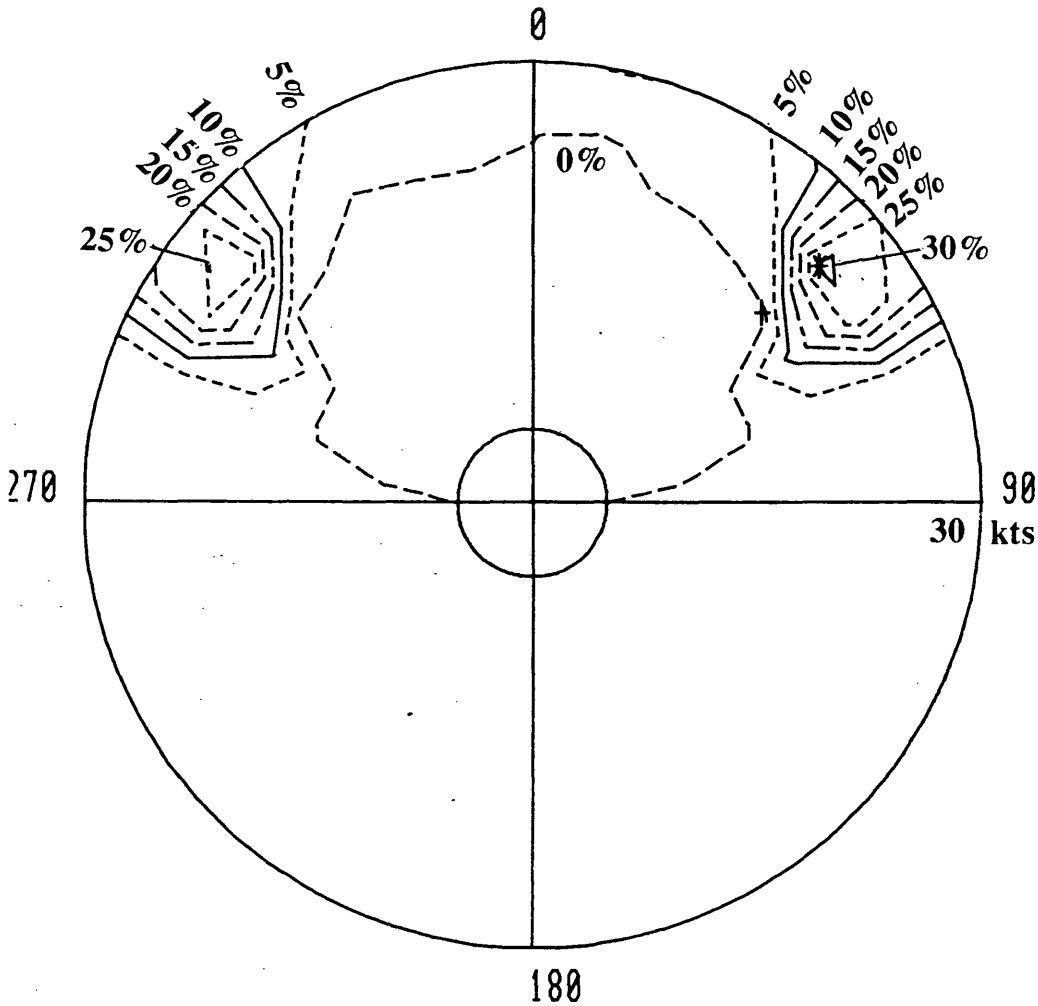

Figure 5.5.10 Variation in total tail rotor dynamic head as calculated using Helistab in conjunction with the Beddoes main rotor wake model.

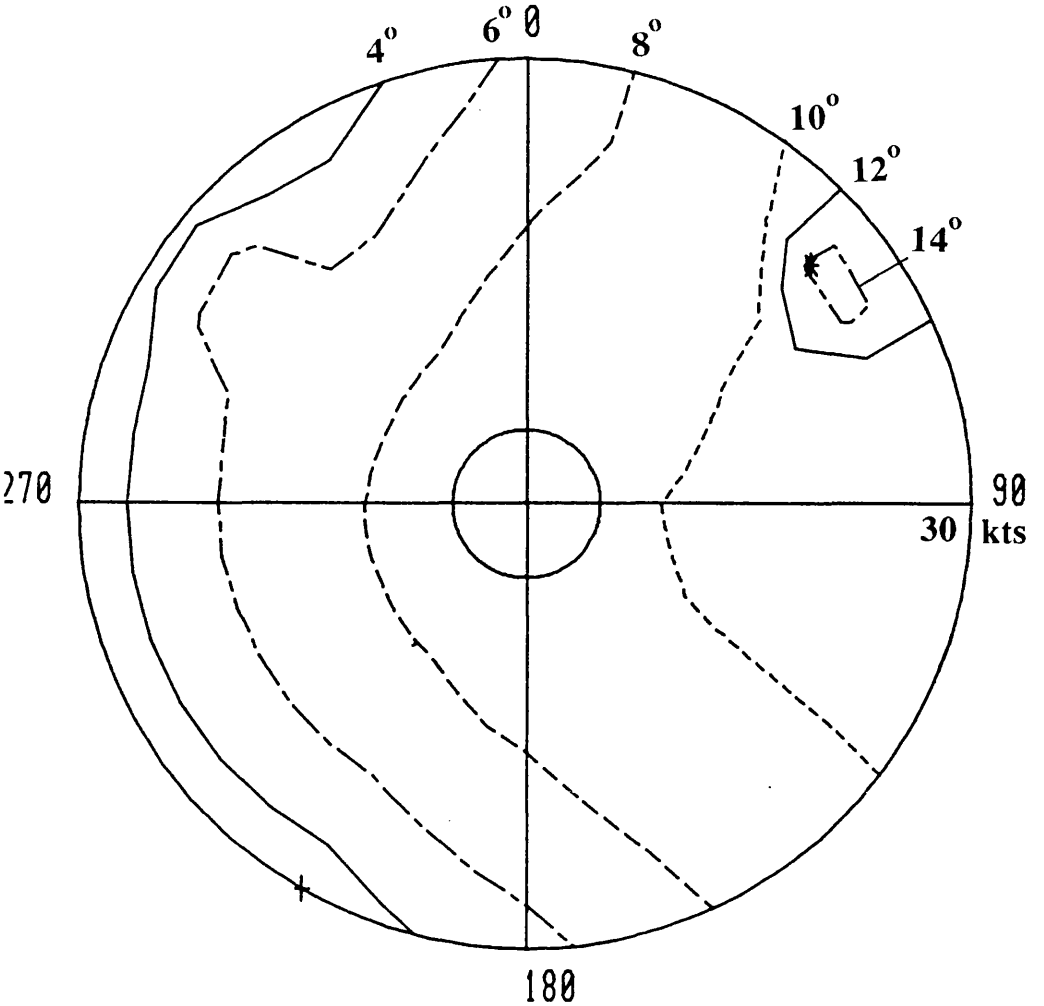

Figure5.5.11 Variation in tail rotor blade root pitch angle as calculated using Helistab in conjunction with the Beddoes main rotor wake model.

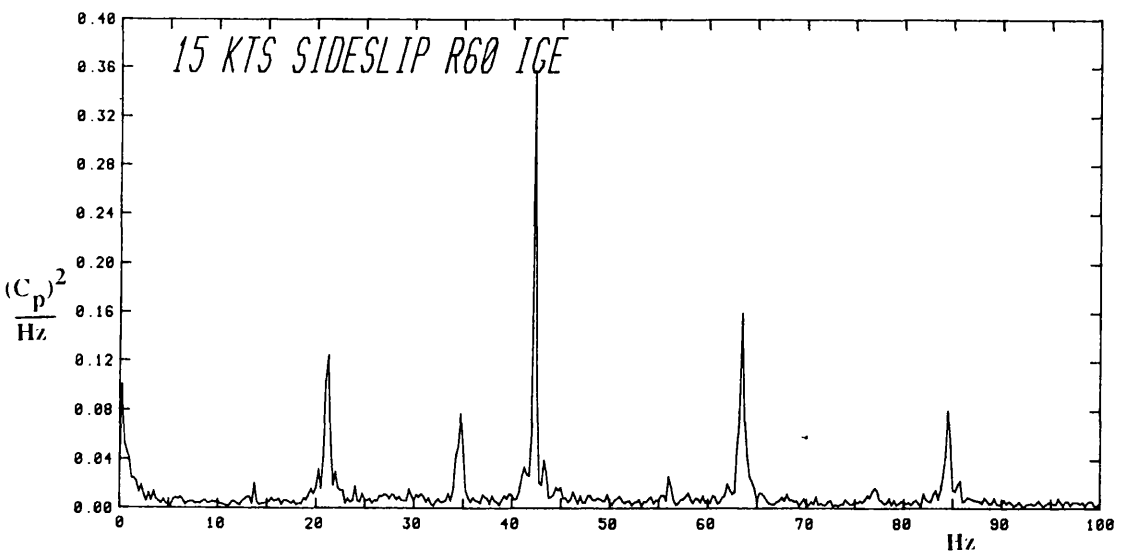

Figure 5.5.12 Frequency content of the 84% tail rotor radius leading edge sensor on the Puma during tail rotor buzz.

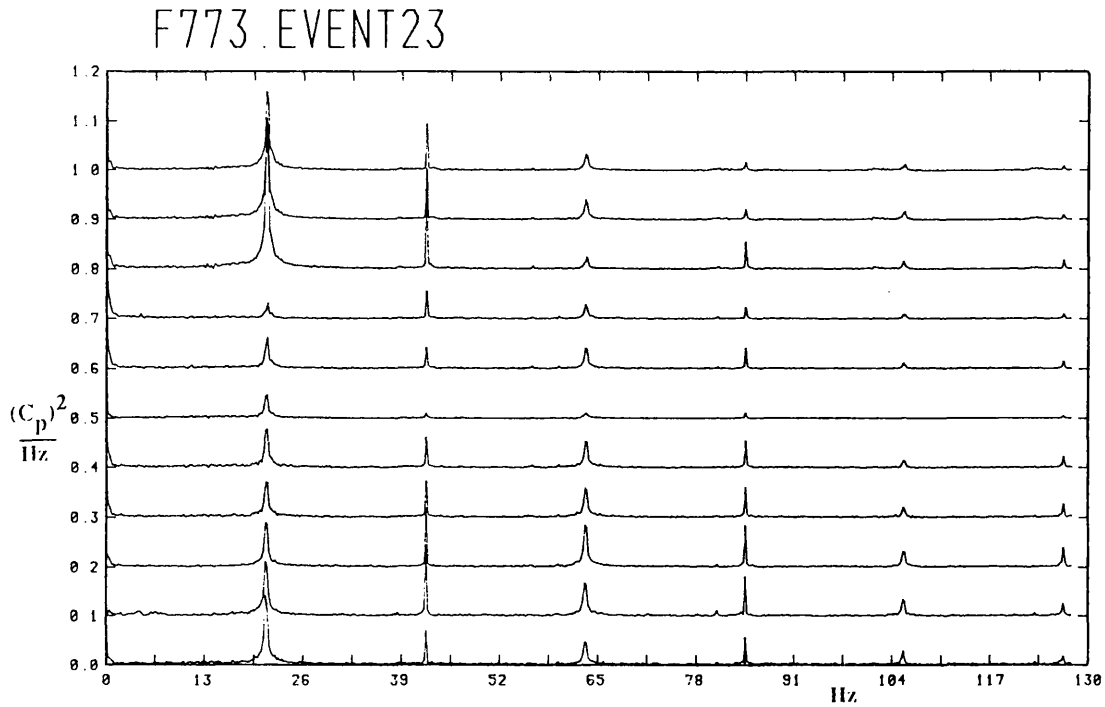

Figure5.6.1 Puma tail rotor blade leading edge sensor frequency content in flight 20kts/180°OGE.

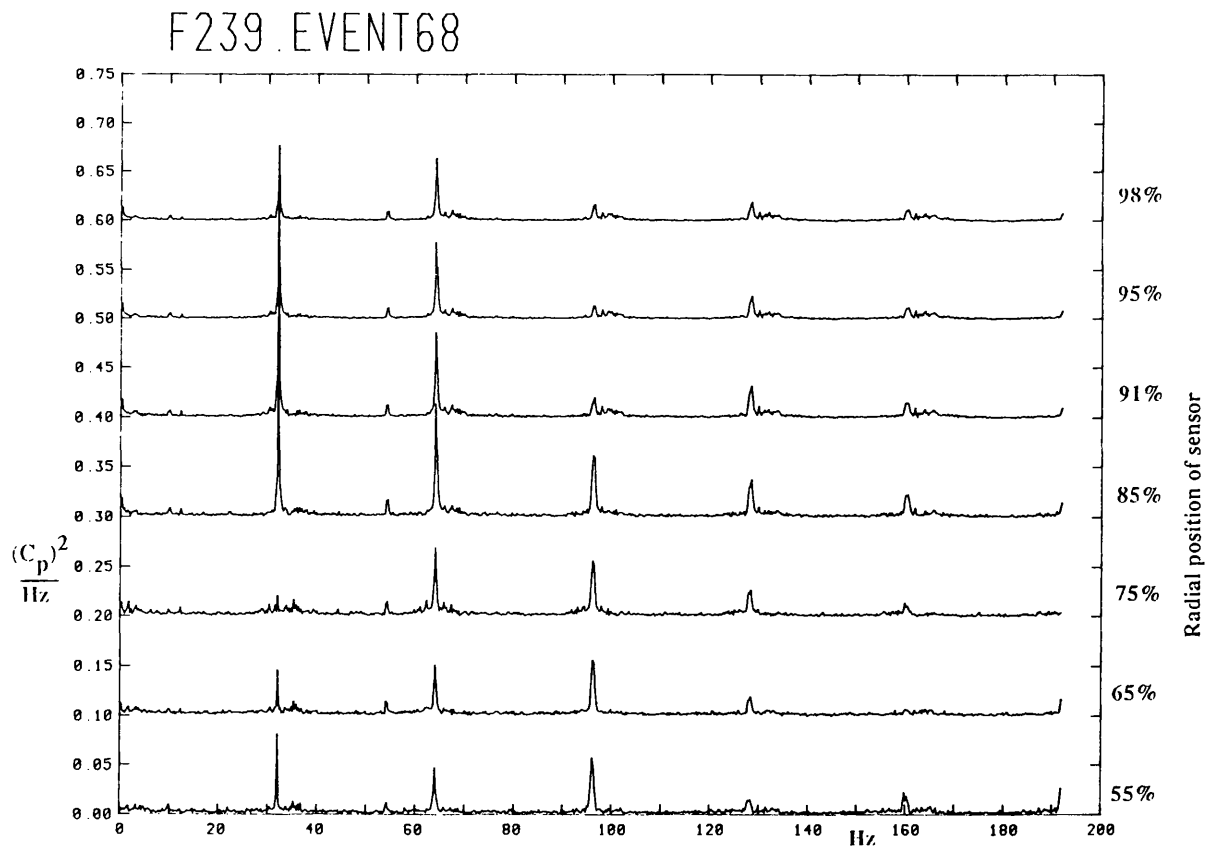

Figure5.6.2 Lynx tail rotor blade leading edge sensor frequency content in flight 30kts/150°OGE.

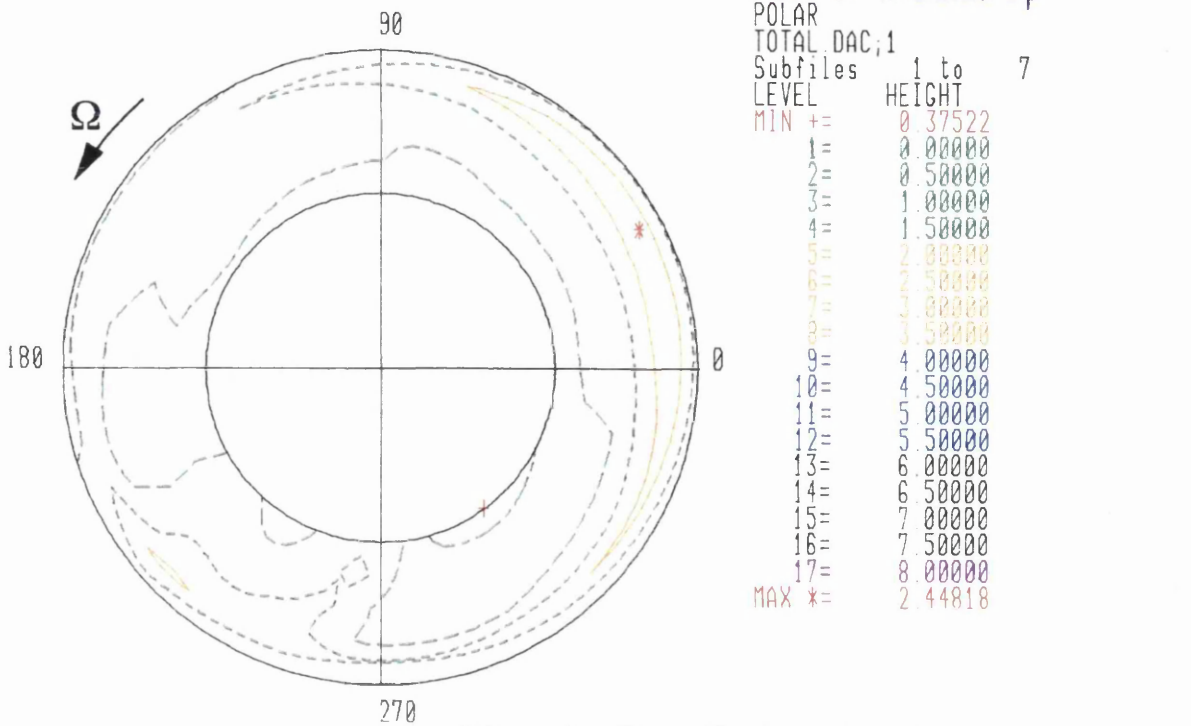

Figure 5.6.3 Lynx AH Mk5 tail rotor leading edge $-C_p$ averaged over 160 revolutions in flight 30kts/150° OGE.

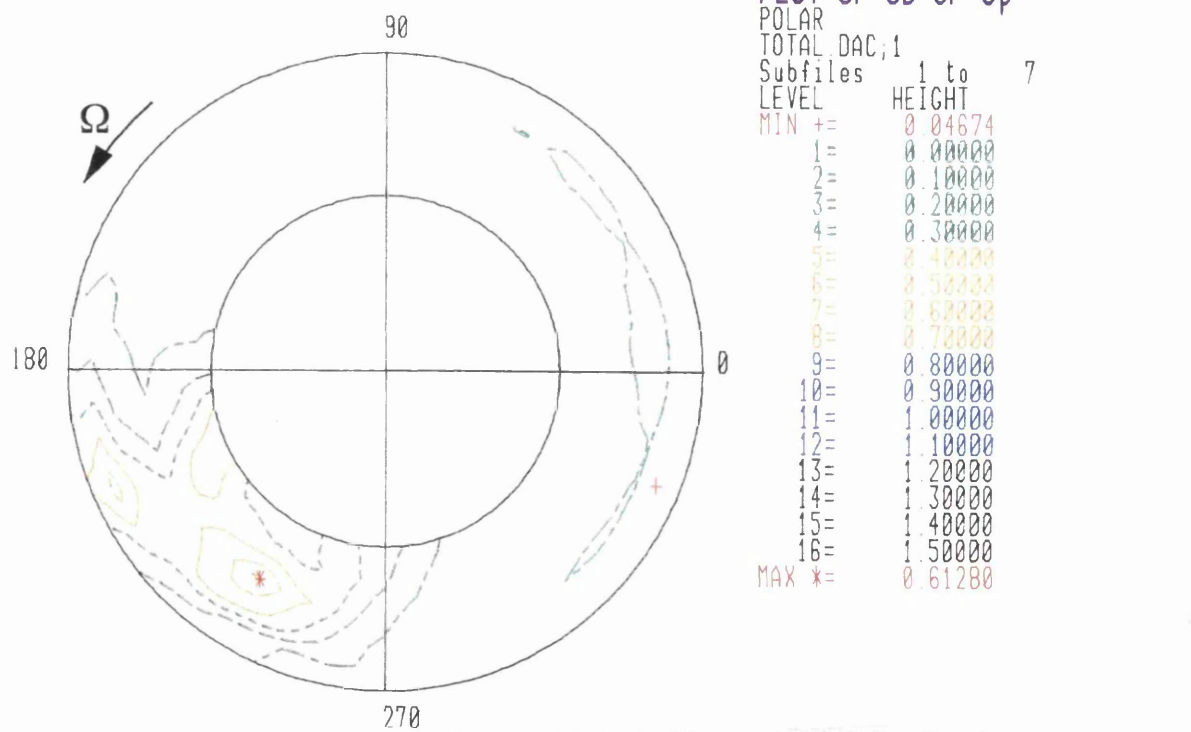

Figure 5.6.4 Standard deviation of Lynx AH Mk5 tail rotor leading edge $-C_p$ over 160 revolutions in flight 30kts/150° OGE.

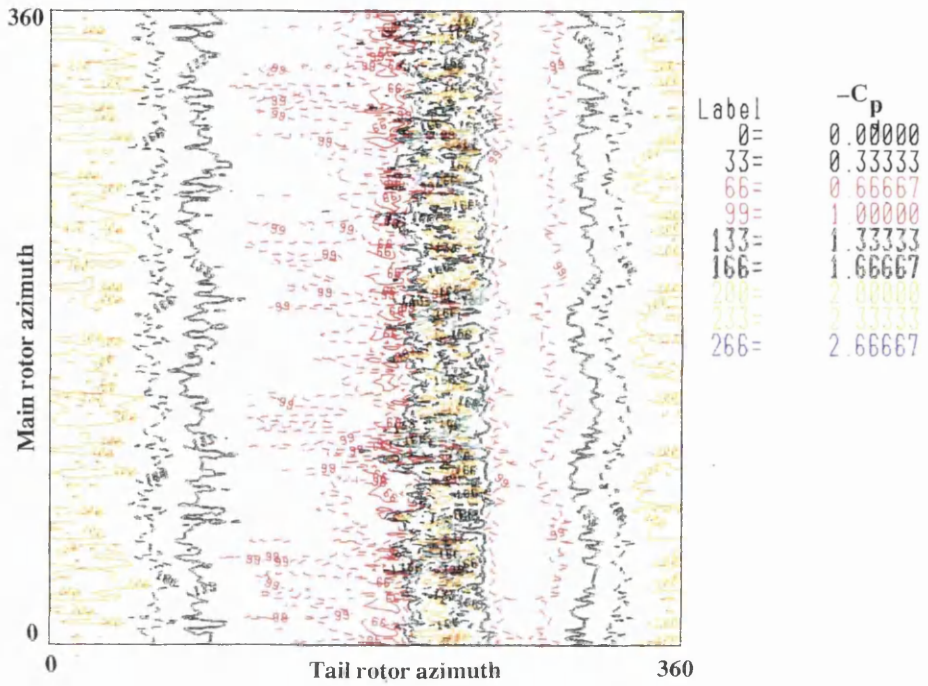

Figure5.6.5 Variation of $-C_p$ with tail rotor azimuth and main rotor azimuth during flight at 30kts/210° OGE. Interpretation of plot is fully explained in text

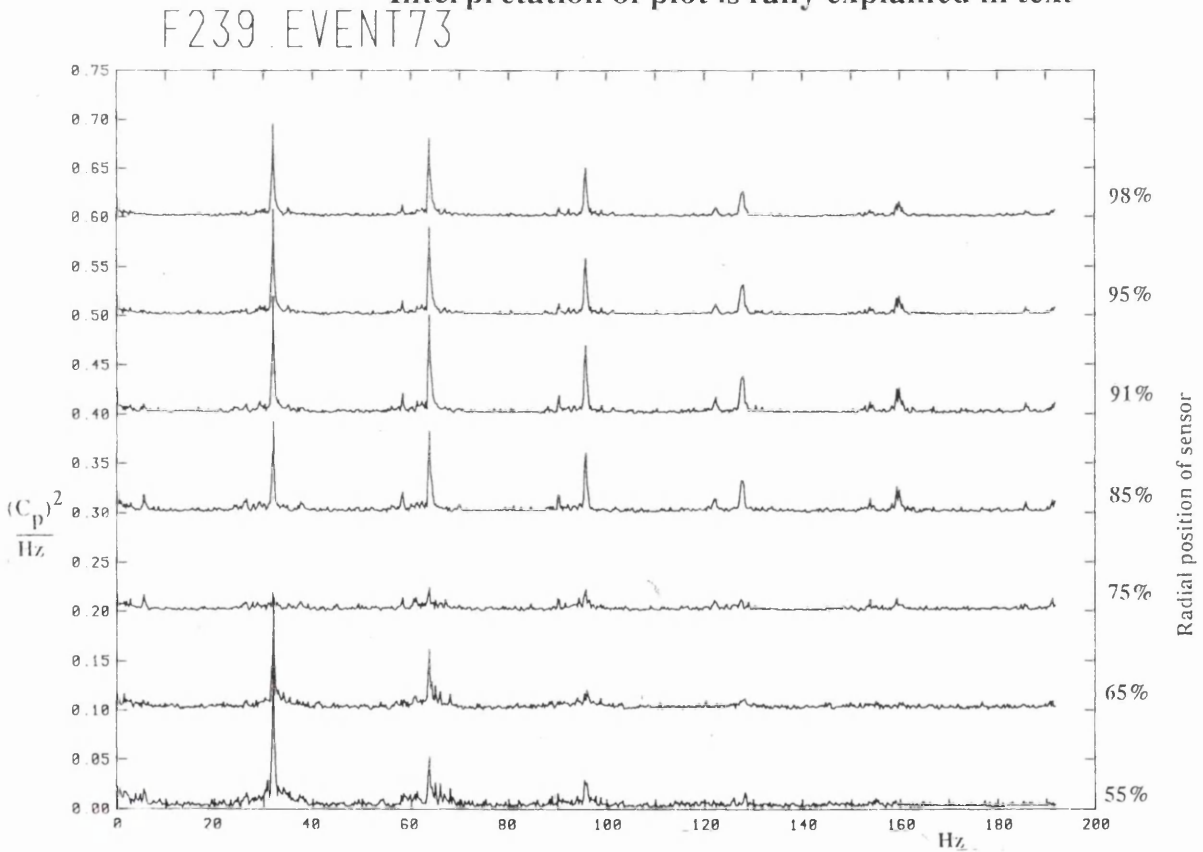

Figure 5.6.6 Lynx leading edge pressure sensor frequency content during flight at 30/kts/300° OGE

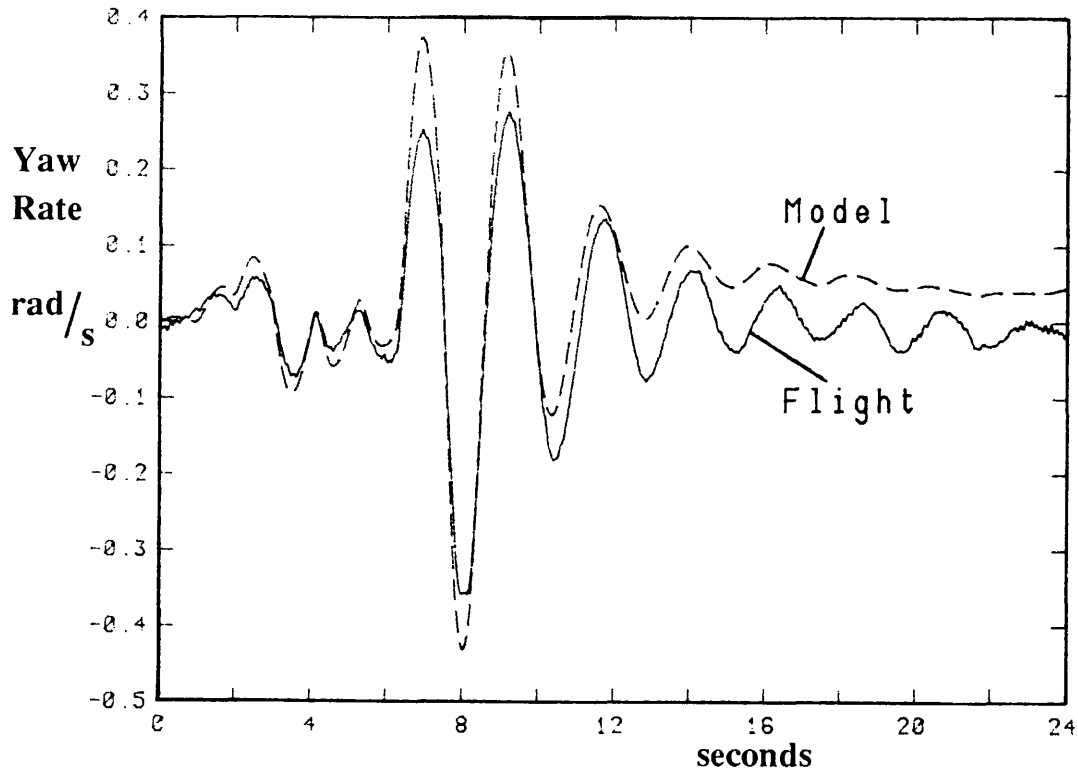

Figure6.2.1 **Figure showing BO105 yaw rate response to a pedal input and Helistab model response to the same input. Flight condition is 80 knots forward flight OGE.**

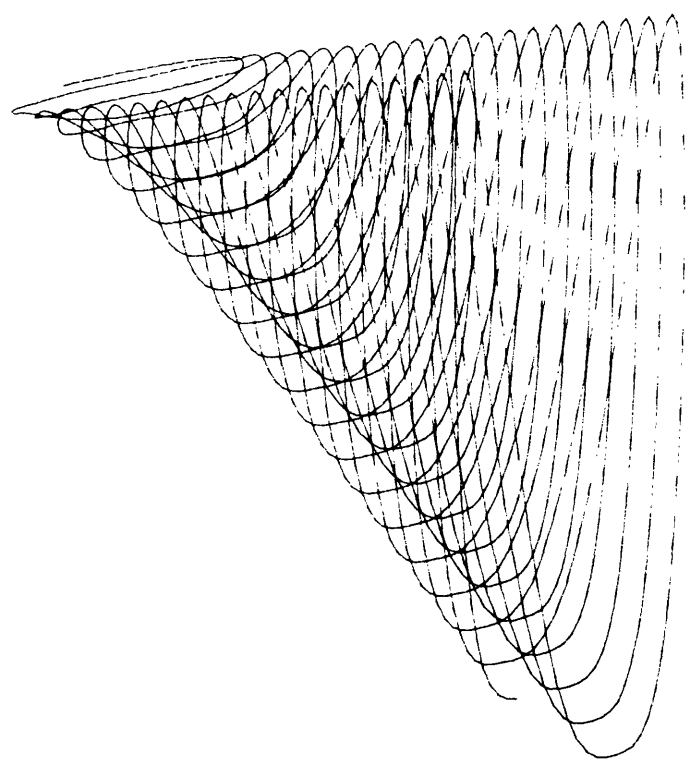

Figure6.3.1 **Beddoes main rotor wake model configured as a Lynx at 30 knots.**

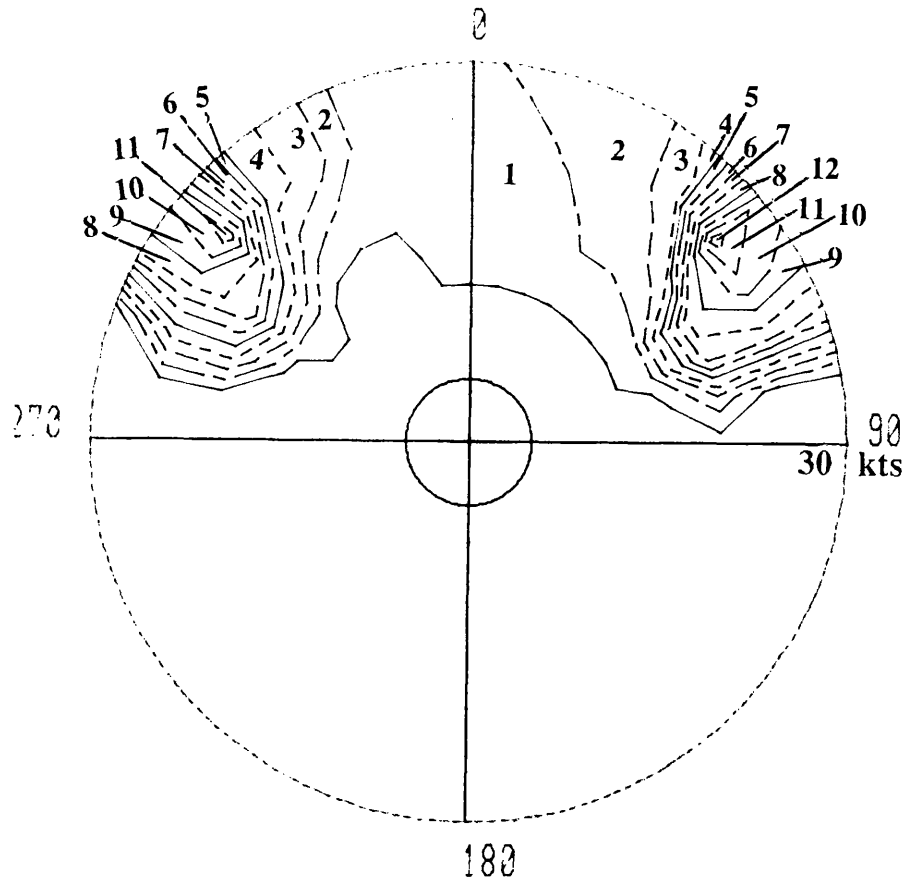

Figure6.3.2 Variation in number of main rotor blade trailing tip vortices passing through the tail rotor disc with flight condition as calculated using Beddoes wake model.

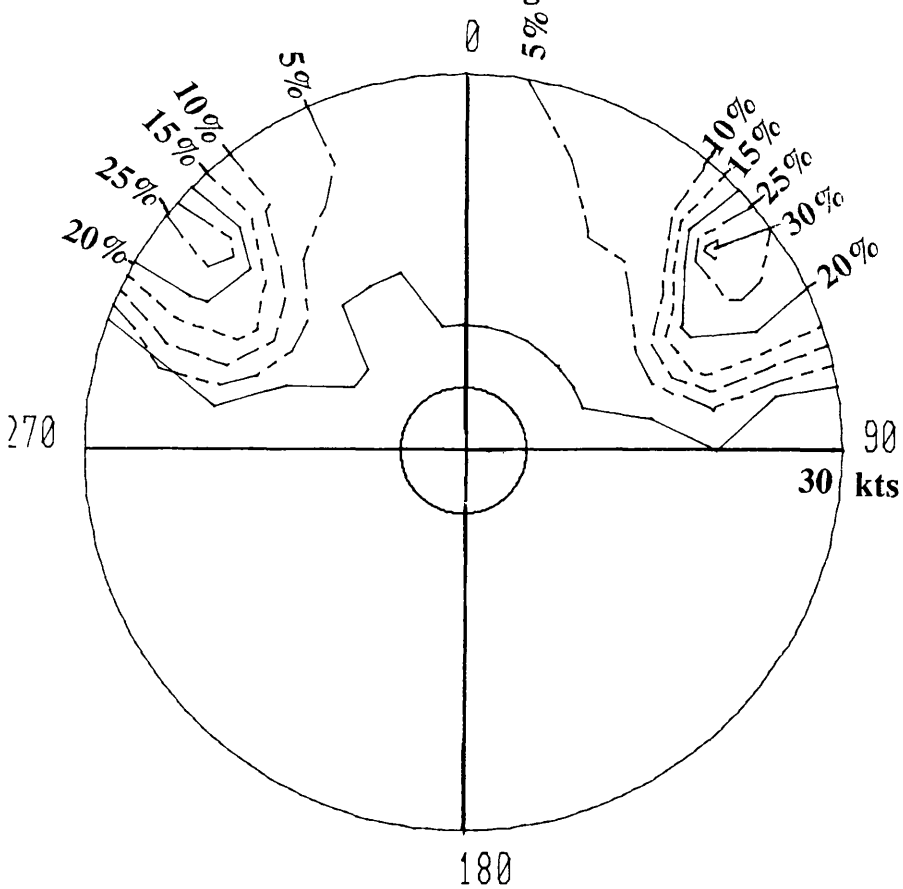

Figure6.3.3 Reduction in tail rotor dynamic head calculated using data from figure 6.3.2

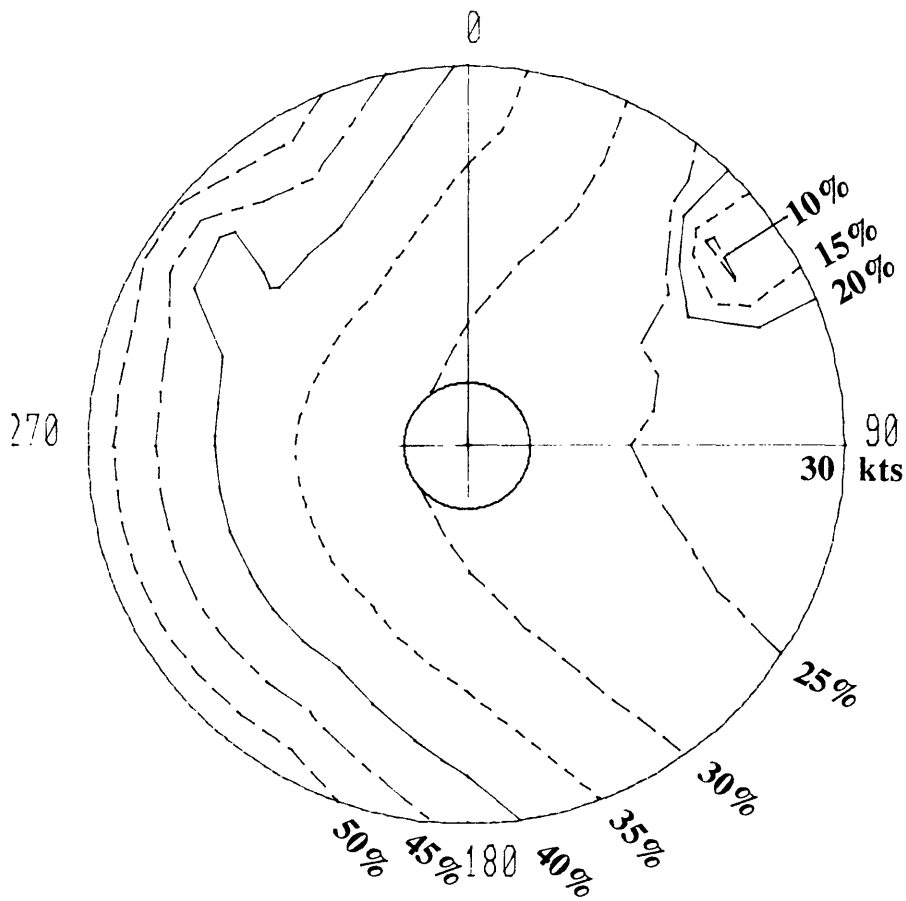

Figure6.3.4 Variation in pedal margin with flight condition as calculated using data from figure 6.3.3. Compare with figure 1.4.2.

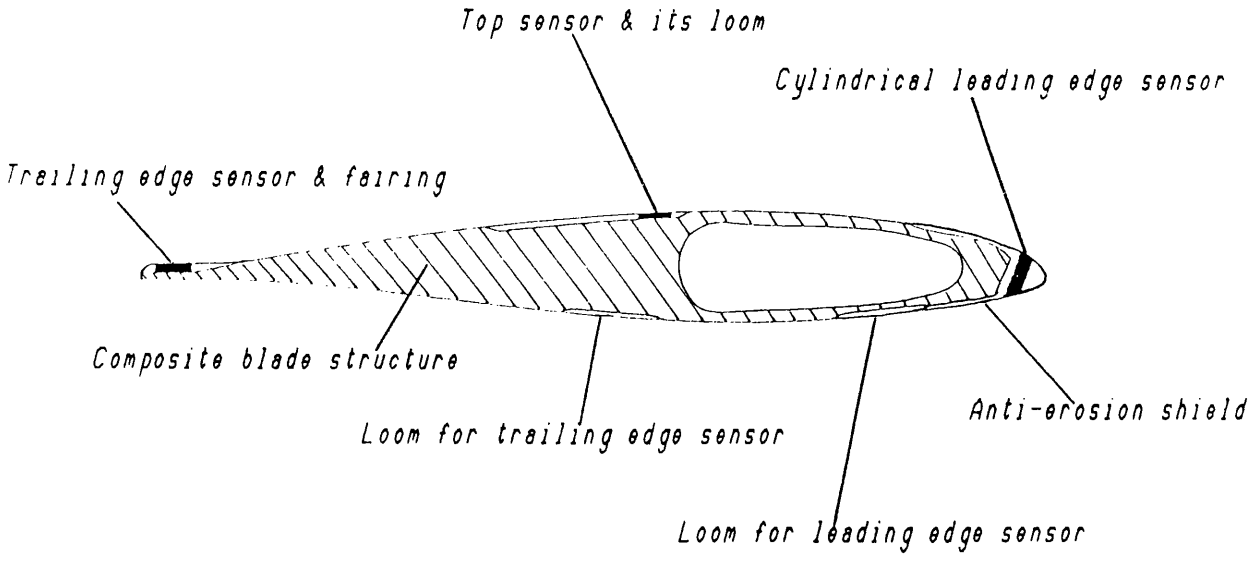

Figure A4.1 Cross section through proposed Lynx AH Mk7 pressure instrumented tail rotor blade.

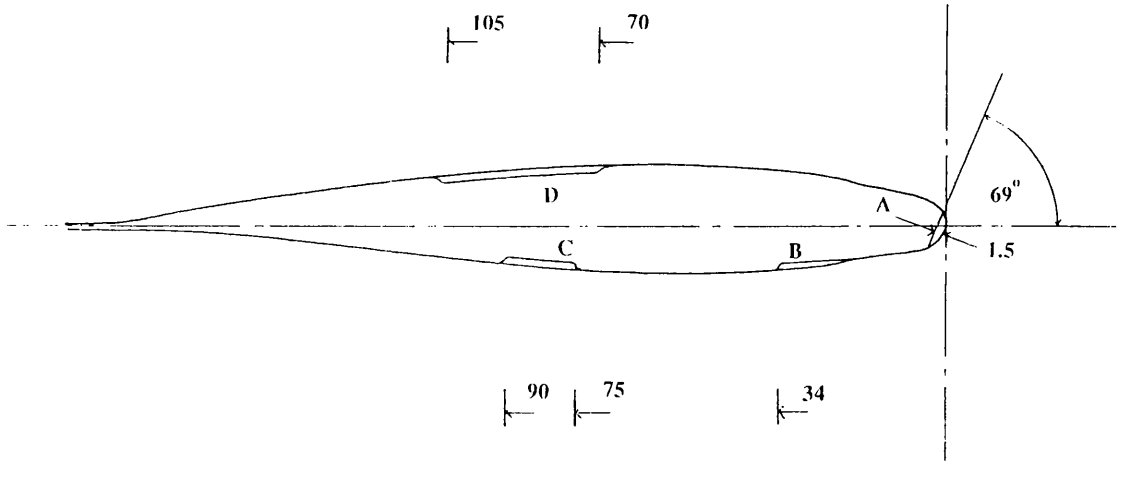

Figure A4.2 Cross section through Lynx AH Mk7 tail rotor blade core showing depressions required. Dimensions in mm.

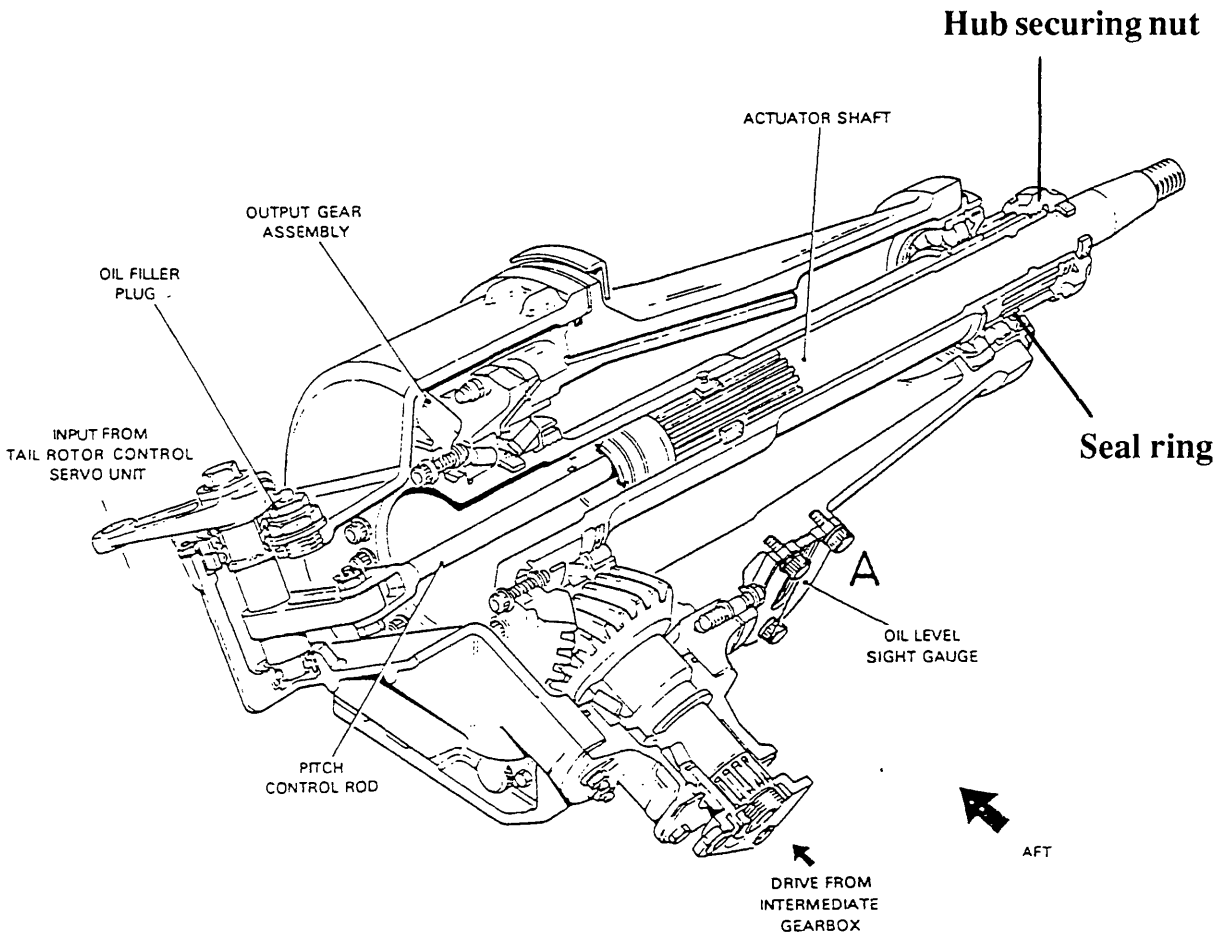

Figure A4.3 **Section of Lynx AH Mk7 tail rotor gearbox showing the seal ring to be modified for thrust measurement.**